Magnetic Bearings

Eric Maslen
University of Virginia
Department of Mechanical, Aerospace, and Nuclear Engineering
Charlottesville, Virginia

Revised June 5, 2000

Contents

List of Figures

List of Tables

Chapter 1

Electromagnetism

The central physical concept enabling magnetic bearing technology is that of magnetism. This chapter provides a brief review of magnetism including ferromagnetism. These notes were extracted from a very detailed and complete exposition by Lorrain and Corson[1]

1.1 Fundamental magnetic forces

The development follows a reasonably direct course. First, it is demonstrated that magnetic fields are really a relativistic distortion of the electric field of a moving charge and the resulting forces are obtained directly from Coulomb's law, which was first reported in about 1785. It is then demonstrated that the typical drift velocities in conductors are small enough to ignore the higher order relativistic terms. Next, it is shown that the force between two conductors is due only to the magnetic effect: the forces due to the electric field (computed in the stationary frame) cancel.

1.1.1 Lorentz force

Measured in a reference frame in which two charged particles are stationary, the force between the two charged particles is given by the fundamental relationship known as Coulomb's law:

$$\mathbf{F}_{b2} = \frac{Q_a Q_b}{4\pi\epsilon_0 r_2^3}\mathbf{r}_2 \tag{1.1}$$

where $\mathbf{r}_2$ is the radial vector between the two particles, as measured in the charge frame and $\epsilon_0 = 8.854 \times 10^{-12}$ Coul^2/Joule-m is the permittivity of a vacuum.

Assume that the charged particles are moving in parallel relative to a stationary observer. It can be shown through a straightforward application of the Lorentz transforms that, in the observer's frame of reference, the force acting on particle a by the charge of

[1]Lorrain, Paul and Corson, Dale, *Electromagnetic Fields and Waves*, W. H. Freeman and Company, San Francisco, 1970.

particle b is observed as:

$$\mathbf{F}_{b1} = \frac{\gamma Q_a Q_b \mathbf{r}_1}{4\pi\epsilon_0 r_2^3} + \mathbf{v} \times \frac{\gamma Q_a Q_b \mathbf{v} \times \mathbf{r}_1}{4\pi\epsilon_0 c^2 r_2^3} \tag{1.2}$$

where $\gamma = 1/\sqrt{1-(V/c)^2}$. The first term is the expected effect due to the attraction or repulsion of charges. The second term is a relativistic effect due to the motion of the charged particles. It is customary to define the term

$$\mathbf{E} \doteq \frac{\gamma Q_a \mathbf{r}_1}{4\pi\epsilon_0 r_2^3} \tag{1.3}$$

as the electric field at b due to the charge at a and the term

$$\mathbf{B} \doteq \frac{\gamma Q_a \mathbf{v} \times \mathbf{r}_1}{4\pi\epsilon_0 c^2 r_2^3} \tag{1.4}$$

as the magnetic field at b due to the motion of the charged particle a. The combination of coefficients $1/\epsilon_0 c^2 = \mu_0 = 4\pi \times 10^{-7}$ N/A^2 is called the *permeability* of a vacuum.

In this manner, the magnetic field is recognized to be simply a distortion of the electric field as seen by the observer in the stationary system, due to relativistic effects. Since the additional term arises from direct application of the Lorentz transforms, the effect is referred to as the Lorentz force:

$$\mathbf{F} = Q(\mathbf{E} + \mathbf{v} \times \mathbf{B}) \tag{1.5}$$

1.1.2 Conductors

A commonly encountered source of magnetic field is the motion of charge in a conductor, referred to as electric current. In a conductor, it is assumed that the carrier charges (free electrons) are uniformly distributed throughout the volume of the conductor and that the conductor has a net charge of zero: it contains the same number of protons as electrons. Let the volume density of carrier charges be called q so that the total charge in a differential volume dv is $dQ = qdv$. The electric current in the conductor is the rate at which charge passes through a control surface. If these carrier charges have a velocity, $\mathbf{v}$, then the total current passing through a given section of the conductor is

$$\mathbf{I} = \int_S \mathbf{v} \cdot \mathbf{n} q da = q \int_S \mathbf{v} \cdot \mathbf{da} = qA\overline{\mathbf{v}} \tag{1.6}$$

in which $\overline{\mathbf{v}}$ is the mean carrier velocity, or the drift velocity. Thus, the drift velocity can be computed from the current and the carrier density:

$$\overline{\mathbf{v}} = \frac{1}{qA}\mathbf{I} \tag{1.7}$$

In copper conductors, the maximum current density (current per unit cross sectional area) which can be sustained without damage to the conductor is on the order of 2×10^7

A/m^2. The free carrier charge density can be estimated from the atom density in copper. Copper has an atomic mass of 63.5 AMU and a specific mass of 8.89 which implies that it has about 8.4×10^{22} atoms per cubic centimeter (recall Avogadro's number of 6.022×10^{23} atoms per mole.) Further, copper has only one electron in its outermost or valence shell. Assuming that the single outer shell electron in elemental copper is the only one available as a carrier electron in the conductor, then since each electron carries a charge of 1.6×10^{-19} Coulombs, the carrier density, q, is about 1.4×10^{10} Coulomb/m^3. Consequently, the drift velocity is on the order of

$$v \approx \frac{1}{qA} I = \frac{1}{q} J = \frac{2 \times 10^7 \text{Coul}}{\text{sec m}^2} \frac{\text{m}^3}{1.4 \times 10^{10} \text{Coul}} = 0.0014 \text{m/sec}^2$$

This represents an upper bound because: a) the assumed current density is an upper bound and b) the assumed number of conduction electrons per atom is probably a lower bound. Thus, the drift velocity is low enough that the Lorentz corrections to the radius in (1.4) are neglible: $\gamma = 1.0$ to 15 significant digits. As a result, the terms $\mathbf{E}$ and $\mathbf{B}$ in (1.5) can be computed non-relativistically for most problems in the design and analysis of magnetic bearings.

Given the small magnitude of the drift velocity, it seems likely that no relativistic effects would be discernable and that, therefore, the magnetic force would be negligible. However, when considering the forces between two conductors, the forces produced by the electric field of the electrons in one of the conductors are *exactly* cancelled by the forces produced by the electric field of the protons because the conductor is electrically neutral. The protons produce no magnetic (relativistic) effect because they are stationary relative to the reference frame of the conductor. Thus, the remaining term which is relativistic is all that is detected.

As a point of comparison, the electric and magnetic forces acting on one moving point charge due to the presence and motion of another point charge can be compared: is

$$\frac{|\mathbf{v} \times \mathbf{B}|}{|\mathbf{E}|} \leq \frac{v^2}{c^2}$$

Thus, for charges moving at the speeds typical of conductors, the magnetic force is smaller than the electric force by a factor of at least 10^{23}!

Of course, when the conductor itself is in motion, the bulk velocity of the conductor will contribute to the magnetic field induced by the electrons, but in this case the protons will also produce a magnetic field which will cancel that due to the conductor frame velocity of the electrons. Consequently, even if the conductor is in motion, the magnetic field produced is only that due to the current in the conductor. This is reasonable since one would not expect to be able to generate a magnetic field simply by *moving* an electrically neutral conductor carrying no electric current.

1.1.3 Magnetic field due to a general distribution of moving charges

The magnetic field at a point in space due to the motion of any charges in its neighborhood can be computed by treating (1.4) as the differential field due to a differential charge and

then integrating over the entire volume enclosing the moving charges:

$$\mathbf{B} = \int_V \frac{\mu_0 dQ \mathbf{v} \times \mathbf{r}}{4\pi r^3} \tag{1.8}$$

Defining the *carrier charge density*, q, as the amount of charge per unit volume (treating it as no longer a discrete quantity), the term dQ is replaced with qdv:

$$\mathbf{B} = \int_V \frac{\mu_0 q dv \mathbf{v} \times \mathbf{r}}{4\pi r^3} \tag{1.9}$$

Finally, the *current density*, $\mathbf{J}$, is defined as the product of the carrier charge density and its local velocity:

$$\mathbf{J} \doteq q\mathbf{v} \tag{1.10}$$

to produce the *Biot–Savart law*

$$\mathbf{B} = \frac{\mu_0}{4\pi} \int_V \frac{\mathbf{J} \times \mathbf{r}}{r^3} dv \tag{1.11}$$

1.1.4 Maxwell's Equations

From the previous definitions of the magnetic field (1.4) and the electric field (1.3), it is possible (and fairly direct) to obtain Maxwell's equations:

$$\nabla \cdot \mathbf{E} = \frac{q}{\epsilon_0} \tag{1.12}$$

$$\nabla \times \mathbf{E} = -\frac{\partial \mathbf{B}}{\partial t} \tag{1.13}$$

$$\nabla \cdot \mathbf{B} = 0 \tag{1.14}$$

$$\nabla \times \mathbf{B} = \mu_0 \left(\mathbf{J} + \epsilon_0 \frac{\partial \mathbf{E}}{\partial t} \right) \tag{1.15}$$

or, in integral form,

$$\int_S \mathbf{E} \cdot \mathbf{ds} = \frac{1}{\epsilon_0} \int_V q dv \tag{1.16}$$

$$\int_S \mathbf{B} \cdot \mathbf{ds} = 0 \tag{1.17}$$

in which S is a closed surface surrounding a volume V, and

$$\oint_L \mathbf{E} \cdot \mathbf{dl} = -\frac{\partial}{\partial t} \int_S \mathbf{B} \cdot \mathbf{ds} \tag{1.18}$$

$$\oint_L \mathbf{B} \cdot \mathbf{dl} = \mu_0 \int_S \left(\mathbf{J}_m + \epsilon_0 \frac{\partial \mathbf{E}}{\partial t} \right) \cdot \mathbf{d}s \tag{1.19}$$

in which L is a closed path around an open surface S.

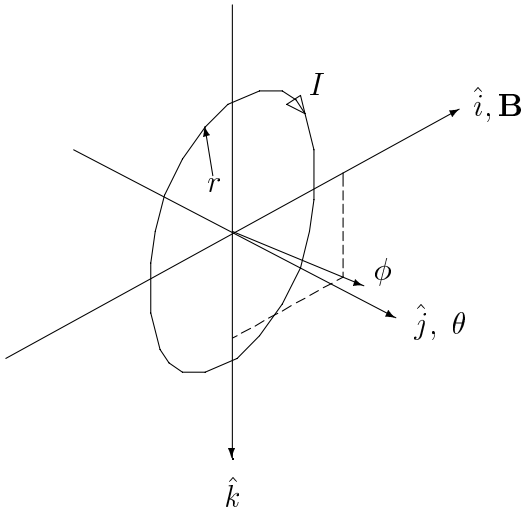

Figure 1.1: Current carrying coil in a uniform magnetic field.

1.2 Magnetic force on a current carrying loop

An elementary problem of interest in understanding magnetic forces is that of the force acting on a current carrying loop in a uniform magnetic field. Assume a planar, circular loop of radius r with current I which is oriented so that its axis forms an angle θ relative to the magnetic field vector, $\mathbf{B}$. Figure 1.1 illustrates the geometry. The force acting on a differential element of the loop at an angle ϕ can be computed using (1.5):

$$\mathbf{dF} = dQ\ \mathbf{v} \times \mathbf{B} \tag{1.20}$$

The product $dQ\mathbf{v}$ is equal to the current times the length of the differential element:

$$dQ\mathbf{v} = I\mathbf{dl} \tag{1.21}$$

to yield

$$\mathbf{dF} = I\ \mathbf{dl} \times \mathbf{B} \tag{1.22}$$

> Note that, in computing the force acting on the coil, we do not consider the interaction between the current and its *own* $\mathbf{B}$ field. Clearly, an electron cannot exert a force on itself, but the other electrons comprising the overall current could (and do) exert a force on any given electron. However, if the current is modelled as distributed over a finite wire area and the net force acting on the wire due to the magnetic field generated by the wire itself is computed, it is found to be zero. This should be no great surprise, because while the average amplitude of the $\mathbf{B}$ field within the wire may be quite high, the average orientation is zero. This is because the field induced by the current circulates around the current. By contrast, an externally imposed field will not circulate around the current and the average orientation (and magnitude) of the externally imposed field will not be zero within the area of the wire.

Choosing a coordinate frame where the $\hat{i}$ vector is parallel to $\mathbf{B}$, the axis of the coil lies in the $\hat{i} - \hat{k}$ plane, and the center of the coil lies at the origin, we can componentiate these

vectors and perform the computation:

$$\mathbf{B} = B\hat{i} \quad , \quad \mathbf{dl} = r\left(\cos\phi\sin\theta\hat{i} - \sin\phi\hat{j} + \cos\phi\cos\theta\hat{k}\right)d\phi$$

to obtain

$$\mathbf{dF} = rBI\left(\cos\phi\cos\theta\hat{j} + \sin\phi\hat{k}\right)d\phi$$

The total force acting on the loop is obtained by integrating this expression through the range of ϕ:

$$\mathbf{F} = rBI\int_0^{2\pi}\left(\cos\phi\cos\theta\hat{j} + \sin\phi\hat{k}\right)d\phi = 0$$

That is, there is no *net* force acting on a current carrying loop in a *uniform* magnetic field. Later, it will be shown that a diverging magnetic field will produce a force on such a coil and that this is what leads to the attractive or repulsive forces between magnets.

The differential moment acting on the loop is obtained by

$$\mathbf{dC} = \mathbf{r} \times \mathbf{dF}$$

in which the radius is

$$\mathbf{r} = r\left(\sin\phi\sin\theta\hat{i} + \cos\phi\hat{j} + \sin\phi\cos\theta\hat{k}\right)$$

which provides

$$\mathbf{dC} = r^2BI\left(0.5\sin 2\phi\sin^2\theta\hat{i} - \sin^2\phi\sin\theta\hat{j} + 0.25\sin 2\phi\sin 2\theta\hat{k}\right)d\phi$$

The total moment is obtained by integrating:

$$\begin{aligned}\mathbf{C} &= r^2BI\int_0^{2\pi}\left(0.5\sin 2\phi\sin^2\theta\hat{i} - \sin^2\phi\sin\theta\hat{j} + 0.25\sin 2\phi\sin 2\theta\hat{k}\right)d\phi \\ &= -\pi r^2BI\sin\theta\hat{j}\end{aligned} \tag{1.23}$$

Thus, a positive rotation $\theta\hat{j}$ produces a negative, or restoring, moment $-\pi r^2BI\sin\theta\hat{j}$ (which is oriented along the same axis): the coil tends to align its axis with the magnetic field.

Further, the magnetic field at the center of the coil due to the current in the coil can be computed using (1.4):

$$\begin{aligned}\mathbf{B} &= \int_L \mu_0\frac{dQ\mathbf{v}\times\mathbf{r}}{4\pi r^3} \\ &= \frac{\mu_0 I}{4\pi r^3}\int_L \mathbf{dl}\times\mathbf{r} \\ &= \frac{\mu_0 I}{4\pi r}\int_0^{2\pi}\cos\theta\hat{i} + \sin\theta\hat{k}\;d\phi \\ &= \frac{\mu_0 I}{2r}\left(\cos\theta\hat{i} + \sin\theta\hat{k}\right)\end{aligned}$$

The *magnetic dipole moment*, $\mathbf{m}$, due to the motion of a charge distribution Q in a volume V about a point a is defined as

$$\mathbf{m} \doteq \frac{1}{2}\int_V \mathbf{r}_a \times dQ\mathbf{v} \tag{1.24}$$

For the present problem, the moving charge distribution is confined to the wire, so the dipole moment is

$$\mathbf{m} = \frac{1}{2}\oint \mathbf{r} \times I\mathbf{dl}$$

where the integration is taken around the coil loop. The dipole moment for this coil is found to be

$$\mathbf{m} = \pi r^2 I\left(\cos\theta\hat{i} + \sin\theta\hat{k}\right) \tag{1.25}$$

In terms of this dipole moment, the magnetic field at the center of the coil is thus

$$\mathbf{B} = \frac{\mu_0}{2\pi r^3}\mathbf{m} \tag{1.26}$$

This field is aligned with the axis of the loop in the direction indicated by ϕ in Figure 1.1. Centering a set of spherical coordinates at the center of the coil with the ϕ rotational coordinate aligned with the symmetry of the coil, the spherical components of the field are:

$$B_R = \frac{\mu_0}{2\pi}\frac{|m|}{R^3}\cos\theta$$

$$B_\theta = \frac{\mu_0}{4\pi}\frac{|m|}{R^3}\sin\theta$$

in which R is the distance from the center of the coil to the point of measurement and the angle θ is the angle between the axis of the coil and the radial vector to the measurement point. Figure 1.2 shows the orientation of this axisymmetric field throughout the space surrounding the coil. The lines simply connect adjacent vectors and the spacing between the lines is an indication of the magnitude of the field: closely spaced lines indicate a high magnitude.

When the coil is fully aligned with the external field, the coil's field tends to reinforce the external field, rather than cancelling it. Because this current carrying loop is both a source of the B field as well as a sink of it, it is referred to as a magnetic dipole.

1.3 Ferromagnetism

Materials are made up of atoms and atoms have electrons which move in circular orbits and, therefore, generate magnetic fields. In general, the magnetic fields are randomly oriented and the aggregate effect is zero. However, in *ferromagnetic* materials, it is observed that regions of the material exhibit coherence so that the motions of the electrons tend to be so coordinated as to produce a net magnetic field. These regions are called the *magnetic domains* of the material.

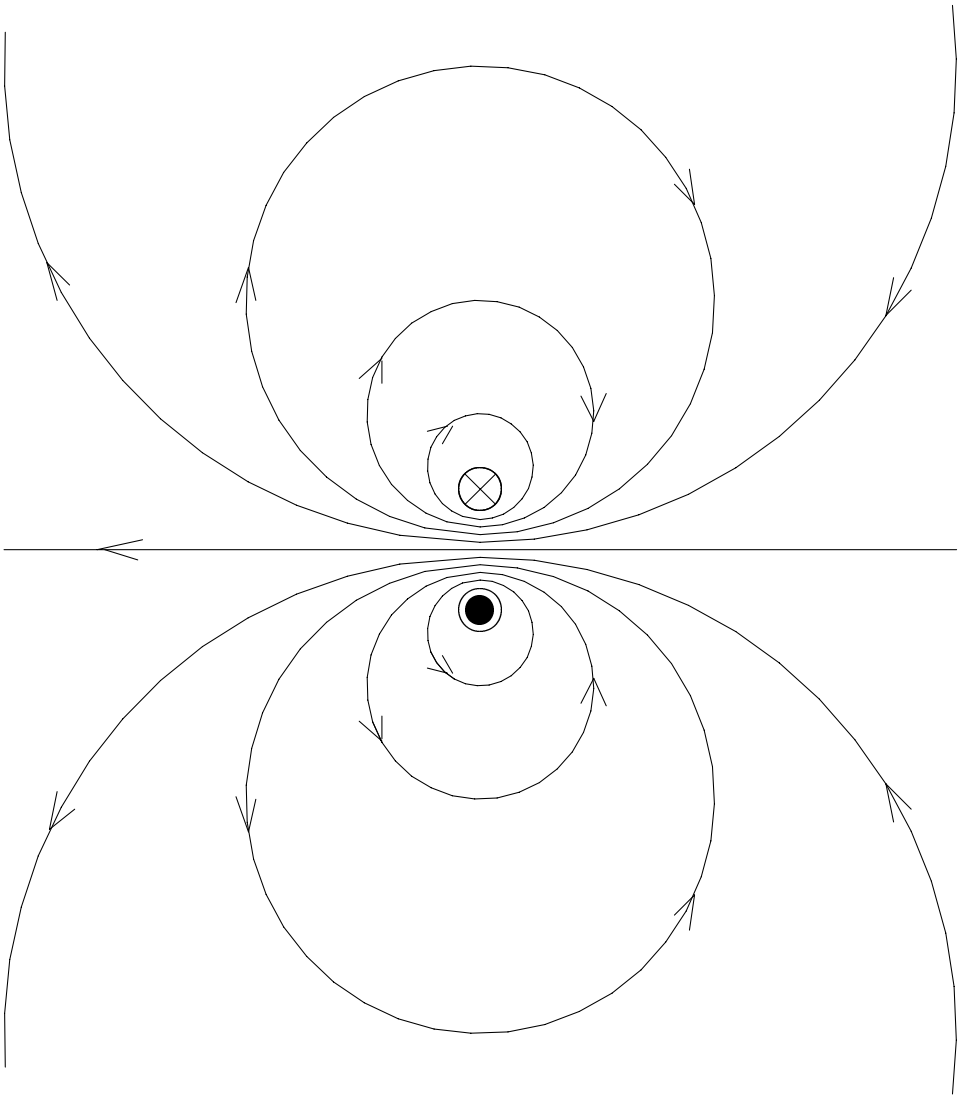

Figure 1.2: Magnetic field surrounding a current carrying coil.

This behavior should, in a way, not be surprising. Assume that there are finite volumes within the conductive material where electrons can travel freely without dissipation. If so, then one free electron may tend to move in some motion around the surface of this volume, forming a current carrying loop. This loop will generate a magnetic field and tend to align any other such loops (electron trajectories) within the volume with itself. The actual orientation of this aggregate motion would be determined by the geometric details of the domain as well as the electrical properties of the boundary surface.

What distinguishes ferromagnetic materials from other materials, then, is the tendency to exhibit these magnetic domains.

In order to see the significance of these domains, imagine them to be a collection of current carrying coils, or dipoles, distributed throughout the volume of the material. In the absence of any external fields, the dipoles are randomly oriented. One might object by observing that the dipoles themselves generate a magnetic field in the material which ought to produce some alignment. However, if the orientation of the dipoles is initially random (made so by some superior effort) then the average magnetic field passing through any volume of reasonable scale would be expected to be zero. Thus, absent any external stimulus, the domains might be randomly oriented and would stay so. Further, noting that the (initial) orientation of the domains is probably selected by random geometric and electrical influences, it is reasonable to assume that, if the domains are rotated by application of an external field and then the external field is removed, then they should tend to return to their initial orientation. This suggests some sort of moment stiffness and conjures up a picture of a collection of coils on gimbals with torsional springs acting at the gimbal axes to return the coil orientation (dipole axis) to some nominal value in the absence of other influences.

Suppose, now, that a magnetic field is imposed on such a material: perhaps it is placed at the center of a large current carrying coil. If the domains maintained their initial, random positions, then there would be no effect and the average magnetic field intensity at the center of the external coil would be the same as if the material were not present. However, if the domains align themselves with the field imposed by the coil, then there will be a substantial increase in the field intensity throughout the volume of the material, relative to what it would be if the domains were not aligned. Clearly, the softer the imagined gimbal springs are made, the more the domains will tend to align themselves with the imposed field and the more the field will be intensified.

For a single domain with an effective center field of

$$\mathbf{B}_c = \frac{\mu_0 I}{2r}\left(\cos\theta\hat{i} + \sin\theta\hat{k}\right)$$

the moment due to the external field (aligned along the $\hat{i}$ axis) is

$$\mathbf{M} = -\pi r^2 BI\sin\theta\hat{j}$$

If we posit an initial alignment θ_0 and a gimbal stiffness K, then the moment due to the gimbal stiffness is

$$\mathbf{M}_g = -K(\theta - \theta_0)\hat{j}$$

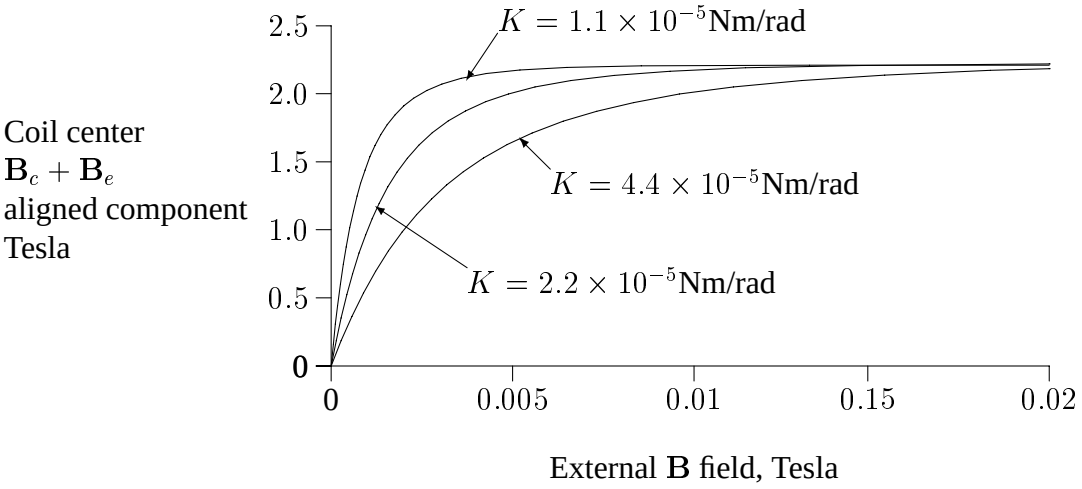

Figure 1.3: Coil center field strength as a function of applied field.

so that the equilibrium orientation is

$$\mathbf{M} + \mathbf{M}_g = 0 \quad \Rightarrow \quad \pi r^2 BI \sin\theta + K\theta = K\theta_0$$

The net field at the center of the coil is the sum of that due to the coil itself and the externally imposed field. Figure 1.3 shows the component of this field parallel to the imposed field as a function of the imposed field for $r = 0.001$m, $I = 3500$A, $\theta_0 = \pi/2$, and various values of K. The significant features are that the field demonstrates substantial amplification at low levels of applied field and demonstrates a saturation effect where the coil becomes fully aligned with the applied field and further increases in the applied field produce only equal gains in the center field.

This spring aligned gimballed coil model for the domains of a ferromagnetic material is useful in that it provides some insight to the general properties of such materials. First, if the spring is quite soft, the domains will align themselves with the external field quite easily, producing a very high initial amplification of the field whereas if the spring is quite stiff, the amplification is lower. This amplification effect is referred to as the *relative permeability* of the material. Saturation is achieved when all of the domains in the material are completely aligned with the external field. The amplitude of the added field is determined by the dipole strength of the domains and is independent of the stiffness of the gimbal.

Thus, the saturation density and relative permeability are expected to be somewhat unrelated properties of the material. In fact, there is some correlation: materials with very high relative permeability tend to have lower saturation densities while materials with very high saturation densities have more moderate relative permeabilities.

Ampére is credited with suggesting an internal model for ferromagnetic materials consisting of a distribution of such small dipoles as shown in Figure 1.4. In this model, the many internal dipoles are partially aligned to the applied magnetic field. The net effect of the many current loops is an equivalent surface current, as indicated in Figure 1.4. This equivalent surface current is related to the applied field: it is zero when the applied field is zero, increases in proportion to the applied field until all of the domains are nearly aligned and finally reaches a fixed value determined not by the applied field but by the strengths

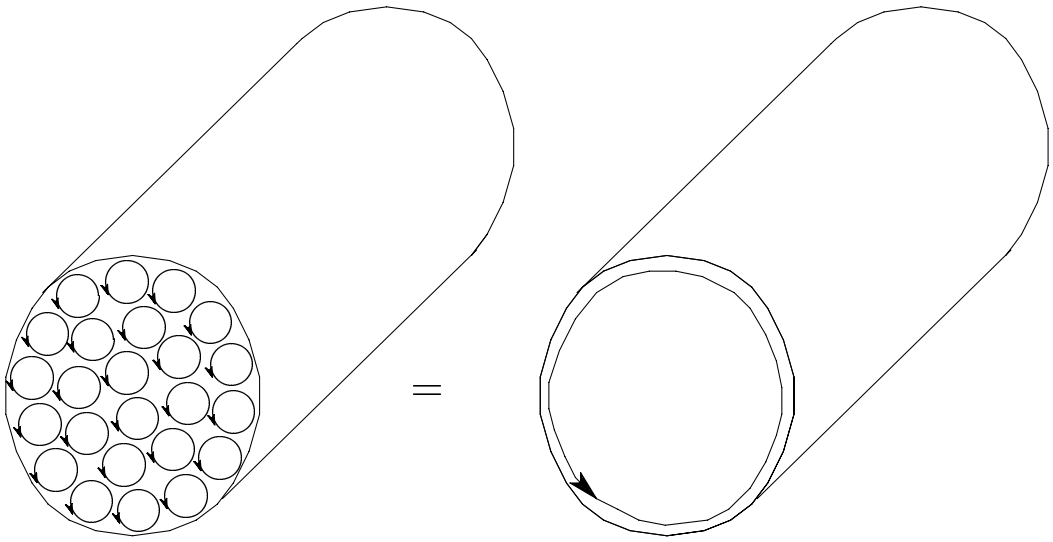

Figure 1.4: Internal model of a ferromagnetic material: many dipoles partially aligned with the imposed field.

of the internal dipoles. The reason that the internal current loops can be represented by a single surface current is that the effects of adjacent counterflowing currents within the volume of the material tend to cancel each other but, at the surface, no such cancellation takes place. This model of ferromagnetic materials being equivalent to a surface current surrounding the volume of the material is a powerful model, especially in treating permanent magnets.

1.3.1 Hysteresis

The model described above for a ferromagentic material is entirely reversible: if a field is imposed, the domains tend to align themselves with it, but once the field is removed, the domains will return to their initial alignment. If the model for the gimbal spring is changed from being a perfectly elastic spring to one with a tendency to yield at high stress, then those domains which are rotated the most will not return to their original orientation after removal of the aligning field, relaxing instead to some intermediate orientation.

1.3.2 Permanent magnets

A permanent magnet is simply a ferromagnetic material in which the orientation of the dipoles is strongly fixed: K is very large at moderate temperature. The orientation of the dipoles in a permanent magnet can be fixed by exposing the magnet to a strong aligning field while the temperature is elevated. If the temperature is dropped while maintaining the field, the new, aligned orientation is retained and the material is said to be magnetized. In this manner, a permanent magnet can be modelled as an equivalent surface current of *fixed* magnitude: the extremely stiff alignment of the domains maintains the alignment of the internal domains regardless of any imposed external magnetic field.

1.4 Magnetic forces: field divergence

In Section 1.2, it was demonstrated that no net force acts on a circular current carrying coil exposed to a *uniform* magnetic field, $\mathbf{B}$. Suppose, however, that the field is circularly uniform with axis coincident with the axis of the coil and that the field has a constant radial component, B_r, and a constant axial component, B_a, at every point on the coil. Such a field can be established by placing another current carrying coil in a plane parallel to the subject coil with its axis coincident to the subject coil's axis. The field is described by:

$$\mathbf{B} = B_a\hat{i} + B_r\cos\phi\hat{j} + B_r\sin\phi\hat{k} \tag{1.27}$$

while the coil geometry is described by

$$\mathbf{dl} = r\left(-\sin\phi\hat{j} + \cos\phi\hat{k}\right)d\phi \tag{1.28}$$

(the angular misalignment, θ, of Figure 1.1 is equal to zero in this analysis.) The force, then, is

$$\mathbf{F} = -2\pi r B_r I\hat{i} \tag{1.29}$$

What is signficant about this computation is that the force acting on the coil is due to the radial component of the field, not the axial component. That is, the force acts orthogonal to the useful component of the field.

1.4.1 Forces on a ferromagnetic disk

Suppose that a disk of ferromagnetic material is aligned with a current carrying loop, as shown in Figure 1.5. The field from the current carrying loop will tend to align the domains in the ferromagnetic disk, giving rise to an effective surface current, I_s. This current is essentially proportional to the axial component of the field imposed by the coil:

$$I_s = \beta B_{a,c}$$

The force acting on the ferromagnetic disk is determined by the radial component of the imposed magnetic field *alone*. To see that the field produced by the surface current itself does not affect the force, recognise that, if the surface current were to arise but the external coil were not present, no net force would act on the disk: otherwise the disk could push on itself, particularly if it were a permanent magnet. Thus,

$$f_a = -2\pi r B_{r,c} I_s = -2\pi\beta r B_{r,c} B_{a,c}$$

Of course, regardless of the actual shape of the field developed by the external coil, the strength of the radial component of the field is proportional to the strength of the axial component[2]:

$$B_{r,c} = \sigma B_{a,c}$$

[2] For points far from the center of the source coil, the ratio of radial to axial field is $3r/2Z$ where Z is the axial separation between the source coil and the plane of the disk.

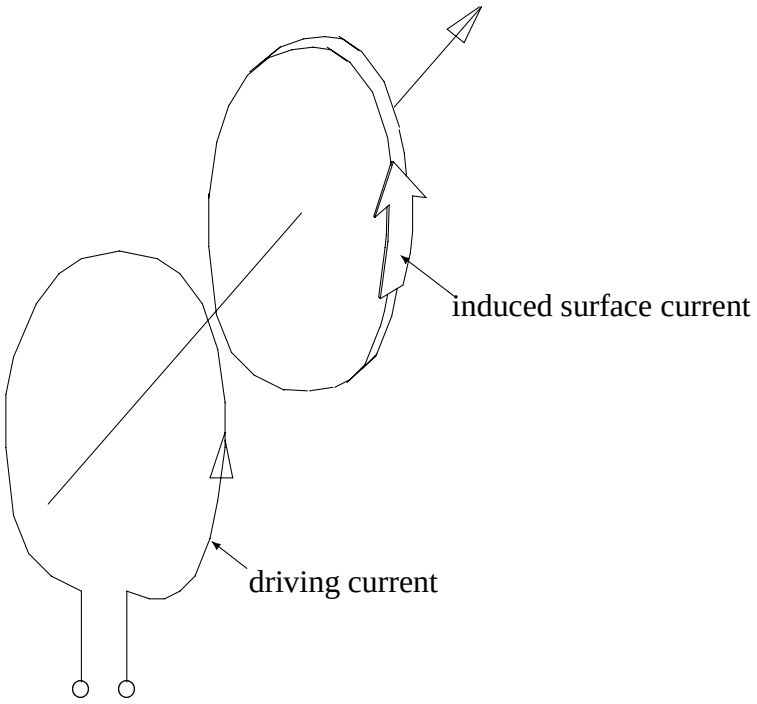

Figure 1.5: Ferromagnetic disk in a magnetic field.

which produces the relationship

$$f_a = -2\pi\beta\sigma r B_{a,c}^2$$

Thus, the axial force is related to the square of the strength of the axial component of the *applied* magnetic field. However, this familiar dependency hides the job performed by each component of the applied field:

1. the axial component of the applied field aligns the domains of the ferromagnetic material, leading to a net surface current.

2. this surface current then interacts with the radial component of the applied magnetic field according to the Lorentz force equation (1.5) to generate a force on the disk.

This scenario is important because it means that a ferromagnetic disk introduced to a *uniform* magnetic field would experience no force. Further, a non-ferromagnetic disk introduced to a field experiences no force because no surface currents are established: there are no domains to align.

1.4.2 Definition of H and χ

Because analysis of forces acting on ferromagnetic bodies requires a distinction between the field which would have been had the domains not aligned and the actual field, a quantity distinct from $\mathbf{B}$ is defined, called the *magnetic field intensity*:

$$\mathbf{H} = \frac{1}{\mu_0}\mathbf{B}_c$$

where $\mathbf{B}_c$ is the magnetic field which would arise in the absence of the ferromagnetic material. The effect that imposing this field $\mathbf{H}$ on the ferromagnetic material has is to orient the local dipole moments. Thus, a measure of the effect on the material is the average dipole moment per unit volume:

$$\mathbf{M} = \mathbf{m}N$$

in which $\mathbf{m}$ is the *average* dipole moment per domain and N is the number of domains per unit volume. Although the dipole moments are, in reality, discrete, $\mathbf{M}$ is an expression for a continuous quantity whose volume integral is the same as the vector sum of all of the moments of all of the domains. Noting that the degree of alignment of the magnetic domains is essentially proportional to $\mathbf{B}_c$ and, therefore, to $\mathbf{H}$, the magnetic susceptibility of the material is defined by

$$\mathbf{M} = \chi\mathbf{H}$$

This represents a constitutive model for the magnetic material and is, as written, linear. After a bunch of vector algebra, it can be shown that the magnetic field within the ferromagnetic material is given by

$$\mathbf{B} = \mu_0(\mathbf{H} + \mathbf{M})$$

That is, it is the superposition of the imposed field intensity $\mathbf{H}$ and the induced field intensity $\mathbf{M}$. In this manner, since $\mathbf{M}$ is related to $\mathbf{H}$ by the linear constitutive law, the relationship between $\mathbf{B}$ and $\mathbf{H}$ within the (assumed linear) ferromagnetic material is

$$\mathbf{B} = \mu_0(\mathbf{H} + \mathbf{M}) = \mu_0(1 + \chi)\mathbf{H}$$

The quantity $1 + \chi$ is called the *relative permeability*, μ_r.

1.4.3 Maxwell's stress tensor

A more rigorous computation of the forces acting on a ferromagnetic body in a magnetic field is obtained using Maxwell's stress tensor, which can be derived in the following manner[3]. Assume that the domain currents can be represented as a net current density with some distribution throughout the volume of the material. If the domains are uniformly aligned then, by Ampère's model, the current is entirely concentrated at the periphery of the material. In any case, we can define an effective current density

$$\mathbf{J}_M = \nabla \times \mathbf{M}$$

where $\mathbf{M}$ is the volume differential dipole moment in the material. Further, if there are any free currents in the volume, they lead to a non–zero curl in $\mathbf{H}$:

$$\mathbf{J}_F = \nabla \times \mathbf{H}$$

[3]These notes were lifted from Joe Keith's dissertation.

Given this, the total force acting on the ferromagnetic body is obtained through the volume integral

$$\mathbf{F} = \int (\mathbf{J}_M + \mathbf{J}_F) \times \mathbf{B}\, dv$$

or,

$$\mathbf{F} = \int (\nabla \times \mathbf{H} + \nabla \times \mathbf{M}) \times \mathbf{B}\, dv$$

Since the *total* magnetic field (due to the imposed field and the domain alignment) is given by $\mathbf{B} = \mu_0 (\mathbf{H} + \mathbf{M})$, this becomes

$$\mathbf{F} = \frac{1}{\mu_0} \int (\nabla \times \mathbf{B}) \times \mathbf{B}\, dv$$

Apply the vector identities

$$\oint (\mathbf{B} \cdot \mathbf{B}) d\mathbf{S} - 2 \oint \mathbf{B}(\mathbf{B} \cdot d\mathbf{S}) = 2 \int \mathbf{B} \times (\nabla \times \mathbf{B}) dv - 2 \int \mathbf{B}(\nabla \cdot \mathbf{B}) dv$$

and

$$(\nabla \times \mathbf{B}) \times \mathbf{B} = -\mathbf{B} \times (\nabla \times \mathbf{B})$$

to obtain

$$\mathbf{F} = \frac{1}{\mu_0} \oint \mathbf{B}(\mathbf{B} \cdot d\mathbf{S}) - \frac{1}{2\mu_0} \oint (\mathbf{B} \cdot \mathbf{B}) d\mathbf{S} - \frac{1}{\mu_0} \int \mathbf{B}(\nabla \cdot \mathbf{B})\, dv$$

Gauss' Law states that, for static fields or fields varying at a moderate rate,

$$\nabla \cdot \mathbf{B} = 0$$

so that the last term disappears:

$$\mathbf{F} = \frac{1}{\mu_0} \oint \mathbf{B}(\mathbf{B} \cdot d\mathbf{S}) - \frac{1}{2\mu_0} \oint (\mathbf{B} \cdot \mathbf{B}) d\mathbf{S}$$

This integration can be represented very compactly using Maxwell's stress tensor, defined in the absence of electric fields ($\mathbf{E} = 0$) as:

$$T_{ij} = \frac{1}{\mu_0} \left(B_i B_j - \frac{1}{2} \delta_{ij} B_{ij}^2 \right)$$

where $\delta_{ij} = 1$ if $i = j$ and $\delta_{ij} = 0$ if $i \neq j$. With this convenient device, the force can be compactly expressed as

$$\mathbf{F} = \oint \overline{\mathbf{T}} \cdot d\mathbf{S}$$

Note that, if the magnetic field is perpendicular to the surface of the iron everywhere on the surface, then the force becomes

$$\mathbf{F} = \frac{1}{2\mu_0} \oint |\mathbf{B}|^2 d\mathbf{S} \tag{1.30}$$

This perpendicularity obtains when the relative permeability of the magnet iron is very high: this is the usual assumption made in computing the force on a ferromagnetic body.

Note that, as in the previous heuristic discussion of the ferromagnetic disk, the body forces arise due to the Lorentz type interaction between the applied magnetic field and the currents within the volume of the body – in this case, the equivalent domain currents. In the sequel, computations of magnetic forces acting on ferromagnetic objects will be accomplished using (1.30) since this form of the computation turns out to be very much the most convenient one in magnetic systems with very high permeability materials.

Chapter 2

Magnetic Actuator Analysis

In analyzing the behavior of a magnetic actuator, the primary objective is to determine the forces generated by the actuator in response to voltages applied to its coils and motion of the actuated device. Once this analysis is well established, it can be used in the design of actuators both in that it provides insight to the effects of the various design parameters and in that the analysis can be used to evaluate design choices.

Generally, the analysis problem is: given the stator iron geometry and coil winding configuration, the position of the rotor, and the currents in the stator coils, what forces are applied to the stator. An associated question is: what is the electrical relationship between voltages applied to the coils and the resulting currents? This question arises because, while it is common to analyze the device as if the coil currents were known, they must be established by a power amplifier of some sort. The power amplifier applies a voltage time history to the coils of the actuator in an attempt to establish the desired (assumed) coil currents. How this is accomplished and what requirements it places on the amplifier depends upon the desired time history of the coil currents and upon the electrical characteristics of the actuator.

The analysis of the coil/geometry – force relationship and of the electrical properties is generally done using a fairly simple one–dimensional representation of the magnetic structure of the actuator. This approach is referred to as magnetic circuit analysis. Analagous to electrical circuit analysis, the approach models the iron elements as essentially waveguides for the magnetic fields established by the actuator coils. As such, the analysis tends to miss some effects – especially that part of the magnetic field which lies outside of the iron of the actuator. It also assumes field uniformity within large elements of the actuator. By making the assumptions that give rise to these errors, the analysis becomes very simple and quick, making it suitable for analytic evaluation and rapid design iteration.

In the end, predictions made with a magnetic circuit analysis should be checked using a more detailed approach like finite element analysis. Such tools are more cumbersome to use, but allow examination of detail issues in the design of the actuator which cannot be revealed by the circuit analysis. Finite element analyis can also accurately account for the magnetic field which lies outside of the iron and thereby properly account for its effect on the actuator forces and electrical properties.

Table 2.1: Physical Quantities

B	magnetic flux density	Tesla	T
Φ	magnetic flux	Tesla-meter^2	Tm^2
μ	permeability	Tesla-meter per Ampere	Tm/A
μ_r	relative permeability	–	
H	magnetomotance	Amperes per meter	A/m
ℓ	length	meters	m
f	force	Newtons	N
σ	electrical conductivity	mhos-meter	$(\Omega$ m$)^{-1}$
J	current density	Amperes/meter^2	A/m^2
I	current	Amperes	A

permeability of free space: $\mu_0 = 4\pi \times 10^{-7}$Tm/A

2.1 Magnetic forces

As developed in the preceding Chapter, the force acting on a body due to the magnetic field in which it is immersed can be computed using Maxwell's stress tensor:

$$\underline{f} = \int_s \int \mathbf{T} \cdot \underline{da} \quad \approx \quad \frac{1}{2\mu_0} \int_s \int |\underline{B}|^2 \underline{da}$$

This approximation is good if rotor material is highly permeable: the source of error comes from that component of the magnetic field which is not orthogonal to the surface of the ferromagnetic body.

Thus, in order to compute f, the magnetic field, B, must be known everywhere on the surface of the body.

2.2 Material properties: constitutive law

Magnetic materials exhibit a flux density in response to an imposed magnetomotance:

$$\underline{B}(t) = \mu(t, H, ...)\underline{H}(t)$$

where $\underline{B}$ and $\underline{H}$ are vectors and μ is a tensor. For isotropic materials at low frequencies, μ is diagonal with all elements the same so that

$$\underline{B}(t) \parallel \underline{H}(t) \quad \Rightarrow \quad \underline{B} = \mu \underline{H}$$

2.2.1 Initial Hysteresis Curve

Permeability is the slope of BH the curve. The initial permeability is low, the center permeability is high, and the asymptotic permeability is μ_o. The assymptotic behavior is called *saturation*: a loss of permeability at high B (H). This occurs because all of the magnetic domains in the ferromagnetic material have become aligned with the applied field and the material can no longer amplify the applied field.

The shape of the $B - H$ curve is described by the magnetic model.

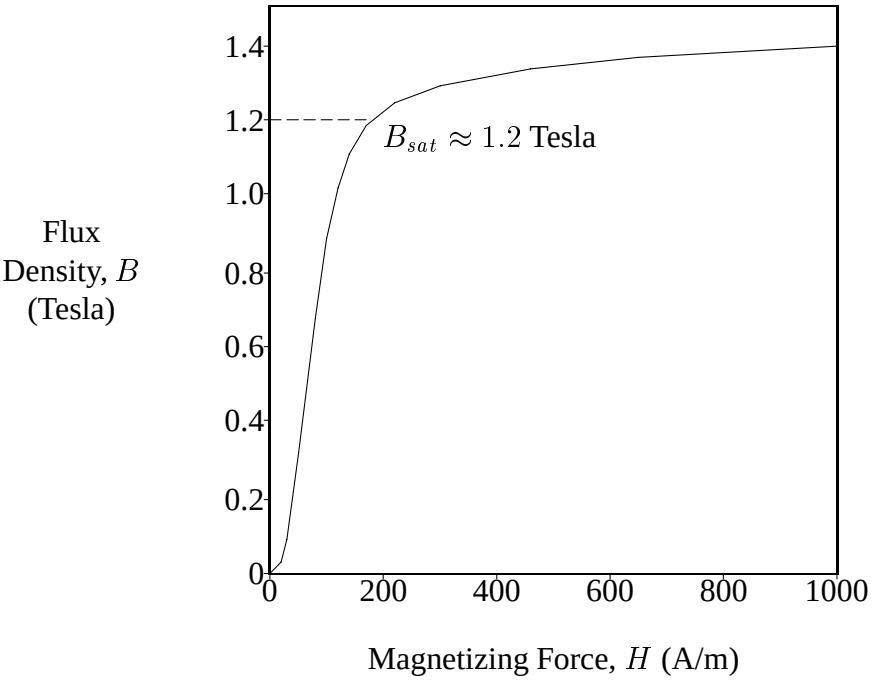

Figure 2.1: Silicon Iron: B *vs* H

Table 2.2: Typical Saturation Densities

material	B_{sat} (Tesla)
3% Silicon Iron	$\approx 1.2 - 1.6$
Vanadium Permendur, Hyperco	$\approx 2.2 - 2.4$

Simplest

$$B = \mu H$$

Add saturation

$$B = \begin{cases} B_{\text{sat}}: & \mu H > B_{\text{sat}} \\ \mu H: & -B_{\text{sat}} < \mu H < B_{\text{sat}} \\ -B_{\text{sat}}: & \mu H < -B_{\text{sat}} \end{cases}$$

Use smooth BH curve

$$B = \mu_o(1 + \mu_r(H))H$$

In addition to the static shape of the $B - H$ curve, the magnetic model can describe the dynamic properties of the relationship:

eddy current effects in a non–rotating system can be described through a frequency dependent permeability.

$$B = \mu_{fd}(s)H \quad : \qquad \mu_{fd}(s) = \mu \left[\frac{\tanh\left(\sqrt{s\sigma\mu}\frac{d}{2}\right)}{\sqrt{s\sigma\mu}\frac{d}{2}} \right]$$

hysteresis makes the $B - H$ relationship multivalued:

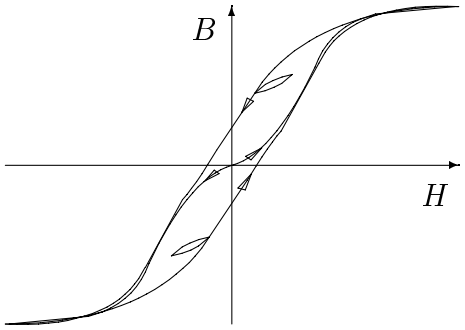

2.3 Field governing equations (Maxwell)

1. magnetomotance:

$$\underline{\nabla} \times \underline{H} = \underline{J}$$

2. conservation of flux:

$$\underline{\nabla} \cdot \underline{B} = 0$$

Simplification: Assume that all of the flux lies in a plane and that all of the current flows perpendicular to that plane:

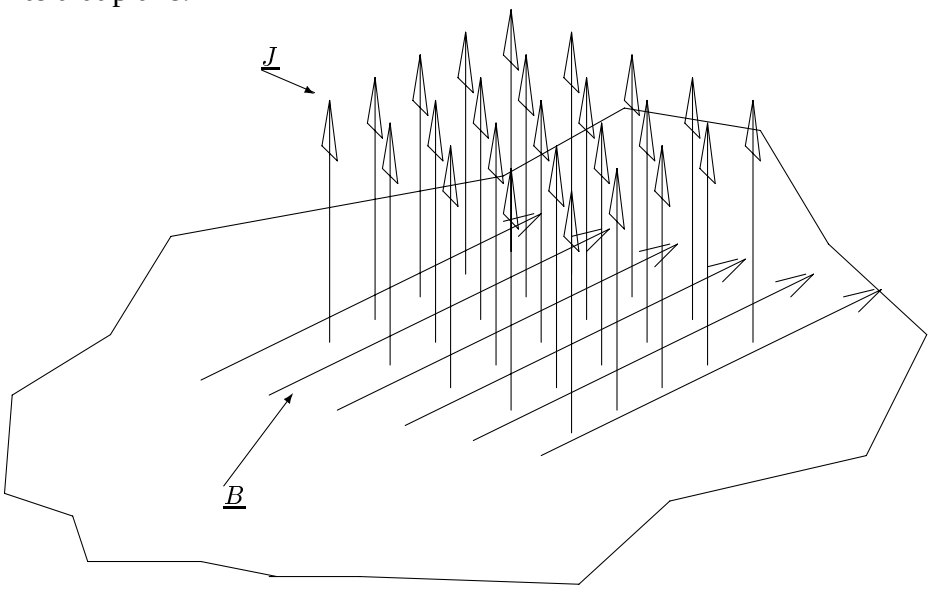

2.3.1 Magnetomotance

$$\int_A \underline{\nabla} \times \underline{H} \cdot \underline{da} = \int_A \underline{J} \cdot \underline{da}$$

(Green's theorem)

$$\int_A \underline{\nabla} \times \underline{H} \cdot \underline{da} = \oint \underline{H} \cdot \underline{d\ell}$$

(2D)

$$\oint \underline{H} \cdot \underline{d\ell} = \int_A J da$$

Lumped Model: Magnetomotance

$$\oint \underline{H} \cdot \underline{d\ell} = \int_A J da$$

Assume:

- path $d\ell$ parallel to H
- path can be broken into n_s segments where H is constant
- J is confined to electromagnet coils
- J is uniform in n_c coils

Ampére's loop law:

$$\sum_{i=1}^{n_s} H_i \ell_i = \sum_{i=1}^{n_c} N_i I_i \qquad (JA = NI)$$

Finally, assume that the permeability is constant in each segment:

$$B_i = \mu_i H_i$$

to get

$$\sum_{i=1}^{n_s} \frac{B_i \ell_i}{\mu_i} = \sum_{i=1}^{n_c} N_i I_i$$

Be careful about sign conventions. If the loop is taken in a clockwise direction, then the currents are assumed positive passing into the analysis plane and the fluxes B are assumed positive in the direction of the integration.

2.3.2 Conservation of Flux

$$\underline{\nabla} \cdot \underline{B} = 0$$

In integral form:

$$\int_s \int \underline{B} \cdot \underline{da} = 0$$

Lumped Model: assume that the perimeter can be broken into n_p discrete patches: B is perpendicular to each patch

$$\sum_{i=1}^{n_p} \int_{A_i} B_i da = 0$$

further, B is *uniform* over each perimeter patch

$$\int_{A_i} B_i da = B_i A_i = \Phi_i$$

Finally,

$$\sum_{i=1}^{n_p} \Phi_i = 0$$

Be careful about signs: it is assumed that the integral is performed over a solid volume and that da is an outward directed normal to the surface. Therefore, the convention in the summation is that a positive Φ_i is directed *out* of the volume.

2.4 Lumped Model: Forces

$$\underline{f} = \frac{1}{2\mu_0} \int_s \int |\underline{B}|^2 \underline{da}$$

Assume:

- surface can be broken into n_a patches
- B is constant in each of these patches

$$\underline{f} = \frac{1}{2\mu_0} \sum_{i=1}^{n_a} B_i^2 \underline{A}_i$$

where $\underline{A}_i$ is an *outward* directed normal to the surface patch with magnitude equal to its area.

2.4.1 Zero Leakage – Circuit Model

It is common to assume, for high permeability magnetic structures with SMALL air gaps, that all flux is confined to the iron and the gap volumes.

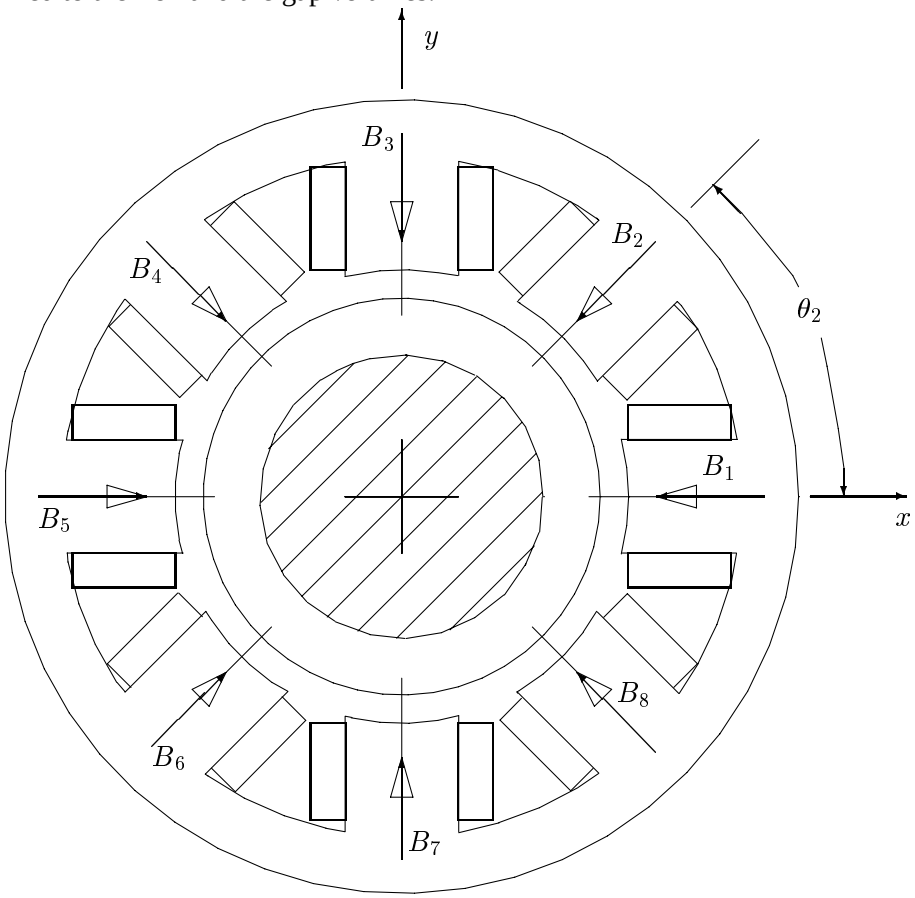

This means that test volumes for flux conservation consider only fluxes travelling within the material and are typically placed at junctions in the structure where flux has a multiple possible directions.

2.5 Calculation of Forces: simplest

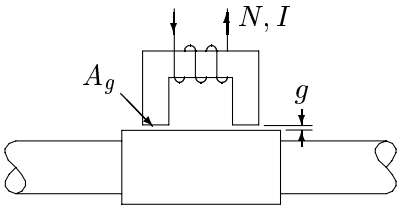

Ampére's loop law:

$$\frac{B_1\ell_1}{\mu_1} + \frac{B_2\ell_2}{\mu_2} + \frac{B_{g1}\ell_{g1}}{\mu_{g1}} + \frac{B_{g2}\ell_{g2}}{\mu_{g2}} = NI$$

Conservation of flux, assuming constant areas:

$$B_1 = B_2 = B_{g1} = B_{g2} = B$$

Assume *infinite* permeability

$$\frac{\ell_1}{\mu_1}, \frac{\ell_2}{\mu_2} \ll \frac{\ell_g}{\mu_g} \qquad \mu_g = \mu_o$$

$$2\frac{B\ell_g}{\mu_g} = NI \quad \Rightarrow \quad B = \frac{\mu_o NI}{2g}$$

$$\underline{f} = \frac{1}{2\mu_0}\sum_{i=1}^{n_a} B_i^2 \underline{A}_i$$

Since we assume zero leakage, external flux only appears in gap areas:

$$f = \frac{2B^2 A_g}{2\mu_0} = \frac{B^2 A_g}{\mu_0}$$

Substitute previous solution for B:

$$B = \frac{\mu_o NI}{2g}$$

to obtain

$$f = \frac{\mu_o N^2 I^2 A_g}{4g^2}$$

2.5.1 Simple example

Assume that the coil carries 100 turns of wire, that the width of each air gap is 1 cm, that the air gap length is 0.5 mm, and that the thickness of the structure (into the plane) is 2 cm. In this case, $g = 0.0005$m and $A_g = 0.0002$ m^2. As usual, $\mu_0 = 4\pi \times 10^{-7}$N/A^2. Thus, the force is

$$f = \frac{4\pi \times 10^{-7} 100^2 I^2 0.0002}{4 0.0005^2} = 2.51 I^2$$

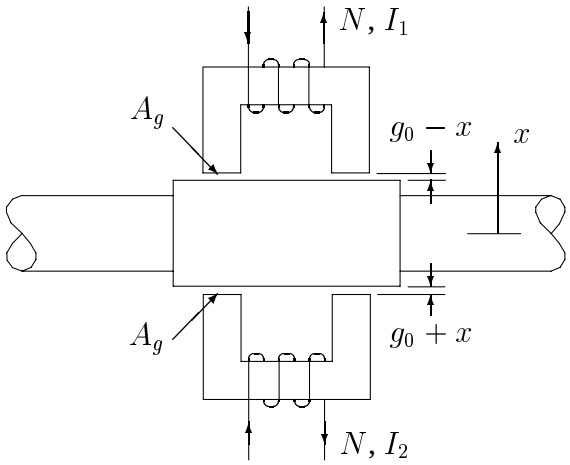

Figure 2.2: Opposing magnets: a push–pull arrangement.

Assuming that the material is silicon iron, saturation occurs when $B \approx 1.6$:

$$B = \frac{\mu_o N I}{2g} = 1.6 \quad \Rightarrow \quad I_{\text{sat}} = \frac{2gB_{\text{sat}}}{\mu_0 N} = 12.73\text{A}$$

so that the maximum force which the actuator can attain is about

$$f_{\max} = 2.51 \times 12.73^2 = 406.9\text{N}$$

Since the total gap area is 0.0004 m^2, this corresponds to an effective "magnetic pressure" of 406.9/0.0004 = 1.02 MN/m^2 = 1.02 MPa. In English units, this becomes 147.5 PSI. Thus, for silicon iron assuming a saturation density of 1.6 Tesla, the maximum magnetic pressure is about 1 MPa or 148 PSI.

2.6 Linearization

The device described in the preceding section can generate force only in the upward direction. Such an arrangement can be usable if the gravitational acceleration provides sufficient downward force to meet the system's dynamic requirements. In most applications, or where the orientation of the actuator is horizontal, this is not adequate and a pair of opposed magnets are used in combination to provide forces in either direction. The scheme is indicated in Figure 2.2.

The net force generated by this scheme is

$$f = \frac{\mu_o N^2 A_g}{4} \left(\frac{I_1^2}{(g_o - x)^2} - \frac{I_2^2}{(g_o + x)^2} \right)$$

As a matter of convenience, introduce bias linearization:

$$I_1 = \max(I_b + i_p, 0)$$

$$I_2 = \max(I_b - i_p, 0)$$

Why limit $I_1, I_2 \geq 0$? Recall definition of I_{sat}:

$$B_{\text{sat}} = \frac{\mu_o N I_{\text{sat}}}{2g_o}$$

Suppose $I_b = \alpha I_{\text{sat}}$. Maximum upper force is reached when

$$I_1 = I_{\text{sat}} \quad \Rightarrow \quad i_p = I_{\text{sat}}(1-\alpha)$$

at this condition,

$$I_2 = \alpha I_{\text{sat}} - (1-\alpha) I_{\text{sat}} = (2\alpha - 1) I_{\text{sat}}$$

Net force is

$$f_{\max} = \frac{\mu_o N^2 A_g}{4g_o} \left(I_{\text{sat}}^2 - I_2^2 \right)$$

Clearly, the best solution is to have $I_2 = 0$ when $I_1 = I_{\text{sat}}$. If $\alpha < 0.5$ then I_2 reaches zero *before* I_1 reaches I_{sat}: clamp I_2 at zero. If $\alpha > 0.5$ then I_2 is still positive when I_1 reaches I_{sat}.

$$f = \frac{\mu_o N^2 A_g}{4} \left(\frac{(I_b + i_p)^2}{(g_o - x)^2} - \frac{(I_b - i_p)^2}{(g_o + x)^2} \right) \quad : \quad |i_p| < I_b$$

Linearize about operating point, $x = x_0$ $i_p = i_{p,0}$:

$$f = f|_{x=x_0, i_p=i_{p,0}} + \left.\frac{\partial f}{\partial i_p}\right|_{x=x_0, i_p=i_{p,0}} (i_p - i_{p,0}) + \left.\frac{\partial f}{\partial x}\right|_{x=x_0, i_p=i_{p,0}} (x - x_0) + \ldots$$

Define "actuator gain":

$$K_i \doteq \left.\frac{\partial f}{\partial i_p}\right|_{x=x_0, i_p=i_{p,0}}$$

and "open loop stiffness":

$$K_x \doteq - \left.\frac{\partial f}{\partial x}\right|_{x=x_0, i_p=i_{p,0}}$$

so that

$$f = f_0 + K_i(i_p - I_{p,0}) - K_x(x - x_0) + \ldots$$

2.6.1 Actuator Gain – use $x_0 = 0$

$$\begin{aligned} K_i \doteq \left.\frac{\partial f}{\partial i_p}\right|_{x=x_0, i_p=i_{p,0}} &= \frac{\mu_0 N^2 A_g}{4g_0^2} \left(2(I_b + i_p)(+1) - 2(I_b - i_p)(-1)\right) \\ &= \frac{\mu_0 N^2 I_b A_g}{g_0^2} \end{aligned} \tag{2.1}$$

Actuator gain increases in proportion to bias current, inversely with gap squared.

In terms of flux density:

$$B_b = \frac{\mu_0 N I_b}{2g_0} \quad \Rightarrow \quad I_b = \frac{2g_0 B_b}{N\mu_0}$$

so that

$$K_i = \frac{\mu_0 N^2 A_g}{g_0^2}\frac{2g_0 B_b}{N\mu_0} = \frac{2NB_bA_g}{g_0} \tag{2.2}$$

These terms are more fundamental and give a direct indication of sensitivities: increased actuator gain comes from increased bias density or reduced gap.

Ampere-Turns: Comments

The magnetomotive force is generated by the electromagnet coil(s).

These coils are created by winding wire around a form. If small wire is used, then many turns can be put into 1 cm^2 whereas if large wire is used, then only a few turns can be put into the same space.

It turns out that the total copper area per coil area is about constant. This is so because small wire has thinner insulation than large wire. As a result, for a given coil area, the area of copper is nearly independent of the number of turns. For commercial windings, the ratio of copper area to coil area is about 0.5. The limit is about 0.7.

Wire performance is limited, thermally, in terms of the current *density* it can carry: small wire carries a small current and large wire carries a large current. Generally, this limit is about 600 A/cm^2.

Thus, for a given coil area, the maximum available magnetomotance is a fixed number of Ampere-turns, no matter what wire size or number of turns is used:

$$NI_{\max} \approx 600 \times 0.5A_c = 300A_c$$

Force is related to:

- actuator gain times current (amps): $f = K_i i_p$

  or

- actuator gain divided by turns times ampere turns: $f = \frac{K_i}{N} N i_p$

$$\frac{K_i}{N} = \frac{2B_bA_g}{g_0}$$

2.7 Open Loop Stiffness – use $x_0 = 0$

$$\begin{aligned} K_x &\doteq -\left.\frac{\partial f}{\partial x}\right|_{x=x_0, i_p=i_{p,0}} \\ &= -\frac{\mu_0 N^2 A_g}{4}\left((-2)\frac{(I_b+i_{p,0})^2}{(g_0-x_0)^3}(-1) - (-2)\frac{(I_b-i_{p,0})^2}{(g_0+x_0)^3}(+1)\right) \\ &= -\frac{\mu_0 N^2 A_g}{g_0^3}\left(I_b^2 + i_{p,0}^2\right) \end{aligned} \tag{2.3}$$

Open loop stiffness is *negative* and increases with increased bias current or reduced gap.

In terms of bias flux density (let $i_{p,0} = 0$):

$$K_x = -\frac{4B_b^2 A_g}{\mu_o g_0} \tag{2.4}$$

2.8 Force Slew Rate

$$\left|\frac{df}{dt}\right|_{\max} \approx K_i \left|\frac{di}{dt}\right|_{\max}$$

(ingore nonlinear terms, effect of K_x)

Current slew rate:

$$\left|\frac{di}{dt}\right|_{\max} \approx \frac{V_{\max}}{L}$$

(ignore coil resistance)

Coil inductance:

$$L = N\frac{d\Phi}{di} = NA_g\frac{dB}{di} = \frac{N^2 A_g \mu_o}{2g_0}$$

Available slew:

$$\left|\frac{df}{dt}\right|_{\max} = \frac{2I_b V_{\max}}{g_0} = \frac{2\alpha I_{\text{sat}} V_{\max}}{g_0}$$

Usually, choose $I_{\text{sat}} = I_{\max}$ for the amplifier

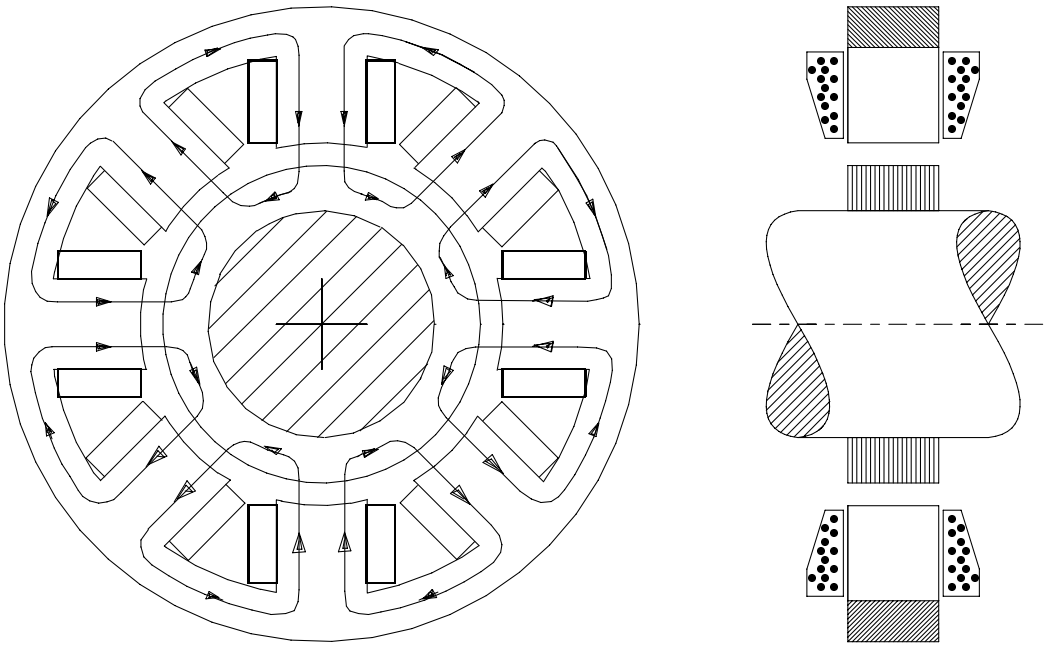

Figure 2.3: Typical 8–pole radial actuator.

2.9 Design Tradeoffs

Open–loop stiffness is undesirable, actuator gain is desirable:

$$\frac{K_x}{K_i/N} = -2\frac{B_b}{\mu_0} = -2\frac{\alpha B_{\text{sat}}}{\mu_0}$$

This says that large B_b or α is bad.
However, available slew rate:

$$\left|\frac{df}{dt}\right|_{\max} = \frac{2I_b V_{\max}}{g_0} = \frac{2\alpha I_{\text{sat}} V_{\max}}{g_0}$$

For a given amplifier, want large α and small gap.

2.10 Generalize

- stators often single piece – no discrete “horse shoes”
- one stator may provide several force components
- stator may be highly cross–coupled

1. identify number of flux densities to find: n_b
2. identify independent flux loops: n_l
3. account for all current linked by each loop

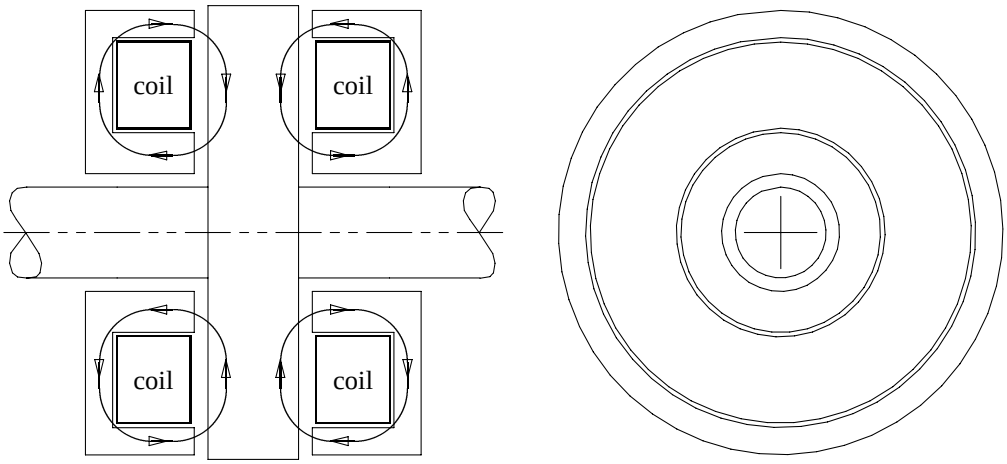

Figure 2.4: Typical 4–pole thrust actuator.

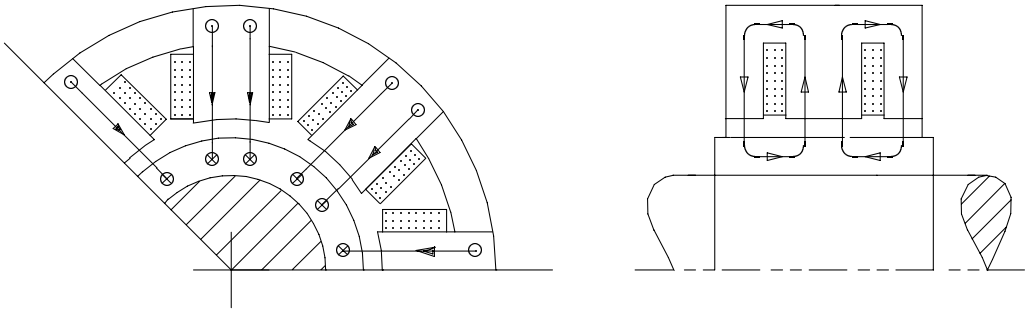

Figure 2.5: Homopolar radial actuator

4. identify independent flux conservation nodes: n_n
5. should have $n_n + n_l = n_b$
6. find gaps as functions of position ($x, y, \ldots$)
7. write n_l loop equations, n_n conservation equations
8. express coil currents as functions of controller output, biasing
9. solve for fluxes
10. compute net force by vector addition of each gap force

2.10.1 Example

Ignore iron flux, compute only gap fluxes: $n_b = 6$

Five independent flux loops:

$$\frac{1}{\mu_0}(B_1 g_1 - B_2 g_2) = N_1 I_1 - N_2 I_2$$

$$\frac{1}{\mu_0}(B_2 g_2 - B_3 g_3) = N_2 I_2 - N_3 I_3$$

$$\frac{1}{\mu_0}(B_3 g_3 - B_4 g_4) = N_3 I_3 - N_4 I_4$$

$$\frac{1}{\mu_0}(B_4 g_4 - B_5 g_5) = N_4 I_4 - N_5 I_5$$

$$\frac{1}{\mu_0}(B_5 g_5 - B_6 g_6) = N_5 I_5 - N_6 I_6$$

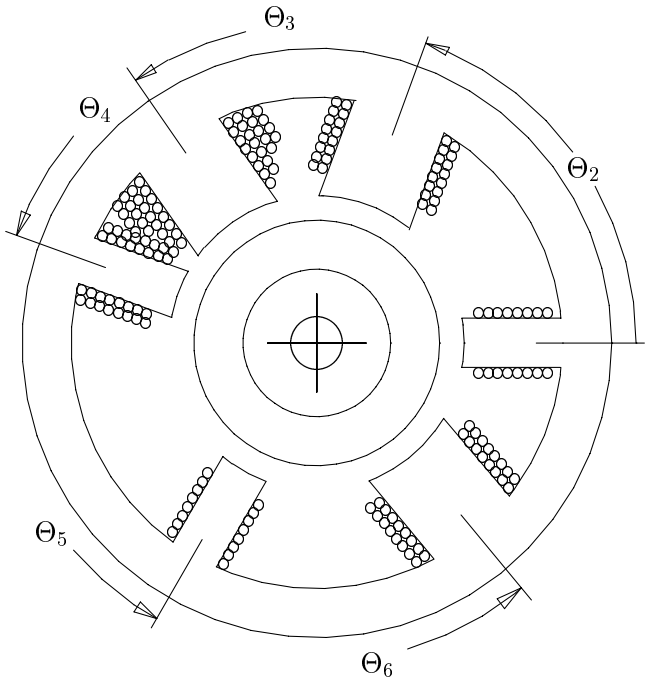

One independent flux conservation equation:

$$B_1 A_1 + B_2 A_2 + B_3 A_3 + B_4 A_4 + B_5 A_5 + B_6 A_6 = 0$$

Forces:

$$f_x = \frac{1}{2\mu_0}\left(B_1^2 A_1 \cos\Theta_1 + \ldots B_6^2 A_6 \cos\Theta_6\right)$$

$$f_y = \frac{1}{2\mu_0}\left(B_1^2 A_1 \sin\Theta_1 + \ldots B_6^2 A_6 \sin\Theta_6\right)$$

Gaps:

$$g_1 = g_{1,0} - x\cos\Theta_1 - y\sin\Theta_1$$

$$\vdots$$

$$g_6 = g_{6,0} - x\cos\Theta_6 - y\sin\Theta_6$$

Summarize:
Define the impedance matrix

$$\mathcal{R}(x,y) \doteq \frac{1}{\mu_0}\begin{bmatrix} g_1 & -g_2 & 0 & 0 & 0 & 0 \\ 0 & g_2 & -g_3 & 0 & 0 & 0 \\ 0 & 0 & g_3 & -g_4 & 0 & 0 \\ 0 & 0 & 0 & g_4 & -g_5 & 0 \\ 0 & 0 & 0 & 0 & g_5 & -g_6 \\ \mu_0 A_1 & \mu_0 A_2 & \mu_0 A_3 & \mu_0 A_4 & \mu_0 A_5 & \mu_0 A_6 \end{bmatrix}(x,y)$$

and linkage matrix

$$\mathcal{N} \doteq \begin{bmatrix} N_1 & -N_2 & 0 & 0 & 0 & 0 \\ 0 & N_2 & -N_3 & 0 & 0 & 0 \\ 0 & 0 & N_3 & -N_4 & 0 & 0 \\ 0 & 0 & 0 & N_4 & -N_5 & 0 \\ 0 & 0 & 0 & 0 & N_5 & -N_6 \\ 0 & 0 & 0 & 0 & 0 & 0 \end{bmatrix}$$

Define vector summation, x:

$$\mathcal{A}_x \doteq \frac{1}{2\mu_0}\begin{bmatrix} A_1\cos\Theta_1 & 0 & 0 & 0 & 0 & 0 \\ 0 & A_2\cos\Theta_2 & 0 & 0 & 0 & 0 \\ 0 & 0 & A_3\cos\Theta_3 & 0 & 0 & 0 \\ 0 & 0 & 0 & A_4\cos\Theta_4 & 0 & 0 \\ 0 & 0 & 0 & 0 & A_5\cos\Theta_5 & 0 \\ 0 & 0 & 0 & 0 & 0 & A_6\cos\Theta_6 \end{bmatrix}$$

and vector summation, y:

$$\mathcal{A}_x \doteq \frac{1}{2\mu_0}\begin{bmatrix} A_1\sin\Theta_1 & 0 & 0 & 0 & 0 & 0 \\ 0 & A_2\sin\Theta_2 & 0 & 0 & 0 & 0 \\ 0 & 0 & A_3\sin\Theta_3 & 0 & 0 & 0 \\ 0 & 0 & 0 & A_4\sin\Theta_4 & 0 & 0 \\ 0 & 0 & 0 & 0 & A_5\sin\Theta_5 & 0 \\ 0 & 0 & 0 & 0 & 0 & A_6\sin\Theta_6 \end{bmatrix}$$

This provides the linear set of equations

$$\mathcal{R}(x,y)\underline{B} = \mathcal{N}\underline{I}$$

and the pair of quadratic equations

$$f_x = \underline{B}^\top \mathcal{A}_x \underline{B}$$

and

$$f_y = \underline{B}^\top \mathcal{A}_y \underline{B}$$

2.10.2 Force Components

Solve for the force components in terms of the coil currents (and rotor position, x and y):

$$f_x = \underline{I}^\top \mathcal{N}^\top \mathcal{R}^{-\top}(x,y)\mathcal{A}_x \mathcal{R}^{-1}(x,y)\mathcal{N}\underline{I}$$

$$f_y = \underline{I}^\top \mathcal{N}^\top \mathcal{R}^{-\top}(x,y)\mathcal{A}_y \mathcal{R}^{-1}(x,y)\mathcal{N}\underline{I}$$

2.10.3 General linearization

Assume that the coil currents are selected according to a law with the linear form:

$$\underline{I} = \mathcal{C}\left\{\begin{array}{c} i_x \\ i_y \\ i_b \end{array}\right\} = \mathcal{C}\underline{\hat{I}}$$

where i_b is a fixed biasing term, i_x controls the force in the $x-$ direction, and i_y controls the force in the $y-$ direction. Recall the definition of the actuator gain:

$$K_i \doteq \frac{\partial f}{\partial i}$$

Thus, in general, the actuator gain is a matrix function. In the present case, the actuator gain would be defined by

$$K_i \doteq \frac{\partial f}{\partial \underline{\hat{I}}}$$

Thus, the top row of K_i is:

$$K_{i_x} = \left.\frac{\partial f_x}{\partial \underline{\hat{I}}}\right|_{0,0} = 2\underline{\hat{I}}^\top \mathcal{C}^\top \mathcal{N}^\top \mathcal{R}^{-\top}(0,0)\mathcal{A}_x \mathcal{R}^{-1}(0,0)\mathcal{N}\mathcal{C}$$

and the second row is

$$K_{i_y} = \left.\frac{\partial f_y}{\partial \underline{\hat{I}}}\right|_{0,0} = 2\underline{\hat{I}}^\top \mathcal{C}^\top \mathcal{N}^\top \mathcal{R}^{-\top}(0,0)\mathcal{A}_y \mathcal{R}^{-1}(0,0)\mathcal{N}\mathcal{C}$$

The open loop stiffness can be derived in a similar fashion:

$$K_x = \begin{bmatrix} K_{xx} & K_{xy} \\ K_{yx} & K_{yy} \end{bmatrix}$$

where

$$K_{ij} \doteq \frac{\partial f_i}{\partial j}$$

from which it follows that

$$K_{ij} = \hat{\underline{I}}_0^\top \mathcal{C}^\top \mathcal{N}^\top \left(\frac{\partial}{\partial j} \mathcal{R}^{-\top}(x,y) \mathcal{A}_i \mathcal{R}^{-1}(x,y) + \mathcal{R}^{-\top}(x,y) \mathcal{A}_i \frac{\partial}{\partial j} \mathcal{R}^{-1}(x,y) \right) \mathcal{N} \mathcal{C} \hat{\underline{I}}_0 \qquad (2.5)$$

where $\hat{\underline{I}}_0$ represents the current control reference vector at the nominal operating point. Noting that

$$\frac{\partial A(x) A^{-1}(x)}{\partial x} = \frac{\partial A}{\partial x} A^{-1} + A \frac{\partial A^{-1}}{\partial x} = 0$$

the derivatives of the reluctance matrix can be computed as

$$\frac{\partial \mathcal{R}^{-1}}{\partial j} = -\mathcal{R}^{-1} \frac{\partial \mathcal{R}}{\partial j} \mathcal{R}^{-1}$$

where the inverses and partial derivative are evaluated at the nominal operating point: typically, $x = 0, y = 0$.

2.11 Examples

2.11.1 Two horseshoes

Assume that the geometry is as indicated in Figure 2.6. Let the width of the pole pieces be 3.5 cm and the thickness (perpendicular to the Figure) be 5.0 cm. The nominal air gap, g, is 0.75 mm. Each coil has 85 turns and the bias flux density is set to 0.45 Tesla. This means that the bias current, I_b, is

$$I_b = \frac{2 g_0 B_b}{N \mu_0} = \frac{2 \times 0.00075 \times 0.45}{85 \times 4\pi \times 10^{-7}} = 6.32 \text{ Amps}$$

From (2.1), the actuator gain is then

$$K_i = \frac{\mu_0 N^2 I_b A_g}{g_0^2} = \frac{4\pi \times 10^{-7} \times 85^2 \times 6.32 \times 0.035 \times 0.05}{0.00075^2} = 178.5 \text{ N/A}$$

The open loop stiffness is given by (2.3):

$$K_x = -\frac{\mu_o N^2 A_g}{g_0^3} \left(I_b^2 + i_{p,0}^2 \right) = -\frac{4\pi \times 10^{-7} \times 85^2 \times 0.035 \times 0.05 \times 6.32^2}{0.00075^3} = -1.52 \times 10^6 \text{ N/m}^2$$

The same analysis can be repeated using the formalisms introduced in Section 2.10. The impedance matrix is found by using the two independent loops. No conservation of flux condition is required because the magnetic circuit has no branches:

$$\mathcal{R} = \frac{1}{\mu_0} \begin{bmatrix} 2(g_0 - x) & 0 \\ 0 & 2(g_0 + x) \end{bmatrix}$$

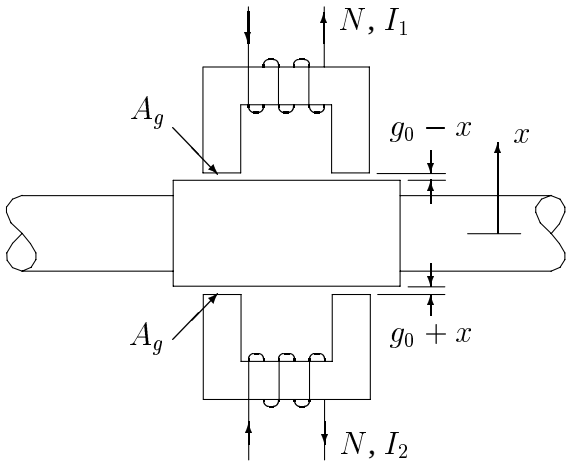

Figure 2.6: Push–pull magnet scheme.

The linkage matrix is also very simple:

$$\mathcal{N} = \begin{bmatrix} N & 0 \\ 0 & N \end{bmatrix}$$

This produces the relationship between the coil currents and the gap fluxes:

$$\mathcal{R} \begin{Bmatrix} B_1 \\ B_2 \end{Bmatrix} = \mathcal{N} \begin{Bmatrix} I_1 \\ I_2 \end{Bmatrix}$$

The current selection scheme relates the coil currents to some control terms:

$$\begin{Bmatrix} I_1 \\ I_2 \end{Bmatrix} = \begin{bmatrix} 1 & 1 \\ -1 & 1 \end{bmatrix} \begin{Bmatrix} i_p \\ I_b \end{Bmatrix}$$

so that the current selection matrix is

$$\mathcal{C} = \begin{bmatrix} 1 & 1 \\ -1 & 1 \end{bmatrix}$$

The force summation matrix is

$$\mathcal{A}_x = \frac{1}{2\mu_0} \begin{bmatrix} 2A_g & 0 \\ 0 & -2A_g \end{bmatrix}$$

Thus, the force is given by:

$$\begin{aligned}
f_x &= \hat{\underline{I}}^\top \mathcal{C}^\top \mathcal{N}^\top \mathcal{R}^{-\top} \mathcal{A}_x \mathcal{R} \mathcal{N} \mathcal{C} \hat{\underline{I}} \\
&= \frac{\mu_0}{2} \{i_p \; I_b\} \begin{bmatrix} 1 & -1 \\ 1 & 1 \end{bmatrix} \begin{bmatrix} N & 0 \\ 0 & N \end{bmatrix} \begin{bmatrix} \frac{1}{2(g_0-x)} & 0 \\ 0 & \frac{1}{2(g_0+x)} \end{bmatrix} \begin{bmatrix} 2A_g & 0 \\ 0 & -2A_g \end{bmatrix} \\
&\qquad \begin{bmatrix} \frac{1}{2(g_0-x)} & 0 \\ 0 & \frac{1}{2(g_0+x)} \end{bmatrix} \begin{bmatrix} N & 0 \\ 0 & N \end{bmatrix} \begin{bmatrix} 1 & 1 \\ -1 & 1 \end{bmatrix} \begin{Bmatrix} i_p \\ I_b \end{Bmatrix} \\
&= \frac{\mu_0}{2} \{i_p \; I_b\} \begin{bmatrix} N & -N \\ N & N \end{bmatrix} \begin{bmatrix} N\frac{A_g}{2(g_0-x)^2} & N\frac{A_g}{2(g_0-x)^2} \\ N\frac{A_g}{2(g_0+x)^2} & -N\frac{A_g}{2(g_0+x)^2} \end{bmatrix} \begin{Bmatrix} i_p \\ I_b \end{Bmatrix} \\
&= \frac{\mu_0 N^2 A_g}{4} \{i_p \; I_b\} \begin{bmatrix} 1 & -1 \\ 1 & 1 \end{bmatrix} \begin{bmatrix} \frac{1}{(g_0-x)^2} & \frac{1}{(g_0-x)^2} \\ \frac{1}{(g_0+x)^2} & -\frac{1}{(g_0+x)^2} \end{bmatrix} \begin{Bmatrix} i_p \\ I_b \end{Bmatrix} \\
&= \frac{\mu_0 N^2 A_g}{4} \{i_p \; I_b\} \begin{bmatrix} \frac{1}{(g_0-x)^2} - \frac{1}{(g_0+x)^2} & \frac{1}{(g_0-x)^2} + \frac{1}{(g_0+x)^2} \\ \frac{1}{(g_0-x)^2} + \frac{1}{(g_0+x)^2} & \frac{1}{(g_0-x)^2} - \frac{1}{(g_0+x)^2} \end{bmatrix} \begin{Bmatrix} i_p \\ I_b \end{Bmatrix} \\
&= \frac{\mu_0 N^2 A_g g_0 x}{(g_0-x)^2(g_0+x)^2} \left(i_p^2 + I_b^2\right) + \frac{\mu_0 N^2 A_g (g_0^2+x^2)}{(g_0-x)^2(g_0+x)^2} I_b i_p
\end{aligned}$$

Evaluated at $x = 0$:

$$f_x = \frac{\mu_0 N^2 I_b i_p A_g}{g_0^2}$$

The actuator gain is

$$\begin{aligned}
K_{i_x} &= \left. \frac{\partial f_x}{\partial \hat{\underline{I}}} \right|_0 \\
&= 2\hat{\underline{I}}^\top \mathcal{C}^\top \mathcal{N}^\top \mathcal{R}^{-\top}(0) \mathcal{A}_x \mathcal{R}^{-1}(0) \mathcal{N} \mathcal{C} \\
&= \frac{\mu_0 N^2 A_g}{2} \{i_p \; I_b\} \left[\begin{array}{cc} \frac{1}{(g_0-x)^2} - \frac{1}{(g_0+x)^2} & \frac{1}{(g_0-x)^2} + \frac{1}{(g_0+x)^2} \\ \frac{1}{(g_0-x)^2} + \frac{1}{(g_0+x)^2} & \frac{1}{(g_0-x)^2} - \frac{1}{(g_0+x)^2} \end{array} \right] \Bigg|_{x=0} \\
&= \frac{\mu_0 N^2 A_g}{(g_0-x)^2(g_0+x)^2} \left[\begin{array}{cc} 2i_p g_0 x + I_b \left(g_0^2 + x^2\right) & i_p \left(g_0^2 + x^2\right) + 2I_b g_0 x \end{array} \right] \Bigg|_{x=0}
\end{aligned}$$

Evaluated at the point $x = 0$:

$$K_{i_x} = \frac{\mu_0 N^2 A_g}{g_0^2} \left[\begin{array}{cc} I_b & i_p \end{array} \right]$$

Thus, the sensitivity of the output force to the control term, i_p, is the same as computed previously using the simpler analysis.

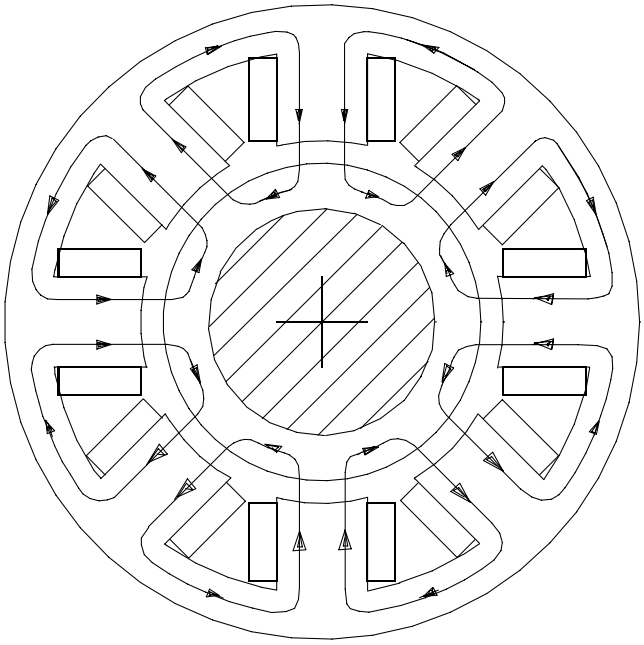

Figure 2.7: Eight pole stator example.

Finally, the open–loop stiffness is (2.5):

$$\begin{aligned}
K_{xx} &= -\frac{1}{2\mu_0}\hat{\underline{I}}_0^\top \mathcal{C}^\top \mathcal{N}^\top \left(\mathcal{R}^{-\top} \frac{\partial \mathcal{R}^\top}{\partial x} \mathcal{R}^{-\top} \mathcal{A}_x \mathcal{R}^{-1} + \mathcal{R}^{-\top} \mathcal{A}_x \mathcal{R}^{-1} \frac{\partial \mathcal{R}}{\partial x} \mathcal{R}^{-1} \right) \mathcal{N}\mathcal{C}\hat{\underline{I}}_0 \\
&\quad \left(\text{where it is noted that: } \frac{\partial \mathcal{R}}{\partial x} = \frac{2}{\mu_0} \begin{bmatrix} -1 & 0 \\ 0 & 1 \end{bmatrix} \right) \\
&= \frac{2N^2 A_g}{\mu_0^2} \underline{I}_0^\top \mathcal{R}^{-\top} \left(\begin{bmatrix} -1 & 0 \\ 0 & 1 \end{bmatrix} \mathcal{R}^{-\top} \begin{bmatrix} 1 & 0 \\ 0 & -1 \end{bmatrix} + \begin{bmatrix} 1 & 0 \\ 0 & -1 \end{bmatrix} \mathcal{R}^{-1} \begin{bmatrix} -1 & 0 \\ 0 & 1 \end{bmatrix} \right) \mathcal{R}^{-1} \underline{I}_0 \\
&= -\frac{\mu_0 N^2 A_g}{2} \underline{I}_0^\top \begin{bmatrix} \frac{1}{(g_0-x)^3} & 0 \\ 0 & \frac{1}{(g_0+x)^3} \end{bmatrix} \underline{I}_0 \\
&= -\frac{\mu_0 N^2 A_g}{2} \left(\frac{(I_b+i_p)^2}{(g_0-x)^3} + \frac{(I_b-i_p)^2}{(g_0+x)^3} \right)
\end{aligned}$$

Evaluated at $x = 0$:

$$K_{xx} = -\frac{\mu_0 N^2 A_g}{g_0^3} \left(I_b^2 + i_p^2 \right)$$

Again, this is the same expression as was obtained previously using the simpler analysis.

2.11.2 Heteropolar radial stator

The advantage of the generalized analysis lies in its ability to treat more complex circuits with interactions which are more difficult to visualize. As an example, consider the eight pole actuator pictured in Figure 2.7. Ignoring the finite permeability of the stator and rotor iron, the reluctance

matrix can be obtained using seven loop equations and a single conservation of flux equation:

$$\mathcal{R} = \frac{1}{\mu_0}\begin{bmatrix} -g_1 & g_2 & 0 & 0 & 0 & 0 & 0 & 0 \\ 0 & -g_2 & g_3 & 0 & 0 & 0 & 0 & 0 \\ 0 & 0 & -g_3 & g_4 & 0 & 0 & 0 & 0 \\ 0 & 0 & 0 & -g_4 & g_5 & 0 & 0 & 0 \\ 0 & 0 & 0 & 0 & -g_5 & g_6 & 0 & 0 \\ 0 & 0 & 0 & 0 & 0 & -g_6 & g_7 & 0 \\ 0 & 0 & 0 & 0 & 0 & 0 & -g_7 & g_8 \\ \mu_0 A_g & \mu_0 A_g & \mu_0 A_g & \mu_0 A_g & \mu_0 A_g & \mu_0 A_g & \mu_0 A_g & \mu_0 A_g \end{bmatrix}$$

in which

$$\begin{aligned} g_1 &= g - x \\ g_2 &= g - 0.707x - 0.707y \\ g_3 &= g - y \\ g_4 &= g + 0.707x - 0.707y \\ g_5 &= g + x \\ g_6 &= g + 0.707x + 0.707y \\ g_7 &= g + y \\ g_8 &= g - 0.707x + 0.707y \end{aligned}$$

Assuming that all of the coils carry N turns, the linkage matrix is

$$\mathcal{N} = N\begin{bmatrix} 1 & -1 & 0 & 0 & 0 & 0 & 0 & 0 \\ 0 & 1 & -1 & 0 & 0 & 0 & 0 & 0 \\ 0 & 0 & 1 & -1 & 0 & 0 & 0 & 0 \\ 0 & 0 & 0 & 1 & -1 & 0 & 0 & 0 \\ 0 & 0 & 0 & 0 & 1 & -1 & 0 & 0 \\ 0 & 0 & 0 & 0 & 0 & 1 & -1 & 0 \\ 0 & 0 & 0 & 0 & 0 & 0 & 1 & -1 \\ 0 & 0 & 0 & 0 & 0 & 0 & 0 & 0 \end{bmatrix}$$

The force summation matrices are

$$\mathcal{A}_x = \frac{A_g}{2\mu_0}\begin{bmatrix} 1 & 0 & 0 & 0 & 0 & 0 & 0 & 0 \\ 0 & 0.707 & 0 & 0 & 0 & 0 & 0 & 0 \\ 0 & 0 & 0 & 0 & 0 & 0 & 0 & 0 \\ 0 & 0 & 0 & -0.707 & 0 & 0 & 0 & 0 \\ 0 & 0 & 0 & 0 & -1 & 0 & 0 & 0 \\ 0 & 0 & 0 & 0 & 0 & -0.707 & 0 & 0 \\ 0 & 0 & 0 & 0 & 0 & 0 & 0 & 0 \\ 0 & 0 & 0 & 0 & 0 & 0 & 0 & 0.707 \end{bmatrix}$$

and

$$\mathcal{A}_y = \frac{A_g}{2\mu_0}\begin{bmatrix} 0 & 0 & 0 & 0 & 0 & 0 & 0 & 0 \\ 0 & 0.707 & 0 & 0 & 0 & 0 & 0 & 0 \\ 0 & 0 & 1 & 0 & 0 & 0 & 0 & 0 \\ 0 & 0 & 0 & 0.707 & 0 & 0 & 0 & 0 \\ 0 & 0 & 0 & 0 & 0 & 0 & 0 & 0 \\ 0 & 0 & 0 & 0 & 0 & -0.707 & 0 & 0 \\ 0 & 0 & 0 & 0 & 0 & 0 & -1 & 0 \\ 0 & 0 & 0 & 0 & 0 & 0 & 0 & -0.707 \end{bmatrix}$$

Finally, the coil currents must be related to some control parameters. One choice of a coil selection law is

$$\underline{I} = \mathcal{C}\hat{\underline{I}} = \begin{bmatrix} 1 & 0 & 1 \\ -0.707 & -0.707 & -1 \\ 0 & 1 & 1 \\ 0.707 & -0.707 & -1 \\ -1 & 0 & 1 \\ 0.707 & 0.707 & -1 \\ 0 & -1 & 1 \\ -0.707 & 0.707 & -1 \end{bmatrix} \begin{Bmatrix} i_{p,x} \\ i_{p,y} \\ I_b \end{Bmatrix}$$

The actuator gain can be found from (2.10.3):

$$\begin{aligned} K_{i_x} &= \left.\frac{\partial f_x}{\partial \hat{\underline{I}}}\right|_{0,0} \\ &= 2\hat{\underline{I}}^\top \mathcal{C}^\top \mathcal{N}^\top \mathcal{R}^{-\top}(0,0)\mathcal{A}_x \mathcal{R}^{-1}(0,0)\mathcal{N}\mathcal{C} \end{aligned}$$

The sensitivity of the impedance matrix to variations in x is:

$$\frac{\partial \mathcal{R}}{\partial x} = \frac{1}{\mu_0}\begin{bmatrix} 1 & -0.707 & 0 & 0 & 0 & 0 & 0 & 0 \\ 0 & 0.707 & 0 & 0 & 0 & 0 & 0 & 0 \\ 0 & 0 & 0 & 0.707 & 0 & 0 & 0 & 0 \\ 0 & 0 & 0 & -0.707 & 1 & 0 & 0 & 0 \\ 0 & 0 & 0 & 0 & -1 & 0.707 & 0 & 0 \\ 0 & 0 & 0 & 0 & 0 & -0.707 & 0 & 0 \\ 0 & 0 & 0 & 0 & 0 & 0 & 0 & -0.707 \\ 0 & 0 & 0 & 0 & 0 & 0 & 0 & 0 \end{bmatrix}$$

while the sensitivity to variations in y is:

$$\frac{\partial \mathcal{R}}{\partial y} = \frac{1}{\mu_0}\begin{bmatrix} 0 & -0.707 & 0 & 0 & 0 & 0 & 0 & 0 \\ 0 & 0.707 & -1 & 0 & 0 & 0 & 0 & 0 \\ 0 & 0 & 1 & -0.707 & 0 & 0 & 0 & 0 \\ 0 & 0 & 0 & 0.707 & 0 & 0 & 0 & 0 \\ 0 & 0 & 0 & 0 & 0 & 0.707 & 0 & 0 \\ 0 & 0 & 0 & 0 & 0 & -0.707 & 1 & 0 \\ 0 & 0 & 0 & 0 & 0 & 0 & -1 & 0.707 \\ 0 & 0 & 0 & 0 & 0 & 0 & 0 & 0 \end{bmatrix}$$

The actuator gain evaluated at $x = y = 0$ is

$$\begin{aligned} K_{i_x} &= \left.\frac{\partial f_x}{\partial \hat{\underline{I}}}\right|_0 \\ &= 2\hat{\underline{I}}^\top \mathcal{C}^\top \mathcal{N}^\top \mathcal{R}^{-\top}(0)\mathcal{A}_x \mathcal{R}^{-1}(0)\mathcal{N}\mathcal{C} \\ &= \frac{\mu_0 A_g N^2}{g^2} \left\{ \begin{array}{ccc} i_{p,x} & i_{p,y} & I_b \end{array} \right\} \left[\begin{array}{ccc} 0 & 0 & 4 \\ 0 & 0 & 0 \\ 4 & 0 & 0 \end{array} \right] \\ &= \frac{4\mu_0 A_g N^2}{g^2} \left[\begin{array}{ccc} I_b & 0 & i_{p,x} \end{array} \right] \end{aligned}$$

and

$$\begin{aligned} K_{i_y} &= \left.\frac{\partial f_y}{\partial \hat{\underline{I}}}\right|_0 \\ &= 2\hat{\underline{I}}^\top \mathcal{C}^\top \mathcal{N}^\top \mathcal{R}^{-\top}(0)\mathcal{A}_y \mathcal{R}^{-1}(0)\mathcal{N}\mathcal{C} \\ &= \frac{\mu_0 A_g N^2}{g^2} \left\{ \begin{array}{ccc} i_{p,x} & i_{p,y} & I_b \end{array} \right\} \left[\begin{array}{ccc} 0 & 0 & 0 \\ 0 & 0 & 4 \\ 0 & 4 & 0 \end{array} \right] \\ &= \frac{4\mu_0 A_g N^2}{g^2} \left[\begin{array}{ccc} 0 & I_b & i_{p,y} \end{array} \right] \end{aligned}$$

The total actuator gain matrix becomes:

$$K_i = \frac{4\mu_0 A_g N^2}{g^2} \left[\begin{array}{ccc} I_b & 0 & i_{p_{x,0}} \\ 0 & I_b & i_{p_{y,0}} \end{array} \right]$$

The last column corresponds to perturbations in the bias current, which is held to zero. So the last column can be discarded to provide the simpler actuator gain

$$K_i = \frac{4\mu_0 A_g N^2 I_b}{g^2}$$

The open–loop stiffness matrix elements are computed from (2.5):

$$K_{ij} = \hat{\underline{I}}_0^\top \mathcal{C}^\top \mathcal{N}^\top \left(\frac{\partial}{\partial j}\mathcal{R}^{-\top}(x,y)\mathcal{A}_i \mathcal{R}^{-1}(x,y) + \mathcal{R}^{-\top}(x,y)\mathcal{A}_i \frac{\partial}{\partial j}\mathcal{R}^{-1}(x,y) \right) \mathcal{N}\mathcal{C}\hat{\underline{I}}_0$$

so that

$$\begin{aligned} K_{xx} &= \hat{\underline{I}}_0^\top \mathcal{C}^\top \mathcal{N}^\top \left(\frac{\partial}{\partial x}\mathcal{R}^{-\top}(x,y)\mathcal{A}_x \mathcal{R}^{-1}(x,y) + \mathcal{R}^{-\top}(x,y)\mathcal{A}_x \frac{\partial}{\partial x}\mathcal{R}^{-1}(x,y) \right) \mathcal{N}\mathcal{C}\hat{\underline{I}}_0 \\ &= -\frac{\mu_0 A_g N^2}{g^3} \left(3i_{p_{x,0}}^2 + i_{p_{y,0}}^2 + 4I_b^2 \right) \end{aligned}$$

The remaining terms can be computed in a similar manner to yield

$$K_x = -\frac{\mu_0 A_g N^2}{g^3} \left[\begin{array}{cc} 3i_{p_{x,0}}^2 + i_{p_{y,0}}^2 + 4I_b^2 & i_{p_{x,0}} i_{p_{y,0}} \\ i_{p_{x,0}} i_{p_{y,0}} & i_{p_{x,0}}^2 + 3i_{p_{y,0}}^2 + 4I_b^2 \end{array} \right]$$

If the nominal operating currents are zero, then the open–loop stiffness loses its cross–coupling terms and becomes, simply

$$K_x = -\frac{4\mu_0 A_g N^2 I_b^2}{g^3}$$

For the case where $x = y = 0$, the bias flux density can be computed as

$$B_b = \frac{\mu_0 N I_b}{g}$$

so that, in terms of the bias density, the actuator gain and open–loop stiffness become

$$K_i = \frac{4A_g N B_b}{g} \quad , \quad K_x = -\frac{4A_g B_b^2}{\mu_0 g}$$

Finally, the inductance can be computed for use in calculating the available slew rate. Using Faraday's law, the voltage across each coil is proportional to the rate of change of total flux passing through the coil:

$$V_i = N_i \frac{d\Phi_i}{dt} = N_i A_i \frac{dB_i}{dt}$$

or, in vector form,

$$\underline{V} = \mathcal{W} \frac{d}{dt} \underline{B}$$

in which $\mathcal{W} \doteq \text{ diag}[N_i A_i]$. Recalling the previous definitions of the impedance matrix and the linkage matrix,

$$\mathcal{R}\underline{B} = \mathcal{N}\underline{I}$$

or,

$$\underline{B} = \mathcal{R}^{-1}\mathcal{N}\underline{I}$$

so that

$$\underline{V} = \mathcal{W} \frac{d}{dt} \left(\mathcal{R}^{-1}\mathcal{N}\underline{I} \right)$$

The definition of inductance is the matrix expression

$$L \doteq \mathcal{W} \frac{d\underline{B}}{d\underline{I}} = \mathcal{W}\mathcal{R}^{-1}\mathcal{N}$$

which gives

$$\underline{V} = L \frac{d\underline{I}}{dt} + \frac{dL}{dt}\underline{I}$$

The latter term is the back-EMF due to rotor motion:

$$\begin{aligned} \frac{dL}{dt} &= \mathcal{W} \frac{d\mathcal{R}^{-1}}{dt} \mathcal{N} \\ &= -\mathcal{W}\mathcal{R}^{-1} \frac{d\mathcal{R}}{dt} \mathcal{R}^{-1}\mathcal{N} \\ &= -\mathcal{W}\mathcal{R}^{-1} \left(\frac{\partial \mathcal{R}}{\partial x}\frac{dx}{dt} + \frac{\partial \mathcal{R}}{\partial y}\frac{dy}{dt} \right) \mathcal{R}^{-1}\mathcal{N} \end{aligned}$$

Generally, the journal velocity term is substantially smaller than the current term is.

For the present 8 pole stator, the inductance matrix can be computed as

$$L = \frac{\mu_0 N^2 A_g}{8g} \begin{bmatrix} 7 & -1 & -1 & -1 & -1 & -1 & -1 & -1 \\ -1 & 7 & -1 & -1 & -1 & -1 & -1 & -1 \\ -1 & -1 & 7 & -1 & -1 & -1 & -1 & -1 \\ -1 & -1 & -1 & 7 & -1 & -1 & -1 & -1 \\ -1 & -1 & -1 & -1 & 7 & -1 & -1 & -1 \\ -1 & -1 & -1 & -1 & -1 & 7 & -1 & -1 \\ -1 & -1 & -1 & -1 & -1 & -1 & 7 & -1 \\ -1 & -1 & -1 & -1 & -1 & -1 & -1 & 7 \end{bmatrix}$$

The slew rate limitation is then imposed by:

$$\underline{V} = L\frac{d}{dt}\underline{I} = L\mathcal{C}\frac{d}{dt}\hat{\underline{I}} = L\mathcal{C}K_i^{-1}\frac{d}{dt}\underline{f}$$

where the last column of $\mathcal{C}$, corresponding to the constant bias current, has been stricken. Noting that $L\mathcal{C}$ is not square, premultiply the equation by the transpose of this quantity to obtain

$$\mathcal{C}^\top L^\top \underline{V} = \mathcal{C}^\top L^\top L\mathcal{C}K_i^{-1}\frac{d}{dt}\underline{f}$$

or,

$$\frac{d}{dt}\underline{f} = K_i\left(\mathcal{C}^\top L^\top L\mathcal{C}\right)^{-1}\mathcal{C}^\top L^\top \underline{V}$$

For the nominal operating point, this expression can be reduced to

$$\frac{d}{dt}\underline{f} = \frac{I_b}{g}\begin{bmatrix} 1 & -0.707 & 0 & 0.707 & -1 & 0.707 & 0 & -0.707 \\ 0 & -0.707 & 1 & -0.707 & 0 & 0.707 & -1 & 0.707 \end{bmatrix}\underline{V}$$

Assuming that $|V_i| \leq V_{\text{sup}}$, the maximum force slew rate is given by

$$\left|\frac{d\underline{f}}{dt}\right|_\infty \leq \frac{4.828 V_{\text{sup}} I_b}{g}$$

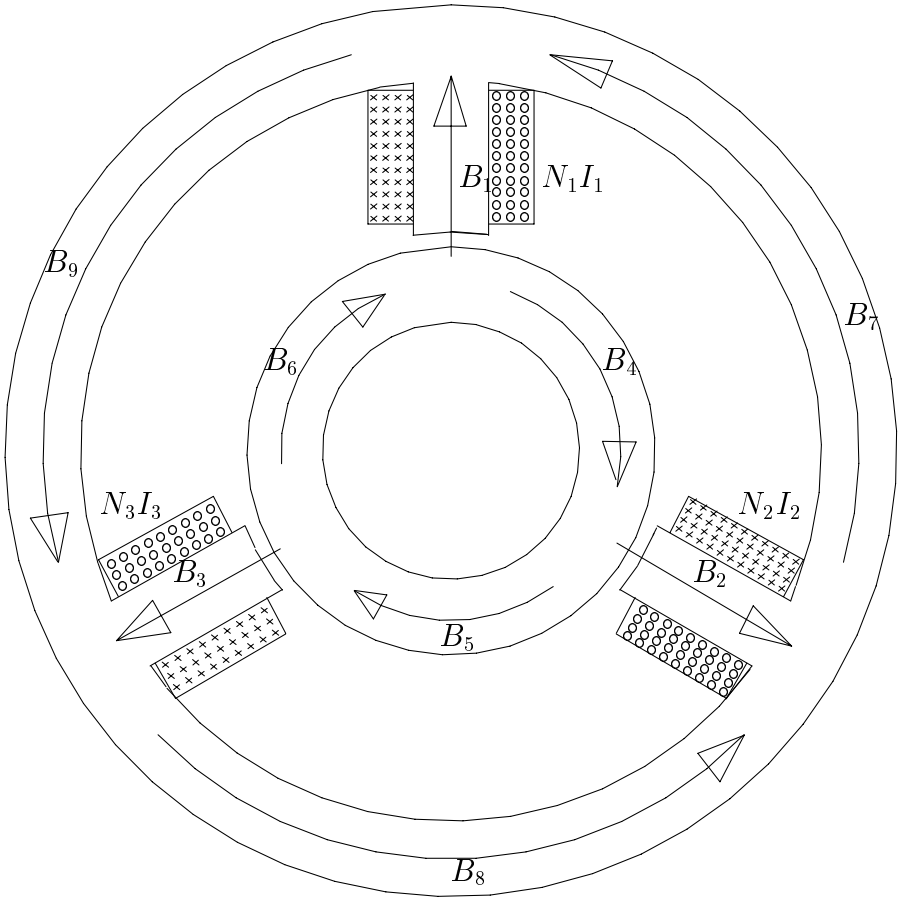

Figure 2.8: Three pole stator

2.11.3 Three pole stator

Consider the simple three pole stator depicted in Figure 2.8.

1. select a sign convention for the currents and fluxes, identify the currents and fluxes.
2. find as many independent loop equations as are available:

$$-B_1\frac{g_1}{\mu_0} - B_1\frac{\ell_1}{\mu_0\mu_r} + B_4\frac{\ell_4}{\mu_0\mu_r} + B_2\frac{g_2}{\mu_0} + B_2\frac{\ell_2}{\mu_0\mu_r} + B_7\frac{\ell_7}{\mu_0\mu_r} = N_1I_1 - N_2I_2$$

$$-B_2\frac{g_2}{\mu_0} - B_2\frac{\ell_2}{\mu_0\mu_r} + B_5\frac{\ell_5}{\mu_0\mu_r} + B_3\frac{g_3}{\mu_0} + B_3\frac{\ell_3}{\mu_0\mu_r} + B_8\frac{\ell_8}{\mu_0\mu_r} = N_2I_2 - N_3I_3$$

$$B_4\frac{\ell_4}{\mu_0\mu_r} + B_5\frac{\ell_5}{\mu_0\mu_r} + B_6\frac{\ell_6}{\mu_0\mu_r} = 0$$

$$B_7\frac{\ell_7}{\mu_0\mu_r} + B_8\frac{\ell_8}{\mu_0\mu_r} + B_9\frac{\ell_9}{\mu_0\mu_r} = 0$$

3. find the remaining equations using conservation of flux:

$$B_1 A_1 + B_7 A_7 - B_9 A_9 = 0$$

$$B_2 A_2 + B_8 A_8 - B_7 A_7 = 0$$

$$B_3 A_3 + B_9 A_9 - B_8 A_8 = 0$$

$$B_6 A_6 - B_1 A_1 - B_4 A_4 = 0$$

$$B_4 A_4 - B_2 A_2 - B_5 A_5 = 0$$

4. Summarize these equations in the form of the impedance and linkage matrices:

$$\mathcal{R} = \frac{1}{\mu_0} \begin{bmatrix} -g_1 - \frac{\ell_1}{\mu_r} & g_2 + \frac{\ell_2}{\mu_r} & 0 & \frac{\ell_4}{\mu_r} & 0 & 0 & \frac{\ell_7}{\mu_r} & 0 & 0 \\ 0 & -g_2 - \frac{\ell_2}{\mu_r} & g_3 + \frac{\ell_3}{\mu_r} & 0 & \frac{\ell_5}{\mu_r} & 0 & 0 & \frac{\ell_8}{\mu_r} & 0 \\ 0 & 0 & 0 & \frac{\ell_4}{\mu_r} & \frac{\ell_5}{\mu_r} & \frac{\ell_6}{\mu_r} & 0 & 0 & 0 \\ 0 & 0 & 0 & 0 & 0 & 0 & \frac{\ell_7}{\mu_r} & \frac{\ell_8}{\mu_r} & \frac{\ell_9}{\mu_r} \\ A_1 & 0 & 0 & 0 & 0 & 0 & A_7 & 0 & -A_9 \\ 0 & A_2 & 0 & 0 & 0 & 0 & -A_7 & A_8 & 0 \\ 0 & 0 & A_3 & 0 & 0 & 0 & 0 & -A_8 & A_9 \\ A_1 & 0 & 0 & A_4 & 0 & -A_6 & 0 & 0 & 0 \\ 0 & A_2 & 0 & -A_4 & A_5 & 0 & 0 & 0 & 0 \end{bmatrix}$$

$$\mathcal{N} = \begin{bmatrix} N_1 & -N_2 & 0 \\ 0 & N_2 & -N_3 \\ 0 & 0 & 0 \\ 0 & 0 & 0 \\ 0 & 0 & 0 \\ 0 & 0 & 0 \\ 0 & 0 & 0 \\ 0 & 0 & 0 \\ 0 & 0 & 0 \end{bmatrix}$$

5. Construct the force summation matrices. Note that only B_1 through B_3 actually produce any force:

$$\mathcal{A}_x = \frac{1}{2\mu_0} \begin{bmatrix} 0 & 0 & 0 & 0 & 0 & 0 & 0 & 0 & 0 \\ 0 & A_2 \cos 30^\circ & 0 & 0 & 0 & 0 & 0 & 0 & 0 \\ 0 & 0 & -A_3 \cos 30^\circ & 0 & 0 & 0 & 0 & 0 & 0 \\ 0 & 0 & 0 & 0 & 0 & 0 & 0 & 0 & 0 \\ 0 & 0 & 0 & 0 & 0 & 0 & 0 & 0 & 0 \\ 0 & 0 & 0 & 0 & 0 & 0 & 0 & 0 & 0 \\ 0 & 0 & 0 & 0 & 0 & 0 & 0 & 0 & 0 \\ 0 & 0 & 0 & 0 & 0 & 0 & 0 & 0 & 0 \\ 0 & 0 & 0 & 0 & 0 & 0 & 0 & 0 & 0 \end{bmatrix}$$

$$\mathcal{A}_y = \frac{1}{2\mu_0}\begin{bmatrix} A_1 & 0 & 0 & 0 & 0 & 0 & 0 & 0 & 0 \\ 0 & -A_2\sin 30^\circ & 0 & 0 & 0 & 0 & 0 & 0 & 0 \\ 0 & 0 & -A_3\sin 30^\circ & 0 & 0 & 0 & 0 & 0 & 0 \\ 0 & 0 & 0 & 0 & 0 & 0 & 0 & 0 & 0 \\ 0 & 0 & 0 & 0 & 0 & 0 & 0 & 0 & 0 \\ 0 & 0 & 0 & 0 & 0 & 0 & 0 & 0 & 0 \\ 0 & 0 & 0 & 0 & 0 & 0 & 0 & 0 & 0 \\ 0 & 0 & 0 & 0 & 0 & 0 & 0 & 0 & 0 \\ 0 & 0 & 0 & 0 & 0 & 0 & 0 & 0 & 0 \end{bmatrix}$$

Note that both $\mathcal{A}_x$ and $\mathcal{A}_y$ are indefinite, as required to produce forces in arbitrary directions.

6. Since the current vector has dimension of only three, it is not possible (or necessary) to pick a current selection matrix, $\mathcal{C}$. It will be assumed equal to the identity matrix:

$$\mathcal{C} = \begin{bmatrix} 1 & 0 & 0 \\ 0 & 1 & 0 \\ 0 & 0 & 1 \end{bmatrix}$$

7. Establish the relationship between the gaps and the rotor position:

$$g_1 = g - y$$

$$g_2 = g + \sin 30^\circ y - \cos 30^\circ x$$

$$g_3 = g + \sin 30^\circ y + \cos 30^\circ x$$

To continue the example, assume that the areas are all equal: $A_1 = A_2 = \ldots = A_9 = A$. Further, assume that the coils all have the same number of turns: $N_1 = N_2 = N_3 = N$. Finally, assume that the iron lengths in the back iron (ℓ_7, ℓ_8, ℓ_9) are all 900 times the nominal gap, g; the leg iron lengths are all 300 times the nominal gap; and the rotor iron lengths are all 600 times the nominal gap. Finally, assume that the iron relative permeability is 3000:

$$\ell_1 = \ell_2 = \ell_3 = 300g$$

$$\ell_4 = \ell_5 = \ell_6 = 600g$$

$$\ell_7 = \ell_8 = \ell_9 = 900g$$

$$\mu_r = 3000$$

With these assumptions, the *nominal* impedance matrix (at $x = y = 0$) is

$$\mathcal{R} = \frac{g}{\mu_0}\begin{bmatrix} -1.1 & 1.1 & 0 & 0.2 & 0 & 0 & 0.3 & 0 & 0 \\ 0 & -1.1 & 1.1 & 0 & 0.2 & 0 & 0 & 0.3 & 0 \\ 0 & 0 & 0 & 1 & 1 & 1 & 0 & 0 & 0 \\ 0 & 0 & 0 & 0 & 0 & 0 & 1 & 1 & 1 \\ 1 & 0 & 0 & 0 & 0 & 0 & 1 & 0 & -1 \\ 0 & 1 & 0 & 0 & 0 & 0 & -1 & 1 & 0 \\ 0 & 0 & 1 & 0 & 0 & 0 & 0 & -1 & 1 \\ 1 & 0 & 0 & 1 & 0 & -1 & 0 & 0 & 0 \\ 0 & 1 & 0 & -1 & 1 & 0 & 0 & 0 & 0 \end{bmatrix}$$

in which those rows corresponding to entirely zero rows in $\mathcal{N}$ have been normalized to 1.0. The sensitivities of the impedance matrix to rotor displacement are easily computed as

$$\frac{\partial \mathcal{R}}{\partial x} = \frac{\sqrt{3}}{2\mu_0} \begin{bmatrix} 0 & -1 & 0 & 0 & 0 & 0 & 0 & 0 & 0 \\ 0 & 1 & 1 & 0 & 0 & 0 & 0 & 0 & 0 \\ 0 & 0 & 0 & 0 & 0 & 0 & 0 & 0 & 0 \\ 0 & 0 & 0 & 0 & 0 & 0 & 0 & 0 & 0 \\ 0 & 0 & 0 & 0 & 0 & 0 & 0 & 0 & 0 \\ 0 & 0 & 0 & 0 & 0 & 0 & 0 & 0 & 0 \\ 0 & 0 & 0 & 0 & 0 & 0 & 0 & 0 & 0 \\ 0 & 0 & 0 & 0 & 0 & 0 & 0 & 0 & 0 \\ 0 & 0 & 0 & 0 & 0 & 0 & 0 & 0 & 0 \end{bmatrix}$$

and

$$\frac{\partial \mathcal{R}}{\partial y} = \frac{1}{\mu_0} \begin{bmatrix} -1 & 0.5 & 0 & 0 & 0 & 0 & 0 & 0 & 0 \\ 0 & -0.5 & 0.5 & 0 & 0 & 0 & 0 & 0 & 0 \\ 0 & 0 & 0 & 0 & 0 & 0 & 0 & 0 & 0 \\ 0 & 0 & 0 & 0 & 0 & 0 & 0 & 0 & 0 \\ 0 & 0 & 0 & 0 & 0 & 0 & 0 & 0 & 0 \\ 0 & 0 & 0 & 0 & 0 & 0 & 0 & 0 & 0 \\ 0 & 0 & 0 & 0 & 0 & 0 & 0 & 0 & 0 \\ 0 & 0 & 0 & 0 & 0 & 0 & 0 & 0 & 0 \\ 0 & 0 & 0 & 0 & 0 & 0 & 0 & 0 & 0 \end{bmatrix}$$

The linkage matrix becomes

$$\mathcal{N} = N \begin{bmatrix} 1 & -1 & 0 \\ 0 & 1 & -1 \\ 0 & 0 & 0 \\ 0 & 0 & 0 \\ 0 & 0 & 0 \\ 0 & 0 & 0 \\ 0 & 0 & 0 \\ 0 & 0 & 0 \\ 0 & 0 & 0 \end{bmatrix}$$

Finally, the force summation matrices become

$$\mathcal{A}_x = \frac{A\sqrt{3}}{4\mu_0} \begin{bmatrix} 0 & 0 & 0 & 0 & 0 & 0 & 0 & 0 & 0 \\ 0 & 1 & 0 & 0 & 0 & 0 & 0 & 0 & 0 \\ 0 & 0 & -1 & 0 & 0 & 0 & 0 & 0 & 0 \\ 0 & 0 & 0 & 0 & 0 & 0 & 0 & 0 & 0 \\ 0 & 0 & 0 & 0 & 0 & 0 & 0 & 0 & 0 \\ 0 & 0 & 0 & 0 & 0 & 0 & 0 & 0 & 0 \\ 0 & 0 & 0 & 0 & 0 & 0 & 0 & 0 & 0 \\ 0 & 0 & 0 & 0 & 0 & 0 & 0 & 0 & 0 \\ 0 & 0 & 0 & 0 & 0 & 0 & 0 & 0 & 0 \end{bmatrix}$$

$$\mathcal{A}_y = \frac{A}{4\mu_0}\begin{bmatrix} 2 & 0 & 0 & 0 & 0 & 0 & 0 & 0 & 0 \\ 0 & -1 & 0 & 0 & 0 & 0 & 0 & 0 & 0 \\ 0 & 0 & -1 & 0 & 0 & 0 & 0 & 0 & 0 \\ 0 & 0 & 0 & 0 & 0 & 0 & 0 & 0 & 0 \\ 0 & 0 & 0 & 0 & 0 & 0 & 0 & 0 & 0 \\ 0 & 0 & 0 & 0 & 0 & 0 & 0 & 0 & 0 \\ 0 & 0 & 0 & 0 & 0 & 0 & 0 & 0 & 0 \\ 0 & 0 & 0 & 0 & 0 & 0 & 0 & 0 & 0 \\ 0 & 0 & 0 & 0 & 0 & 0 & 0 & 0 & 0 \end{bmatrix}$$

With these simplifications, the force components become

$$\begin{aligned} f_x &= \underline{I}^\top \mathcal{N}^\top \mathcal{R}^{-\top}(x,y)\mathcal{A}_x\mathcal{R}^{-1}(x,y)\mathcal{N}\underline{I} \\ &= \frac{0.1199\mu_0 N^2 A}{g^2}\underline{I}^\top \begin{bmatrix} 0 & -1 & 1 \\ -1 & 1 & 0 \\ 1 & 0 & -1 \end{bmatrix}\underline{I} \end{aligned}$$

$$\begin{aligned} f_y &= \underline{I}^\top \mathcal{N}^\top \mathcal{R}^{-\top}(x,y)\mathcal{A}_y\mathcal{R}^{-1}(x,y)\mathcal{N}\underline{I} \\ &= \frac{0.0693\mu_0 N^2 A}{g^2}\underline{I}^\top \begin{bmatrix} 2 & -1 & -1 \\ -1 & -1 & 2 \\ -1 & 2 & -1 \end{bmatrix}\underline{I} \end{aligned}$$

The actuator gain is

$$K_i = \frac{\partial \underline{f}}{\partial \underline{I}} = \frac{\mu_0 N^2 A}{g^2}\begin{bmatrix} 0.1199(I_3 - I_2) & 0.1199(I_2 - I_1) & 0.1199(I_1 - I_3) \\ 0.0693(2I_1 - I_2 - I_3) & 0.0693(2I_3 - I_1 - I_2) & 0.0693(2I_2 - I_1 - I_3) \end{bmatrix}$$

The linkage matrix, $\mathcal{N}$, is singular. For this example problem, coil currents satisfying $I_1 = I_2 = I_3$ lie in the null space of $\mathcal{N}$, which means that such a coil current arrangement does not produce any magnetic flux. In order to always produce the most flux relative to the amount of current used, the coil currents should be selected so that no component of the current vector lies in the null space of $\mathcal{N}$. That is, the coil current vector should be orthogonal to $\{111\}$. One possible method of choosing the currents to satisfy this requirement is

$$\begin{Bmatrix} I_1 \\ I_2 \\ I_3 \end{Bmatrix} = \begin{bmatrix} 1 & 0 \\ 0 & 1 \\ -1 & -1 \end{bmatrix}\begin{Bmatrix} I_1 \\ I_2 \end{Bmatrix}$$

This choice of coil currents leads to the simplification in the force law:

$$f_x = \frac{0.1199\mu_0 N^2 A}{g^2}\{I_1 I_2\}\begin{bmatrix} -3 & -3 \\ -3 & 0 \end{bmatrix}\begin{Bmatrix} I_1 \\ I_2 \end{Bmatrix} = -\frac{0.3597\mu_0 N^2 A}{g^2}(I_1^2 + I_1 I_2)$$

$$f_y = \frac{0.2079\mu_0 N^2 A}{g^2}\{I_1 I_2\}\begin{bmatrix} 1 & -1 \\ -1 & -2 \end{bmatrix}\begin{Bmatrix} I_1 \\ I_2 \end{Bmatrix} = \frac{0.2079\mu_0 N^2 A}{g^2}\left(I_1^2 - 2I_1 I_2 - 2I_2^2\right)$$

Notice that, even in the centered ($x = y = 0$) condition, these force relationships are nonlinear in the currents. By contrast, the double horseshoe and the eight pole actuators were both linear in the current control variable(s). This nonlinearity of the three pole actuator is fundamental to its operation.

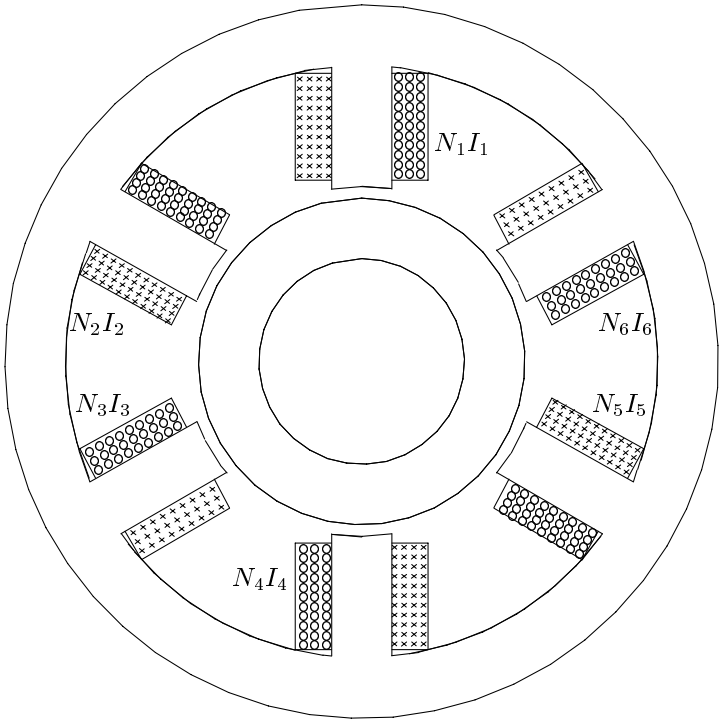

Figure 2.9: Six pole actuator.

2.11.4 Six pole actuator

A final example of interest is the six pole actuator shown in Figure 2.9. In this example, it is assumed that the relative permeability of the iron is high enough that the flux density can be computed at least approximately without reference to the flux in the backiron or journal: only the gap fluxes will be computed explicitly so that it is assumed that all of the terms having the form $B_i\ell_i/\mu_0\mu_r$ are essentially zero. Further, assume that the gap areas are all the same and that the coils all have the same number of turns. With these assumptions, the impedance and linkage matrices are:

$$\mathcal{R} = \frac{1}{\mu_0}\begin{bmatrix} g_1 & -g_2 & 0 & 0 & 0 & 0 \\ 0 & g_2 & -g_3 & 0 & 0 & 0 \\ 0 & 0 & g_3 & -g_4 & 0 & 0 \\ 0 & 0 & 0 & g_4 & -g_5 & 0 \\ 0 & 0 & 0 & 0 & g_5 & -g_6 \\ 1 & 1 & 1 & 1 & 1 & 1 \end{bmatrix}$$

$$\mathcal{N} = N\begin{bmatrix} 1 & -1 & 0 & 0 & 0 & 0 \\ 0 & 1 & -1 & 0 & 0 & 0 \\ 0 & 0 & 1 & -1 & 0 & 0 \\ 0 & 0 & 0 & 1 & -1 & 0 \\ 0 & 0 & 0 & 0 & 1 & -1 \\ 0 & 0 & 0 & 0 & 0 & 0 \end{bmatrix}$$

The gaps are related to the journal motion through

$$\begin{aligned} g_1 &= g - y \\ g_2 &= g - 0.5y + 0.866x \\ g_3 &= g + 0.5y + 0.866x \\ g_4 &= g + y \\ g_5 &= g + 0.5y - 0.866x \\ g_6 &= g - 0.5y - 0.866x \end{aligned}$$

The force summation matrices are

$$\mathcal{A}_x = \frac{A}{2\mu_0} \begin{bmatrix} 0 & 0 & 0 & 0 & 0 & 0 \\ 0 & -0.866 & 0 & 0 & 0 & 0 \\ 0 & 0 & -0.866 & 0 & 0 & 0 \\ 0 & 0 & 0 & 0 & 0 & 0 \\ 0 & 0 & 0 & 0 & 0.866 & 0 \\ 0 & 0 & 0 & 0 & 0 & 0.866 \end{bmatrix}$$

and

$$\mathcal{A}_y = \frac{A}{2\mu_0} \begin{bmatrix} 1 & 0 & 0 & 0 & 0 & 0 \\ 0 & 0.5 & 0 & 0 & 0 & 0 \\ 0 & 0 & -0.5 & 0 & 0 & 0 \\ 0 & 0 & 0 & -1 & 0 & 0 \\ 0 & 0 & 0 & 0 & -0.5 & 0 \\ 0 & 0 & 0 & 0 & 0 & 0.5 \end{bmatrix}$$

The coil currents can be profitably chosen according to

$$\begin{Bmatrix} I_1 \\ I_2 \\ I_3 \\ I_4 \\ I_5 \\ I_6 \end{Bmatrix} = \mathcal{C}\hat{\underline{I}} = \begin{bmatrix} 0 & 1 & 1 \\ 0.866 & -0.5 & -1 \\ -0.866 & -0.5 & 1 \\ 0 & 1 & -1 \\ 0.866 & -0.5 & 1 \\ -0.866 & -0.5 & -1 \end{bmatrix} \begin{Bmatrix} i_{p,x} \\ i_{p,y} \\ I_b \end{Bmatrix}$$

With this method of choosing the coil currents, the force components at $x = y = 0$ can be computed as

$$f_x = \frac{\mu_0 N^2 A}{2g^2} \hat{\underline{I}}^\top \begin{bmatrix} 0 & 0 & 3 \\ 0 & 0 & 0 \\ 3 & 0 & 0 \end{bmatrix} \hat{\underline{I}} = \frac{3\mu_0 N^2 A I_b}{g^2} i_{p,x}$$

and

$$f_x = \frac{\mu_0 N^2 A}{2g^2} \hat{\underline{I}}^\top \begin{bmatrix} 0 & 0 & 0 \\ 0 & 0 & 3 \\ 0 & 3 & 0 \end{bmatrix} \hat{\underline{I}} = \frac{3\mu_0 N^2 A I_b}{g^2} i_{p,y}$$

so the force is linear in the control terms, $i_{p,x}$ and $i_{p,y}$ and completely decoupled. The actuator gain is the scalar

$$K_i = \frac{3\mu_0 N^2 A I_b}{g^2}$$

and the linearized force is

$$\underline{f} = K_i \left\{ \begin{array}{c} i_{p,x} \\ i_{p,y} \end{array} \right\} + K_x \left\{ \begin{array}{c} x \\ y \end{array} \right\}$$

The open loop stiffness is easily computed as

$$K_x = -\frac{\mu_0 N^2 A}{2g^3} \left[\begin{array}{cc} 4.5i_{p,x}^2 + 1.5i_{p,y}^2 + 6I_b^2 & 3i_{p,x}i_{p,y} \\ 3i_{p,x}i_{p,y} & 1.5i_{p,x}^2 + 4.5i_{p,y}^2 + 6I_b^2 \end{array} \right]$$

For the unloaded case where the nominal control terms are zero, the open loop stiffness becomes a simple scalar:

$$K_x = -\frac{3\mu_0 N^2 I_b^2 A}{g^3}$$

2.11.5 General n pole symmetric heteropolar stator

In general, for an n pole symmetric stator (where n is even), the coil currents can be chosen according to the rule

$$I_i = (-1)^i \left(\cos\theta_i i_{p,x} + \sin\theta_i i_{p,y} + I_b\right)$$

If this selection scheme is adopted, then the actuator gain and open loop stiffness, evaluated at $x = y = i_{p,x} = i_{p,y} = 0$ will be

$$K_i = \frac{n\mu_0 N^2 I_b A}{2g^2} \quad , \quad K_x = -\frac{n\mu_0 N^2 I_b^2 A}{2g^3}$$

The principal drawback to this coil selection scheme is that none of the coils carry the same current. This implies that none of the coils can be wired in series to be driven by a common amplifier: apparently this scheme requires n power amplifiers. However, if each leg of the stator carries three coils: one for $x-$ control, one for $y-$ control, and one for biasing, then the coil sizes can be adjusted to produce the appropriate weightings and wound in series. In this manner, any n pole symmetric stator can be controlled using only six wires (two for each coil set) and three power amplifiers.

2.11.6 Combined Force and Moment

Figure 2.10 illustrates a simple planar actuator which is capable of producing both the $x-$ and $y-$ components of force as well as a moment about the $z-$ axis. As shown, all of the legs carry the same number of coil turns and three of the legs have the same gap area, A_g, while the two legs on the left side of the stator have half this gap area.

Ampère's loop law is applied to obtain four magnetic flux density equations:

$$\begin{aligned} B_1\frac{g_1}{\mu_0} - B_2\frac{g_2}{\mu_0} &= NI_1 - NI_2 \\ B_2\frac{g_2}{\mu_0} - B_3\frac{g_3}{\mu_0} &= NI_2 - NI_3 \\ B_3\frac{g_3}{\mu_0} - B_4\frac{g_4}{\mu_0} &= NI_3 - NI_4 \\ B_4\frac{g_4}{\mu_0} - B_5\frac{g_5}{\mu_0} &= NI_4 - NI_5 \end{aligned}$$

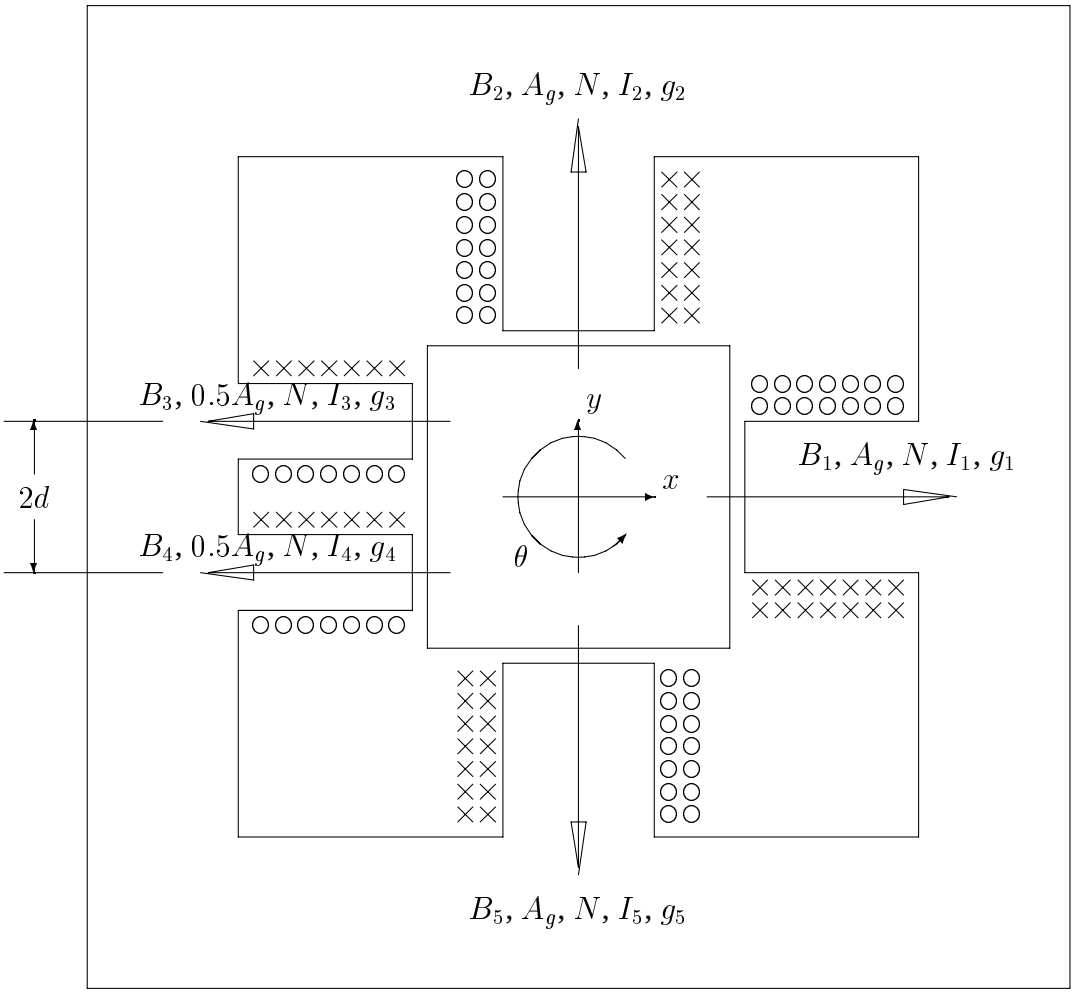

Figure 2.10: Planar actuator which produces two forces and a moment.

Conservation of flux produces a last equation:

$$B_1 A_g + B_2 A_g + 0.5 B_3 A_g + 0.5 B_5 A_g + B_5 A_g = 0$$

The resulting impedance and linkage matrices are

$$\mathcal{R} = \frac{1}{\mu_0} \begin{bmatrix} g_1 & -g_2 & 0 & 0 & 0 \\ 0 & g_2 & -g_3 & 0 & 0 \\ 0 & 0 & g_3 & -g_4 & 0 \\ 0 & 0 & 0 & g_4 & -g_5 \\ 2 & 2 & 1 & 1 & 2 \end{bmatrix} \quad , \quad \mathcal{N} = N \begin{bmatrix} 1 & -1 & 0 & 0 & 0 \\ 0 & 1 & -1 & 0 & 0 \\ 0 & 0 & 1 & -1 & 0 \\ 0 & 0 & 0 & 1 & -1 \\ 0 & 0 & 0 & 0 & 0 \end{bmatrix}$$

The gaps are related to the position of the rotor by

$$\begin{aligned} g_1 &= g_0 - x \\ g_2 &= g_0 - y \\ g_3 &= g_0 + x - d\theta \\ g_4 &= g_0 + x + d\theta \\ g_5 &= g_0 + y \end{aligned}$$

so that the sensitivities of the impedance matrix to the various displacement components are

$$\frac{\partial \mathcal{R}}{\partial x} = \frac{1}{\mu_0} \begin{bmatrix} -1 & 0 & 0 & 0 & 0 \\ 0 & 0 & -1 & 0 & 0 \\ 0 & 0 & 1 & -1 & 0 \\ 0 & 0 & 0 & 1 & 0 \\ 0 & 0 & 0 & 0 & 0 \end{bmatrix}$$

$$\frac{\partial \mathcal{R}}{\partial y} = \frac{1}{\mu_0} \begin{bmatrix} 0 & 1 & 0 & 0 & 0 \\ 0 & -1 & 0 & 0 & 0 \\ 0 & 0 & 0 & 0 & 0 \\ 0 & 0 & 0 & 0 & -1 \\ 0 & 0 & 0 & 0 & 0 \end{bmatrix}$$

$$\frac{\partial \mathcal{R}}{\partial \theta} = \frac{d}{\mu_0} \begin{bmatrix} 0 & 0 & 0 & 0 & 0 \\ 0 & 0 & 0 & 0 & 0 \\ 0 & 0 & 1 & 0 & 0 \\ 0 & 0 & -1 & 1 & 0 \\ 0 & 0 & 0 & 0 & 0 \end{bmatrix}$$

Inspection of the structure of the actuator suggests the current selection scheme:

$$\underline{I} = \begin{bmatrix} 1 & 0 & 0 & 1 \\ 0 & -1 & 0 & -1 \\ -1 & 0 & 1 & 1 \\ -1 & 0 & -1 & 1 \\ 0 & 1 & 0 & -1 \end{bmatrix} \begin{Bmatrix} i_x \\ i_y \\ i_\theta \\ I_b \end{Bmatrix} = C \hat{\underline{I}}$$

Noting that the linkage matrix has a null space of:

$$\text{null}(\mathcal{N}) = \begin{bmatrix} 1 \\ 1 \\ 1 \\ 1 \\ 1 \end{bmatrix}$$

the currents should further be selected to be orthogonal to this null space. A basis for the space orthogonal to the null space is:

$$c = 0.2 \begin{bmatrix} 4 & 3 & 2 & 1 \\ -1 & 3 & 2 & 1 \\ -1 & -2 & 2 & 1 \\ -1 & -2 & -3 & 1 \\ -1 & -2 & -3 & -4 \end{bmatrix}$$

(This matrix was obtained by computing the Moore–Penrose pseudoinverse of the matrix $\mathcal{N}$ and then column reducing the result.) So that the ultimate current selection scheme becomes

$$\underline{I} = c(c^\top c)^{-1} c^\top C \hat{\underline{I}} = \mathcal{C} \hat{\underline{I}}$$

in which

$$\mathcal{C} = \begin{bmatrix} 1.2 & 0 & 0 & 0.8 \\ 0.2 & -1 & 0 & -1.2 \\ -0.8 & 0 & 1 & 0.8 \\ -0.8 & 0 & -1 & 0.8 \\ 0.2 & 1 & 0 & -1.2 \end{bmatrix}$$

Finally, the force summation matrices are obtained by inspection:

$$\mathcal{A}_x = \frac{A_g}{2\mu_0} \begin{bmatrix} 1 & 0 & 0 & 0 & 0 \\ 0 & 0 & 0 & 0 & 0 \\ 0 & 0 & -0.5 & 0 & 0 \\ 0 & 0 & 0 & -0.5 & 0 \\ 0 & 0 & 0 & 0 & 0 \end{bmatrix}$$

$$\mathcal{A}_y = \frac{A_g}{2\mu_0} \begin{bmatrix} 0 & 0 & 0 & 0 & 0 \\ 0 & 1 & 0 & 0 & 0 \\ 0 & 0 & 0 & 0 & 0 \\ 0 & 0 & 0 & 0 & 0 \\ 0 & 0 & 0 & 0 & -1 \end{bmatrix} \quad , \quad \mathcal{A}_\theta = \frac{A_g d}{4\mu_0} \begin{bmatrix} 0 & 0 & 0 & 0 & 0 \\ 0 & 0 & 0 & 0 & 0 \\ 0 & 0 & 1 & 0 & 0 \\ 0 & 0 & 0 & -1 & 0 \\ 0 & 0 & 0 & 0 & 0 \end{bmatrix}$$

With these characteristic matrices computed, the force components can be determined at the nominal centered condition ($x = y = \theta = 0$):

$$f_x = \hat{\underline{I}}^\top \mathcal{C}^\top \mathcal{N}^\top \mathcal{R}^{-\top} \mathcal{A}_x \mathcal{R}^{-1} \mathcal{N} \mathcal{C} \hat{\underline{I}} = \frac{\mu_0 N^2 A_g}{2g^2} \hat{\underline{I}}^\top \begin{bmatrix} 0 & 0 & 0 & 2 \\ 0 & 0 & 0 & 0 \\ 0 & 0 & -1 & 0 \\ 2 & 0 & 0 & 0 \end{bmatrix} \hat{\underline{I}} = \frac{\mu_0 N^2 A_g}{2g^2} \left(4 I_b i_x - i_\theta^2 \right)$$

$$f_y = \hat{\underline{I}}^\top \mathcal{C}^\top \mathcal{N}^\top \mathcal{R}^{-\top} \mathcal{A}_y \mathcal{R}^{-1} \mathcal{N} \mathcal{C} \hat{\underline{I}} = \frac{\mu_0 N^2 A_g}{2g^2} \hat{\underline{I}}^\top \begin{bmatrix} 0 & 0 & 0 & 0 \\ 0 & 0 & 0 & 2 \\ 0 & 0 & 0 & 0 \\ 0 & 2 & 0 & 0 \end{bmatrix} \hat{\underline{I}} = \frac{2\mu_0 N^2 A_g I_b}{g^2} i_y$$

$$f_\theta = \hat{\underline{I}}^\top \mathcal{C}^\top \mathcal{N}^\top \mathcal{R}^{-\top} \mathcal{A}_\theta \mathcal{R}^{-1} \mathcal{N} \mathcal{C} \hat{\underline{I}} = \frac{\mu_0 N^2 A_g d}{2g^2} \hat{\underline{I}}^\top \begin{bmatrix} 0 & 0 & -1 & 0 \\ 0 & 0 & 0 & 0 \\ -1 & 0 & 0 & 1 \\ 0 & 0 & 1 & 0 \end{bmatrix} \hat{\underline{I}} = \frac{\mu_0 N^2 A_g d}{g^2} (I_b i_\theta - i_x i_\theta)$$

Each of the forces is linear in its respective control term, but the moment and x forces are coupled through the product terms $i_x i_\theta$ so that the actuator gain matrix looks like:

$$K_i = \frac{2\mu_0 N^2 A_g I_b}{g^2} \begin{bmatrix} I_b & 0 & -0.25 i_\theta \\ 0 & I_b & 0 \\ -0.25 d i_\theta & 0 & 0.5 d (I_b - 0.5 i_x) \end{bmatrix}$$

Thus, the linearization is not perfect nor is the system completely decoupled. However, if the nominal operating point is $i_x = i_y = i_\theta = 0$, then the system is decoupled as desired.

This failure to be perfectly decoupled and linearized is a consequence of the structure of the actuator and can be alleviated by simply adding a second leg on the right side of the actuator, as shown in Figure 2.11. For this device, the coil current selection law

$$\underline{I} = \frac{1}{3} \begin{bmatrix} 3 & 0 & -3 & 2 \\ 0 & -3 & 0 & -4 \\ -3 & 0 & 3 & 2 \\ -3 & 0 & -3 & 2 \\ 0 & 3 & 0 & -4 \\ 3 & 0 & 3 & 2 \end{bmatrix} \begin{Bmatrix} i_x \\ i_y \\ i_\theta \\ I_b \end{Bmatrix}$$

produces the force relationships (at centered condition):

$$f_x = \hat{\underline{I}}^\top \mathcal{C}^\top \mathcal{N}^\top \mathcal{R}^{-\top} \mathcal{A}_x \mathcal{R}^{-1} \mathcal{N} \mathcal{C} \hat{\underline{I}} = \frac{\mu_0 N^2 A_g}{2g^2} \hat{\underline{I}}^\top \begin{bmatrix} 0 & 0 & 0 & 2 \\ 0 & 0 & 0 & 0 \\ 0 & 0 & 0 & 0 \\ 2 & 0 & 0 & 0 \end{bmatrix} \hat{\underline{I}} = \frac{2\mu_0 N^2 I_b A_g}{g^2} i_x$$

$$f_y = \hat{\underline{I}}^\top \mathcal{C}^\top \mathcal{N}^\top \mathcal{R}^{-\top} \mathcal{A}_y \mathcal{R}^{-1} \mathcal{N} \mathcal{C} \hat{\underline{I}} = \frac{\mu_0 N^2 A_g}{2g^2} \hat{\underline{I}}^\top \begin{bmatrix} 0 & 0 & 0 & 0 \\ 0 & 0 & 0 & 2 \\ 0 & 0 & 0 & 0 \\ 0 & 2 & 0 & 0 \end{bmatrix} \hat{\underline{I}} = \frac{2\mu_0 N^2 I_b A_g}{g^2} i_y$$

$$f_\theta = \hat{\underline{I}}^\top \mathcal{C}^\top \mathcal{N}^\top \mathcal{R}^{-\top} \mathcal{A}_\theta \mathcal{R}^{-1} \mathcal{N} \mathcal{C} \hat{\underline{I}} = \frac{\mu_0 N^2 A_g d}{2g^2} \hat{\underline{I}}^\top \begin{bmatrix} 0 & 0 & 0 & 0 \\ 0 & 0 & 0 & 0 \\ 0 & 0 & 0 & 4 \\ 0 & 0 & 4 & 0 \end{bmatrix} \hat{\underline{I}} = \frac{4\mu_0 N^2 I_b A_g d}{g^2} i_\theta$$

Thus, the actuator is linear in the control parameters and fully decoupled. The actuator gain matrix is

$$K_i = \frac{2\mu_0 N^2 A_g I_b}{g^2} \begin{bmatrix} I_b & 0 & 0 \\ 0 & I_b & 0 \\ 0 & 0 & 2 d I_b \end{bmatrix}$$

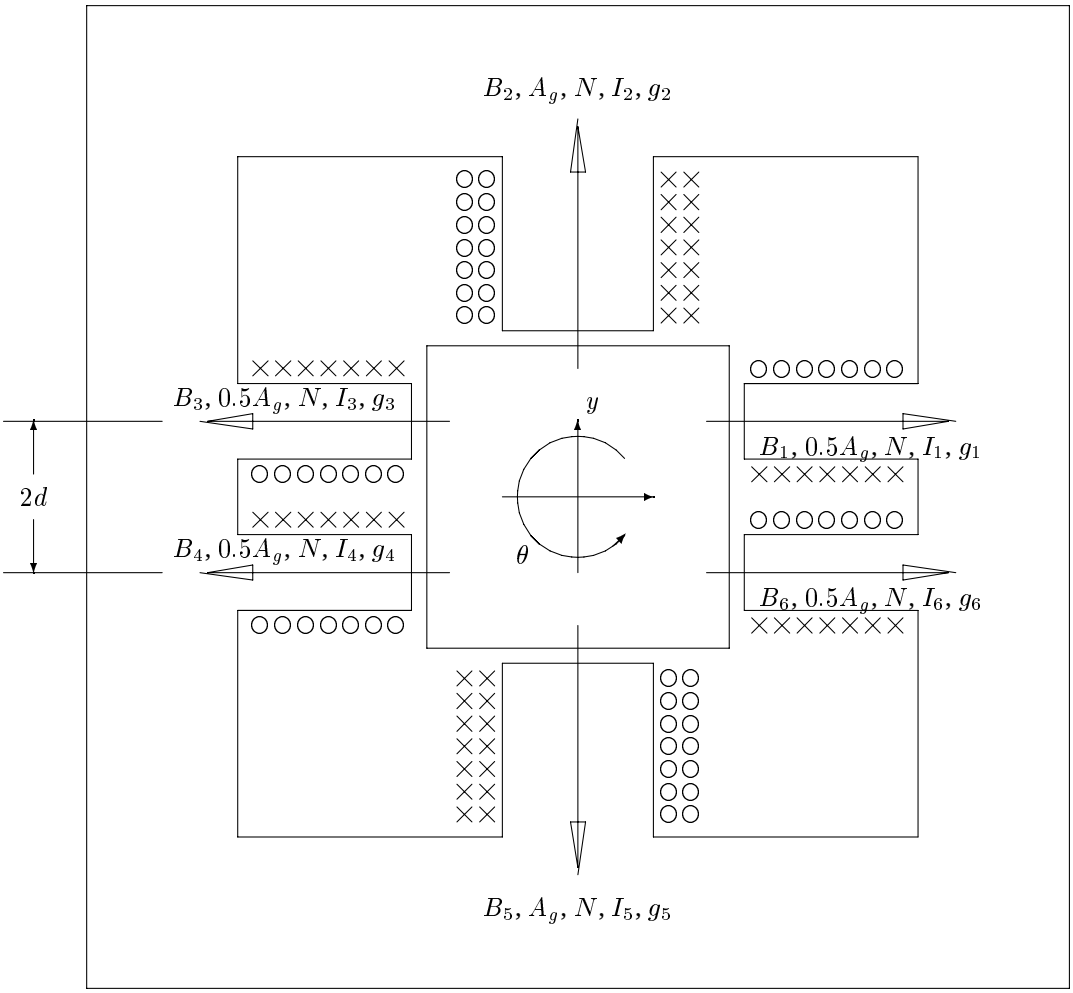

Figure 2.11: Planar actuator with moments - linearizable.

2.12 Load Capacity

The load capacity of a magnetic actuator is most appropriately defined as the maximum force that the actuator can generate in any given direction. Because of the nature of the saturation curve, the actual load capacity of an actuator is, in principal, infinite: the magnetic flux density *can*, physically, be made as large as desired. However, it is more common to compute the load capacity of the actuator as that point where the stator iron begins to substantially saturate. Using magnetic circuit analysis and a linear model of the magnetic material, this means that the actuator capacity is reached whenever ' the flux density, B, in any one of the circuit elements reaches B_{sat}.

For practical actuators, the magnitude of the force that is generated when this limit is reached is always dependent upon the orientation of the force. Thus, it is useful to describe the actuator load capacity using a polar plot where the radius of the plot is an indication of the load capacity at each angular orientation. In cases where it is desirable to characterize the actuator with a single load capacity figure, the minimum radius of this polar plot should be used. This is particularly useful in applications where the orientation of the loads is unknown so that a conservative estimate of the actuator capacity is desired.

Using the simple circuit analysis presented so far and this rather conservative definition of load capacity, the polar capacity of an actuator can be defined mathematically as

$$\overline{f}(\underline{u}) = \max_{\underline{\hat{I}}} \left| \underline{f}(\underline{\hat{I}}) \right|_2 \quad \text{subject to: } \underline{f} = \alpha \underline{u} \text{ and } \left| \underline{B}(\underline{\hat{I}}) \right|_\infty \leq B_{\text{sat}}$$

in which the components of the force vector are given by

$$f_i = \mathcal{C}^\top(\underline{\hat{I}}) \mathcal{N}^\top \mathcal{R}^{-\top} \mathcal{A}_i \mathcal{R}^{-1} \mathcal{N} \mathcal{C}(\underline{\hat{I}}) + w_i$$

the flux density is given by

$$\underline{B} = \mathcal{R}^{-1} \mathcal{N} \mathcal{C}(\underline{\hat{I}})$$

and $\underline{u}$ is a unit vector in the selected direction. The terms w_i represent external loads which act on the journal in conjunction with the actuator force and may be artificially attributed to the actuator in order to properly asssess its net capacity. Typically, these forces will be gravity loads. Note that the coil current selection law, $\mathcal{C}$, may in general be nonlinear; in the preceding discussion it was assumed to be linear at least in the neighborhood of the operating point.

2.12.1 Limiting performance

In evaluating the performance of the coil current selection scheme and in estimating the capacity of an actuator prior to choosing the coil current selection scheme, it is convenient to have an alternative method of evaluating the actuator capacity. Here, rather than imposing a coil current selection scheme, the capacity is based on the gap flux densities, assuming that they can be chosen arbitrarily with the only restriction being that they must satisfy conservation of flux:

$$\overline{f}(\underline{u}) = \max_{\underline{B}} \left| \underline{f}(\underline{\hat{I}}) \right|_2 \quad \text{subject to: } \underline{f} = \alpha \underline{u} \,, \;\; |\underline{B}|_\infty \leq B_{\text{sat}} \,, \;\; \text{and } \underline{A}^\top \underline{B} = 0$$

in which the components of the force are given by

$$f_i = \underline{B}^\top \mathcal{A}_i \underline{B} + w_i$$

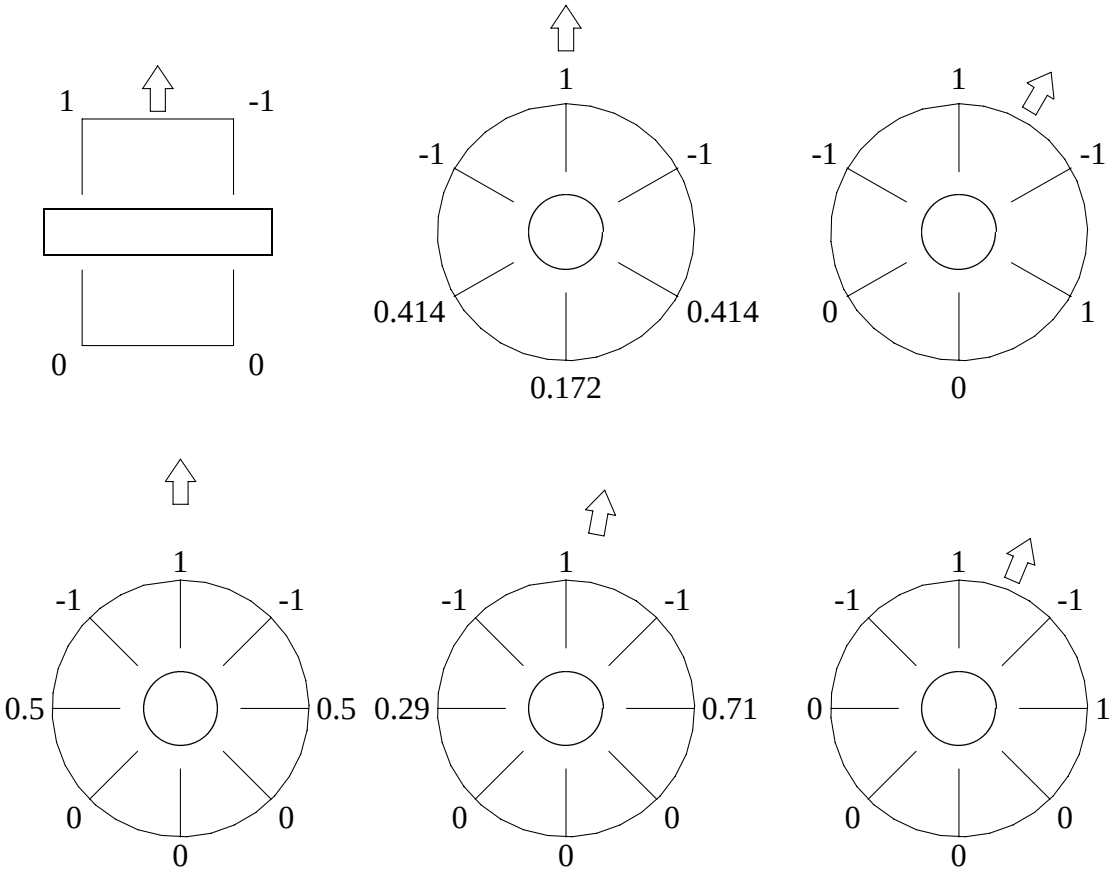

Figure 2.12: Flux density distributions for maximum capacity at various orientations: all densities are normalized by B_{sat}

and the elements of the vector $\underline{A}$ are the gap areas corresponding to each of the gap fluxes in $\underline{B}$.

Figure 2.12 illustrates this limiting performance analysis for several different actuators.

The simplest example is that of the double opposed horseshoe actuator. This device only generates force along a single axis and the flux density is the same in either face of each pole pair. Consequently, the largest vertical force is obtained by driving the gap fluxes in the two upper gaps to saturation while bringing fluxes in the two lower gaps to zero. The diagram illustrates this by identifying the upper left gap density as 1 (meaning $1 \times B_{\text{sat}}$), the upper right gap density as -1 (the sign change is necessary in order to satisfy conservation of flux), and the two lower gaps have 0 flux density. The resulting load capacity is easily computed as:

$$F_{\max} = \frac{A_g B_{\text{sat}}^2}{2\mu_0}\left(1^2 + (-1)^2 - 0^2 - 0^2\right) = \frac{A_g B_{\text{sat}}^2}{\mu_0}$$

For the symmetric eight pole stator, also illustrated in Figure 2.12, the load capacity in any particular direction can be assessed by drawing a line through the center of the device orthogonal to the force orientation. The three poles closest to the load direction on the load side of this line are then assumed to be at alternating signed saturation while the three poles opposite these saturated poles are assumed at zero density. The remaining two poles are used to satisfy flux conservation and load orientation.

For instance, assume that the load orientation is ten degrees from one of the legs. Identifying the flux densities (normalized by the saturation density) of the two "control" legs as B_+ and B_- where B_+ corresponds to the leg on the load side of the dividing line, conservation of flux requires that:

$$B_{\text{sat}}\left(-1 + 1 - 1 + B_+ + B_-\right) = 0 \quad \Rightarrow \quad B_+ = 1 - B_-$$

Load orientation requires that the off–axis force component is zero:

$$\frac{A_g}{2\mu_0}\left(1^2 \sin 10^\circ + (-1)^2 \sin 55^\circ - (-1)^2 \sin 35^\circ + B_-^2 \sin 100^\circ - B_+^2 \sin 80^\circ\right) = 0$$

$$\Rightarrow \quad B_+^2 - B_-^2 = 0.426$$

These two equations can be solved simultaneously to yield

$$B_+ = 0.713 \quad , \quad B_- = 0.287$$

and the total load capacity is

$$\begin{aligned} f_{\max}(10^\circ) &= \frac{A_g B_{\text{sat}}^2}{2\mu_0}\left(1^2 \cos 10^\circ + (-1)^2 \cos 55^\circ + (-1)^2 \cos 35^\circ + B_-^2 \cos 100^\circ + B_+^2 \cos 80^\circ\right) \\ &= 1.23\frac{A_g B_{\text{sat}}^2}{\mu_0} \end{aligned}$$

In general, the load capacity of this actuator can be found in this manner for angles from -22.5° to $+22.5^\circ$ with the result that the load capacity is

$$\overline{f}(\Phi) = \frac{1.207 A_g B_{\text{sat}}^2}{\cos\Phi\mu_0}$$

where Φ is the angle between the load line and the nearest pole. This yields a worst case capacity of $1.207 A_g B_{\text{sat}}^2/\mu_0$ at $\Phi = 0$ (on–pole orientation) and a best case capacity of $1.306 A_g B_{\text{sat}}^2/\mu_0$ at $\Phi =$

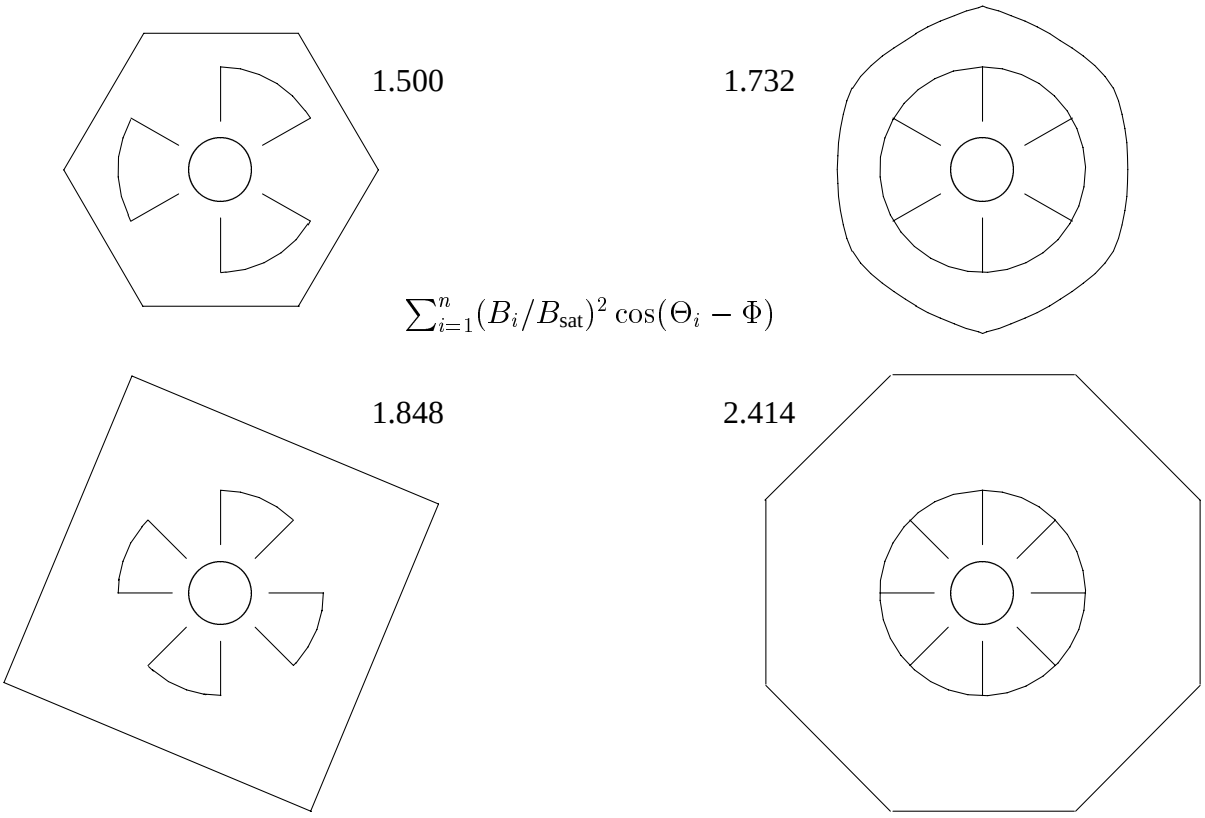

Figure 2.13: Polar plots of saturated pole load capacity for various radial actuators.

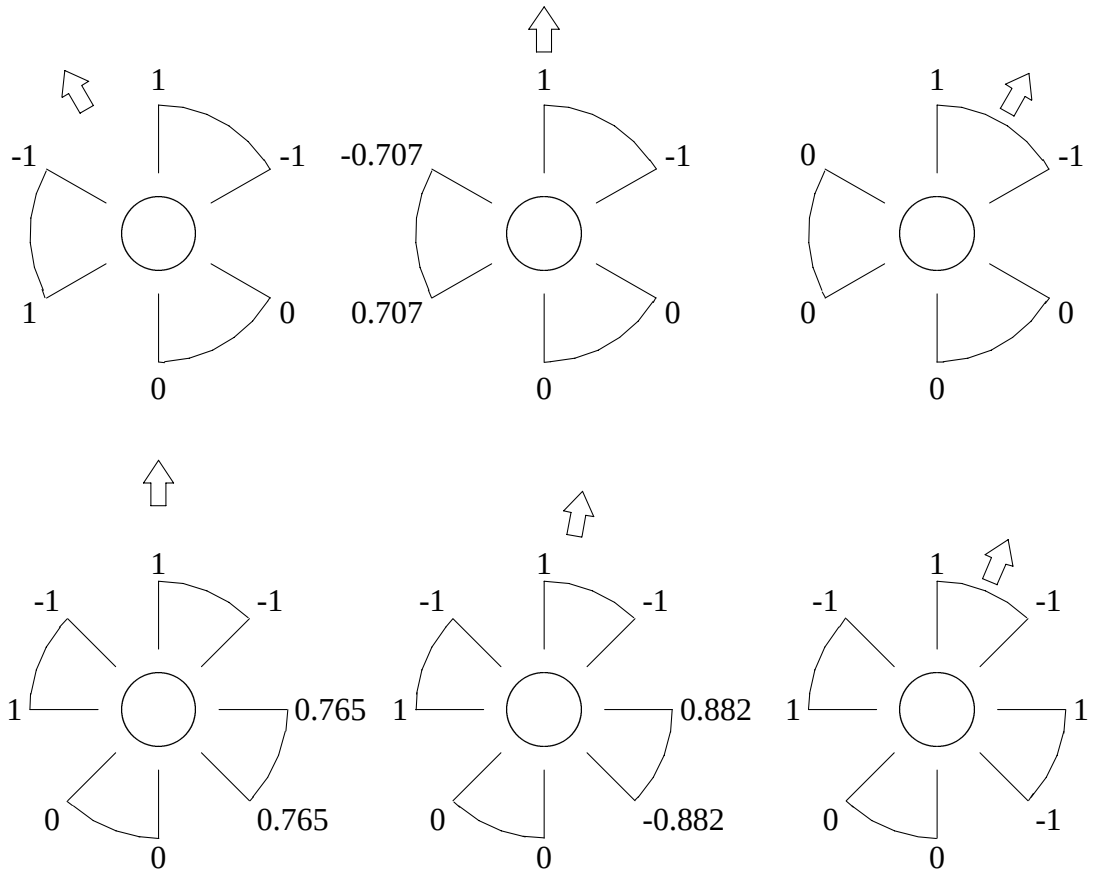

Figure 2.14: Saturation diagrams for radial actuators with horseshoe paired poles.

$22.5°$ (pole bisector orientation). Naturally, since the legs are spaced $45°$ apart, this characterizes the entire polar load capacity. This capacity is illustrated in Figure 2.13.

It is important to note that this analysis depends on the notion that the only constraints on the gap flux densities is that they must be less than the saturation density and that they must satisfy conservation of flux. If the poles of the actuator are organized as horseshoes, either by cutting the stator into magnetically isolated quadrants or by wiring the adjacent coils within quadrants in reverse series, then the gap densities must match (with opposing sign) within each quadrant, as illustrated in Figure 2.14. In this case, the densities can be chosen by setting the quadrant closest to the load line to saturation and then using the adjacent quadrant nearest the load line to correct the force direction. The remaining quadrant fluxes are set to zero. Thus, for a load line within $45°$ of the bisector between adjacent poles of a quadrant, the nearest neighbor quadrant fluxes are chosen according to:

$$1^2 \sin(22.5 + \Phi) - (-1)^2 \sin(22.5 - \Phi) - B(1^2 \sin(67.5 - \Phi) + (-1)^2 \sin(114.5 - \Phi) = 0$$

or,

$$B = \tan \Phi$$

which produces a polar capacity of

$$\overline{f}(\Phi) = \frac{0.9239 B_{\text{sat}}^2 A_g}{\cos \Phi \mu_0}$$

Again, this polar capacity is illustrated in Figure 2.13. The worst case is the on–quadrant orientation where $\Phi = 0$, $B = 0$, and the capacity is $0.9239 B_{\text{sat}}^2 A_g/\mu_0$ while the best case is the between–quadrant orientation where $\Phi = 45°$, $B = 1$, and the capacity is $1.306 B_{\text{sat}}^2 A_g/\mu_0$. Notice that the best case capacity for the horseshoe arrangement is the same as for the more general case, but that the worst case capacity is thirty percent less than for the more general case.

The approach used in analyzing the eight pole radial stator can be easily extended to stators with other *even* multiples of two evenly spaced, equal sized poles. However, the method does not work on stators with *odd* multiples of two evenly spaced legs. The problem is that, with an odd multiple of two, there is an even number of primary (saturated) legs so that these legs automatically satisfy flux conservation. The two control legs must therefore carry the same flux ($B_- = -B_p$) and, since they have the same orthogonal contribution to the direction, it is not possible to use them to correct the load angle. Therefore, more legs must participate.

As an example, consider the six pole stator with evenly spaced, same sized poles. Using the arguments described previously, a line would be drawn orthogonal to the load line. Assuming that the load line does not pass exactly through any of the poles, this would result in three legs on the load side of the line and three on the opposite sign. The two legs on the load side of the line closest to the load line would be assigned alternating saturation. The remaining leg on the load side of the dividing line would be assigned B_+ while its radially opposed leg would be assigned B_-. The remaining legs would be assigned zero flux. Since there are two legs saturated, conservation of flux would require that

$$-1 + 1 + B_+ + B_- = 0 \quad \Rightarrow \quad B_- = -B_+$$

Further, alignment of the bearing force with the specified load direction, Φ, would require that

$$B_+^2 \sin(60 + \Phi) + 1^2 \sin\Phi + (-1)^2 \sin(\Phi - 60) + B_-^2 \sin(\Phi - 120) = 0$$

Using a few trigonometric identities and the prior relationship between B_+ and B_-, this becomes

$$\sin\Phi + \sin(\Phi - 60) = 0$$

This expression is only satisfied at $\Phi = 30°$.

Instead, it turns out that all of the legs will have a non-zero flux density in order to achieve the maximum load capacity for the six pole stator. For instance, consider the case when the load is aligned with one of the poles. In this case, three of the poles can be saturated and the remaining three poles used to satisfy flux conservation. By the symmetry of the problem, the two gaps nearest the dividing line can be assigned the flux density B_1 while the gap opposite the load line can be assigned the flux density B_2. (The pair of gaps *could* be assigned fluxes with opposite sign and still satisfy the directional requirement, but this would greatly increase the flux required in the third pole to satisfy conservation.) Flux conservation requires that

$$(-1) + 1 + (-1) + B_1 + B_2 + B_1 = 0 \quad \Rightarrow \quad 2B_1 + B_2 = 1$$

The total load is

$$\begin{aligned} f &= \frac{A_g B_{\text{sat}}^2}{2\mu_0}\left((-1)^2\cos 60^\circ + 1^2 + (-1)^2\cos 60^\circ - B_1^2\cos 60^\circ - B_2^2 - B_1^2\cos 60^\circ\right) \\ &= \frac{A_g B_{\text{sat}}^2}{2\mu_0}\left(2 - B_1^2 - B_2^2\right) \\ &= \frac{A_g B_{\text{sat}}^2}{2\mu_0}\left(2 - B_1^2 - (1-2B_1)^2\right) \\ &= \frac{A_g B_{\text{sat}}^2}{2\mu_0}\left(1 - 5B_1^2 + 4B_1)\right) \end{aligned}$$

The capacity is maximized by differentiating with respect to B_1 and setting the result to zero:

$$B_1 = 0.4 \quad \Rightarrow \quad B_2 = 0.2$$

The resulting load capacity is

$$\overline{f}(0^\circ) = \frac{0.9 A_g B_{\text{sat}}^2}{\mu_0}$$

In general, the maximal load capacity solution is formulated with the assumption that the two poles closest to the load line are saturated and the remaining legs have densities B_1 through B_4. Flux conservation requires that

$$B_4 = -(B_1 + B_2 + B_3)$$

Alignment requires that

$$\begin{aligned} \sin\Phi + \sin(\Phi - 60) + B_1^2\sin(\Phi - 120) &+ B_2^2\sin(\Phi - 180) + \\ B_3^2\sin(\Phi - 240) &+ B_4^2\sin(\Phi - 300) = 0 \end{aligned}$$

The net force developed is

$$\begin{aligned} f(\Phi) = \frac{A_g B_{\text{sat}}^2}{2\mu_0}\big(&\cos\Phi + \cos(\Phi - 60) + B_1^2\cos(\Phi - 120) \\ &+ B_2^2\cos(\Phi - 180) + B_3^2\cos(\Phi - 240) + B_4^2\cos(\Phi - 300)\big) \end{aligned}$$

A general solution can be formed by substituting the first expression for B_4 into the second expression which represents a constraint. The second expression can then be scaled by a Lagrange multiplier λ and added to the third equation. Solution for λ, B_1, B_2, and B_3 is then obtained by differentiating the augmented load capacity with respect to each of these four variables and equating the resulting expressions to zero. These equations are readily reduced to give $\lambda = \tan(\Phi - 30^\circ)$, two linear equations in the three independent flux densities, and one quadratic equation in the three. The two linear equations can be solved for B_1 and B_2 in terms of B_3 and these results substituted into the last equation to yield a quadratic equation in B_3. This equation is solved for both the minimum and maximum values and each is checked to see if it maximizes the load capacity.

The problem is indeterminate only for $\Phi = 30^\circ$, where $\lambda = 0$: along a pole bisector. In this case, two legs act in the load direction, two legs act orthogonal to the load direction, and two legs act to oppose the load. The first pair are saturated, the last pair are given zero flux, and the middle

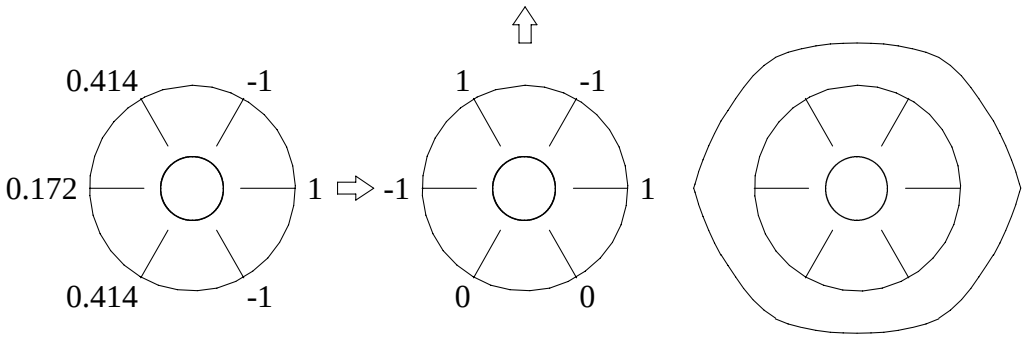

Figure 2.15: Load capacity of the six pole symmetric radial actuator.

pair can be given any flux desired. Continuity with adjacent solutions appears to imply that the two off–axis legs would be saturated. In any case, this orientation produces the worst load capacity of

$$\overline{f}(30^\circ) = \frac{0.866 A_g B_{\text{sat}}^2}{\mu_0}$$

The resulting polar capacity is *nearly* circular, as indicated in Figures 2.13 and 2.15.

2.12.2 Specific Capacity

Drawing on this concept of limiting performance load capacity, it is possible to compute a specific load capacity which is characteristic of a category of stator designs. The specific load capacity is defined for single plane radial stators as the worst orientation load capacity (minimum radius of the polar capacity) divided by the projected area of the journal. The projected area of the journal is simply the length of the journal times its diameter:

$$f_c = \min_{\underline{u}} \frac{\mu_0 \overline{f}(\underline{u})}{B_{\text{sat}}^2 d_j \ell_j} \tag{2.6}$$

As shown in the previous discussion, the load capacity always comes out as a characteristic scale times a product of saturation density and gap area:

$$\min_{\underline{u}} \overline{f}(\underline{u}) = \alpha \frac{A_g B_{\text{sat}}^2}{\mu_0}$$

where the factor α is a property of the stator geometry:

$$\alpha \doteq \min_{\underline{u}} \overline{f}(\underline{u}) \frac{\mu_0}{A_g B_{\text{sat}}^2}$$

Thus,

$$f_c = \frac{\alpha A_g}{d_j \ell_j}$$

For a single plane radial stator with n equal area legs, the area A_g is easily computed if it is postulated that the poles occupy some known percentage of the available circumference. Thus,

Table 2.3: Specific load capacity, symmetric single plane radial stators.

legs	specific capacity			
	general		horseshoe	
	$f_i = 0.5$	$f_i = 0.75$	$f_i = 0.5$	$f_i = 0.75$
3	0.163	0.230	-	-
4	0.177	0.257	-	-
5	0.188	0.276	-	-
6	0.224	0.331	0.194	0.287
7	0.240	0.356	-	-
8	0.235	0.350	0.180	0.268
9	0.236	0.351	-	-
10	0.245	0.365	0.229	0.342
12	0.244	0.364	0.218	0.326
16	0.247	0.369	0.232	0.347
20	0.248	0.371	0.238	0.357
∞	0.250	0.375	0.250	0.375

define the percent iron, f_i, as the ratio between the sum of the arc lengths of the pole faces to the total available circumference:

$$f_i = \frac{n\theta_p(r_j + g)}{2\pi(r_j + g)} = \frac{n\theta_p}{2\pi}$$

This parameter is useful in that it varies from 0 to 1 and has an easily assessed impact on the stator design. Further, for this class of stators, it is easily demonstrated that the factor α depends only upon the number of legs:

$$\alpha = \alpha(n)$$

Having introduced the percent iron, the air gap area *measured at the journal surface* is computed as:

$$A_g = 2r_j\ell_j \cos\left(\frac{\theta_p}{2}\right) = d_j\ell_j \cos\left(\frac{\pi f_i}{n}\right)$$

so that, finally, the specific load capacity becomes

$$f_c = \alpha(n) \cos\left(\frac{\pi f_i}{n}\right)$$

Table 2.3 provides this factor for several symmetric stators with a range of leg numbers assuming either independent gap flux control or a horseshoe arrangement.

To illustrate the use of this figure, assume that a radial actuator is to be designed with a minimum load capacity of 2000 N (450 lb) using material which saturates at 1.6 Tesla. Further, assume that a symmetric geometry having 12 legs is selected, that the iron ratio is selected to be 0.75, and that independent coil control will be used so that arbitrary gap flux distributions can be achieved. For

this geometry, the specific capacity is found in Table 2.3 to be $f_c = 0.364$. Thus, the required load capacity would dicate a journal area of

$$\min_{\underline{u}} \overline{f}(\underline{u}) = \frac{B_{sat}^2 d_j \ell_j f_c}{\mu_0} = \frac{1.6^2 d_j \ell_j 0.364}{4\pi \times 10^{-7}} = 2000 \quad \Rightarrow \quad d_j \ell_j = 26.97 \text{ cm}^2$$

If the journal should be roughly square, then the journal dimensions would be:

$$d_j = \ell_j = \sqrt{26.97} = 5.19 \text{ cm}$$

The journal pressure achieved with this stator is:

$$P_{\min} = \frac{\min_{\underline{u}} \overline{f}(\underline{u})}{d_j \ell_j} = \frac{2000}{0.002697} = 0.74 \text{ MPa} = 107.5 \text{ PSI}$$

For comparison, iron which saturates at 1.6 Tesla can achieve a pressure of $1.6^2/2\mu_0 = 1.02$ MPa $=$ 148 PSI.

The choice of the iron ratio as 0.75 is apparently arbitrary, but it will shortly be demonstrated that increasing the iron ratio reduces the area available for coils and can therefore increase the stator outer diameter. Indeed, given a specific design objective (minimum actuator weight, minimum journal weight, minimum stator diameter, minimum stator length, ...) there is a best choice of iron ratio for each number of legs which is sensitive to the required capacities and the iron saturation density.

Chapter 3

Magnetic Stator Design

Design of actuators proceeds from a collection of performance specifications, primarily governing load capacity, and attempts to minimize some kind of performance index. A principal constraint relates to the thermal performance of the device: the electromagnet coils will generate heat through I^2R or Ohmic losses and these losses must be able to be adequately carried away either by conduction through the stator iron to an external heat sink, by convection to the gas or fluid in which the actuator is immersed, or by radiation to neighboring surfaces. Although a formal treatment of this heat transfer problem can be applied to the design problem, it is more customary to use standard quidelines for sizing the coils to provide adequate heat rejection and then examine the ultimate thermal performance after the design process has made some progress toward a final configuration.

Once the basic configuration of the actuator is selected, most of the actuator geometric parameters are determined in attempt to satisfy the thermal constraint in conjunction with load capacity at magnetic saturation and geometric considerations to preclude premature saturation in the iron structure. The resulting design equations retain as few free variables as can be managed and these are iterated in an effort to optimize the design: find a choice of the free parameters which minimizes the performance index.

3.1 Coil Size

The size of the electromagnet coils is determined by the RMS coil current, expressed in Ampere-turns. The model for the coil currents has the form

$$\underline{I} = \mathcal{C}\hat{\underline{I}} = \mathcal{C}\left\{ \begin{array}{c} K_i^{-1}\underline{f} \\ I_b \end{array} \right\} \tag{3.1}$$

Decompose the coil selection law into that component which relates the currents to the force and that component which relates the currents to the bias:

$$\mathcal{C} = \left[\begin{array}{c|c} \mathcal{C}_f & \mathcal{C}_b \end{array} \right] \quad \Rightarrow \quad \underline{I} = \mathcal{C}_b I_b + \mathcal{C}_f K_i^{-1}\underline{f} \tag{3.2}$$

Finally, limitations on the coil size will be related to the product of coil current and coil turns, so multiply the coil current vector by a matrix whose diagonal terms are the number of turns in each coil:

$$\mathbf{N} = \text{diag}N_i$$

so that

$$\mathbf{N}\underline{I} = \mathbf{N}\mathcal{C}_b I_b + \mathbf{N}\mathcal{C}_f K_i^{-1}\underline{f}$$

Finally, the notation is introduced:

$$\mathcal{I}_b \doteq \mathbf{N}\mathcal{C}_b I_b \quad , \quad [\mathcal{I}_x\ \mathcal{I}_y\ ...] \doteq \mathbf{N}\mathcal{C}_f K_i^{-1}$$

Assume that the force can be written as

$$f_x = f_{x,0} + f_{x,s}\cos\omega t$$

$$f_y = f_{y,0} + f_{y,s}\sin\omega t$$

in which $f_{x,0}$ and $f_{y,0}$ are expected static forces and $f_{x,s}$ and $f_{y,s}$ are expected time varying forces so that coil j has

$$N_j I_j = \mathcal{I}_{b,j} + \mathcal{I}_{x,j}(f_{x,0} + f_{x,s}\cos\omega t) + \mathcal{I}_{y,j}(f_{y,0} + f_{y,s}\sin\omega t)$$

The RMS value is

$$|N_j I_j| = \sqrt{(\mathcal{I}_{b,j} + \mathcal{I}_{x,j}f_{x,0} + \mathcal{I}_{y,j}f_{y,0})^2 + 0.5(\mathcal{I}_{x,j}f_{x,s})^2 + 0.5(\mathcal{I}_{y,j}f_{y,s})^2}$$

Recall that

$$|N_j I_j| \leq f_c J_{\max} A_c$$

where $J_{\max}$ is the maximum copper current density, ≈ 600 A/cm^2 and f_c is the copper factor: ratio of copper area to coil area, ≈ 0.5. This means that

$$A_{c,j} \geq \frac{\sqrt{(\mathcal{I}_{b,j} + \mathcal{I}_{x,j}f_{x,0} + \mathcal{I}_{y,j}f_{y,0})^2 + 0.5(\mathcal{I}_{x,j}f_{x,s})^2 + 0.5(\mathcal{I}_{y,j}f_{y,s})^2}}{f_c J_{\max}}$$

3.2 Six Pole Example

Assume:

- $f_{x,0} = 0 \qquad f_{y,0} = 200\text{N}$
- $f_{x,s} = f_{y,s} = 75\text{N}$

From the examples in Chapter2, the actuator gain for a six pole symmetric stator with independently controlled coils is

$$K_i = \frac{3\mu_0 N^2 A_g I_b}{g_0^2}$$

where the coil selection law was chosen as

$$\mathcal{C} = \begin{bmatrix} 0 & 1 & 1 \\ 0.866 & -0.5 & -1 \\ -0.866 & -0.5 & 1 \\ 0 & 1 & -1 \\ 0.866 & -0.5 & 1 \\ -0.866 & -0.5 & -1 \end{bmatrix}$$

The load capacity of this actuator is given by

$$\min_{\underline{u}} \overline{f}(\underline{u}) = \frac{0.866 B_{sat}^2 A_g}{\mu_0}$$

Assume a saturation density of 1.2 Tesla, so that the capacity is

$$\min_{\underline{u}} \overline{f}(\underline{u}) = \frac{0.8661.2^2 A_g}{\mu_0} = 1.15 \times 10^6 A_g$$

If the gap area is set at $A_g = 0.001\text{m}^2$, then the load capacity is 1145 N. Finally, assume that the nominal gap length is 0.2 mm. This produces an actuator gain of

$$K_i = \frac{3\mu_0 N^2 A_g I_b}{g_0^2} = 0.0942 N^2 I_b$$

The bias current controls the bias flux density:

$$\underline{B_b} = \mathcal{R}^{-1}\mathcal{N}\mathcal{C}_b I_b = \frac{\mu_0 N I_b}{g_0} \left\{ \begin{array}{c} 1 \\ -1 \\ 1 \\ -1 \\ 1 \\ -1 \end{array} \right\}$$

so that the bias current needed to produce a given bias density of B_b is

$$NI_b = \frac{B_b g_0}{\mu_0}$$

The factors $\mathcal{I}_b$, $\mathcal{I}_x$, and $\mathcal{I}_y$ are easily computed as

$$\mathcal{I}_b = 159.15 B_b \left\{ \begin{array}{c} 1 \\ -1 \\ 1 \\ -1 \\ 1 \\ -1 \end{array} \right\} \quad , \quad \mathcal{I}_x = \frac{1}{15.0 B_b} \left\{ \begin{array}{c} 0 \\ 0.866 \\ -0.866 \\ 0 \\ 0.866 \\ -0.866 \end{array} \right\} \quad , \quad \mathcal{I}_y = \frac{1}{15.0 B_b} \left\{ \begin{array}{c} 1 \\ -0.5 \\ -0.5 \\ 1 \\ -0.5 \\ -0.5 \end{array} \right\}$$

The resulting RMS currents and required coil areas are summarized in Table 3.1 for bias flux densities of 0.6 T and 0.3 T. If a bias density of 0.6 Tesla is used, the coils must have a cross sectional area of about 0.4 cm^2. If a lower bias density of 0.3 Tesla is used instead, the coil cross sectional area can be reduced to about 0.31 cm^2.

Table 3.1: RMS coil currents and required coil areas for the six pole stator example.

	$B_b = 0.6$T		$B_b = 0.3$T	
Coil	$\|N_j I_j\|$ RMS (A)	coil area (cm^2)	$\|N_j I_j\|$ RMS (A)	coil area (cm^2)
1	117.6	0.39	92.9	0.31
2	106.7	0.36	70.9	0.24
3	84.6	0.28	28.1	0.09
4	73.5	0.25	12.2	0.04
5	84.6	0.28	28.1	0.09
6	106.7	0.36	70.9	0.24

3.3 Stator Iron Geometry

r_s	stator radius
r_c	coil space radius
r_j	journal radius
r_r	rotor shaft radius
g	air gap length
w	pole width
n_p	number of poles
f_i	iron ratio: $\theta_p n_p / 2\pi$

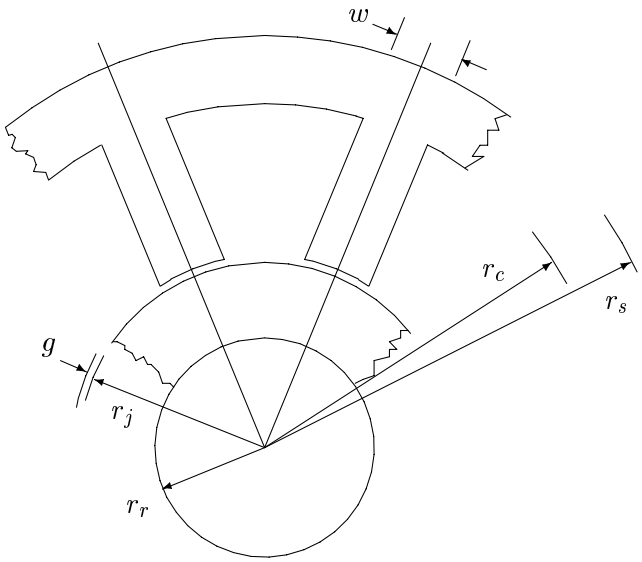

3.4 Geometric Design

Assume that n_p, g, r_r, and f_i are already selected. Decide whether to use flux splitting or not: $\gamma = 0.5$ or 1. Flux splitting is described in Figure 3.1.
Rules:

1. prevent back–iron or journal saturation prior to pole saturation by requiring $r_j - r_r \geq \gamma w$:

$$\begin{aligned} w &= 2(r_j + g)\sin\left(\frac{\pi f_i}{n_p}\right) \\ \Rightarrow \quad r_j - r_r &\geq 2\gamma(r_j + g)\sin\left(\frac{\pi f_i}{n_p}\right) \end{aligned}$$

Thus, computing r_j produces w.

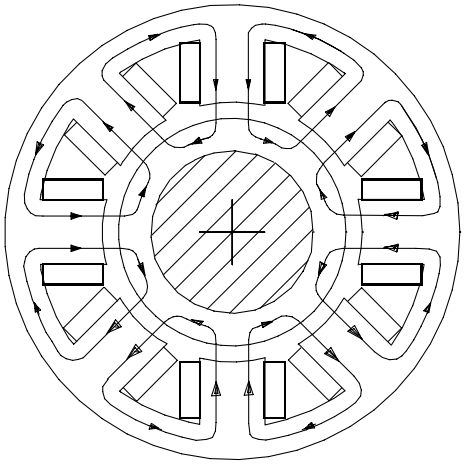

Split flux

- efficient use of iron

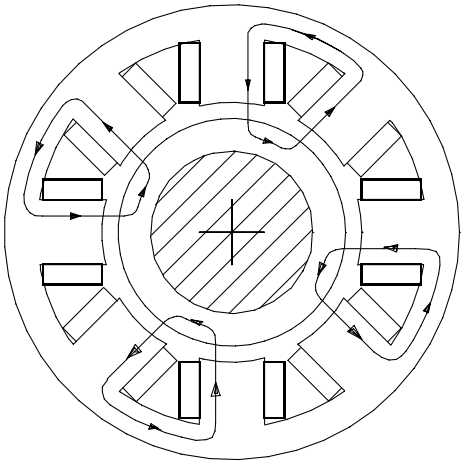

Unsplit flux

- lower rotating losses
- simpler current control

Figure 3.1: Flux splitting.

2. the required A_g can be computed from capacity analysis. Since the preceding computation produced the leg width, the axial length is easily obtained from the gap area:

$$\ell = A_g / w$$

3. match the available coil area, A_v, to the required coil area, A_c: $A_v = \eta A_c$ where $1 \leq \eta \leq 2$. This dictates the radius at the outside of the coil space, r_c. See Figure 3.2.

4. the stator outside diameter is dictated by the coil space radius, leg width, and flux splitting parameter: provide enough back–iron to prevent saturation there.

$$r_s = r_c + \gamma w$$

This approach determines the geometric parameters for symmetric radial stator designs except for the iron ratio f_i, the number of poles n_p, the splitting parameter γ, and the biasing ratio α. Generally, these parameters are chosen iteratively to minimize some performance measure for the actuator. Table 3.2 presents some example criteria along with engineering reasons for selecting the criteria.

Table 3.3 summarizes the free design parameters and indicates each parameter's effect on the design.

3.5 Gap Selection

What controls gap size?

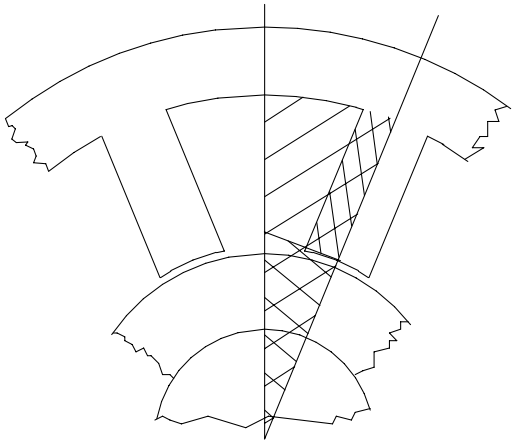

Full Coil Fill

$$r_p \doteq r_j + g$$

$$A_v = \left(r_c^2 \frac{\pi}{n_p} - r_p^2 \tan \frac{\pi}{n_p} - (r_c - r_p)w \right) / 2$$

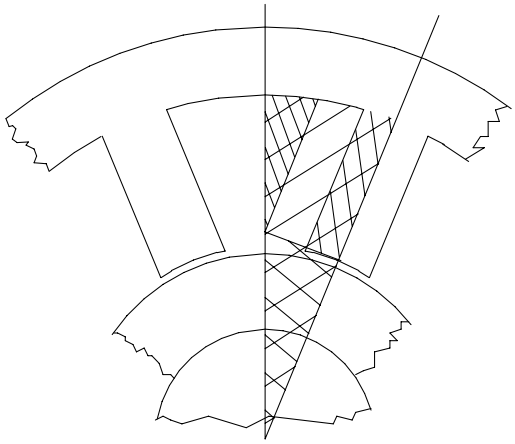

Removable Coils

$$r_p \doteq r_j + g$$

$$A_v = \left[r_p \tan \frac{\pi}{n_p} - \frac{w}{2} \right] (r_c - r_p)$$

Figure 3.2: Coil winding schemes.

Table 3.2: Properties to compute for design comparison.

journal weight, $\pi \rho \ell \left(r_j^2 - r_r^2 \right)$	high weight reduces controllability, rotordynamic performance
journal diameter, $2r_j$	material stress, rotating losses at high RPM: below 2×10^6 DN, ignore
journal length, ℓ	may make shaft longer, degrades rotordynamic performance
stator iron weight + coil weight + journal weight	specific load capacity is capacity/total weight: may be critical
stator axial length with coils	long package can be hard to fit , coil size may require added shaft length

Table 3.3: Free design parameters: symmetric radial actuators.

γ	flux splitting	flux splitting always gives smaller bearings, but higher losses and somewhat more complicated coil current control
n_p	number of poles	generally should increase with increasing shaft size
r_r	rotor shaft radius	usually fixed
f_i	iron ratio	upper limit is based on leakage rules: $2\pi(r_j+g)(1-f_i) > 3g$ lower limit is 0.0 large f_i leads to little space for coils, large stator diameter small f_i leads to unsufficient iron, long axial length
B_{sat}	saturation flux	higher B_{sat} gives more capacity, maybe smaller iron, but need big coils to take advantage of it
α	biasing ratio	up to 0.5: higher gives better slew performance and linearity but increases K_{xx} and coil size

Small gaps:

- require precise machining
- produce sensitivity to thermal/centrifugal growth
- give higher open loop stiffness, stronger variation in K_x with shaft position
- may require high stiffness to prevent excessive rotor motion

Large gaps:

- require require high NI
- produce more flux leakage – more unmodeled magnetic effects

3.5.1 Gap selection: rotordynamics

For rotors, examine the rotordynamics of the shaft/bearing combination: expected rotor response to expected loads, unbalance, ... The gap depends on the bearing dynamic properties which, in turn, depend on size: this implies iteration.

- once journal motions are predicted, use $g \approx 2x_{\max}$
- check K_{xx}, K_{yy}, K_{xy}, K_{yx}: bearing stiffness (closed loop) must be $> 2K_{xx}$.
- open loop stiffnesses too large? make gap larger.
- small journal motion may require high load capacity – high load capacity will mean large K_{xx}: two effects!
- nominal bearing stiffness should be *guided* by $K_b \approx 2f_{cap}/g$

Note: if K_{xx} can't be efficiently made small enough, can use flux feedback in the power amplifiers to eliminate it.

3.6 Example: Six Pole Bearing

Outline:

1. determine load capacity requirements: peak, steady, sinusoidal
2. select bearing configuration
3. use peak capacity to determine required gap area
4. use steady and sinusoidal capacity to determine coil area
5. compute journal diameter, r_j, and pole width, w
6. compute coil space radius to accomodate coil
7. examine solution properties, evaluate design
8. iterate on parameter assumptions

3.6.1 Load capacity, rotor shaft diameter, design parameters

Use something reasonable for capacities, rotor diameter:

- $f_{cap} = 500$ N
- $f_{steady} = 150$ N
- $f_{sinusoidal} = 55$ N
- $r_r = 2$ cm

Initial design parameters:

- iron ratio, $f_i = 0.6$
- gap, $g = 0.2$ mm
- flux splitting? yes: $\gamma = 0.5$
- poles, $n_p = 6$
- saturation flux, B_{sat}: 1.2T
- biasing ratio, $\alpha = 0.5$

3.6.2 Gap area

Use limits from saturation analysis: worst is vertical

$$f_{y,\text{sat}} = \frac{A_g B_{\text{sat}}^2}{2\mu_0}(\sin 60^\circ + \sin 120^\circ) = 500$$

Use $B_{\text{sat}} = 1.2$Tesla.
Solve for gap area:

$$A_g = \frac{2\mu_0 500}{B_{\text{sat}}^2(\sin 60^\circ + \sin 120^\circ)} = 0.000504 \text{ m}^2$$

3.6.3 Find journal radius, pole width

$$r_j - r_r \geq 2\gamma(r_j + g)\sin\left(\frac{\pi f_i}{n_p}\right)$$

$$r_j\left[1 - 2\gamma\sin\left(\frac{\pi f_i}{n_p}\right)\right] \geq r_r + 2\gamma g\sin\left(\frac{\pi f_i}{n_p}\right)$$

$$r_j \geq \frac{r_r + 2\gamma g\sin\left(\frac{\pi f_i}{n_p}\right)}{1 - 2\gamma\sin\left(\frac{\pi f_i}{n_p}\right)} = 2.9 \text{ cm}$$

Use $r_j = 3.0$ cm.

$$w = 2(r_j + g)\sin\left(\frac{\pi f_i}{n_p}\right) = 1.87 \text{ cm}$$

Axial length:

$$\ell = A_g/w = 2.70 \text{ cm}$$

3.6.4 Coil area

From the previous capacity analysis, the dominant term is the biasing, which hasn't changed. Thus, we need about $A_c = 0.4$ cm^2.

Assume a fully packed coil

$$r_p \doteq r_j + g = 3.02 \text{ cm}$$

$$A_v = \left(r_c^2\frac{\pi}{n_p} - r_p^2\tan\frac{\pi}{n_p} - (r_c - r_p)w\right)/2 = 4 \times 10^{-5} \text{ m}^2$$

Solving for r_c gives

$$r_c = 4.21 \text{ cm}$$

Finally, the stator outside dimension is at least

$$r_s \geq r_c + \gamma w = 5.14 \text{ cm}$$

Chapter 4

Power Amplifiers

4.1 Overview

Amplifier purpose:

- controller output will be low power, a voltage proportional to requested current
- actuator input is high power, currents related to desired forces
- amplifier must convert low power controller output signal (voltage) to a high power stator input signal (current)

  this is transconductance operation

General Mechanism:

amplifier regulates flow of energy between a power source and a load

4.1.1 Outline

- Review of components
- Simple Linear Amplifiers, Efficiency
- Regeneration
- Current Sensing
- Stability
- Switching Amplifiers, Efficiency
- Pulse Width Modulation
- Regeneration Revisited
- 3 State Switching
- Flux Feedback
- Other Switching Schemes

4.2 Components

4.2.1 Operational Amplifiers

Linear model:

$$V_a = \gamma\,(V_p - V_m)$$

Characteristics:

$$\gamma = 10^5 - 10^7$$

$$R_m,\ R_p = 10^5 - 10^9\ \Omega$$

Limitations:

$$|I_{out}| < 50 \text{ mA}$$

$$\left|\frac{dV_a}{dt}\right| < 1 - 100\ \text{V}/\mu\text{sec}$$

$$|V_a| < 12 \text{ volts}$$

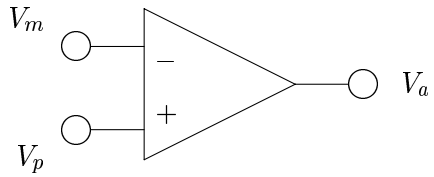

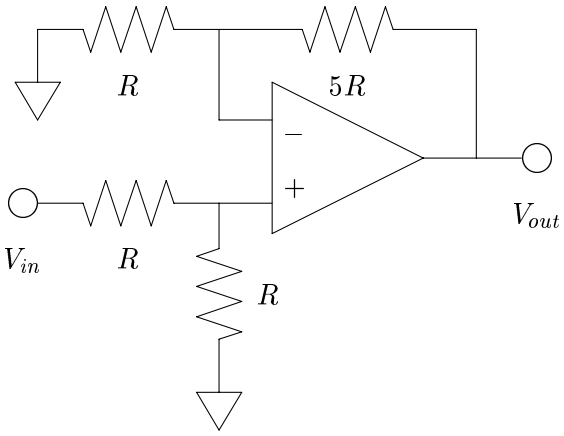

Always used in feedback schemes, op-amp forces circuit response to satisfy $V_m = V_p$.
For circuit shown, $V_{out} = 3V_{in}$.

4.2.2 Output Devices

Bipolar transistor

Linear model:

$$I_c = h_{fe} I_b \qquad V_{be} \approx 0.6 \text{ volts}$$

Switch model:

$$V_{ce} \approx 1 - 3 \text{ volts} \qquad V_{be} > 1 - 2 \text{ volts}$$

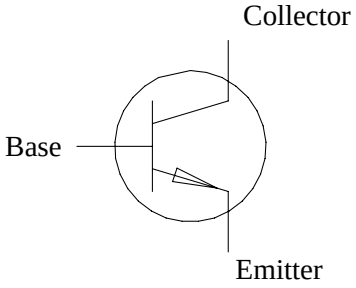

Field effect transistor

Linear model:

$$I_{ds} = g_{fs}(V_{gs} - V_{gst}) \qquad V_{gst} \approx 2 - 4 \text{ volts}$$

Switching model:

$$R_{ds} \approx 0.05 - 1.5 \text{ Ohms} \qquad V_{gs} > 6 \text{ volts}$$

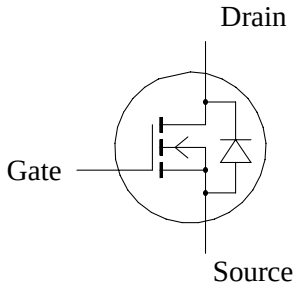

Insulated Gate Bipolar Transistor (IGBT)

Linear model:

$$I_c = g_{fe}(V_{ge} - V_{get}) \qquad V_{get} \approx 4.0 \text{ volts}$$

(similar to an FET) Switch model:

$$V_{ce} \approx 1 - 3 \text{ volts} \qquad V_{ge} > 6 - 10 \text{ volts}$$

(similar to a bipolar transistor)

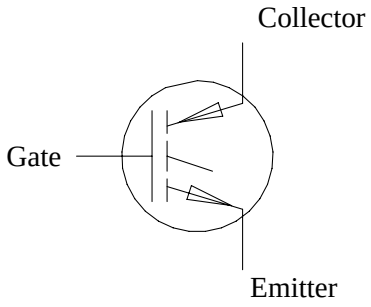

4.3 Linear Amplifier, Monopolar

Transistor model (very simple!):

$$I_c \approx h_{fe} I_b$$

Output voltage:

$$V_{out} = I_e Z_\ell = (1 + h_{fe}) I_b Z_\ell$$

Base current:

$$I_b = \frac{V_{in} - V_b}{R} = \frac{V_{in} - V_{out} - V_{be}}{R}$$

Amplifier voltage gain:

$$V_{out} = \frac{1 + h_{fe}}{R/Z + 1 + h_{fe}} (V_{in} - V_{be})$$

Amplifier current gain:

$$I_{out} = I_e = (1 + h_{fe}) I_b$$

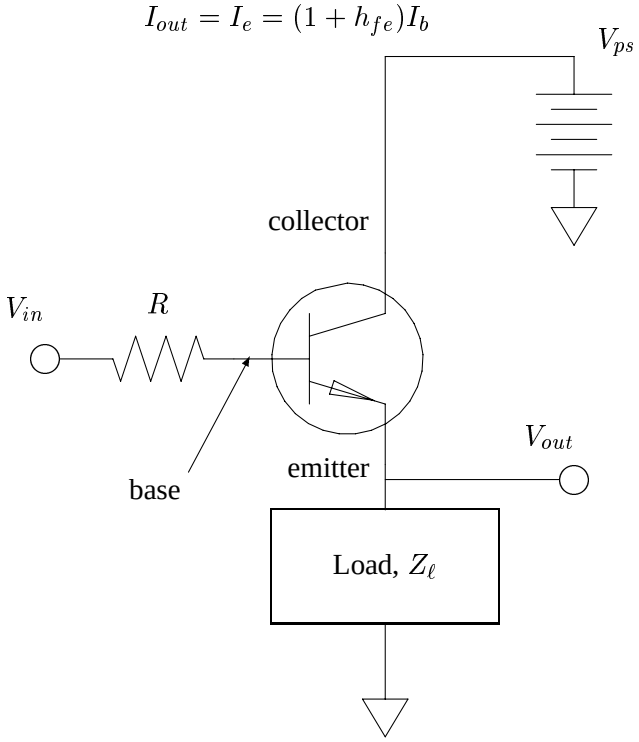

4.3.1 Dissipation

Power is dissipated in this amplifier in both the load and in the output transistor.

The instantaneous load power is

$$W_\ell = V_{out} I_{out} = I_{out}^2 Z_\ell$$

The output transistor power is

$$W_x = (V_{ps} - V_{out}) I_{out}$$

The efficiency of the amplifier is the ratio of power consumed to power delivered:

$$\eta = \frac{1}{T} \int_0^T \frac{W_\ell}{W_x + W_\ell} \, dt = \frac{1}{T} \int_0^T \frac{V_{out} I_{out}}{(V_{ps} - V_{out}) I_{out} + V_{out} I_{out}} \, dt = \frac{\overline{V}_{out}}{V_{ps}}$$

4.3.2 Efficiency Example

Suppose that, in order to accomodate the peak dynamic requirement,

$$V_{ps} = 30 \text{ volts}$$

Further, assume that the load impedance is

$$Z_\ell = 0.033s + 1.62$$

(as in the simple example worked in the last lecture.)

The efficiency of the amplifier at DC under no load condition is computed for the bias current of 0.95 amps:

$$V_{out} = 0.95 \times 1.62 = 1.54 \text{ volts} \quad \Rightarrow \quad \eta = \frac{1.54}{30} = 5.13 \ \%$$

We can only increase electrical efficiency by reducing the power supply voltage, which will reduce the dynamic capacity.

4.4 Monopolar Amplifier Using Feedback

Simple one transistor amplifier gave okay performance:

Amplifier voltage gain:

$$V_{out} = \frac{1 + h_{fe}}{R/Z + 1 + h_{fe}} (V_{in} - V_{be})$$

Amplifier current gain:

$$I_{out} = I_e = (1 + h_{fe}) I_b$$

but it would be nice to get more control over the gain, eliminate the offset, and remove sensitivity to h_{fe} and load impedance.

Op–amp characteristic:

$$V_a = -\gamma V_m$$

Collector current conservation:

$$V_{out} = Z_\ell \left[I_c - \frac{V_{out} - V_m}{R_f} \right]$$

Transistor characteristic:

$$I_c = (1 + h_{fe}) \frac{V_a - (V_{out} + V_{be})}{R_b}$$

Op–amp input impedance:

$$\frac{V_{in} - V_m}{R_i} = -\frac{V_{out} - V_m}{R_f}$$

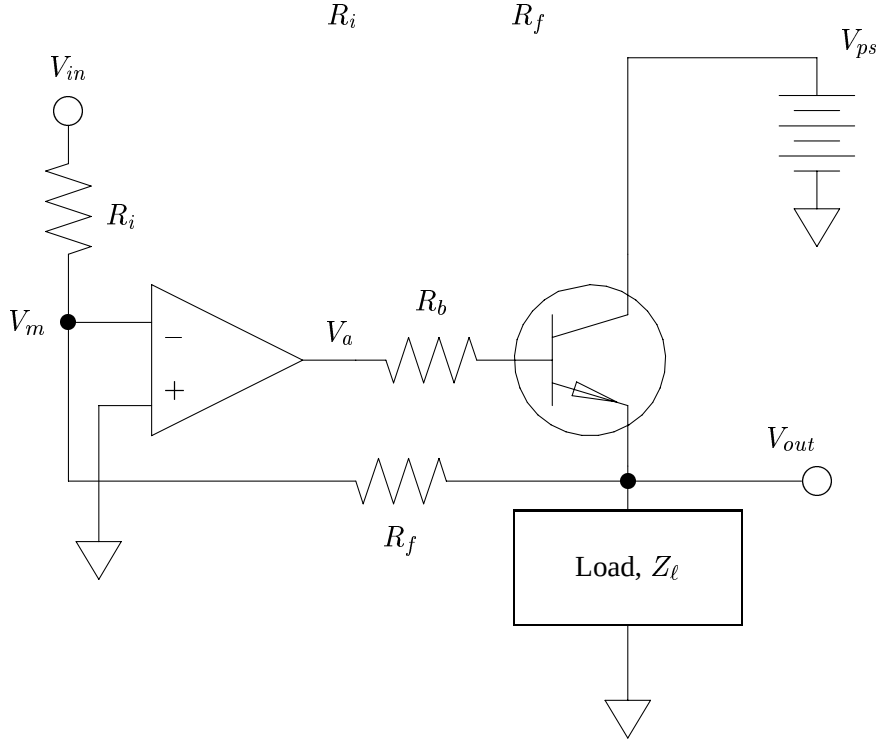

$$V_{out} \left[1 + Z_\ell \left(\frac{1 + h_{fe}}{R_b} + \frac{1}{R_f} + \left[\frac{\gamma(1 + h_{fe})}{R_b} - \frac{1}{R_f} \right] \frac{R_i}{R_i + R_f} \right) \right] =$$

$$- Z_\ell \left[\frac{\gamma(1 + h_{fe})}{R_b} - \frac{1}{R_f} \right] \frac{R_f}{R_f + R_i} V_{in} - Z_\ell \frac{1 + h_{fe}}{R_b} V_{be}$$

In limit as $\gamma \to \infty$:

$$V_{out} = -\frac{R_f}{R_i} V_{in}$$

4.5 Monopolar Amplifier - Transconductance

Current shunt sensor function:

$$V_{out} = I_{load} \frac{R_s R_f}{R_s + R_f} \approx I_{load} R_s$$

Amplifier gain:

$$V_{out} = -\frac{R_f}{R_i} V_{in}$$

Transconductance:

$$I_{load} = -\frac{R_f}{R_i R_s} V_{in}$$

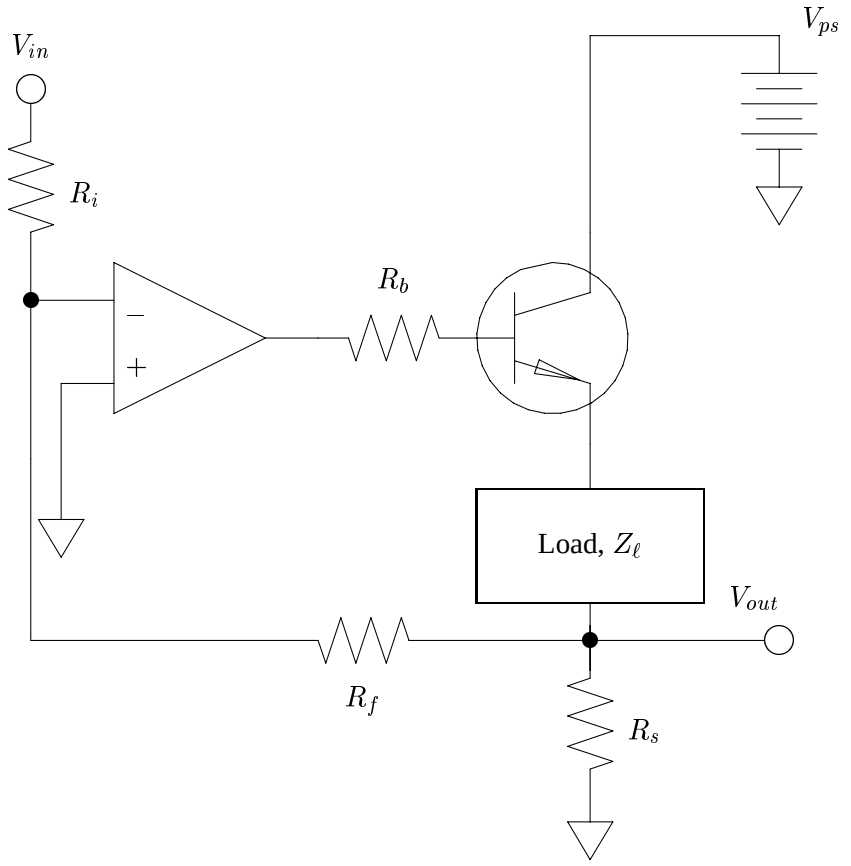

Problem: limited voltage range of op–amp

4.6 Three Transistor Transconductance Amplifier

Additional transistors provide voltage gain.

Transconductance is still

$$I_{load} = -\frac{R_f}{R_i R_s} V_{in}$$

Drawback: amplifier is not regenerative. Can't recapture inductor current, can only dissipate it.

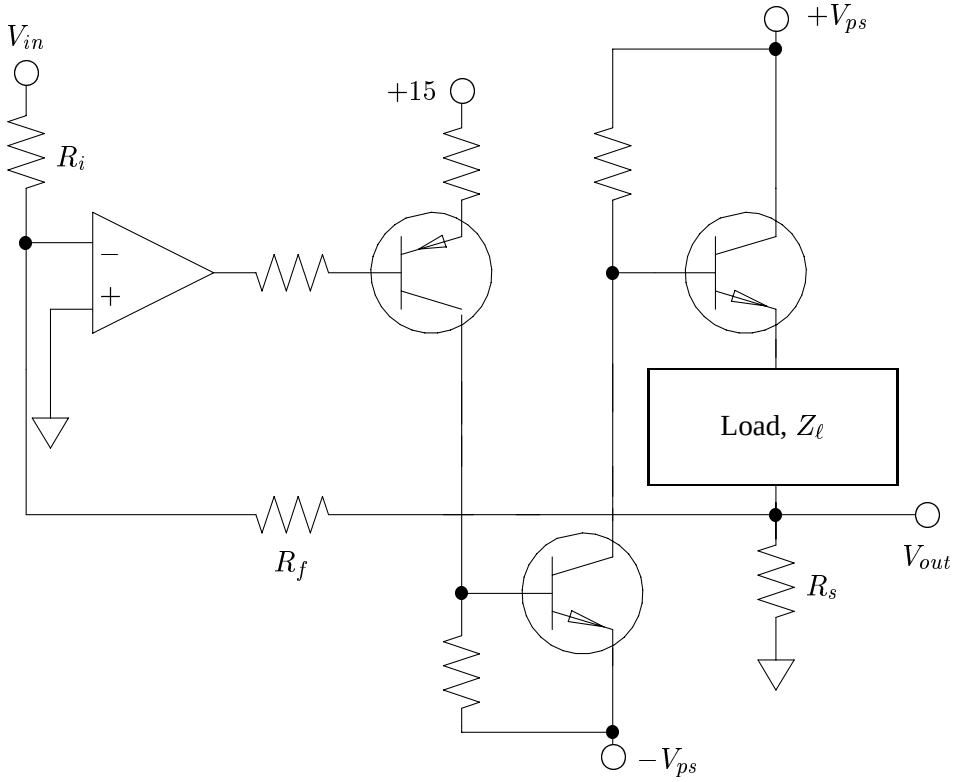

4.6.1 Simplified Model, Inductive Load

Present amplifier:

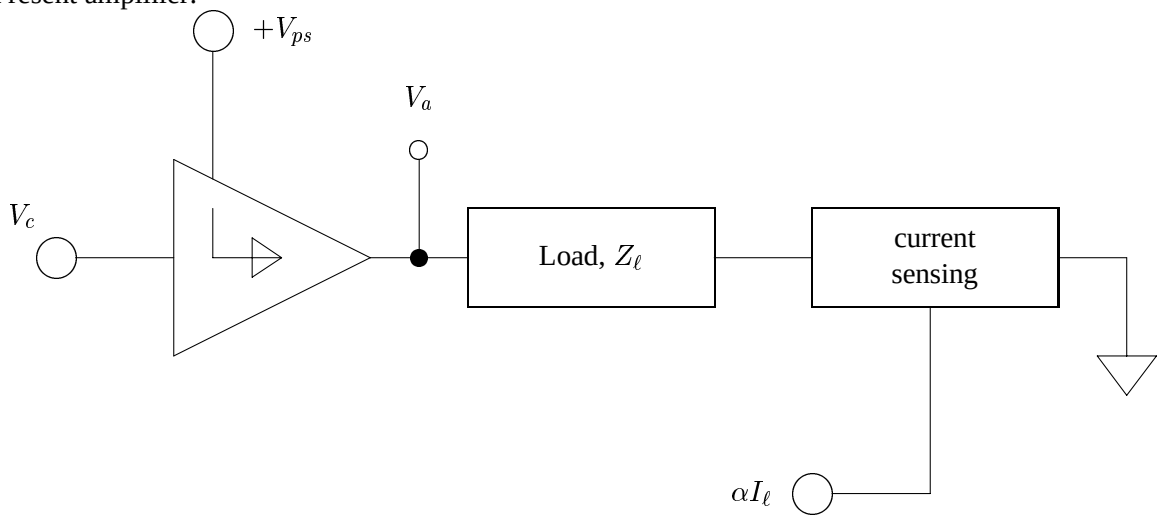

To increase the load current, V_a is made positive.

To decrease the load current, V_a is made negative.

Current is *always* drawn from the power supply, sent through the load, and dumped to ground: no current is ever recovered.

4.6.2 Regenerative Amplifier

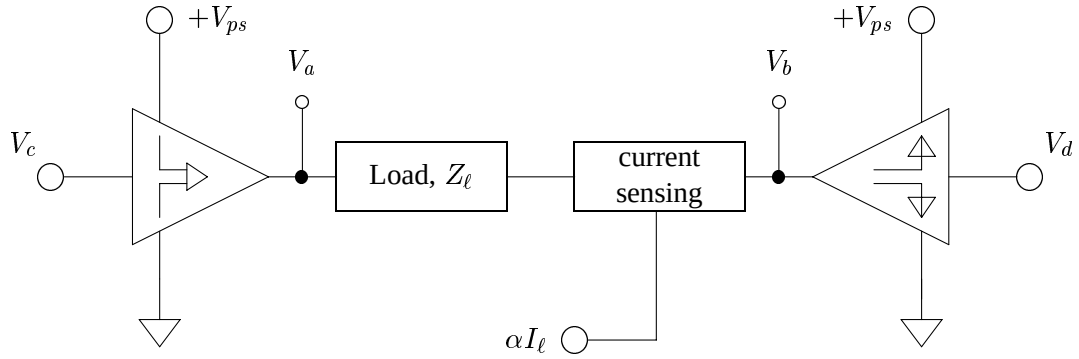

To increase the load current, V_a is made positive, $V_b = 0$.

To decrease the load current, V_b is made positive, $V_a = 0$.

Current is drawn from the power supply when increasing the inductor current, returned to the power supply when decreasing the inductor current.

4.7 Current Sensing

4.7.1 Resistor

Simplest method: resistor as a sensor

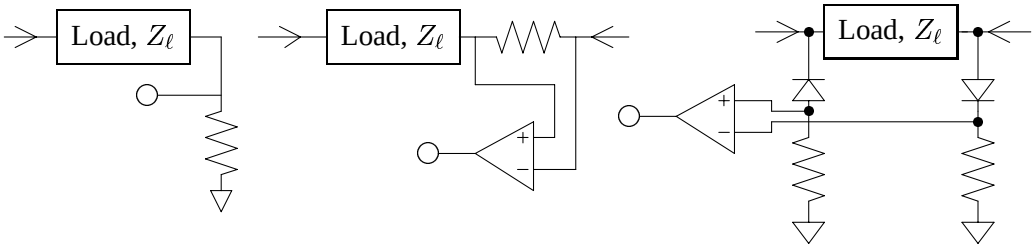

Drawbacks: no isolation from load voltages (can be large), power dissipation in the sense resistor.

4.7.2 Hall Effect Device

Hall effect device senses flux:

$$V_{Hall} = \alpha\Phi$$

Common scheme for measuring currents (works at DC):

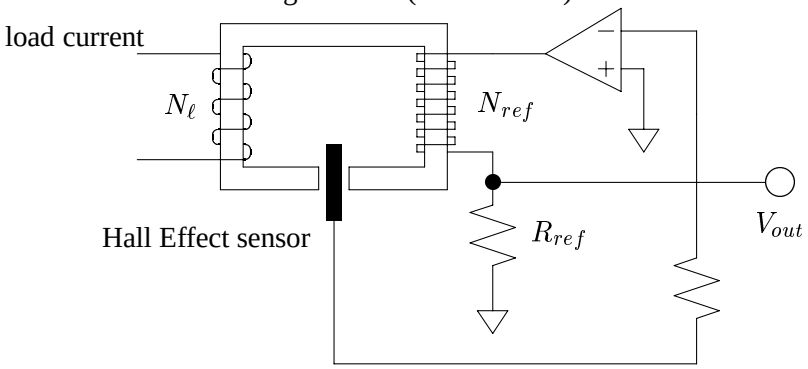

The amplifier modulates the current in the reference coil to make the flux sensed by the Hall Effect sensor be zero.

Thus:

$$N_\ell I_\ell - N_{ref} I_{ref} = 0 \qquad V_{out} = I_{ref} R_{ref} = \frac{R_{ref} N_{ref}}{N_\ell} I_\ell$$

4.8 Stability, Bandwidth

Load model:

$$I(s) = \frac{1}{Ls + R} V(s)$$

Op–amp, transistor stage model:

$$V(s) = -\frac{K}{\tau^2 s + 2\tau\xi s + 1} \left(\frac{R_f V_{in}(s)}{R_i + R_f} + \frac{R_s R_i I(s)}{R_i + R_f} \right)$$

Closed loop model:

$$\frac{I(s)}{V_{in}(s)} = \frac{-K}{(\tau^2 s + 2\tau\xi s + 1)(Ls + R)(R_f / R_s R_i + 1/R_s) + K} \frac{R_f}{R_i R_s}$$

Apparently,

$$\lim_{K \to \infty} \frac{I(s)}{V_{in}(s)} = \frac{R_f}{R_i R_s}$$

Unfortunately, K is limited by stability considerations. Generally, K is chosen to provide an acceptable damping ratio in the closed loop performance.

4.9 General Characteristics

- maximum current: determined by output device capacity
- maximum voltage: device capacity, power supply voltage
- bandwidth: load characteristics, bandwidth of transistor stage
- efficiency: $\eta \approx \overline{V_{out}} / V_{ps}$

Choice of output devices:

high voltage, moderate current: use power FET: low on resistance relative to load

moderate voltage, high currents: use IGBT's: low saturation voltage

4.10 Switching Amplifiers

4.10.1 General Idea of Switching

With a linear amplifier, the voltage across the load varies continuously:

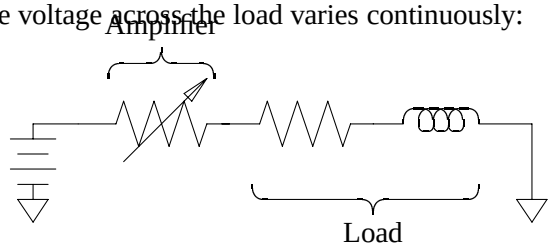

With a switching amplifier, the voltage across the load is either $+V_{ps}$ or $-V_{ps}$:

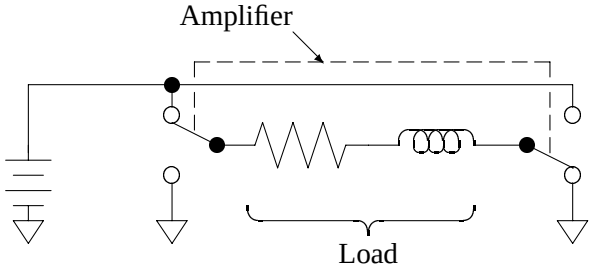

4.10.2 Character of the Switch

For field effect transistors, we can model the switch as:

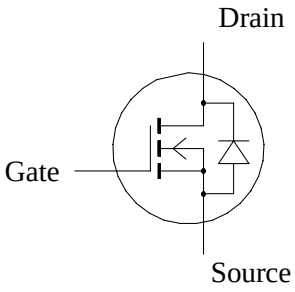

- time between "on" and "off" transitions is t_s
- when "off": no current is conducted
- when "on": device resistance is fixed at R_{on}
- transition from "off" to "on" is:
  - fixed duration, t_r
  - voltage and current vary linearly during transition

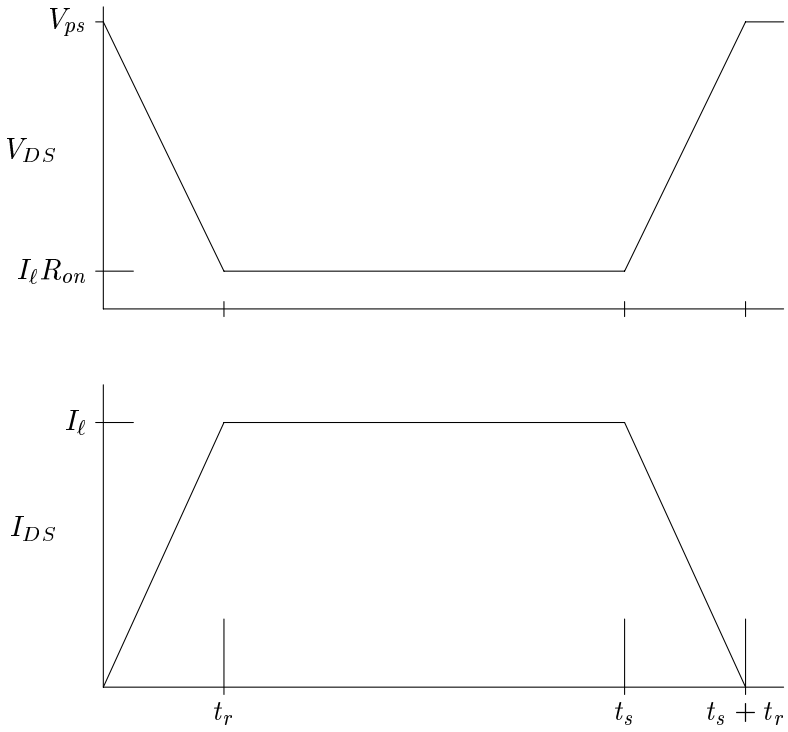

4.10.3 Switching: Duty Cycle

It is common to design the switching *algorithm* so that a pair of transitions occurs every τ seconds (microseconds!)

The *duty cycle* is the percent time spent in the "on" state:

$$t_s = \delta\tau$$

Note: the load is controlled by 4 switches. Two are on while the other two are off. This means that the duty cycle refers to percent time of positive load voltage.

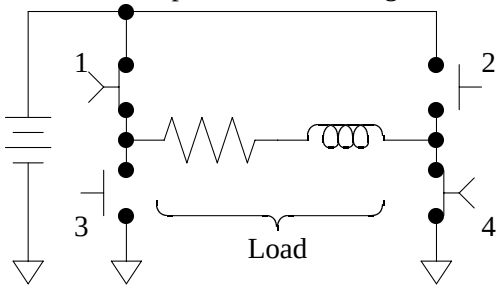

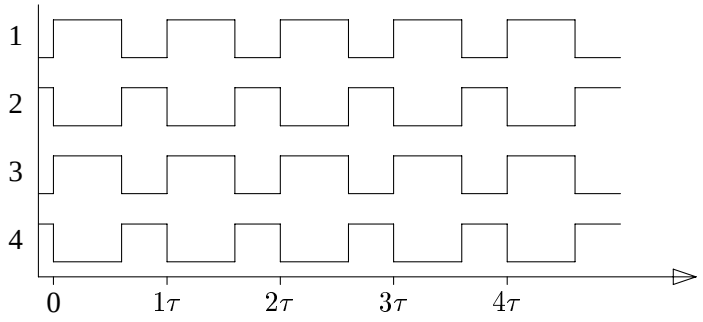

4.10.4 Average Voltage

Assuming that the switch is ideal (ignore t_r, R_{on}) the average voltage drop across the load during one full cycle is:

$$V_{avg} = \frac{1}{\tau}\left(\delta\tau V_{ps} + (1-\delta)\tau(-V_{ps})\right) = (2\delta - 1)V_{ps} \quad : \quad 0 < \delta < 1$$

So the average applied voltage varies continuously between $-V_{ps}$ and $+V_{ps}$.

4.10.5 Average Current

For an inductive load, switching produces a current noise:

$$I = I_0 + \frac{1}{L}\int_0^t V(t)dt = \begin{cases} I_0 + \frac{1}{L}V_{ps}t : & 0 < t < \delta\tau \\ I_0 + \frac{2}{L}V_{ps}\delta\tau - \frac{1}{L}V_{ps}t : & \delta\tau < t < \tau \end{cases}$$

Average current is incremented or decremented by δ:

$$I_{avg} = \frac{1}{\tau}\int_0^\tau I(t)dt = I_0 + \frac{V_{ps}}{L}(2\delta - 1)$$

4.10.6 Switching Waveform

Assume the example:

- bias: $I_b = 0.95$ amps
- power supply: $V_{ps} = 30$ volts
- coil resistance: $R_c = 1.62\Omega$
- coil inductance: $L = 33$ mH

Amplifier properties:

- switching rate, $f_s = 25$ kHz,
  $\tau = 40$ μsec
- output device, $R_{on} = 0.05\Omega$.

Waveform:

$$\frac{dI}{dt} + \frac{R_c + R_{on}}{L} I = \frac{1}{L} V$$

$$\Rightarrow \quad \frac{dI}{dt} + 50.61 I = \pm 909.1$$

at steady state,

$$V_{avg} = I_b(R_c + R_{on}) = 1.59 \;\Rightarrow\; \delta = 0.526$$

$$I(t) = \min \left\{ \begin{array}{l} 0.941 + 17.023 \left(1 - e^{-50.6t}\right) \\ \\ 0.979 - 18.943 \left(1 - e^{-50.6t}\right) \end{array} \right\}$$

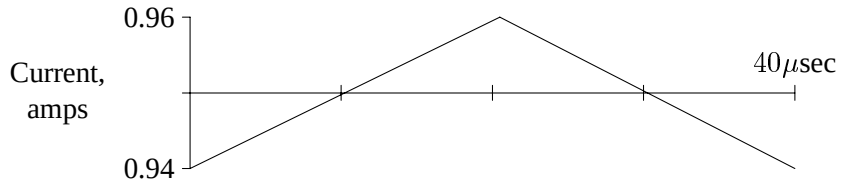

4.10.7 Power Dissipation

Energy is dissipated during transition and during the "on" state:

Transition energy:

$$W_t = \frac{V_{ps} I_\ell + 2 I_\ell^2 R_{on}}{6} t_r$$

"On" state energy:

$$W_{on} = I_\ell^2 R_{on} (\delta\tau - t_r)$$

Total power/cycle (two transitions):

$$W_{cycle} = \frac{V_{ps} I_\ell - I_\ell^2 R_{on}}{3} t_r + I_\ell^2 R_{on} \delta\tau$$

Power:

$$P = \frac{W_{cycle}}{\tau} = \frac{V_{ps} I_\ell - I_\ell^2 R_{on}}{3} f_s t_r + I_\ell^2 R_{on} \delta$$

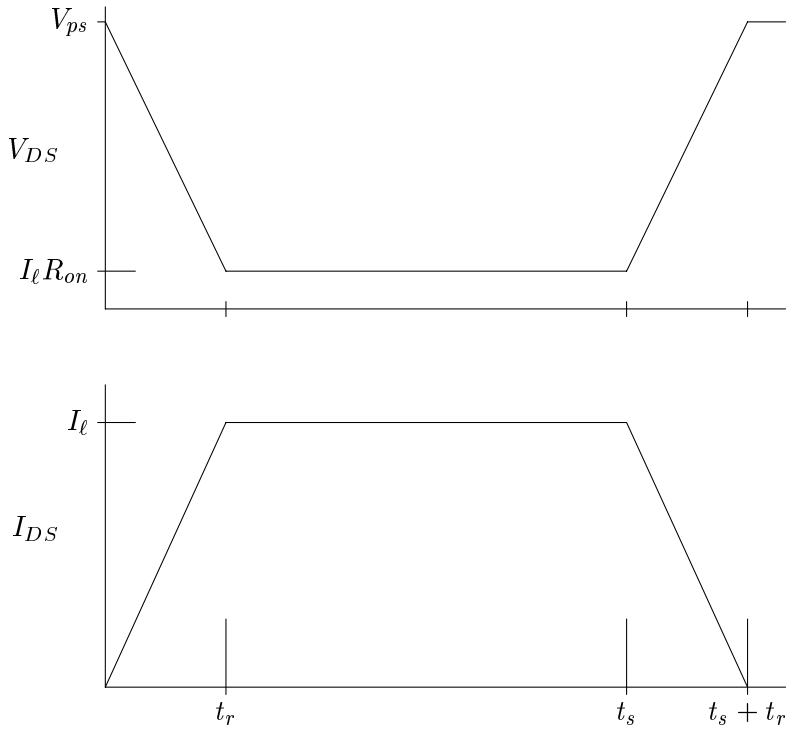

4.10.8 Efficiency

The efficiency is the ratio of power delivered to power consumed. Previously, it was shown that each device in the H bridge consumes

$$P_x = \frac{V_{ps} I_\ell - I_\ell^2 R_{on}}{3} f_s t_r + I_\ell^2 R_{on} \delta$$

Since half of the devices have a duty cycle of δ and the other half have a duty cycle of $1 - \delta$, the total power consumed by the bridge is

$$P_b = \frac{4V_{ps} I_\ell - 4I_\ell^2 R_{on}}{3} f_s t_r + 2I_\ell^2 R_{on}$$

The power delivered to the load is (for constant I_ℓ):

$$P_\ell = I_\ell^2 R_c$$

Let the "on" resistance be $R_{on} = \rho R_c$ so that

$$\eta = \frac{1}{\frac{4}{3}\left[\frac{V_{ps}}{I_\ell R_c} - \rho\right] f_s t_r + (1 + 2\rho)}$$

4.10.9 Efficiency Examples

Consider the simple bearing design developed previously:

$$V_{ps} = 30\text{V} \quad I_\ell = 0.95\text{A} \quad R_c = 1.62\Omega \quad f_s = 25\text{kHz}$$

Example 1:

$$R_{on} = 0.0\Omega$$

$$t_r = 0\text{nsec}$$

$$\eta = 100 \text{ percent}$$

Example 2:

$$R_{on} = 0.05\Omega$$

$$t_r = 50\text{nsec}$$

$$\eta = 91.5 \text{ percent}$$

Example 3:

$$R_{on} = 0.05\Omega$$

$$t_r = 100\text{nsec}$$

$$\eta = 88.9 \text{ percent}$$

Example 4:

$$R_{on} = 0.025\Omega$$

$$t_r = 100\text{nsec}$$

$$\eta = 91.6 \text{ percent}$$

4.11 Transconductance Models

Two approaches:

- Use linear model, treat switching amplifier as voltage gain element

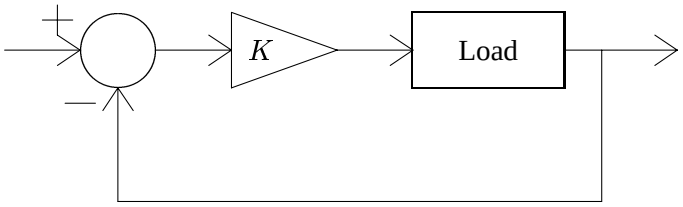

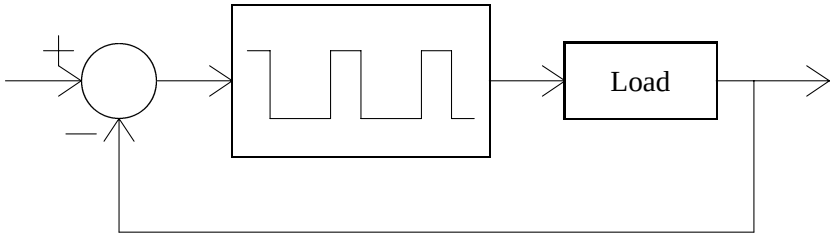

- Treat feedback loop as non-linear, no open–loop model for switching element

4.11.1 Pulse Width Modulation

From prior analysis, we know that the output voltage, averaged over one cycle, is

$$V_{avg} = (2\delta - 1)V_{ps}$$

Thus, if the duty cycle is made proportional to an input voltage:

$$\delta = 0.5 + \frac{K}{2V_{ps}}V_{in}$$

then the amplifier has a defined gain:

$$V_{avg} = KV_{in}$$

This mechanism of varying the duty cycle (pulse width) in proportion to the input voltage is called **P**ulse **W**idth **M**odulation or PWM.

Commonest method of implementing: Input signal is compared to a triangle wave of amplitude A_t and frequency f_s. Output state is determined by the sign of the sum:

$$V_l = V_{ps}\ \text{sign}\left(V_{in} - A_t\Delta(t)\right) \qquad \Delta(t) = \begin{cases} 1 - 4t/\tau & : 0 < t < 0.5\tau \\ 4t/\tau - 3 & : 0.5\tau < t < \tau \end{cases}$$

PWM:

$$V_l = V_{ps}\ \text{sign}\left(V_{in} - A_t\Delta(t)\right) \qquad \Delta(t) = \begin{cases} 1 - 4t/\tau & : 0 < t < 0.5\tau \\ 4t/\tau - 3 & : 0.5\tau < t < \tau \end{cases}$$

For a constant input, V_{in}, the resulting switching decisions occur at:

$$t_{\uparrow} = \frac{\tau}{4}\left(1 - \frac{V_{in}}{A_t}\right) \qquad t_{\downarrow} = \frac{\tau}{4}\left(3 + \frac{V_{in}}{A_t}\right)$$

so the duty cycle is

$$\delta = \frac{t_{\downarrow} - t_{\uparrow}}{\tau} = 0.5\left(1 + \frac{V_{in}}{A_t}\right)$$

and the amplifier gain is

$$K = \frac{V_{ps}}{A_t}$$

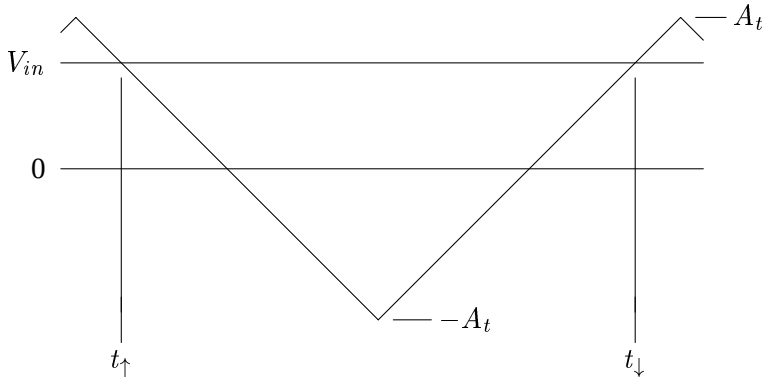

4.11.2 PWM Bandwidth

The load model is

$$I_\ell = \frac{1}{sL + R} V_\ell$$

and the (simplified) amplifier model is

$$V_\ell = \frac{V_{ps}}{A_t}(I_{ref} - I_\ell)$$

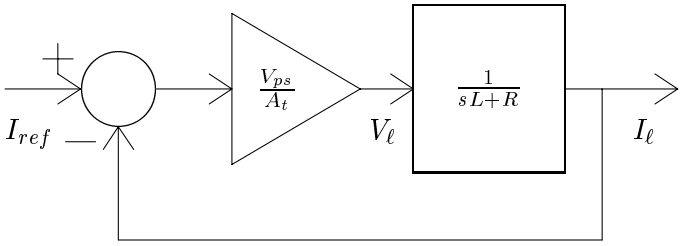

This means that the closed loop transfer function is (solve for I_ℓ in terms of I_{ref})

$$I_\ell = \frac{V_{ps}}{(sL + R)A_t + V_{ps}} I_{ref}$$

The bandwidth occurs where

$$2\pi f_{bw} L A_t = R A_t + V_{ps} \quad \Rightarrow \quad f_{bw} = \frac{R}{2\pi L} + \frac{V_{ps}}{2\pi A_t L}$$

Switching can track the input as long as

$$\frac{d}{dt} A_t \Delta(2\pi t f_s) > \frac{d}{dt}(I_{ref} - I_\ell) \approx \frac{V_{ps}}{L}$$

so that

$$4A_t f_s > \frac{V_{ps}}{L} \quad \Rightarrow \quad A_t > \frac{V_{ps}}{4Lf_s}$$

This suggests an upper limit on the bandwidth of

$$f_{bw,\max} = \frac{4f_s}{2\pi}$$

By Shannon's sampling theorem, more reasonable to expect a usable bandwidth of

$$f_{bw,\max} \approx 0.2 f_s$$

4.11.3 Regeneration

- Positive current
  - Increasing inductor current

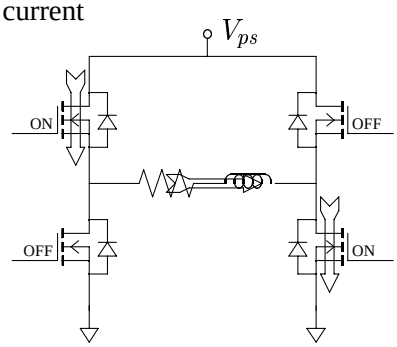

  - Decreasing inductor current

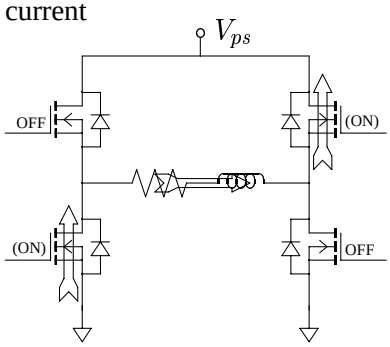

- Negative current
  - Increasing inductor current

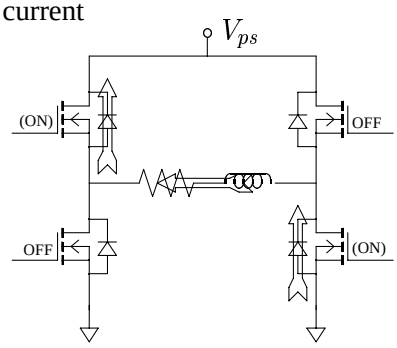

– Decreasing inductor current

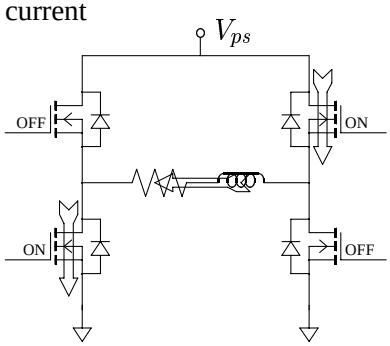

4.12 Power Supply Requirements

Because the amplifier is regenerative, the power supply only has to provide the *average* power: the peaks are delivered by capacitors. Further, the switching mechanism functions as a DC/DC converter: the actual (average) current drawn from the power supply is determined by amplifier efficiency:

$$P_{ps} = V_{ps} I_{avg,ps} = \frac{1}{\eta} I_{avg}^2 R_c$$

so that

$$I_{avg,ps} = \frac{I_{avg}^2 R_c}{\eta V_{ps}} = I_{avg} \frac{V_{avg}}{\eta V_{ps}}$$

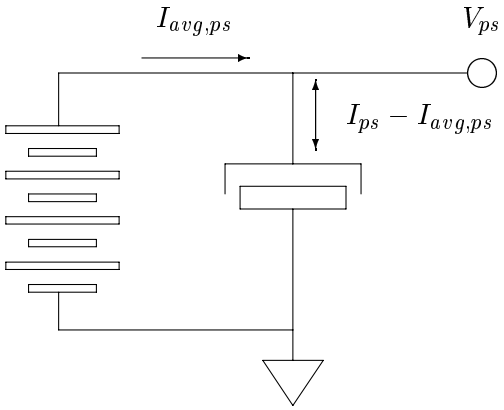

For example, let $R_c = 1.62\Omega$, $V_{ps} = 30$ volts, $I_{avg} = 0.95$ amps, and $\eta = 0.9$:

$$I_{avg,ps} = 54 \text{ mA !}$$

4.13 3–State Output

The H bridge can be controlled to generate a third state where the voltage drop across the load is zero. The advantage is that the load ripple current is much smaller when the load current is changing slowly.

State 1: $I_\ell \uparrow$ State 2: $I_\ell \downarrow$ State 3: $dI/dt \approx 0$

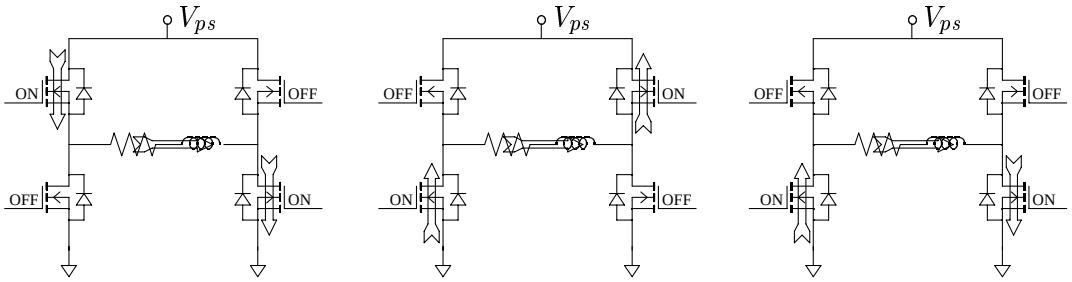

Voltage and current waveforms (constant positive input voltage, $sL + R$ load)

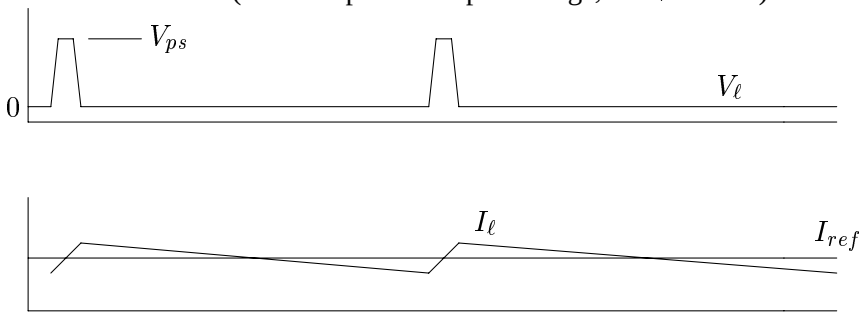

4.13.1 3–State PWM

3–state switching is fairly simple to control. The logic:

- the left and right halves of the bridge are controlled separately
- in each half, either the top or the bottom transistor is on: never both and never neither
- if the input voltage is positive, the output can be increased by turning on the top left transistor (#1).
- if the input voltage is negative, the output can be decreased by turning on the top right transistor (#2).

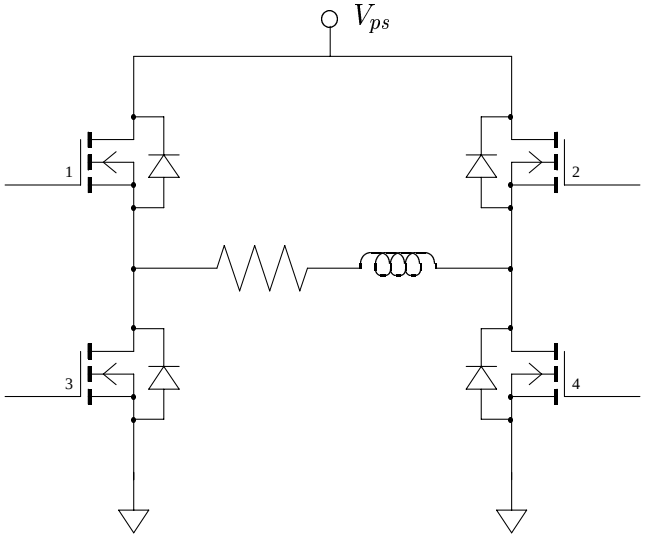

4.13.2 Monopolar PWM Pair

Each half of the bridge is controlled as a monopolar PWM amplifier:

- input signal is compared to triangle wave
  - left half: 0 to A_t
  - right half: $-A_t$ to 0
  - triangle waves are sychronized
- top transistor state determined by sign of difference

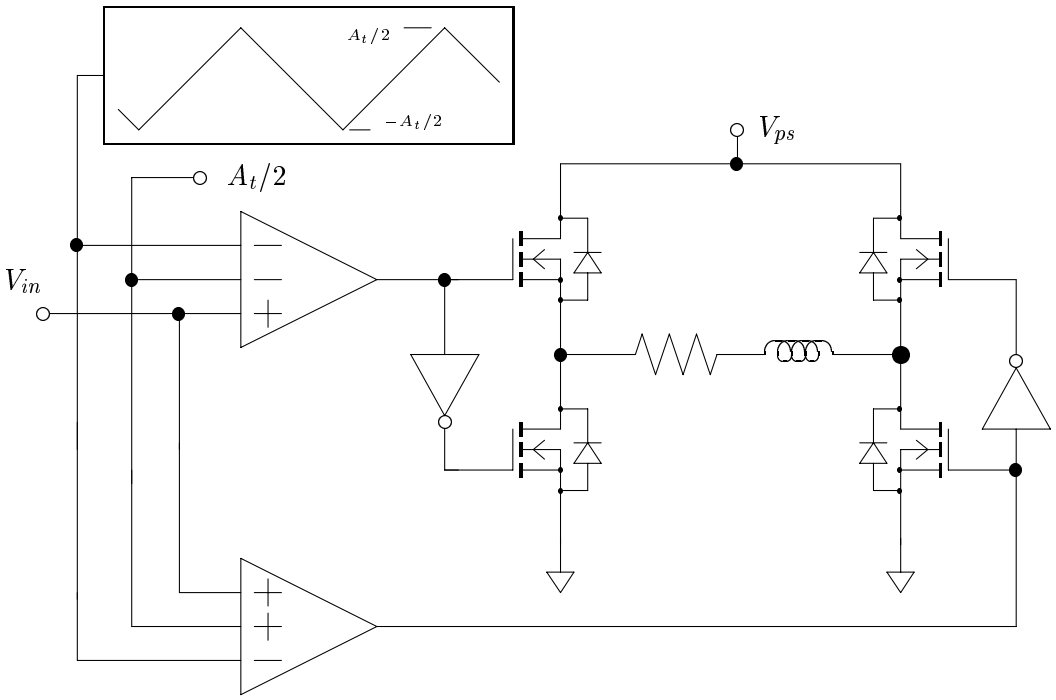

4.13.3 Comparison of 2- and 3-State PWM

amplifier/load properties:

$V_{ps} = 50$ volts

$R = 1.62\Omega$

$L = 33$ mH

$f_s = 25$ kHz

reference signal:

$0.95 + 0.1 \sin 500\pi t$

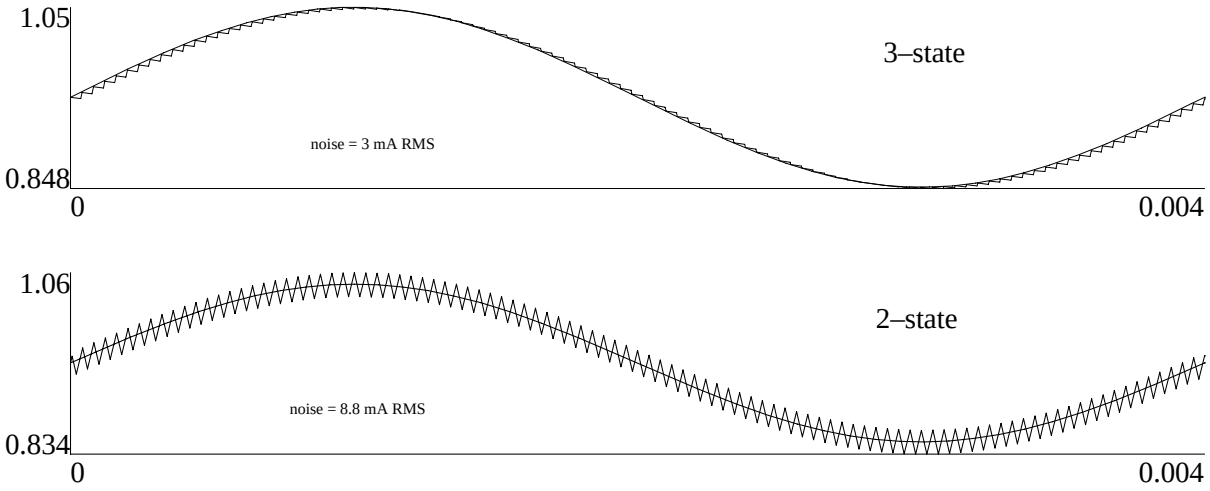

Same Comparison at DC

amplifier/load properties:

$V_{ps} = 50$ volts

$R = 1.62\Omega$

$L = 33$ mH

$f_s = 25$ kHz

reference signal:

0.95

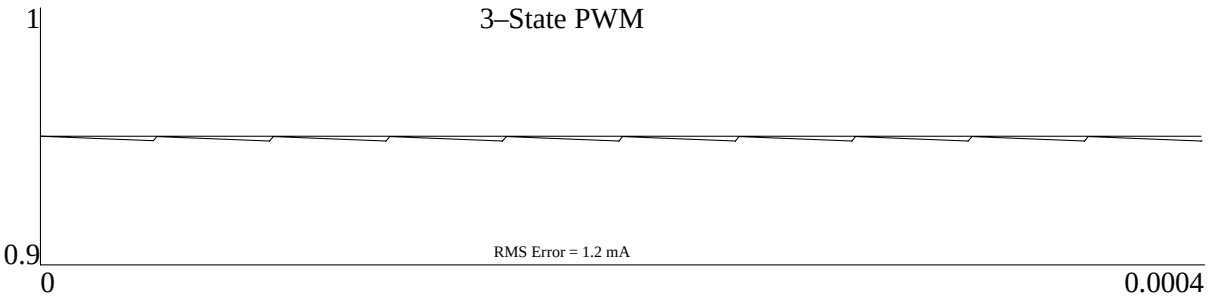

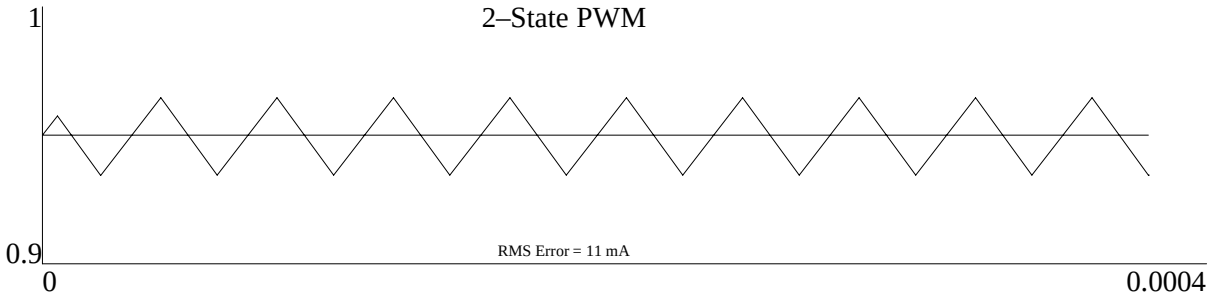

Another Comparison of 2- and 3-State PWM amplifier/load properties:

$V_{ps} = 100$ volts

$R = 0.95\Omega$

$L = 8.3$ mH

$f_s = 25$ kHz

reference signal:

$0.95 + 0.1 \sin 500\pi t$

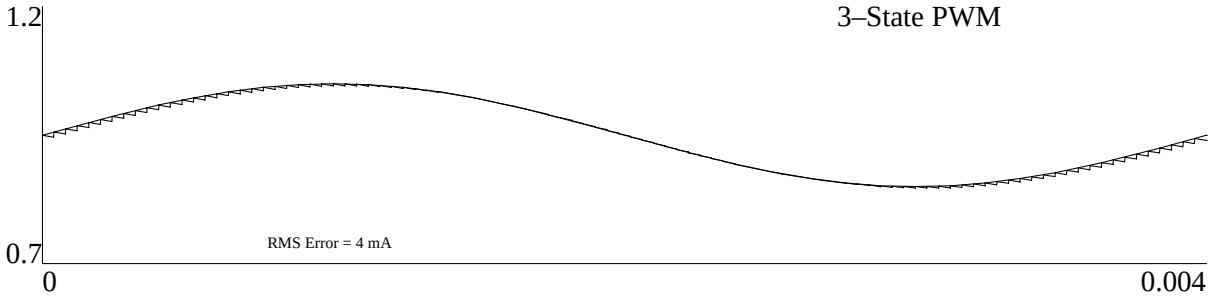

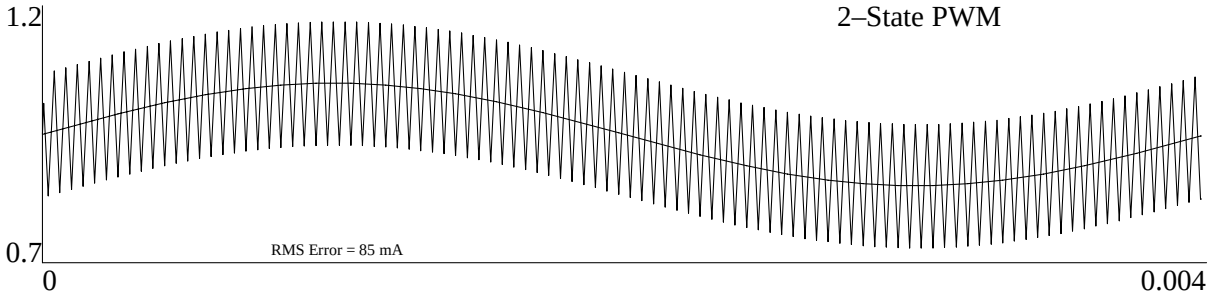

A Final Comparison of 2- and 3-State PWM amplifier/load properties:

$V_{ps} = 200$ volts

$R = 0.95\Omega$

$L = 8.3$ mH

$f_s = 25$ kHz

reference signal:

$0.95 + 0.1 \sin 500\pi t$

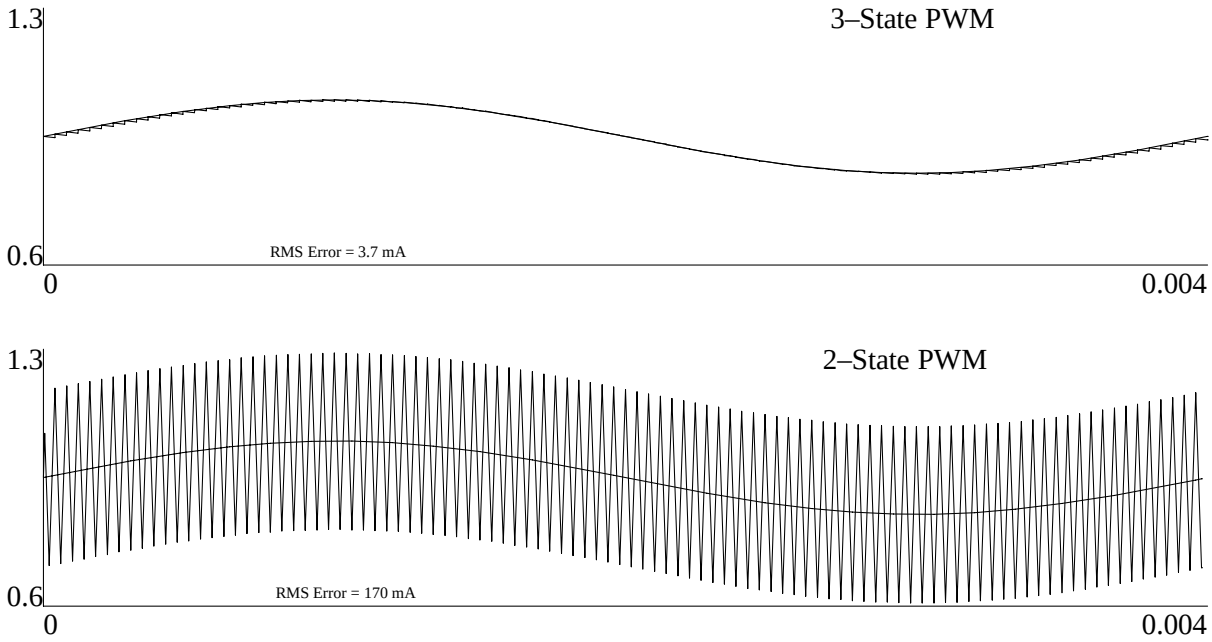

4.14 Current Feedback

Recall the force generated by the simple two horseshoe bearing:

$$f = \frac{1}{\mu_o} A_g \left(B_1^2 - B_2^2 \right)$$

We recast this in terms of the coil currents using

$$B_i = \frac{\mu_0 N I_i}{2g(x) + \ell_{iron}/\mu_r} = \frac{\mu_0 N I_i}{2(g_0 \pm x)}$$

to get

$$f = \frac{\mu_0 N^2 A_g}{2} \left(\frac{I_1^2}{(g_0 - x)^2} - \frac{I_2^2}{(g_0 + x)^2} \right) \qquad \begin{array}{l} I_1 = \max(I_b + i_p, 0) \\ I_2 = \max(I_b - i_p, 0) \end{array} \qquad f \approx K_i i_p - K_x x$$

We control the current by closing a feedback loop in the amplifier which forces the bearing currents to track a request (from the controller)

4.15 Flux Feedback: Why?

Current feedback problems:

- the relationship between force and current depends upon the magnetic properties of the material: saturation, eddy currents, hysteresis, ...
- journal motion produces back-emf which must be overcome by the transconductance amplifier
- open–loop stiffness is destabilizing

With flux linearization:

$$B_1 = B_b + B_p \quad B_2 = B_b - B_p$$

the force–to flux law does not include magnetic properties and has no open–loop stiffness:

$$f = \frac{4}{\mu_o} A_g B_b B_p$$

So, if the amplifier can control the flux directly, sensitivity to gap and $B - H$ effects is eliminated.

4.16 General Amplifier Scheme

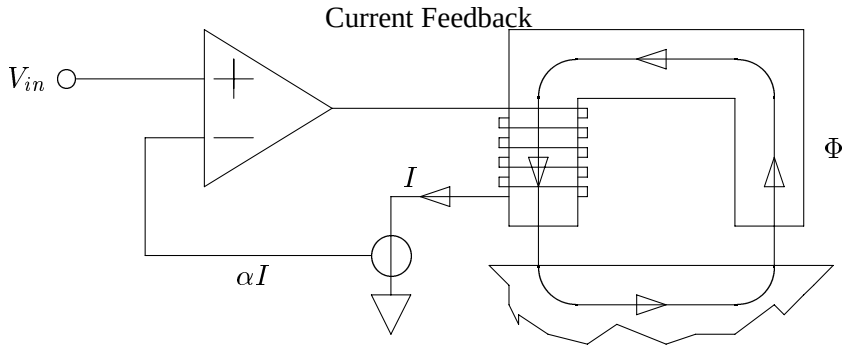

$$I = \frac{V_{in}}{\alpha}$$

Requires a current sensor

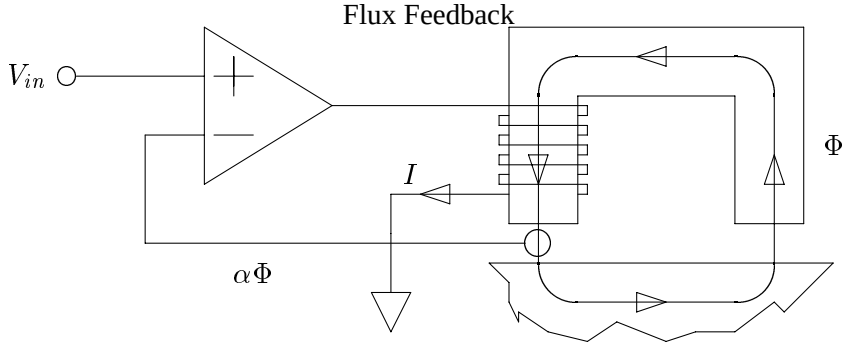

$$\Phi = \frac{V_{in}}{\alpha}$$

Requires a flux sensor

4.16.1 Flux Sensing: Hall Sensors

Principle: $e_0 \propto \Phi I$

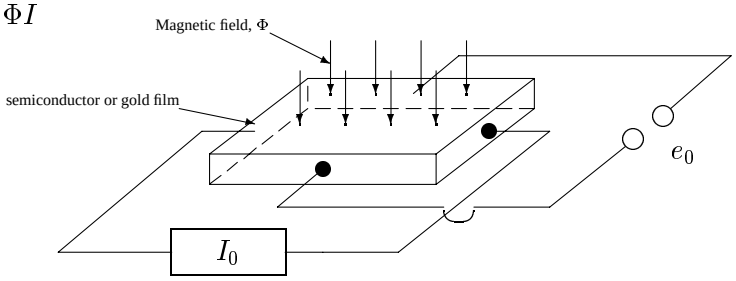

Problems:

- gain is strong function of temperature
- film is at least 0.25 mm thick: extra air gap
- film is fragile

Irony: Current Sensing with Hall Probes

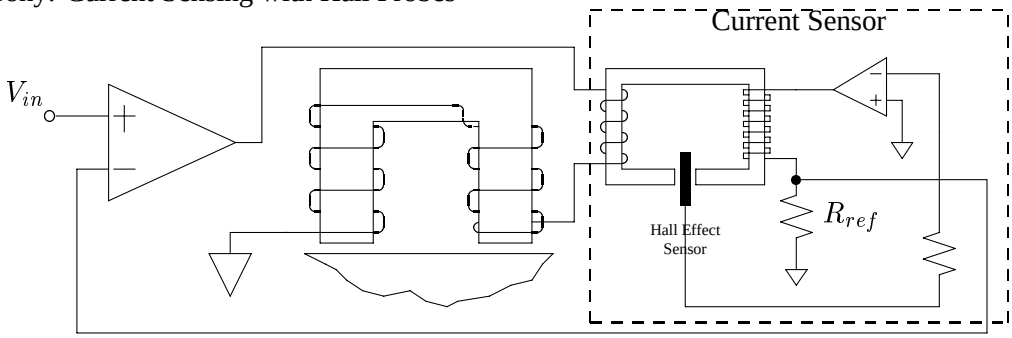

Current is sensed by having it generate another magnetic flux and detecting that flux with a Hall effect sensor!

4.16.2 Flux Sensing: Faraday's Law

For a coil with a flux passing through it:

$$V = N\frac{d\Phi}{dt} + RI$$

This relationship is true independent of hysteresis, eddy currents, magnetic saturation, ...

Thus, the voltage drop across the coil is an indication of the flux:

$$\Phi = \frac{1}{N}\int V - RI\,dt$$

Unfortunately, we can't detect a constant flux this way:

$$\frac{d\Phi}{dt} = 0 \quad \Rightarrow \quad V = RI$$

which is independent of the actual flux.

4.16.3 Flux Detection: Two Schemes

Two models for flux:

$$\begin{aligned}\Phi(t) &= \frac{\mu_0 NA}{2g(t)+f(\Phi,t)}I(t)\\ &\approx \frac{\mu_0 NA}{2g_0+f(\Phi_0)}I-\frac{\mu_0 NAI_0}{(2g_0+f(\Phi_0))^2}\{g-g_0+f(\Phi)-f(\Phi_0)\}\end{aligned}$$

$$\Phi(t) = \frac{1}{N}\int V(t)-RI(t)dt$$

In the frequency domain:

$$\Phi(s) = \frac{\mu_0 NA}{2g_0+f(\Phi_0)}I(s)-\frac{\mu_0 NAI_0}{(2g_0+f(\Phi_0))^2}\{g(s)-g_0+f(\Phi)(s)-f(\Phi_0)\}$$

$$\Phi(s) = \frac{1}{sN}\{V(s)-RI(s)\}$$

Low frequency model:

$$\begin{aligned}\Phi_{LF}(s) &= \frac{a}{sn(s)+a}\Phi(s)\\ &= \frac{\mu_0 NA}{2g_0+f(\Phi_0)}\frac{a}{sn(s)+a}I(s)\\ &\quad -\frac{\mu_0 NAI_0}{(2g_0+f(\Phi_0))^2}\frac{a}{sn(s)+a}\{g(s)-g_0+f(\Phi)(s)-f(\Phi_0)\}\\ &\approx \frac{\mu_0 NA}{2g_0+f(\Phi_0)}\frac{a}{sn(s)+a}I(s)\end{aligned}$$

High frequency model:

$$\Phi_{HF}(s)=\frac{sn(s)}{sn(s)+a}\Phi(s)=\frac{n(s)}{(sn(s)+a)N}\{V(s)-RI(s)\}$$

4.16.4 Flux Detection: Composite Model

Total model:

$$\begin{aligned}\Phi(s) &= \Phi_{LF}(s)+\Phi_{HF}(s)\\ &= \left(\frac{a}{sn(s)+a}+\frac{sn(s)}{sn(s)+a}\right)\Phi(s)\\ &\approx \frac{1}{N(sn(s)+a)}\left(\left[\frac{a\mu_0 N^2 A}{2g_0+f(\Phi_0)}-Rn(s)\right]I(s)+n(s)V(s)\right)\end{aligned}$$

Eliminates effects of:

- eddy currents
- transient or oscillatory rotor motion
- momentary saturation

Cannot eliminate effects of:

- persistent hysteresis
- steady rotor position error
- thermal growth of gaps

4.16.5 Linearized Actuator Model With Flux Feedback

Open loop term is "rolled off" by the low pass filter on the current feedback:

$$f(s) = K_b B_p - \frac{aK_x}{sn(s) + a} x$$

Important note: overcoming eddy current and saturation effects requires LOTS of current (but not lots of voltage).

4.17 Other Algorithms

Some other algorithms which do not treat the switching component as a linear amplifier:

Sample and Hold the sign of the error between actual and reference currents is checked at regular intervals (every τ seconds) and the output state is set depending upon the sign.

Hysteresis the reference and actual currents are compared with a hysteretic amplifier and the output of the amplifier determines the switch state.

Time Delay the reference and actual currents are compared and each time the sign of the error changes, the output state is changed *after* τ seconds.

All have the same objectives:

Limit the switching rate to preserve switching efficiency.
Make the average output current match the average input current

4.17.1 Underlying Concepts

- voltage applied to load is a sequence of states: $+$ or $-$
- number of state changes per second should be limited
- average current after n switches should equal average request
- state changes are made in response to sign changes in current error signal
- closed loop sustains a *limit cycle* at a prescribed frequency

4.17.2 The Limit Cycle: Constant Input

1. initial current is I_0, initial output state is $+$

$$I(t) = I_0 e^{-Rt/L} + \frac{V_{ps}}{R}\left(1 - e^{-Rt/L}\right) \qquad 0 < t < t_-$$

2. state changes at t_-

$$I(t) = \left(I_0 e^{-Rt_-/L} + \frac{V_{ps}}{R}\left(1 - e^{-Rt/L}\right)\right) e^{-R(t-t_-)/L} - \frac{V_{ps}}{R}\left(1 - e^{-R(t-t_-)/L}\right) \; : \; t_- < t < t_+$$

3. state again changes at t_+: current must have returned to I_0:

$$I(t_+) = I_0$$

4. average current should be equal to constant input:

$$\frac{1}{t_+}\int_0^{t_+} I(t)dt = I_{ref}$$

Simpler Form: Ignore R

1. initial error is e_0, initial output state is $+$

$$e(t) = e_0 + \frac{V_{ps}}{L}t \qquad 0 < t < t_-$$

2. state changes at t_-

$$e(t) = e_0 + \frac{V_{ps}}{L}(2t_- - t) \qquad t_- < t < t_+$$

3. state again changes at t_+: current must have returned to I_0:

$$e(t_+) = e_0 \quad \Rightarrow \quad t_+ = 2t_- = \tau$$

4. average current should be equal to constant input:

$$\frac{1}{t_+}\int_0^{t_+} e(t)dt = 0 \quad \Rightarrow \quad e_0 = -\frac{V_{ps}\tau}{4L} \quad , \quad e(t_-) = \frac{V_{ps}\tau}{4L}$$

4.17.3 Key Control Ideas

1. output state switches are correlated to error sign changes (feedback)
2. output state switches cannot occur at sign error instant

Control algorithm must either:

- switch at an error other than zero (PWM, Hysteresis)

or

- switch some time period after zero error (Time delay, sample and hold)

4.17.4 Comparator

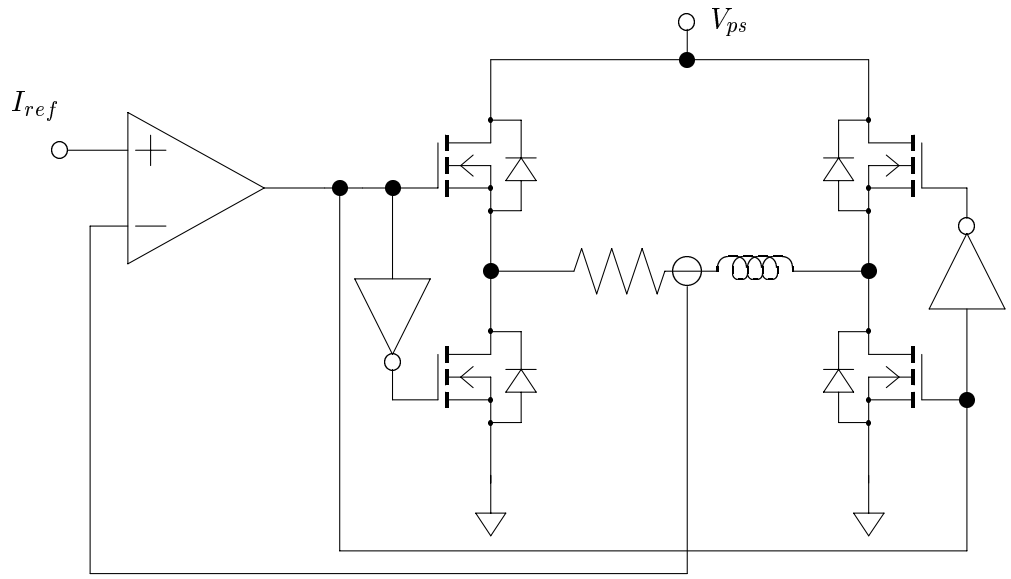

Switching rate depends on comparator characteristics:
VERY RAPID SWITCHING, VERY LOW EFFICIENCY

4.17.5 Sample and Hold

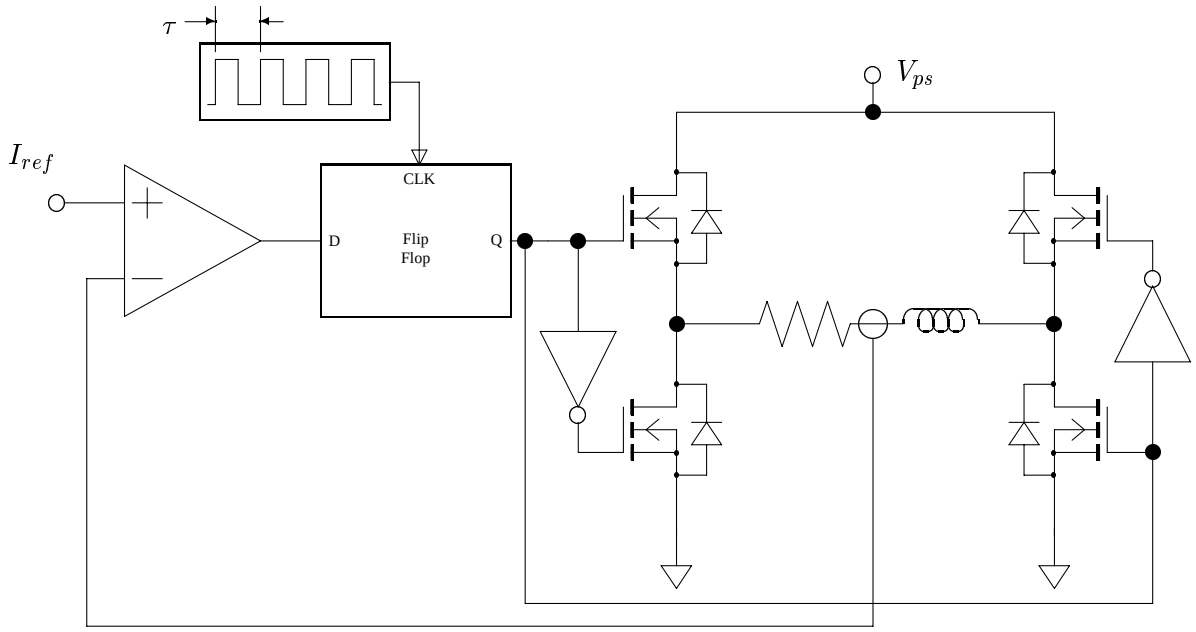

Switching rate:

$$f_s = \frac{1}{\tau}$$

Noise:

$$A_n \approx 2\frac{V_{ps}}{2f_sL}$$

Synchronous; immune to short cycling on noise; high distortion; switching rate set by clock (essentially)

4.17.6 Hysteresis

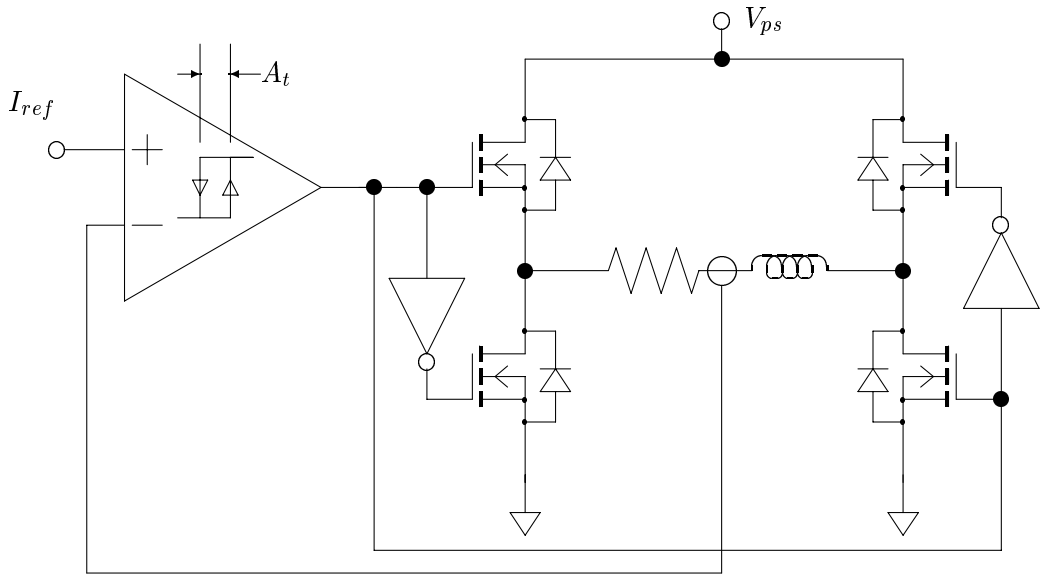

Switching rate:

$$f_s \approx \frac{V_{ps}}{2A_t L}$$

Noise (peak–peak):

$$A_n \approx A_t = \frac{V_{ps}}{2f_s L}$$

Asynchronous; susceptible to short cycling on noise; very low distortion; switching rate depends upon hysteresis depth, power supply voltage, and load impedance.

4.17.7 PWM

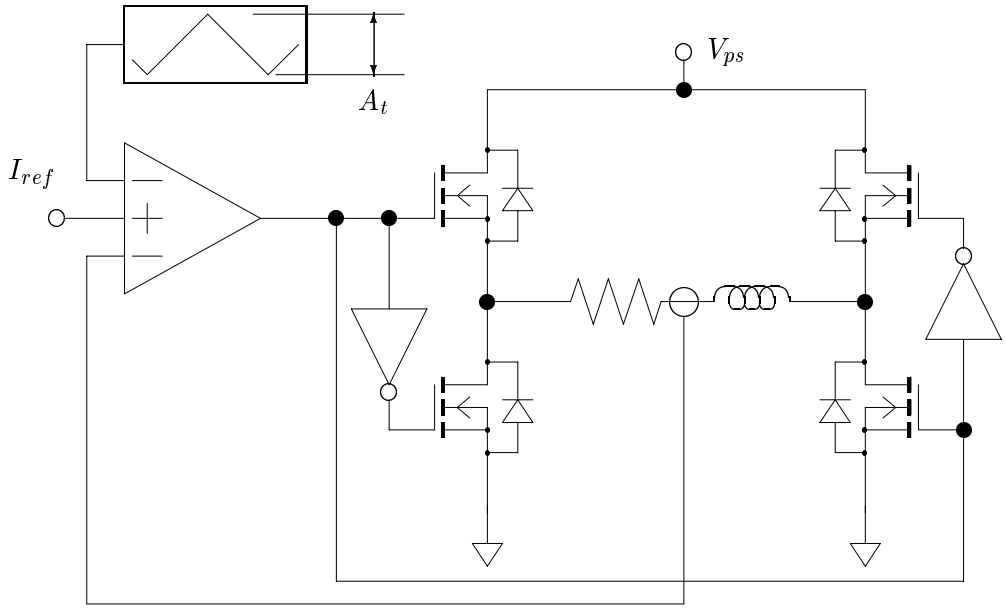

Best bandwidth:

$$A_t \approx \frac{V_{ps}}{2Lf_s}$$

Switching rate:

$$f_s \approx \frac{V_{ps}}{2A_tL}$$

Noise (peak–peak):

$$A_n \approx A_t = \frac{V_{ps}}{2f_sL}$$

Both transitions are asynchronous; susceptible to short cycling on noise; very low distortion; switching rate fixed by clock.

4.17.8 Time Delay

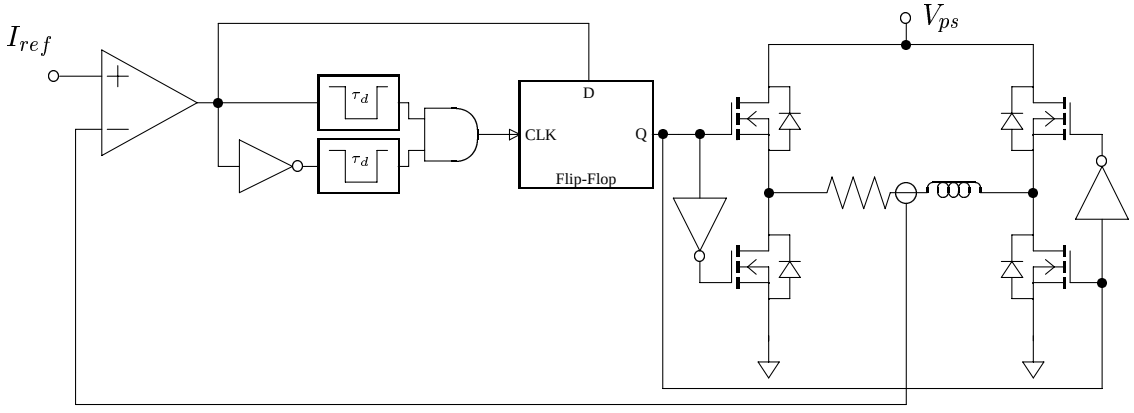

Switching rate:

$$f_s \approx \frac{1}{4\tau_d}$$

Noise (pk–pk):

$$A_n \approx \frac{V_{ps}}{2f_s L}$$

Asynchronous; susceptible to short cycling on noise; very low distortion; switching rate depends upon time delay.

Chapter 5

Stator–Amplifier Matching

5.1 Bearing/Amplifier Design Sequence

1. determine peak, RMS force; peak force slew rate: dynamic requirements
2. select biasing ratio based on linearity or power loss considerations
3. design iron: based on peak force, RMS requirements and thermal model
4. determine amplifier KVa requirement based on slew requirement and gap
5. pick peak current based on availability: dicates coil turns, N, to achieve maximum load capacity

5.1.1 Capacity Requirements

Depend upon:

- system dynamics (rotor dynamics)
- expected loads: unbalance, fluid forces, earthquakes, ...
- allowable load response: clearances, maximum strain, accelerations, ...
- expected controller performance

Note that the allowable response component implies some connection between bearing air gap (a limit on allowed motion) and bearing capacity requirements.

The outcome of this part of the analysis is:

$$f_{\max} \qquad f_{RMS} \qquad \left|\frac{df}{dt}\right|_{\max} \qquad g_0$$

5.1.2 Selecting Biasing Ratio

The biasing ratio is the ratio between the bias current and the current at which the stator iron begins to saturate. The choice of biasing ratio depends on a number of considerations. Since bias current exacts a toll in terms of coil power dissipation and rotating loss, it should be kept as low as possible.

One drawback to low bias is an increase in required power supply voltage in order to protect the actuator's force slew capability.

An additional drawback to low bias may be control complexity: once the control current exceeds the bias current, it is most common to limit the low current coils to 0 which leads to nonlinearity in the current–to–force relationship. If a very simple control is sought, then it may be preferable to use a high biasing ratio (as high as 0.5). More commonly, the biasing ratio is chosen to be high enough to ensure linear operation throughout the normally expected range of actuator loads.

A detailed discussion of methods by which the biasing level may be optimized is beyond the scope of these notes and we will assume that the biasing level will, in general, be selected so as to ensure linear operation throughout the specified RMS load range. In any case, the outcome of this analysis is the biasing ratio,

$$\alpha$$

5.1.3 Iron Size Based on Peak and RMS Loads

Depends on:

- magnetic material: saturation flux density
- general pole configuration: number, spacing, backiron connection
- model for saturation of poles: by quadrant, by sector, single pole, ...
- leakage derating – probably about 0.9, but smaller for large gaps.

Match coil size to allowed RMS current density, coil copper factor, and expected currents:

$$J_{RMS} A_c f_c = N I_{RMS} = N \sqrt{I_b^2 + (f_{RMS}/K_i)^2}$$

$$\Rightarrow \quad A_c = \frac{1}{J_{RMS} f_c} \sqrt{(N I_b)^2 + \left(\frac{f_{RMS} N^2 I_b}{K_i} \right)^2 \frac{1}{(N I_b)^2}}$$

The outcome of this analysis is:

$$\frac{K_i}{N^2 I_b} \qquad \frac{K_x}{N^2 I_b^2} \qquad \frac{L}{N^2} \qquad N I_{\text{sat}}$$

5.1.4 KVa Requirement

For a given choice of iron structure and biasing ratio, the relationship between amplifier capacity, slew requirement, and nominal air gap is:

$$\left| \frac{df}{dt} \right|_{\max} \leq \beta \frac{V_{\max} I_b}{g_0}$$

where β depends upon the stator configuration. Assuming that a biasing ratio has of $\alpha = I_b / I_{\max}$ has been chosen, then

$$\left| \frac{df}{dt} \right|_{\max} \leq \beta \alpha \frac{V_{\max} I_{\max}}{g_0}$$

Table 5.1: Amplifiers Offered by Advanced Motion Controls

Model	$I_{\max}$	$V_{\max}$	kVA	cost ($ US)
100A20	100	200	20.00	800
100A8	100	80	8.00	800
50A20	50	200	10.00	520
50A8	50	80	4.00	520
30A20-AC	30	200	6.00	520
30A8	30	80	2.40	390
25A20	25	200	5.00	390
25A8	25	80	2.00	295
20A14	20	140	2.80	335
16A20-AC	16	200	3.20	439
12A8	12	80	0.96	275
10A8	10	80	0.80	295
5A5	5	50	0.25	198

or,

$$V_{\max} I_{\max} \geq \frac{g_0}{\beta\alpha} \left| \frac{df}{dt} \right|_{\max}$$

Choice of peak currents:

- limited by available devices
- should permit saturation of magnetics:

$$I_{\max} = I_{\text{sat}} \quad \Rightarrow \quad N = \frac{N I_{\text{sat}}}{I_{\max}}$$

For example, Advanced Motion Controls offers the amplifier models listed in Table 5.1. The outcome of this analysis (choice) is the number of coil turns, N

5.1.5 Free Design Parameters: Optimization

The design process, as described above, involves choosing many free parameters which will determine the quality of the final design.

Free Parameters:

- number of poles
- magnetic material (saturation)
- complexity of coil control
- back–iron use (flux splitting)
- iron ratio
- coil packing factor
- amplifier current capacity
- design objective: linear range *vs* slew performance

Performance Measures:

- system weight
- shaft added mass
- power consumption
- system cost
- reliability
- safety (high voltages!)
- package size
- ...

5.2 Design Example

Performance Specifications:

- $f_{\max} = 6500$ N
- $f_{RMS} = 3500$ N
- maximum speed = 8000 RPM
- $df/dt = 5 \times 10^6$ N/sec
- $g_0 = 0.6$ mm
- rotor: $r_r = 5$ cm

Initial Design Choices:

- use 8 poles: $n_p = 8$
- use Vanadium Permendur: $B_{sat} = 2.2$ T
- use flux splitting: $\gamma = 0.5$
- base design on attainable linear limit
- assume coils wound in quadrant pairs

Compute required gap area:

$$A_g = \frac{2\mu_0 f_{\max}}{B_{sat}^2 2\cos 22.5^\circ} = 1.85 \times 10^{-3} \text{ m}^2$$

Choose the iron ratio to give a “square” journal (length = diameter)

$$r_j = (r_r + g_0 \sin(\pi f_i/n_p))/(1 - \sin(\pi f_i/n_p))$$

$$w = 2(r_j + g_0)\sin(\pi f_i/n_p) \qquad \ell = A_g/w$$

$$\begin{aligned} f_i &= 0.35 \\ r_j &= 5.803 \text{ cm} \\ w &= 1.607 \text{ cm} \\ \ell &= 11.514 \text{ cm} \end{aligned}$$

Note that the decision to use a square journal has dictated quite a low iron ratio: only 35 percent. A considerably shorter journal with larger diameter would arise if a higher iron ratio were selected. On the other hand, the larger journal might turn out to be too large: we have not paid any attention to the hoop stresses at the inner diameter of the journal iron, but these stresses can be substantial if the surface speed of the journal is too large. For silicon iron journals, the surface speed should be limited to about 200 m/sec(?), which is equivalent to a DN product of 3.8 million(?). For the present example, the maximum expected shaft speed is 8000 RPM. The computed journal diameter of 5.8 cm then produces a surface speed of only 24 m/sec: well below the level where hoop stress is a concern. In general, the iron ratio is an optimization parameter. When hoop stress is significant, it acts as an upper bound on the useful iron ratio.

5.2.1 Stator Properties

Normalized actuator gain:

$$\frac{K_i}{N^2 I_b} = \frac{4\mu_0 A_g \cos 22.5^\circ}{g_0^2} = 2.38 \times 10^{-2} \text{ N/amp}^2\text{turn}^2$$

Normalized open loop stiffness:

$$\frac{K_x}{N^2 I_b^2} = \frac{4\mu_0 A_g \cos^2 22.5^\circ}{g_0^3} = 36.7 \text{ N/m amp}^2\text{turn}^2$$

Normalized inductance (coil pairs in series):

$$\frac{L}{N^2} = \frac{2\mu_0 A_g}{g_0} = 7.75 \ \mu\text{H/turns}^2$$

Ampere-turns at saturation:

$$NI_{sat} = \frac{B_{sat} g_0}{\mu_0} = 1050 \text{ Ampere-turns}$$

5.2.2 Slew Requirements/Amplifier Selection

Required kVA:

$$\begin{aligned} 0.001 I_{\max} V_{\max} &= 0.001 \frac{NI_{\text{sat}}}{NI_b} \frac{I_b L}{K_i} \left|\frac{df}{dt}\right|_{\max} \\ &= 0.001 \frac{NI_{\text{sat}}}{NI_b} 3.26 \times 10^{-4} \times 5 \times 10^6 \\ &= 1.63 \frac{NI_{\text{sat}}}{NI_b} \end{aligned}$$

Available kVA: pick the 4 kVA amplifier from Advanced Motion:

$$4 = 1.63 \frac{NI_{\text{sat}}}{NI_b} \quad \Rightarrow \quad NI_b = 427 \text{ Ampere-turns}$$

Note: this sets $I_b = 0.41 I_{\text{sat}}$ for a very wide linear range, but probably large coils because the bias is large.

5.3 Design Example Revisited

Performance Specifications:

- $f_{\max} = 6500$ N
- $f_{RMS} = 3500$ N
- maximum speed = 8000 RPM
- $df/dt = 5 \times 10^6$ N/sec
- $g_0 = 0.6$ mm
- rotor: $r_r = 5$ cm

Initial Design Choices:

- use 8 poles: $n_p = 8$
- use Vanadium Permendur: $B_{sat} = 2.2$ T
- do note use flux splitting: $\gamma = 1.0$
- assume coils wound in quadrant pairs

Slew rate chosen by requiring full capacity at maximum running speed:

$$\left|\frac{df}{dt}\right|_{\max} = f_{\max}\Omega_{\max} = 6500 \times 2 \times \pi \times \frac{8000}{60}$$

5.3.1 Size the stator for load capacity

Compute required gap area:

$$A_g = \frac{2\mu_0 f_{\max}}{B_{sat}^2 2\cos 22.5^\circ} = 1.85 \times 10^{-3} \text{ m}^2$$

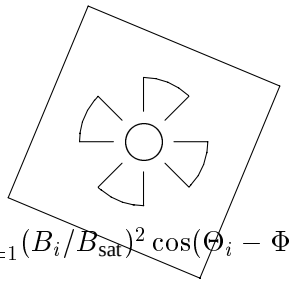

$$\min_\Phi \sum_{i=1}^{n} (B_i/B_{\text{sat}})^2 \cos(\Theta_i - \Phi) = 1.848$$

Choose iron ratio to give “square” journal (length = diameter)

$$r_j = \frac{r_r + 2\gamma g_0 \sin\left(\frac{\pi f_i}{n_p}\right)}{1 - 2\gamma \sin\left(\frac{\pi f_i}{n_p}\right)}$$

$$w = 2(r_j + g_0)\sin\left(\frac{\pi f_i}{n_p}\right) \qquad \ell = \frac{A_g}{w}$$

Solution:

$f_i = 0.28$ $r_j = 6.4228$ cm
$w = 1.4228$ cm $\ell = 12.841$ cm

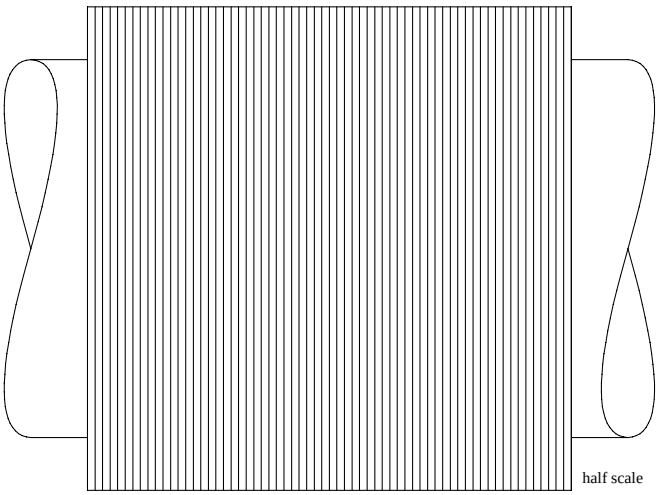

5.3.2 Stator Properties

Normalized actuator gain:

$$\frac{K_i}{N^2 I_b} = \frac{4\mu_0 A_g \cos 22.5^\circ}{g_0^2} = 2.356 \times 10^{-2} \text{ N/amp}^2\text{turn}^2$$

Normalized open loop stiffness:

$$\frac{K_x}{N^2 I_b^2} = \frac{4\mu_0 A_g \cos^2 22.5^\circ}{g_0^3} = 36.3 \text{ N/m amp}^2\text{turn}^2$$

Normalized inductance (coil pairs in series):

$$\frac{L}{N^2} = \frac{2\mu_0 A_g}{g_0} = 7.65 \ \mu\text{H/turns}^2$$

Ampere-turns at saturation:

$$NI_{sat} = \frac{B_{sat} g_0}{\mu_0} = 1050 \text{ Ampere-turns}$$

5.3.3 Slew Requirements/Linearity

Required kVA:

$$\begin{aligned} 0.001 I_{\max} V_{\max} &= 0.001 \frac{NI_{\text{sat}}}{NI_b} \frac{I_b L}{K_i} \left| \frac{df}{dt} \right|_{\max} \\ &= 0.001 \frac{NI_{\text{sat}}}{NI_b} 3.247 \times 10^{-4} \times 5 \times 10^6 \\ &= 1.62 \frac{NI_{\text{sat}}}{NI_b} \end{aligned}$$

Linearity:

actuator is linear while $|I_{p,\max}| < I_b$. 100% linearity would mean that $I_b + I_{p,max} = I_{\text{sat}}$, or $2I_b = I_{\text{sat}}$. In general, the linear range (as a fraction of capacity) is

$$\frac{f_{lin}}{f_{\max}} = \left(\frac{2I_b}{I_{\text{sat}}} \right)^2$$

5.3.4 Amplifier Selection

In this example, $f_{RMS} = 0.538 f_{\max}$ so we might desire that

$$\frac{f_{lin}}{f_{\max}} = 0.538 = \left(\frac{2I_b}{I_{\text{sat}}}\right)^2 \;\Rightarrow\; I_b = 0.367 I_{\text{sat}}$$

This would dictate a kVA capacity of

$$0.001 I_{\max} V_{\max} = \frac{1}{0.367} 1.62 = 4.42 \text{ kVA}$$

Available kVA: pick the 5 kVA amplifier from Advanced Motion:

$$5 = 1.62 \frac{N I_{\text{sat}}}{N I_b} \quad \Rightarrow \quad N I_b \geq 340.2 \text{ A-t}$$

From Advanced Motion Controls:

Model	$I_{\max}$	$V_{\max}$	kVA	cost ($ US)
100A20	100	200	20.00	800
50A20	50	200	10.00	520
100A8	100	80	8.00	800
30A20-AC	30	200	6.00	520
25A20	25	200	5.00	390
50A8	50	80	4.00	520
16A20-AC	16	200	3.20	439
20A14	20	140	2.80	335
30A8	30	80	2.40	390
25A8	25	80	2.00	295
12A8	12	80	0.96	275
10A8	10	80	0.80	295
5A5	5	50	0.25	198

The maximum current for this amplifier is $I_{\max} = 25$ amps so

$$N = \frac{N I_{\text{sat}}}{I_{\max}} = 42 \text{ turns} \qquad I_{\text{sat}} = 25 \text{ amps} \qquad I_b = \max(0.324, 0.367) I_{\text{sat}} = 9.175 \text{ amps}$$

5.3.5 Size the Coil

The RMS perturbation current is:

$$I_{p,RMS} = \frac{f_{RMS}}{K_i} = \frac{f_{RMS} N^2 I_b}{K_i} \frac{1}{N^2 I_b} = \frac{3500}{0.02356} \frac{1}{42^2 9.175} = 9.179 \text{ amps}$$

This gives an RMS coil ampere-turns of

$$N I_{RMS} = 42 \sqrt{9.175^2 + 9.179^2} = 545 \text{ ampere-turns}$$

The required coil area is then

$$J_{rms} f_c A_c = 600 \times 0.5 \times A_c = 545 \quad \Rightarrow \quad A_c = 1.82 \text{ cm}^2$$

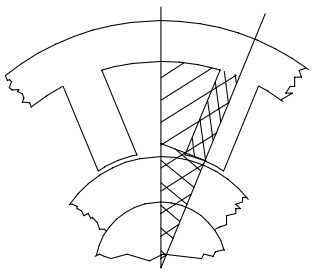

Full Coil Fill

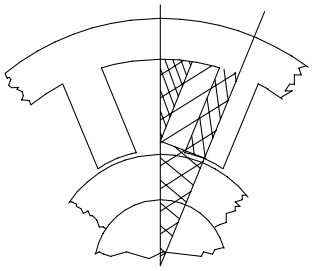

Removable Coils

Use removable coils:

$$r_p \doteq r_j + g_0 = 6.483 \text{ cm}$$

$$A_v = A_c = \left[r_p \tan \frac{\pi}{n_p} - \frac{w}{2} \right] (r_c - r_p)$$

$$\Rightarrow \quad r_c = 7.405 \text{ cm}$$

5.3.6 Completed Design

Stator outer radius is coil space radius plus splitting factor times leg width:

$$r_s = r_c + \gamma w = 7.405 + 1.0 \times 1.4228 = 8.828 \text{ cm}$$

Design performance:

- Stator iron weight: 8.91 kg
- Coil weight (8): 2.52 kg
- Journal weight: 5.14 kg
- Total bearing weight: 16.57 kg
- capacity/weight (at 1G): 40.03
- Total bearing volume: 1135 cm^3
- Bearing axial length: 16.8 cm

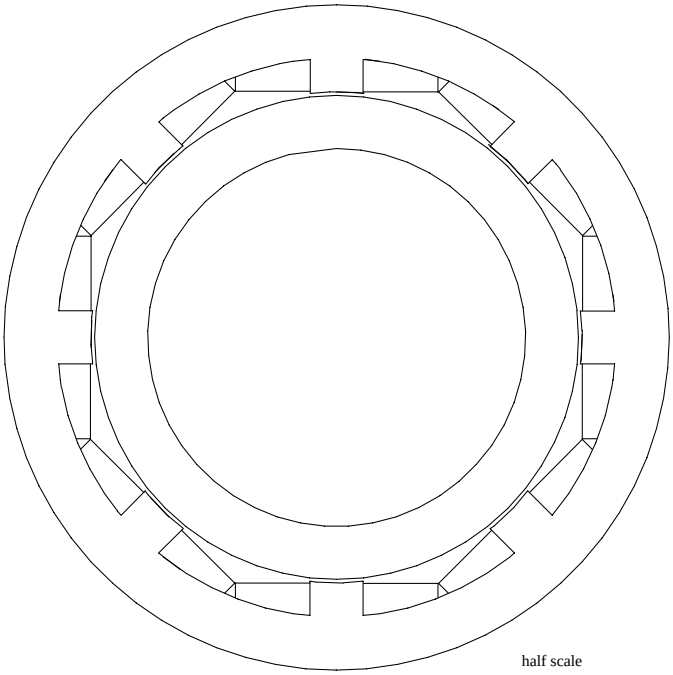

5.4 Design Iteration

Looks like the design has too few poles: try 12 instead. With 12 poles, it's easier to use half back iron ($\gamma = 0.5$) and independent coil control. Otherwise, use the same performance and design criteria.

Compute required gap area:

$$A_g = \frac{2\mu_0 f_{\max}}{B_{sat}^2(1 + 2\cos 30^\circ + 2\cos 60^\circ)} = 0.9044 \times 10^{-3} \text{ m}^2$$

Choose iron ratio to give "square" journal (length = diameter)

$$r_j = \frac{r_r + 2\gamma g_0 \sin\left(\frac{\pi f_i}{n_p}\right)}{1 - 2\gamma \sin\left(\frac{\pi f_i}{n_p}\right)}$$

$$w = 2(r_j + g_0)\sin\left(\frac{\pi f_i}{n_p}\right) \qquad \ell = \frac{A_g}{w}$$

Solution:

$f_i = 0.29$ $\quad r_j = 5.417$ cm
$w = 0.835$ cm $\quad \ell = 10.836$ cm

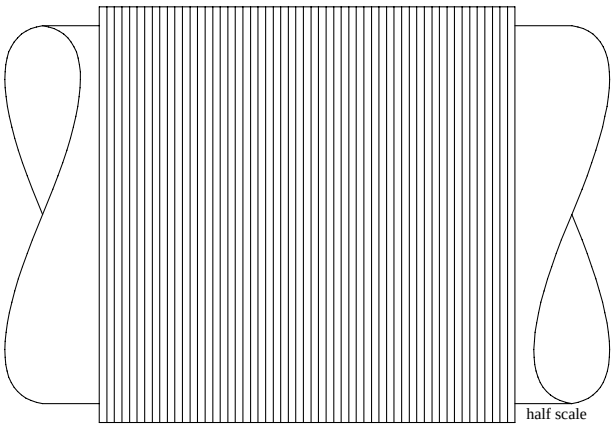

5.4.1 Stator Properties

Normalized actuator gain:

$$\frac{K_i}{N^2 I_b} = \frac{2\mu_0 A_g(1 + 2\cos 30^\circ + 2\sin^2 30^\circ)}{g_0^2} = 2.356 \times 10^{-2} \text{ N/amp}^2\text{turn}^2$$

Normalized open loop stiffness:

$$\frac{K_x}{N^2 I_b^2} = \frac{2\mu_0 A_g(1 + 2\cos^2 30^\circ + 2\sin^2 30^\circ)}{g_0^3} = 31.57 \text{ N/m amp}^2\text{turn}^2$$

Normalized inductance (coils wound separately):

$$\frac{L}{N^2} = \frac{\mu_0 A_g}{g_0} = 1.89 \ \mu\text{H/turns}^2$$

Ampere-turns at saturation:

$$NI_{sat} = \frac{B_{sat} g_0}{\mu_0} = 1050 \text{ Ampere-turns}$$

5.4.2 Slew Requirements/Linearity

Required kVA:

$$\begin{aligned} 0.001 I_{\max} V_{\max} &= 0.001 \frac{NI_{\text{sat}}}{NI_b} \frac{I_b L}{K_i} \left| \frac{df}{dt} \right|_{\max} \\ &= 0.001 \frac{NI_{\text{sat}}}{NI_b} 8.022 \times 10^{-5} \times 5 \times 10^6 \\ &= 0.4011 \frac{NI_{\text{sat}}}{NI_b} \end{aligned}$$

Linearity:

$$\frac{f_{lin}}{f_{\max}} = \left(\frac{2I_b}{I_{\text{sat}}} \right)^2$$

Let $f_{lin} = f_{RMS} = 0.538 f_{\max}$ so that

$$I_b = 0.367 I_{\text{sat}}$$

as in the previous iteration. This requires an amplifier capacity of

$$0.001 I_{\max} V_{\max} = \frac{0.401}{0.367} = 1.09 \text{ kVA}$$

Notice that the previous design, using eight poles, required 4.42 kVA amplifiers. Apparently, the twelve pole design requires much less kVA. However, the twelve pole design uses twelve separate amplifiers whereas the eight pole design used only four. The total kVA for the eight pole design is $4 \times 4.42 = 17.68$ kVA whereas for the twelve pole design, the total capacity required is $12 \times 1.09 = 13.12$ kVA. The slight reduction (25 percent) in required KVa is due to the higher volume efficiency of the iron when independent coil control is used.

5.4.3 Amplifier Selection

Available kVA: pick the 0.96 kVA amplifier from Advanced Motion:

$$0.96 = 0.4011 \frac{N I_{\text{sat}}}{N I_b} = 0.4011 \frac{1050}{N I_b} \quad \Rightarrow \quad N I_b \geq 438.7 \text{ A-t}$$

From Advanced Motion Controls:

Model	$I_{\max}$	$V_{\max}$	kVA	cost ($ US)
100A20	100	200	20.00	800
50A20	50	200	10.00	520
100A8	100	80	8.00	800
30A20-AC	30	200	6.00	520
25A20	25	200	5.00	390
50A8	50	80	4.00	520
16A20-AC	16	200	3.20	439
20A14	20	140	2.80	335
30A8	30	80	2.40	390
25A8	25	80	2.00	295
12A8	12	80	0.96	275
10A8	10	80	0.80	295
5A5	5	50	0.25	198

The maximum current for this amplifier is $I_{\max} = 12$ amps so

$$N = \frac{N I_{\text{sat}}}{I_{\max}} = \frac{1050}{12} = 87.5 \text{ turns} \qquad I_{\text{sat}} = 12 \text{ amps} \qquad I_b = \frac{438.7}{88} = 4.99 \text{ amps}$$

5.4.4 Size the Coil

The RMS perturbation current is:

$$I_{p,RMS} = \frac{f_{RMS}}{K_i} = \frac{f_{RMS} N^2 I_b}{K_i} \frac{1}{N^2 I_b} = \frac{3500}{0.02356} \frac{1}{88^2 4.99} = 3.84 \text{ amps}$$

This gives an RMS coil ampere-turns of

$$NI_{RMS} = 88\sqrt{4.99^2 + 3.844^2} = 554 \text{ ampere-turns}$$

The required coil area is then

$$J_{rms} f_c A_c = 600 \times 0.5 \times A_c = 554 \quad \Rightarrow \quad A_c = 1.85 \text{ cm}^2$$

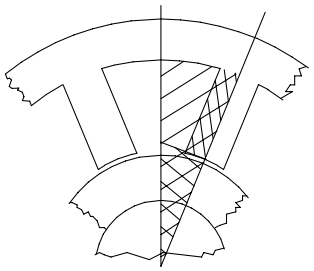

Full Coil Fill

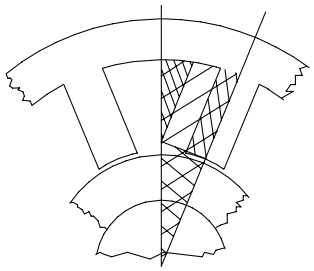

Removable Coils

Use removable coils:

$$r_p \doteq r_j + g_0 = 5.477 \text{ cm}$$

$$A_v = A_c = \left[r_p \tan\frac{\pi}{n_p} - \frac{w}{2} \right] (r_c - r_p)$$

$$\Rightarrow \quad r_c = 7.239 \text{ cm}$$

5.4.5 Completed Design

Stator outer radius is coil space radius plus splitting factor times leg width:

$$r_s = r_c + \gamma w = 7.239 + 0.5 \times 0.835 = 7.656 \text{ cm}$$

This stator is considerably smaller in diameter than the previous design.

5.5 Effect of Iron Ratio on Journal Radius

Figures 5.1 and 5.2 illustrate the effect of iron ratio on journal size. Each figure plots the function

$$\frac{r_j}{r_r} = \frac{1 + 2\gamma \frac{g}{r_r} \sin\left(\frac{\pi f_i}{n_p}\right)}{1 - 2\gamma \sin\left(\frac{\pi f_i}{n_p}\right)}$$

as a function of f_i for gap ratios, g/r_r, ranging from 0.001 through 0.1. In each case, the journal size is largest with the highest gap ratio. Each plot shows both the case with no flux splitting ($\gamma = 1$) and with flux splitting ($\gamma = 0.5$).

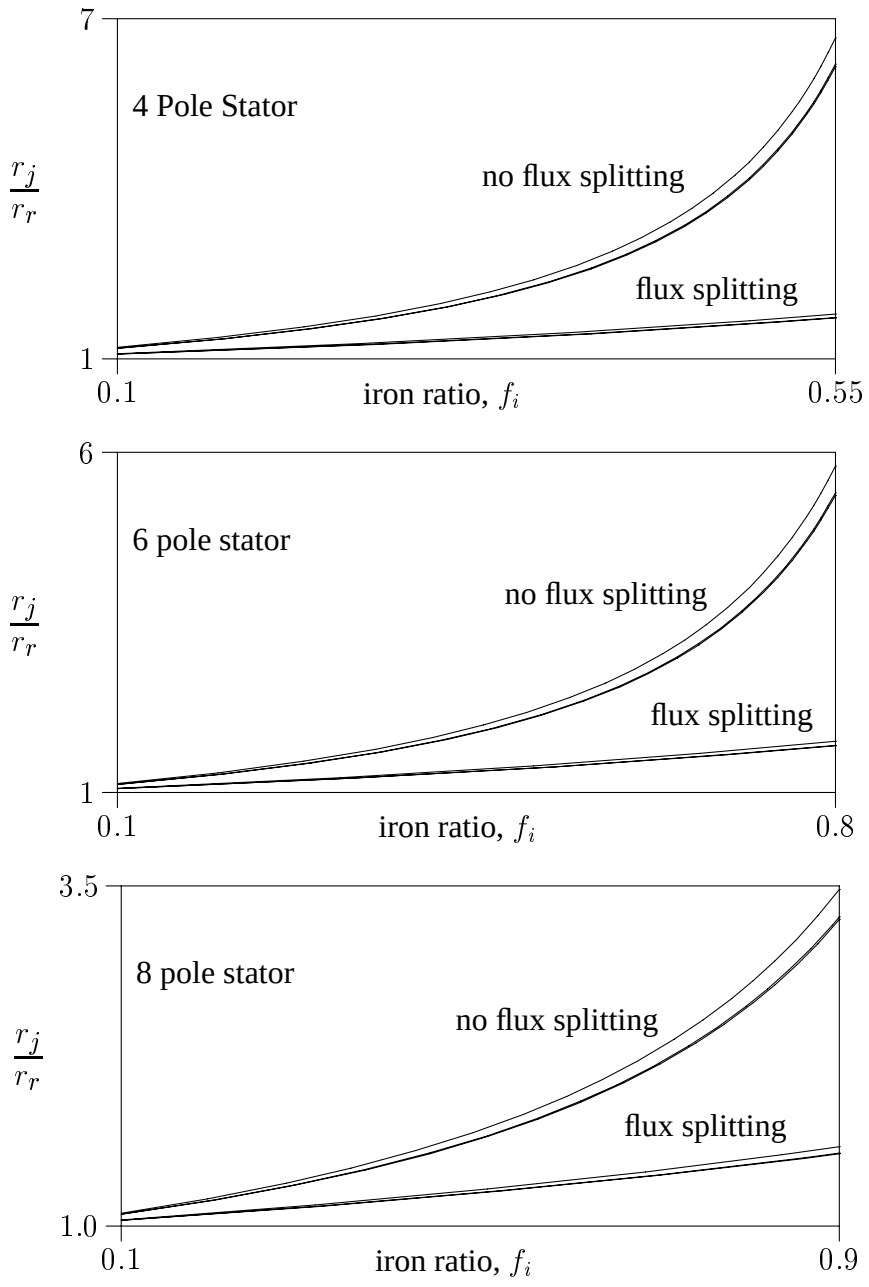

Figure 5.1: Effect of iron ratio on journal size: 4, 6, and 8 pole stators.

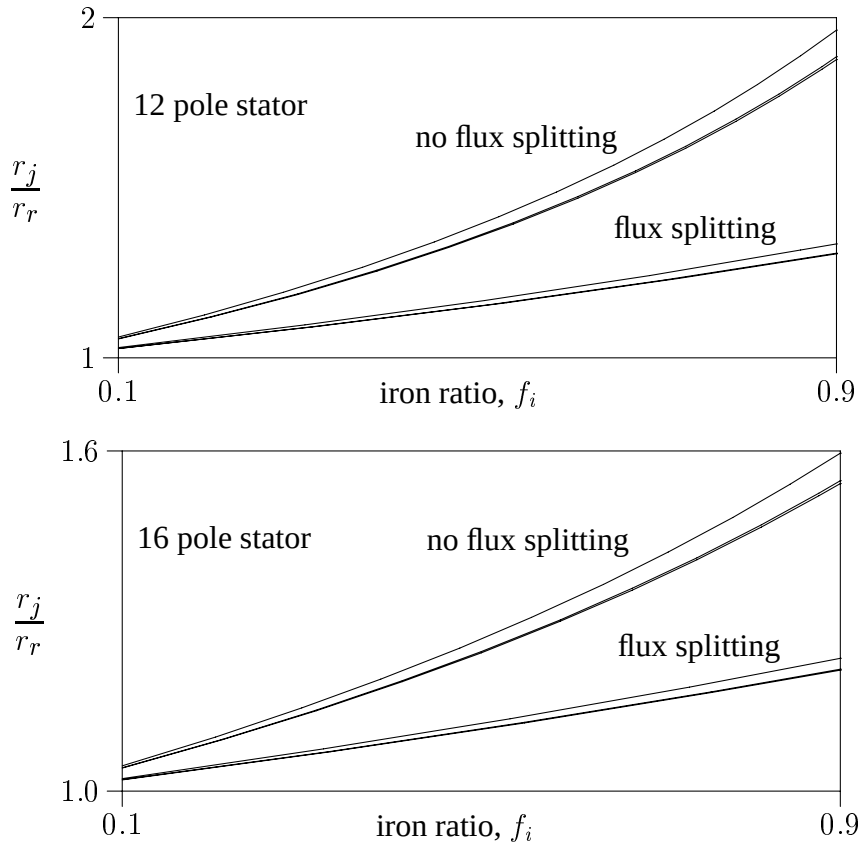

Figure 5.2: Effect of iron ratio on journal size: 12 and 16 pole stators.

Chapter 6

Position Sensors

6.1 General Sensor Characteristics

- noncontacting
- singlevalued: $f(x, y)$ is invertible
- bandwidth should exceed amplifier/magnetic bandwidth
- commercial applications require durability, stability, and low cost
- usable feedback gains usually limited by signal–to–noise ratio
- commonly employed in differential pairs to eliminate effects of thermal or centripetal stress growth

6.2 Points of Comparison

gap requirements: since the probes are all non–contacting, there is a gap lying between the sensitive portion of the probe and the sensed target. This gap is commonly filled with some substance – a process fluid or air. In some cases, the gap is evacuated. The various probes each place a different set of restrictions on what properties this intervening material must have.

bandwidth: the sensor gain as a function of frequency of motion is assumed constant out to some frequency beyond which the gain drops rapidly with increasing frequency. This breakpoint is called the bandwidth and describes the maximum frequency of motion which the sensor can usefully measure.

linearity: ideally, the output of the sensor is described by $v_{out} = ax + b$ where a is the sensor gain and b is some offset. In fact, the sensor output is not perfectly linear, so linearity is a measure of the discrepancy between a linear model and the actual input–output relationship.

cost: self–evident

compatibility with cans: in many magnetic bearing applications, it is desirable to isolate the sensors and magnetic actuators from either the process fluid or process vacuum. In order to do this, it is often necesary to introduce a mechanical barrier (or "can") between these components and the shaft/sensor target which is immersed in the process fluid. Each sensor type is able to operate with such a mechanical barrier, but each places different restrictions on the mechanical, electrical, or magnetic properties of this barrier.

magnetic noise susceptibility: because the sensor usually operates in close proximity to the magnetic bearings which can have substantial leakage magnetic fluxes, the sensitivity of the sensor to this leakage flux may have a significant impact on the overal system performance. In extreme cases, leakage flux may render a sensitive sensor inoperative.

standoff distance: This is a measure of how close the sensitive portion of the sensor must be to the target surface. In some applications, it is difficult or impossible to place the sensor close to the surface so a large allowable standoff distance is required.

6.3 Acoustic Probes – Ultrasonic

- gap requirements: consistent density
- bandwidth: should be $>$ 5 kHz
- linearity: very good
- cost: ???
- compatibility with cans: potentially very good
- magnetic noise susceptibility: very good with piezo devices
- standoff distance: inverse with bandwidth
- problems: diffuse acoustic field, stray echos, machine noise rejection

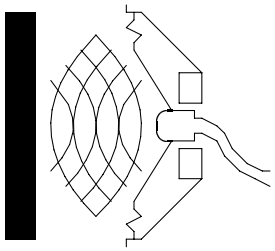

- acoustic impedance depends on target position
- measure with tuned resonant circuit: measure electrical impedance of transducer

6.4 Capacitance Probes

- gap requirements: consistent dielectric strength
- bandwidth: very high
- linearity: moderate (hyperbolic sensitivity to gap)
- cost: moderate to high
- compatibility with cans: must be nonconductive
- magnetic noise susceptibility: significant for switching noise
- standoff distance: small

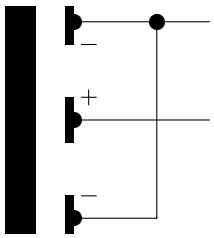

- capacitance is a function of gap
- use at fixed frequency for noise rejection

6.5 Optical Probes: Interferometric

- gap: transparent, consistent refractive index
- target: reflective
- bandwidth: high, > 2 kHz
- linearity: best possible
- cost: very high

- cans: must be transparent (glass)
- magnetic noise susceptibility: none
- standoff distance: arbitrary

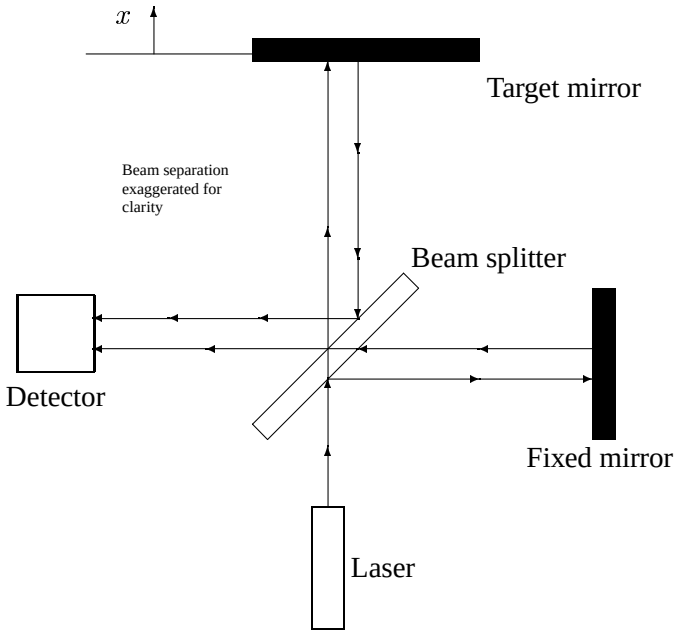

- reconverged beams interfere
- electronics count interference fringes
- quadrature required to detect direction

6.6 Optical Probes: Reflectance

- gap requirements: transparent, consistent absorbtion and refractive index
- target: consistent reflectivity
- bandwidth: extremely high, > 10 kHz
- linearity: excellent
- cost: moderate
- compatibility with cans: must be transparent (glass)
- magnetic noise susceptibility: none
- standoff distance: small, strong effect on sensitivity

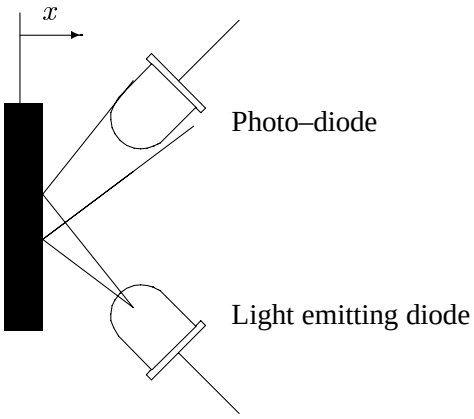

- intensity of reflected light varies with gap
- can minimize optical noise effects with LED frequency modulation, single frequency detection

6.7 Optical Probes: Occlusion

- gap: transparent, consistent absorbtion and refractive index
- target: (prefer non-reflective)
- bandwidth: extremely high, > 10 kHz
- linearity: excellent
- cost: moderate
- cans: must be transparent (glass)
- magnetic noise susceptibility: none
- standoff distance: can be large, small effect on sensitivity

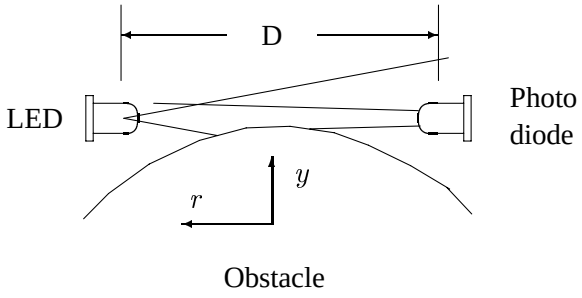

- intensity of transmitted light varies with target motion

- can minimize optical noise effects with LED frequency modulation, single frequency detection

6.8 Differential Occlusion, Thermal Compensation

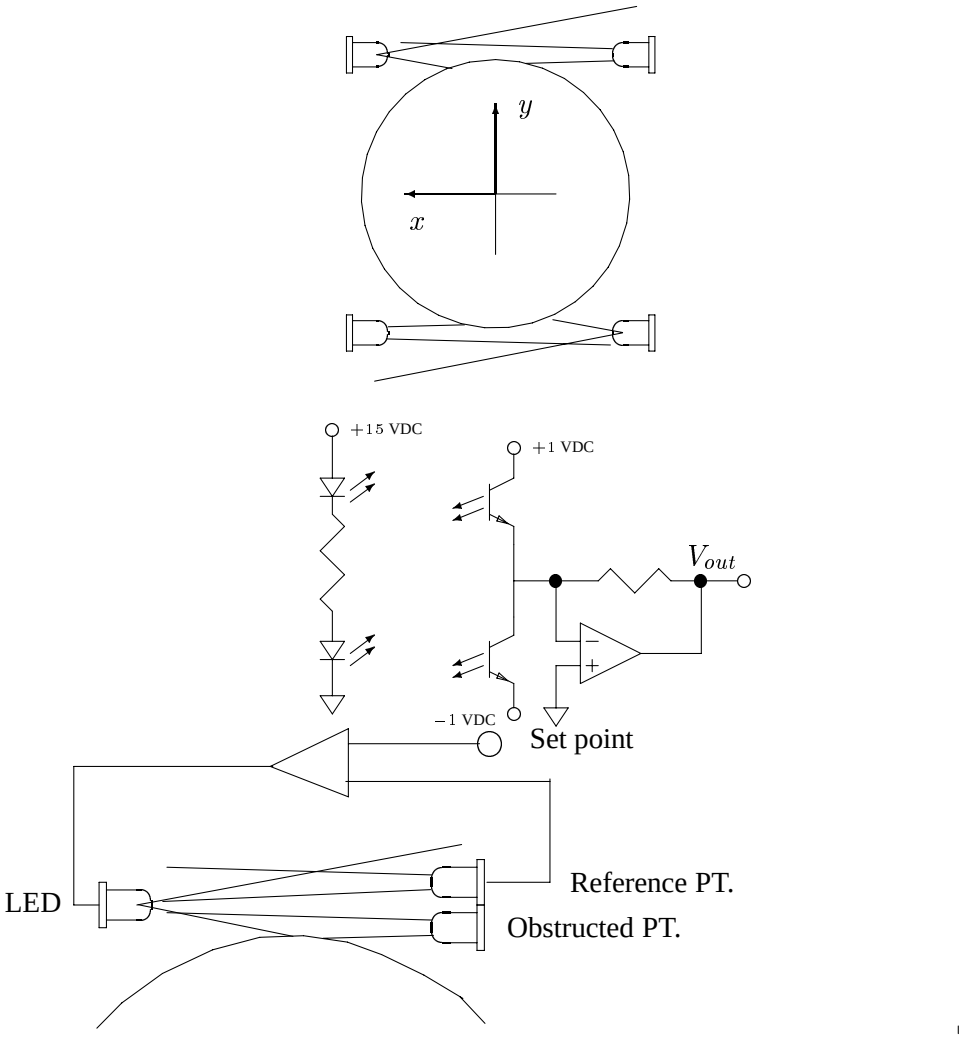

- feedback keeps PT output constant
- compensates for aging, temperature effects in LED
- if PT characteristics are the same, compensates for aging, temperature effects in PT's.

6.9 Eddy Current Probes

- gap requirements: nonconductive
- target requirements: consistent electrical conductivity, permeability
- bandwidth: 2–4 kHz
- linearity: good
- cost: high
- compatibility with cans: must be thin and nonconductive
- mag. noise susceptibility: moderate
- standoff distance: small, strong effect on sensitivity, probe size

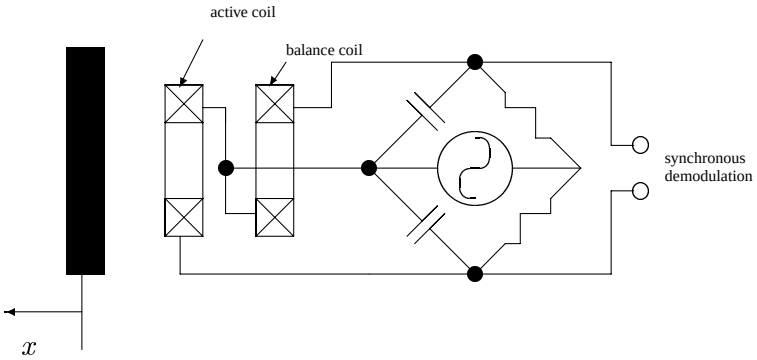

- active coil induces target eddy currents
- eddy currents depend on gap
- eddy currents make active circuit have higher losses than balance circuit
- change in impedances unbalances the bridge

6.10 Problems with Eddy Current Probes

- small mismatch in 1 MHz carrier in adjacent probes can cause large “beat” frequency output signal (0.1 % error $\rightarrow$ 500 Hz)
- “electrical runout” on shaft can be hard to eliminate: small variations in permeability due to machining
- switching noise from magnetic bearings can couple strongly into eddy current probe signals
- cannot conveniently be used outside of a can

- sensor tips are expensive, hard to use in a distributed sensing array (to average surface effects)

6.11 Hall Effect Probes

- gap requirements: short gap
- bandwidth: high with non–conductive cans
- linearity: moderate
- cost: low
- compatibility with cans: must be thin
- magnetic noise susceptibility: very high
- standoff distance: small, strong effect on sensitivity

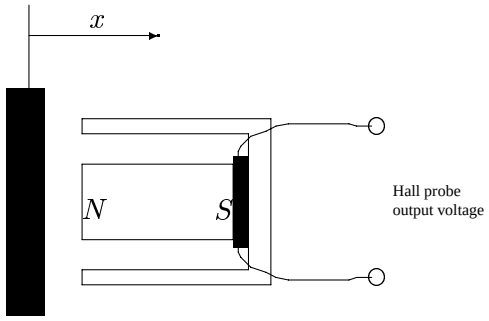

- permanent magnet establishes Φ
- Φ varies inversely with x
- Hall output varies in proportion to Φ

6.12 Variable Reluctance Probes

- gap requirements
- bandwidth: to 2 kHz (limited by eddy current effects)
- linearity: good

- cost: moderate
- compatibility with cans: must be thin
- magnetic noise susceptibility: high
- standoff distance: small, strong effect on sensitivity

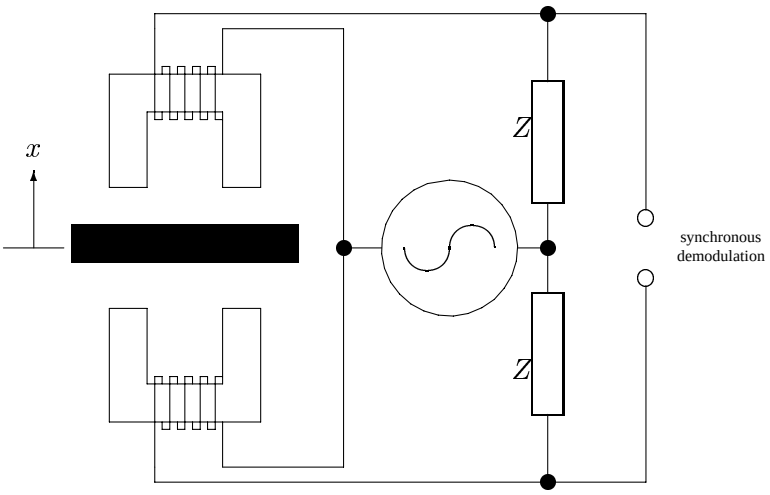

- each coil impedance varies inversely with gap
- resistance is matched to nominal coil impedance
- output voltage is very linear in gap

6.13 Differential Variable Reluctance

Bridge operation:

$$v_1 = \frac{Z(\omega)}{j\omega L_1 + Z(\omega)} V \qquad v_2 = \frac{Z(\omega)}{j\omega L_2 + Z(\omega)} V$$

$$L_1 = \frac{\alpha}{g_0 - x} \qquad L_2 = \frac{\alpha}{g_0 + x}$$

$$v_1 - v_2 = \frac{2j\omega Z(\omega) V}{Z^2(\omega)(g^2 - x^2) - \omega^2\alpha + 2j\omega\alpha Z(\omega) g} x$$

$Z(\omega)$ is matched to nominal coil impedance:

$$Z(\omega) = \omega \frac{\alpha}{g}$$

so that

$$v_1 - v_2 \approx \frac{V}{g}x$$

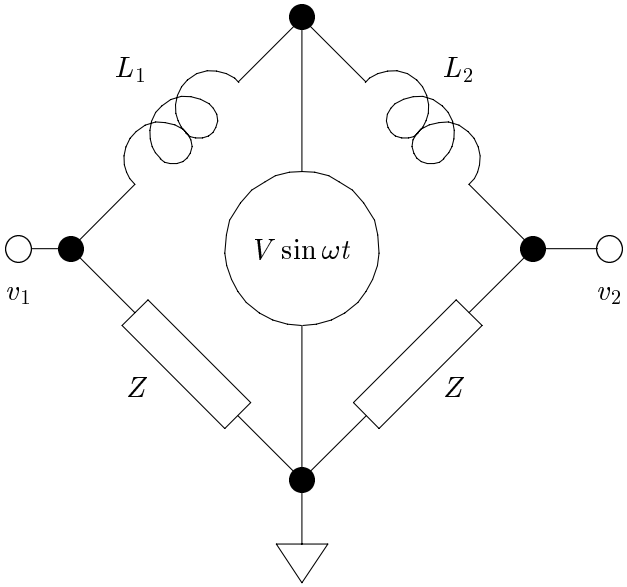

6.14 Synchronous Demodulation

Bridge output:

$$v_1 - v_2 = \frac{V}{g}x \sin \omega t$$

Take product with bridge drive:

$$V \sin \omega t \times (v_1 - v_2) = \frac{V^2}{g}x \sin^2 \omega t$$

Low pass filter (average over 1/2 cycle):

$$\frac{V^2}{g}\frac{\omega}{\pi}\int_t^{t+\frac{\pi}{\omega}} x \sin^2 \omega t dt \approx \frac{V^2}{g}x$$

This is essentially convolution and is very effective at removing noise at frequencies other than ω.

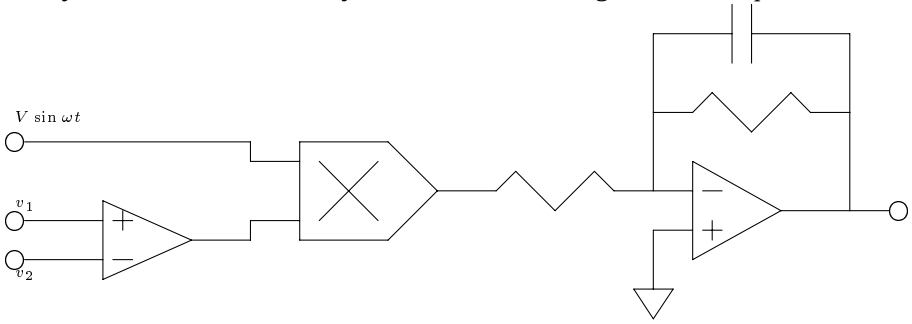

6.15 Signal Processing Waveforms: $x < 0$

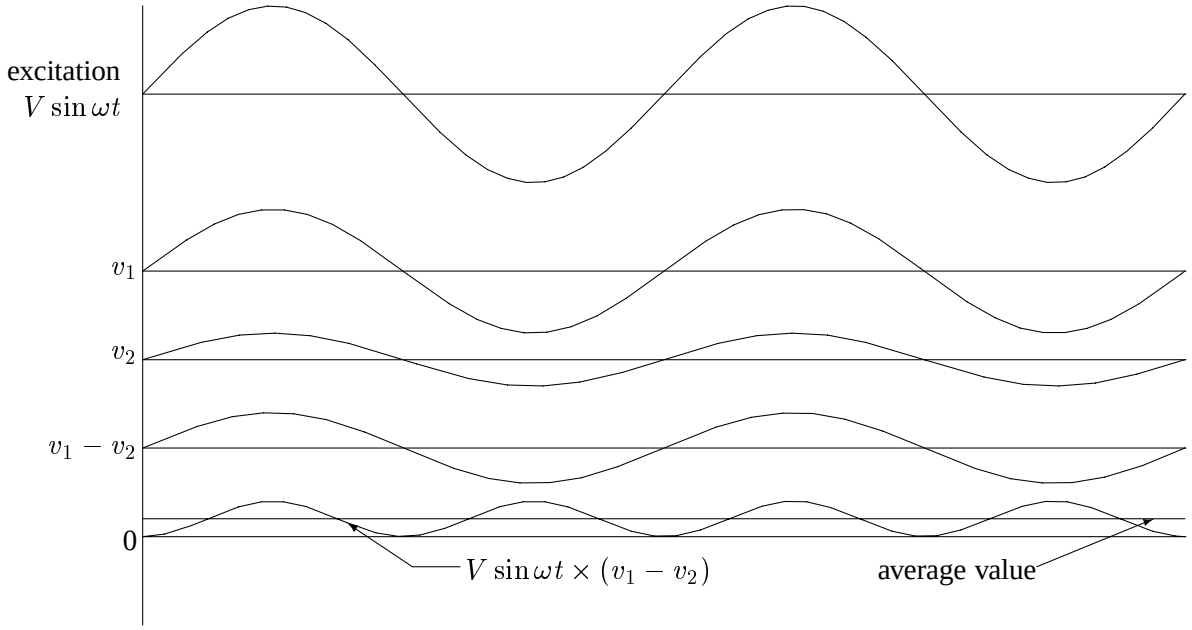

6.16 Signal Processing Waveforms: $x > 0$

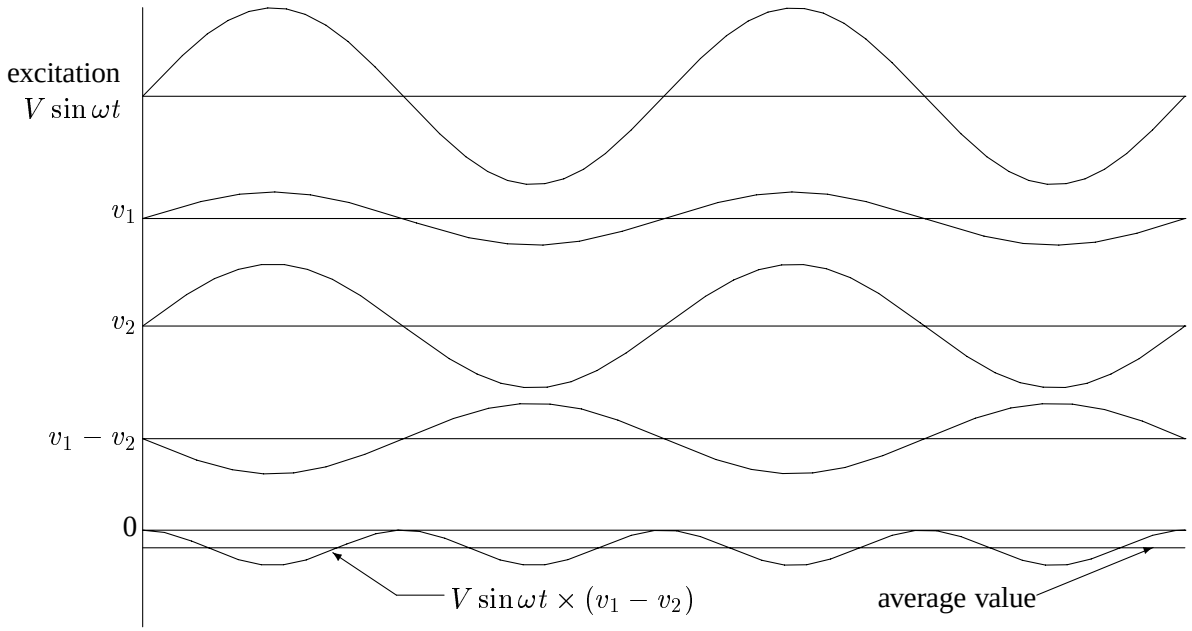

6.17 Signal Processing Waveforms: $x = 0$

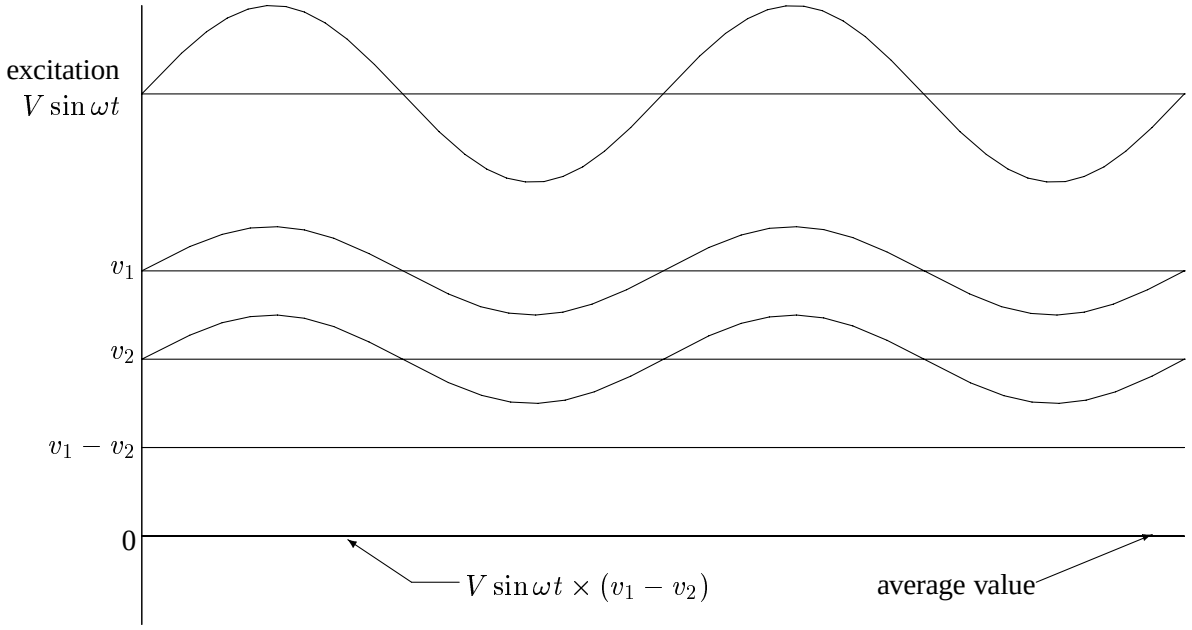

6.18 Problems with Variable Reluctance

- very susceptible to stray field from magnetic bearings: keep probe flux as high as possible
- maximum driving frequency is limited by eddy currents
- minimum driving frequency is limited by bandwidth requirements

  bandwidth $< 0.2\ \omega$
- iron reluctance should be small compared to air gap. At high frequencies, this requires thin lams, short iron paths
- short iron paths leave little room for coils: conflicts with desire to keep gap flux large

6.19 Self Sensing Stators: Basic Concepts

- the bearing stator is a variable reluctance sensor

- coil currents and voltages are available
- coil current and voltage are functionally related by gap length (ignore magnetic non-idealities)
- this function should be invertible to yield gaps or shaft position

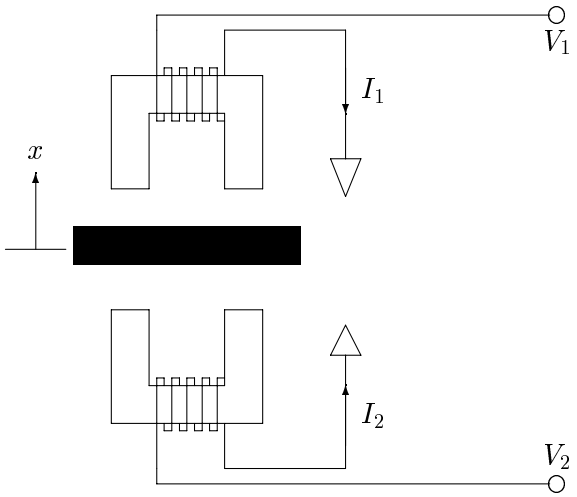

6.20 Motivation

- Specific:
  - reduce wire count
  - reduce components in harsh environment
  - eliminate sensor–actuator noncollocation
  - reduce bearing package length/volume
- Generic:
  - reduce cost
  - increase reliability
  - improve system dynamics

6.21 Prior Research (Patents)

- Bleuler and Vischer
  state estimation and switch demodulation
- Jayawant
  switch demodulation
- Okada
  switch demodulation / synchronous demodulation
- Ianello
  switch demodulation / differential rectification

6.22 General Methods

- state estimation
  - actuator and system are considered integrated
  - actuator is voltage in / current out
  - journal position is obtained by state estimation
  - plant transfer function has pole–zero pairs in RHP
- parameter estimation
  - actuator and system are spectrally separated
  - actuator is voltage in / current out
  - position of journal is a parameter of magnetic model
  - standard approach: forward filtering of current waveform

6.23 Gap Dynamics

$$\begin{aligned} V_1 &= \frac{d}{dt} L_1 I_1 + R I_1 \\ &= I_1 \frac{dL}{dt} + L_1 \frac{dI}{dt} + R I_1 \\ &= I_1 \frac{\mu_0 N^2 A}{(g-x)^2} \frac{dx}{dt} + \frac{\mu_0 N^2 A}{g-x} \frac{dI_1}{dt} + R I_1 \end{aligned}$$

$$V_2 = -I_2 \frac{\mu_0 N^2 A}{(g+x)^2} \frac{dx}{dt} + \frac{\mu_0 N^2 A}{g+x} \frac{dI_2}{dt} + RI_2$$

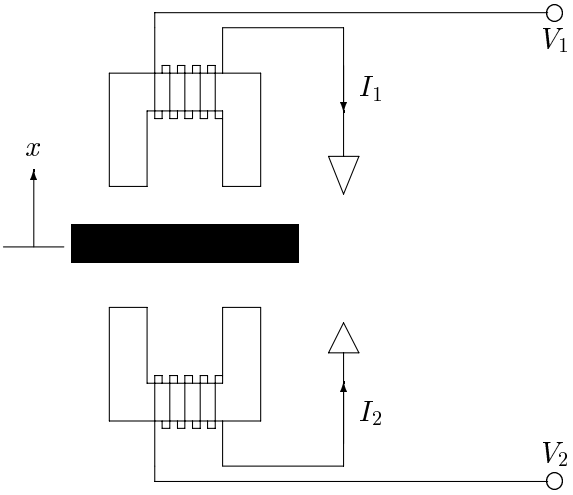

coil voltage is sum of resistive term, inductive (depends on gap), and motion back–EMF

6.24 Parameter Estimation: Ideal Filtering

Assume that switching effect is much stronger than the journal induced back–emf:

$$LdI/dt \gg IdL/dt$$

so that

$$V = \frac{\mu_0 N^2 A}{g-x} \frac{dI}{dt} + RI$$

Further, V is a square wave with amplitude V_{ps} and duty cycle δ.

The switching waveform is a triangle wave with the form:

$$I(t) \approx \begin{cases} I_0 + \frac{V_{ps}}{L} t & 0 < t < \delta\tau \\ I_0 + \frac{V_{ps}}{L}(2\delta\tau - t) & \delta\tau < t < \tau \end{cases}$$

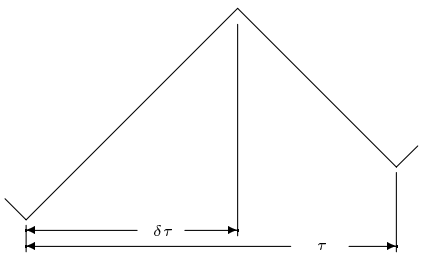

6.25 Step 1: High Pass Filter

Remove the average value:

$$I_f(t) = \begin{cases} \frac{2V_{ps}}{L}(1-\delta)(t-0.5\delta\tau) & 0 < t < \delta\tau \\ -\frac{2V_{ps}}{L}\delta(t-0.5(\delta+1)\tau) & \delta\tau < t < \tau \end{cases}$$

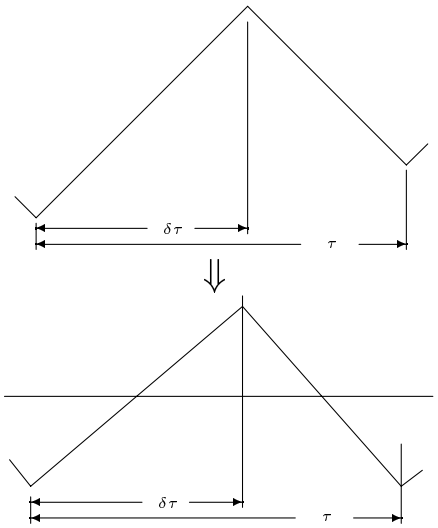

Highpass filter: poles in Butterworth configuration at about $0.1\omega_s$ (0.13 was used in the prototype)

6.26 Step 2: Rectify

Rectify this result:

$$I_r(t) = |I_f(t)| = \begin{cases} \frac{2V_{ps}}{L}(1-\delta)(0.5\delta\tau - t) & 0 < t < 0.5\delta\tau \\ \frac{2V_{ps}}{L}(1-\delta)(t-0.5\delta\tau) & 0.5\delta\tau < t < \delta\tau \\ \frac{2V_{ps}}{L}\delta(0.5(\delta+1)\tau - t) & \delta\tau < t < \frac{(1+\delta)\tau}{2} \\ \frac{2V_{ps}}{L}\delta(t-0.5(\delta+1)\tau) & \frac{(1+\delta)\tau}{2} < t < \tau \end{cases}$$

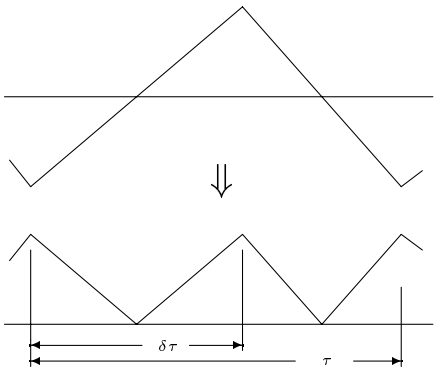

Use a conventional precision rectifier.

6.27 Step 3: Average (Low Pass Filter)

Finally, average the result over one full cycle:

$$\begin{aligned} I_a &= \frac{1}{\tau}\int_0^{\tau} I_r(t)dt = \frac{1}{2}\delta(1-\delta)\frac{V_{ps}\tau}{L} \\ &= \delta(1-\delta)\frac{V_{ps}}{2L_0}\frac{g_0 \pm x}{g_0} \end{aligned}$$

Resulting signal is:

- proportional to the gap
- affected by the duty cycle

Low pass filter, poles at about $0.1\omega_s$, in Butterworth configuration.
(0.05 was used in the prototype)

6.28 Sample Waveforms

Compare actual beam deflection to waveform filter: pinned beam

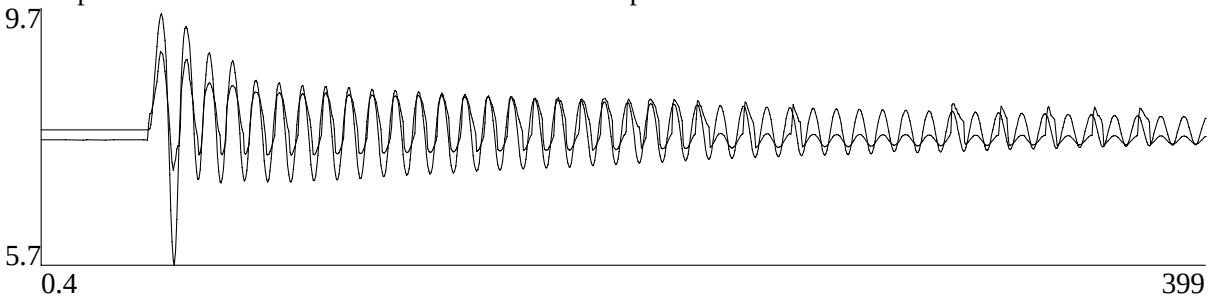

unforced rotor response, duty cycle is constant

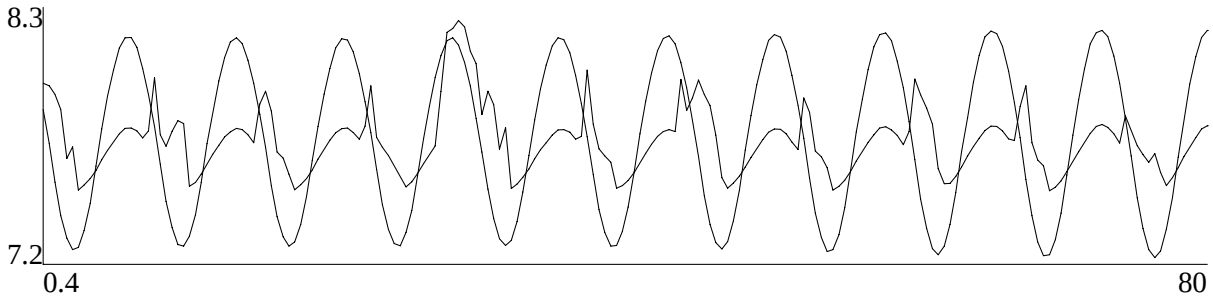

forced rotor response, duty cycle varies sinusoidally

6.29 Duty Cycle Dependency

Duty cycle produces variations in bearing force:

$$\delta \propto \frac{df}{dt}$$

$\Rightarrow$ filtered output depends on:

- gap (displacement)
- force

Two approaches to eliminate force dependency:

1. scaling compensation:

$$g_0 + x = I_a \frac{2L_0 g_0}{V_{ps}\delta(1-\delta)}$$

2. parameter estimation:

   run a parallel simulation of the bearing and adjust the simulated gap to make the filtered simulated current waveform match the filtered measured waveform

6.30 Scaling Compensation

Looks easiest to compensate for δ by scaling.

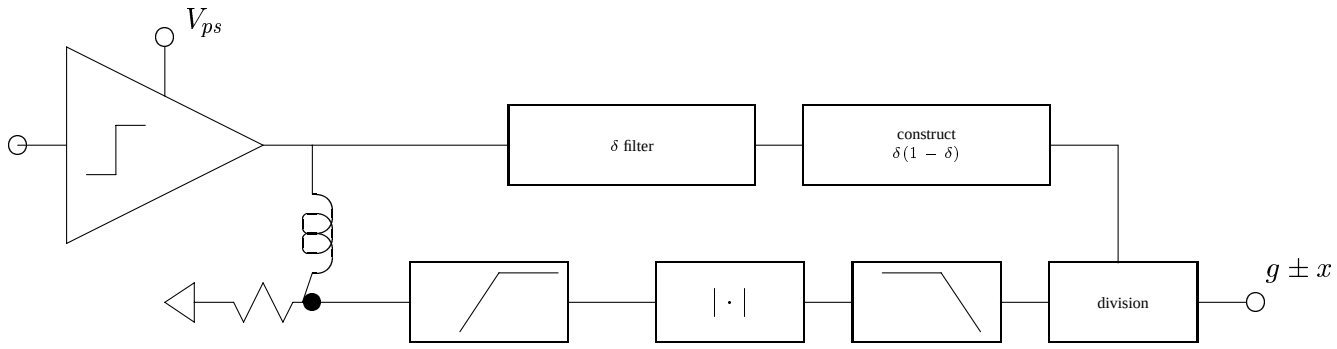

However:

- division is complicated and time consuming
- direct measurement of δ requires additional delay and filtering
- end result is only as good as the forward filter performance: actual circuits will not match the idealized circuits

6.31 Parameter Estimation

Instead, run a simulation of the bearing magnetic dynamics:

- apply the same voltage to the simulation as to the actual bearing
- filter the output with identically the same filter
- force the two filter outputs to be the same by choice of the gap in the simulation

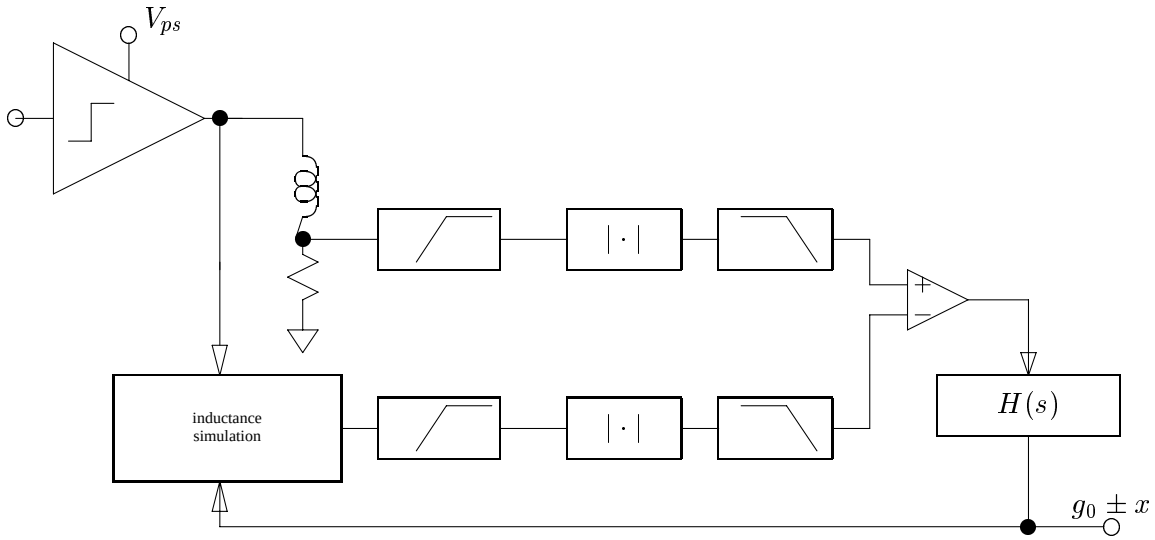

Output quality is primarily determined by simulation quality and $H(s)$.

6.32 Bearing Simulation

Recall coil voltages:

$$V = \mp I\frac{\mu_0 N^2 A}{(g \pm x)^2}\frac{dx}{dt} + \frac{\mu_0 N^2 A}{g \pm x}\frac{dI}{dt} + RI \quad \Rightarrow \quad \frac{dI}{dt} = \frac{g \pm x}{\mu_0 N^2 A}(V - RI) \pm I\frac{1}{g \pm x}\frac{dx}{dt}$$

If we ignore the back–emf due to rotor motion, we get

$$\frac{dI}{dt} = \frac{g \pm x}{\mu_0 N^2 A}(V - RI)$$

Simulation block looks like:

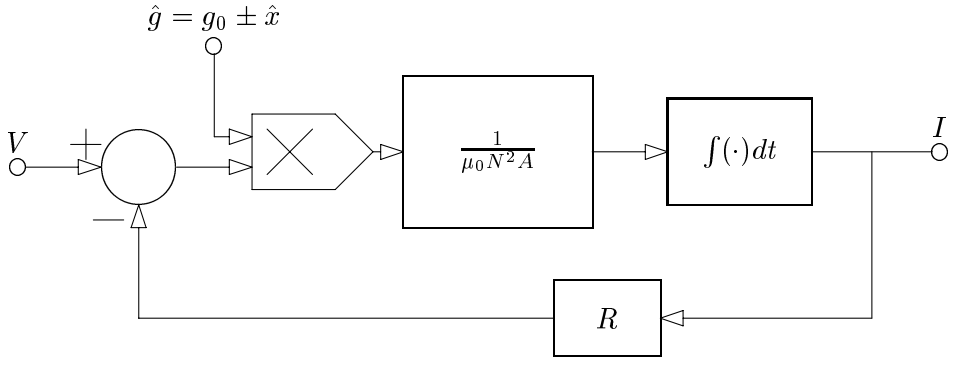

6.33 The Feedback, $H(s)$

The job of the feedback controller, $H(s)$, is to use the error between the two filtered current waveforms to produce an estimate of the gap and, in doing so, force the error to zero.

The system is nonlinear, but can be linearized and shown to be essentially first order. As a result, we can stabilize the loop with a phase lag compensator: proportional–integral control with finite bandwidth:

$$H(s) = \left(\frac{a}{s} + b\right)\frac{1}{\tau s + 1} = \frac{bs + a}{s(\tau s + 1)}$$

Gap parameter estimator bandwidth will depend upon τ and b. These are limited by the dynamic response of the forward path filter.

prototype: $a = 0.2$, $b = 0.0001$, $\tau \approx 10^{-4}$.

6.34 Sample Waveforms

Compare actual beam deflection to estimator output: pinned beam

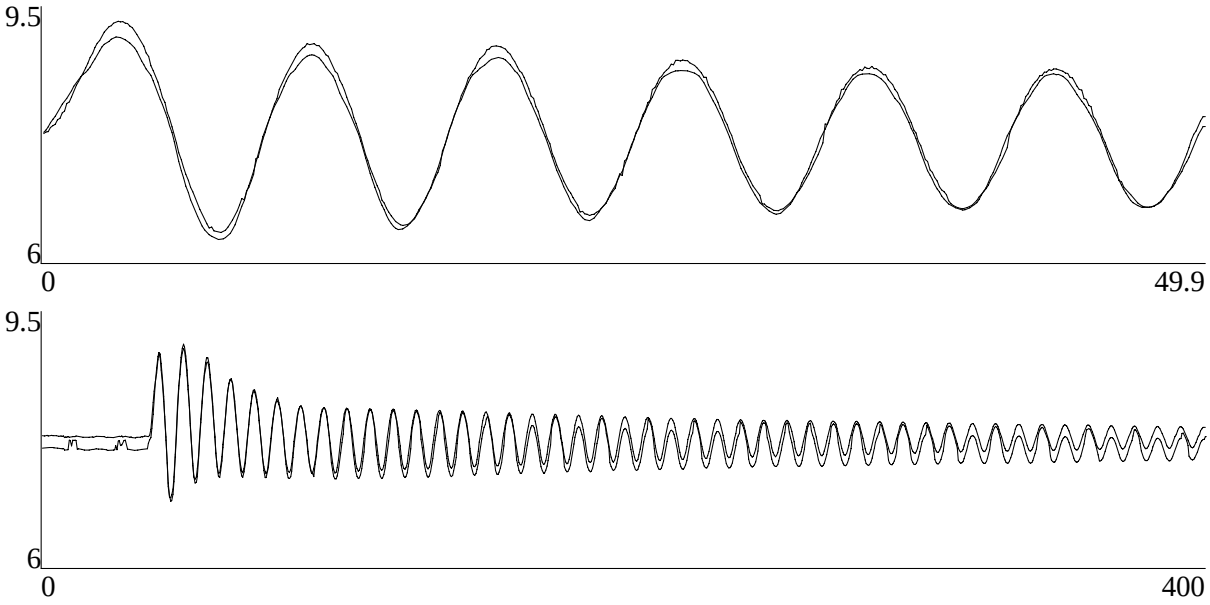

unforced rotor response, duty cycle is constant

6.35 Another Sample Waveform

Compare actual beam deflection to estimator output: pinned beam

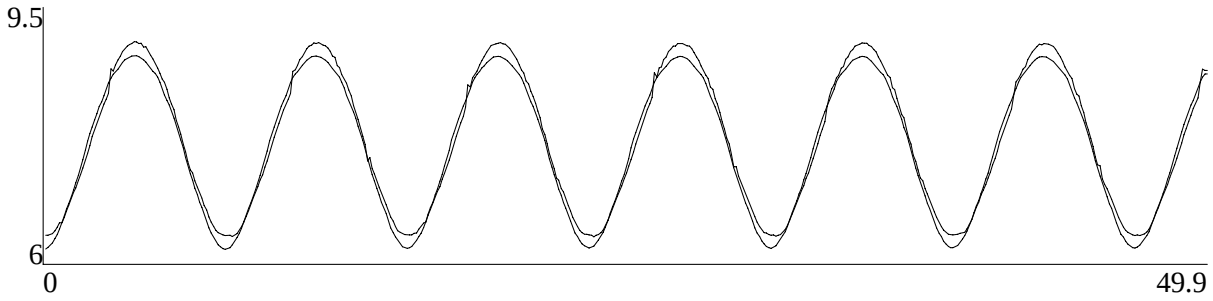

forced rotor response, duty cycle varies sinusoidally

6.36 Prototype Performance

Bandwidth:

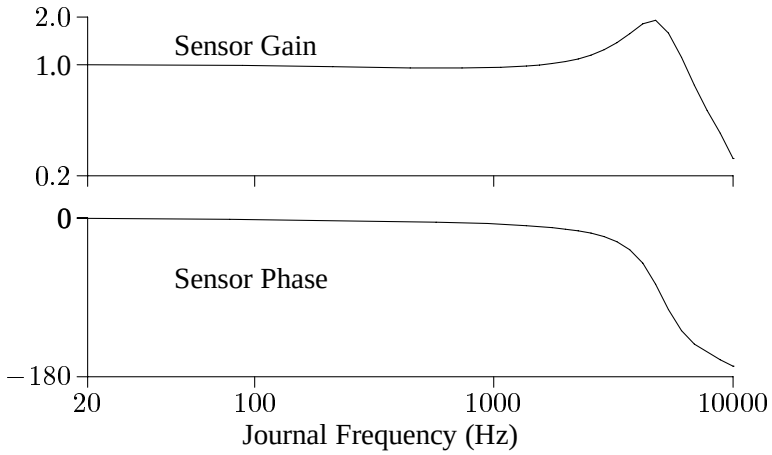

Noise:

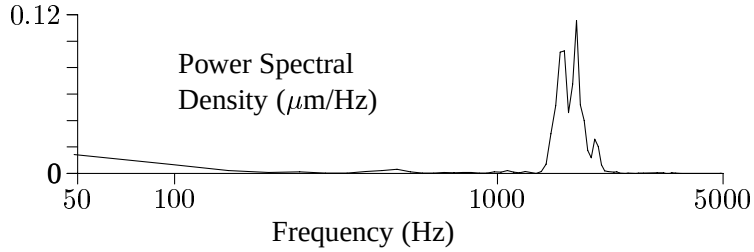

Linearity:

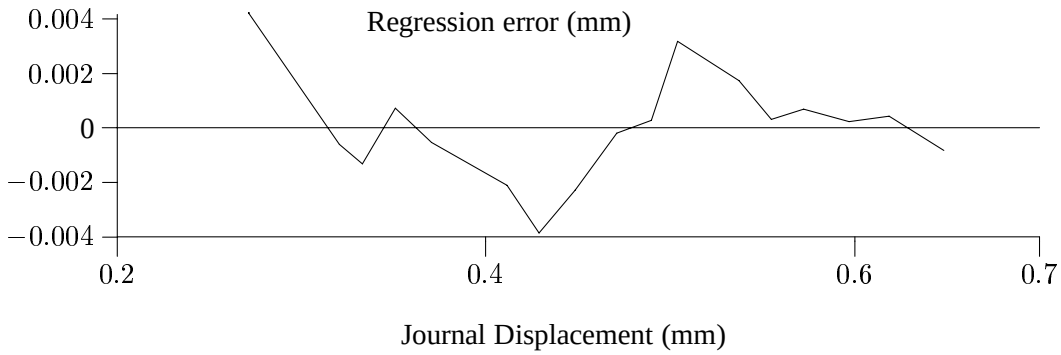

6.37 Drawbacks

- sensitivity

  at sensor frequencies, iron reluctance is large compared to air gap:

$$L = \frac{\mu_o N^2 A}{2g + \ell/\mu_r}$$

$$S_g^L \doteq \frac{\partial L}{\partial g}\frac{g_0}{L_0} = -\frac{2g_0}{2g_0 + \ell/\mu_r}$$

  for typical geometry: $g \approx 0.5$mm, $\ell \approx 100$mm, $\mu_r(20\text{ kHz}) \approx 100$

$$\Rightarrow S_g^L \approx -0.5$$

- linearity

  at high force (high flux density), permeability is a function of current

6.38 Saturation Effects

1. as gap **decreases** and force increases, iron begins to saturate
2. iron saturation produces a loss in relative permeability
3. loss in relative permeability looks like loss of inductance
4. loss of inductance is interpreted as an **increase** in gap length

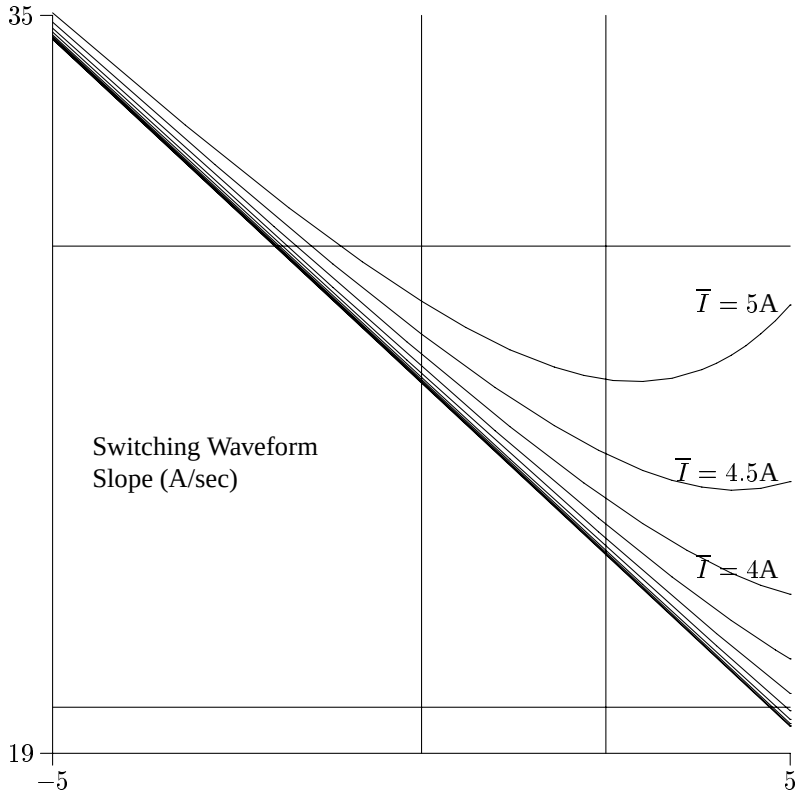

This is a problem for high performance applications, eg.: aircraft jet engines.

6.39 Future Work

- demonstrate on test rig
- incorporate saturation nonlinearity into estimator
- develop and demonstrate coupled stator methods

6.40 Including Saturation

Rearrange simulation model:

$$V - IR = N\frac{d\Phi}{dt} \quad \Rightarrow \quad \frac{dB}{dt} = \frac{1}{NA_g}(V - IR)$$

$$B = \frac{\mu_0 NI}{2g + \ell/\mu_r} \quad \Rightarrow \quad I = \frac{1}{\mu_0 N}(2g + \ell/\mu_r)B$$

0

The relative permeability (at a given frequency) depends only upon B:

$$\frac{\ell}{\mu_r} = f(B)$$

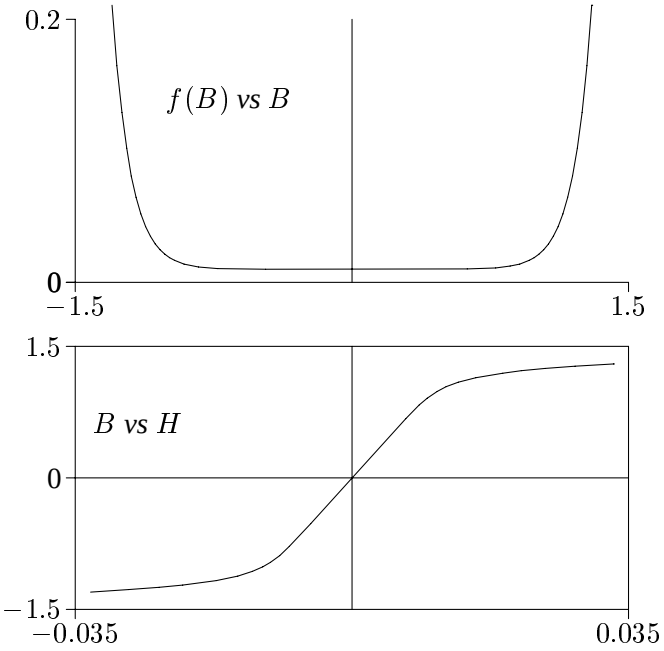

6.41 Revised Simulation Model

The new simulation model, including saturation, is:

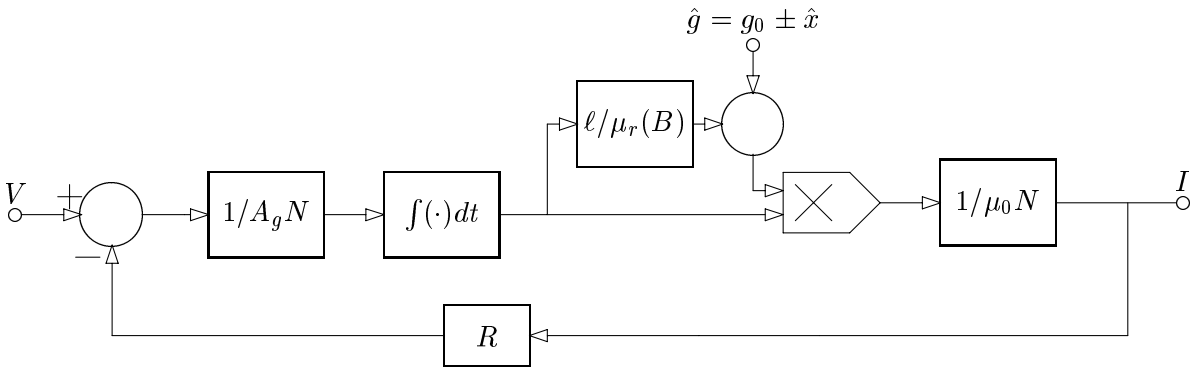

Note that this model **does not neglect "velocity" effects.**

6.42 Differential Gaps

Opposing coils sense motion differentially:

$$g_1 = g_0 + g_t - x$$

$$g_2 = g_0 + g_t + x$$

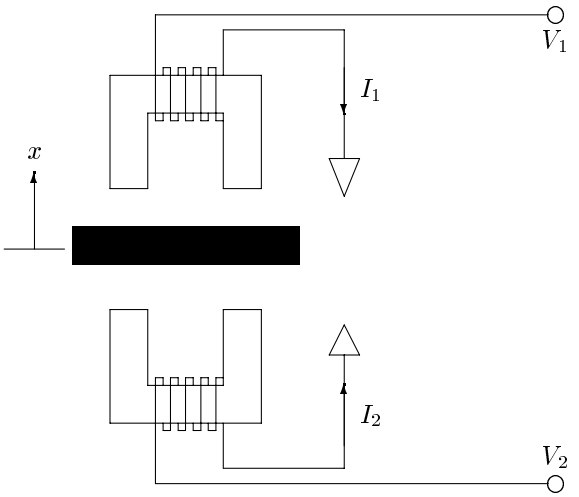

The gap estimates for the two gaps should not be independent!

6.43 Differential Processor

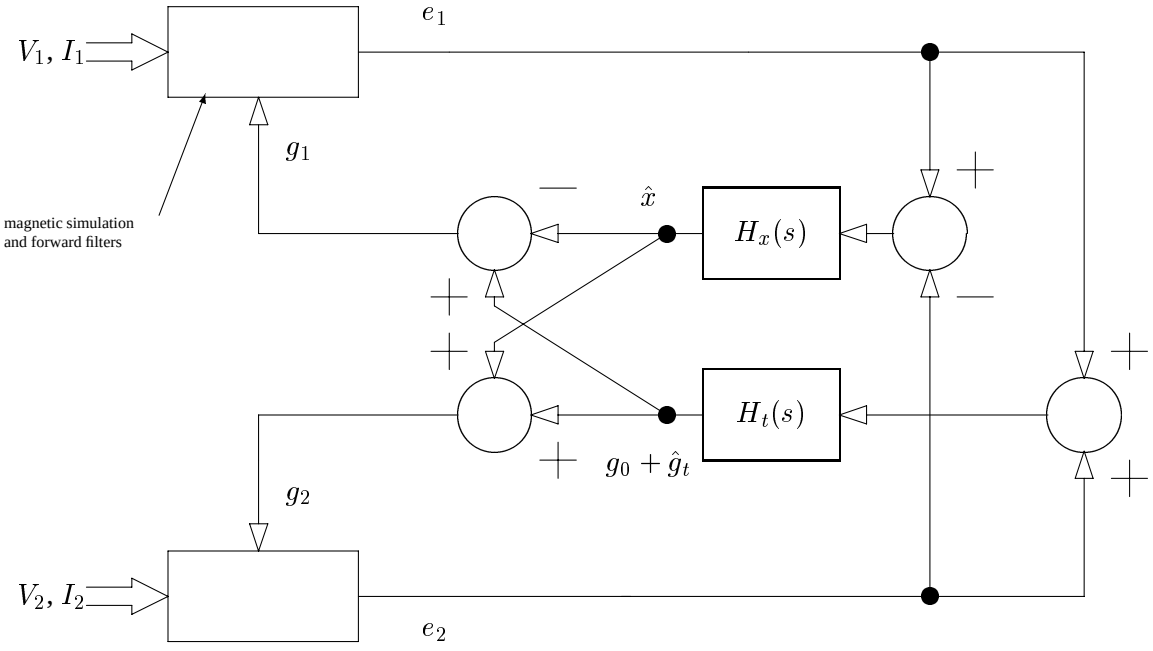

$H_x(s)$ produces a fast loop for estimating displacement, x
$H_t(s)$ produces a slow loop for estimating thermal or centrifugal growth, g_t

Chapter 7

Controllers

7.1 General Structure

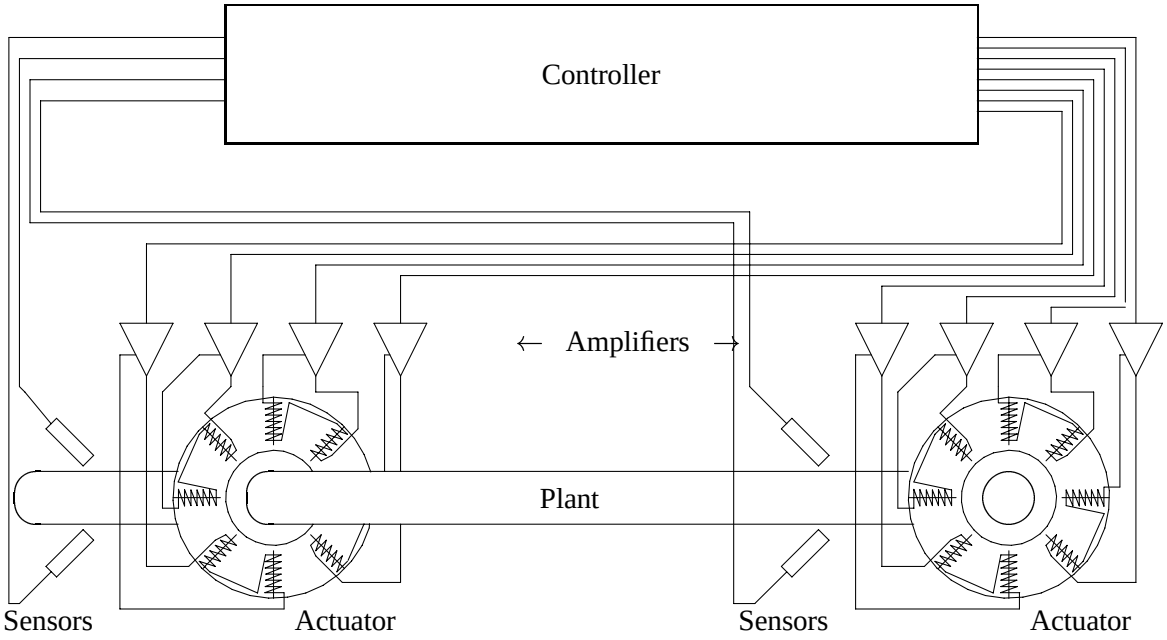

7.2 Controller Roles

Primary tasks:

- coordinate transformation of sensor signals

- collection of any other parameters needed by control algorithm
- generation of control current (or flux) *requests*:
  execute control algorithm
- coordinate transformation, biasing of amplifier signals

Secondary tasks:

- permit modification of control algorithm
- implement diagnostic measurements

7.3 Controller Implementation

7.3.1 Analog

- Generally restricted to performing linear math, implementation of linear filters:

$$G(s) = a\frac{\prod s - z_i}{\prod s - p_i}$$

- Some nonlinearity using diodes, analog multipliers
- Use op-amps, resistors and capacitors. Inductors are avoided because of size, weight, non-ideality.
- Problems: component drift, reliability of potentiometers, general characteristics of filters are fixed by circuits.
- Advantages: inexpensive, compact, fundamental simplicity

7.3.2 Digital

- Fastest when performing linear math (difference equations):

$$G(s) = a\frac{\prod s - z_i}{\prod s - p_i}$$

- Can implement nonlinear equations too, but at greater computational expense.
- Use digital signal processors, A/D converters, D/A converters
- Problems: electrical complexity, higher incidence of component failure, cost.
- Advantages: easier to modify algorithms, implement complex algorithms, perform data acquisition functions (diagnostics, monitoring)

7.4 Analog Filter Components

Scaling amplifier:

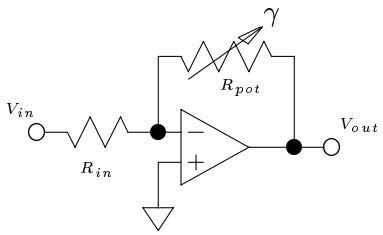

$$V_{out} = -\gamma \frac{R_{pot}}{R_{in}} V_{in}$$

Integrator:

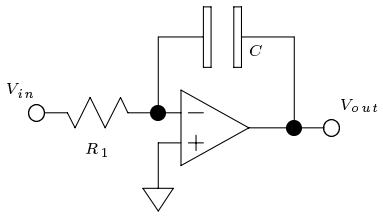

$$V_{out}(s) = -\frac{R}{sC} V_{in}(s)$$

Low pass filter:

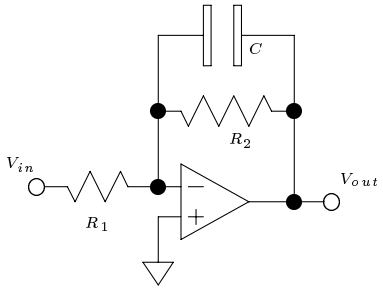

$$V_{out}(s) = -\frac{R_2}{R_1} \frac{1}{sCR_2 + 1} V_{in}(s)$$

Summing amplifier:

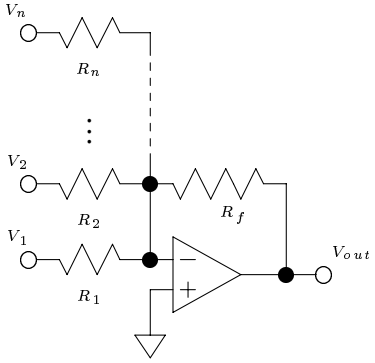

$$V_{out} = -\gamma R_f \left(\frac{1}{R_1} V_1 + \frac{1}{R_2} V_2 + \ldots + \frac{1}{R_n} V_n \right)$$

Differentiator:

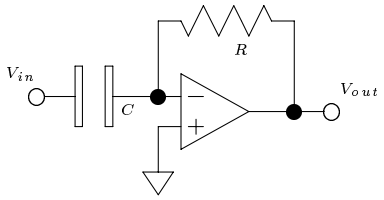

$$V_{out}(s) = -sCRV_{in}(s)$$

High Pass Filter:

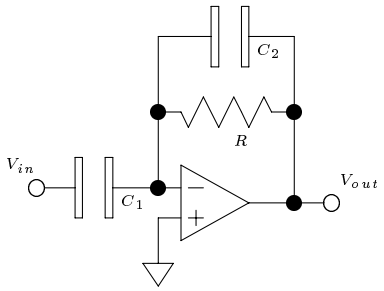

$$V_{out}(s) = -\frac{sC_1R}{1 + sC_2R} V_{in}(s)$$

Phase Lead:

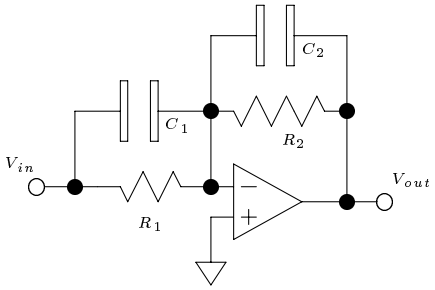

$$V_{out}(s) = -\frac{sC_1R_1 + 1}{sC_2R_2 + 1} \frac{R_2}{R_1} \; V_{in}(s)$$

Buffer voltage follower:

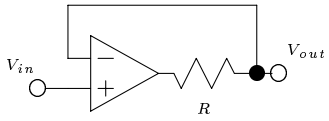

$$V_{out} = V_{in}$$

Limiter:

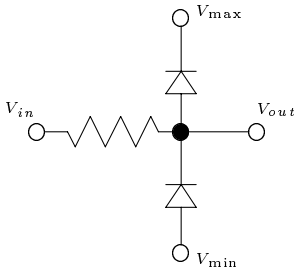

$$V_{out} = \begin{cases} V_{\min} & : \ V_{in} < V_{\min} \\ V_{in} & : \ V_{\min} < V_{in} < V_{\max} \\ V_{\max} & : \ V_{\max} < V_{in} \end{cases}$$

Rectifier:

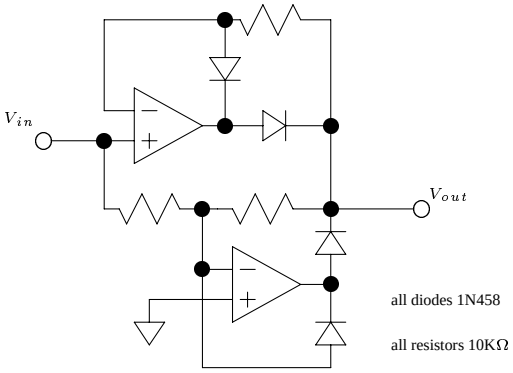

$$V_{out} = |V_{in}|$$

Square Function:

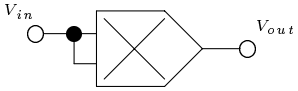

$$V_{out} = V_{in}^2$$

Square Root Circuit:

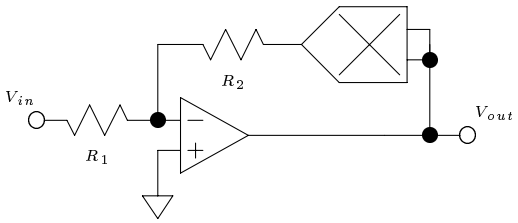

$$V_{out} = -\frac{R_2}{R_1}\sqrt{V_{in}}$$

$$(\ V_{in} \leq 0 \ )$$

Notch Filter

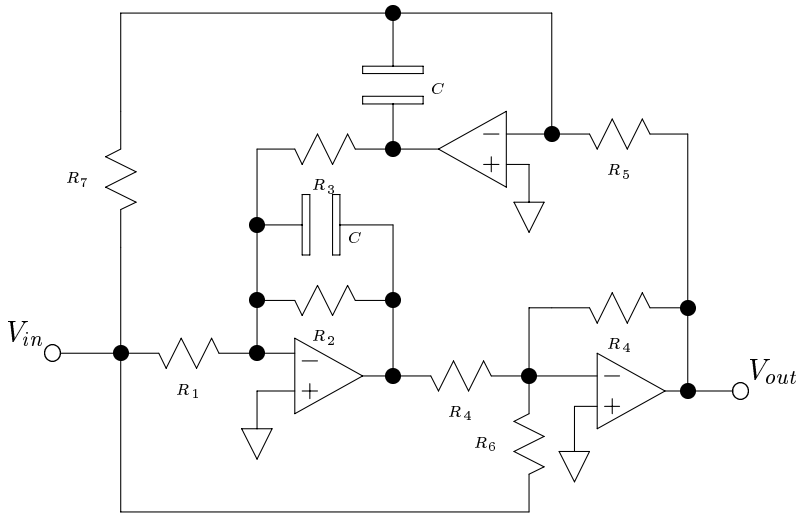

$$V_{out}(s) = \frac{G(s^2 + \omega_0^2)}{s^2 + 2\xi\omega_0 s + \omega_0^2} V_{in}(s)$$

$$\omega_0 = \frac{1}{C\sqrt{R_3 R_5}} \quad G = -\frac{R_2}{R-1}$$

$$\xi = \frac{1}{2\omega_0 R_2 C}$$

assuming that

$$R_2 R_6 = R_1 R_4 \quad R_4 R_7 = R_5 R_6$$

PID Controller: Component Based

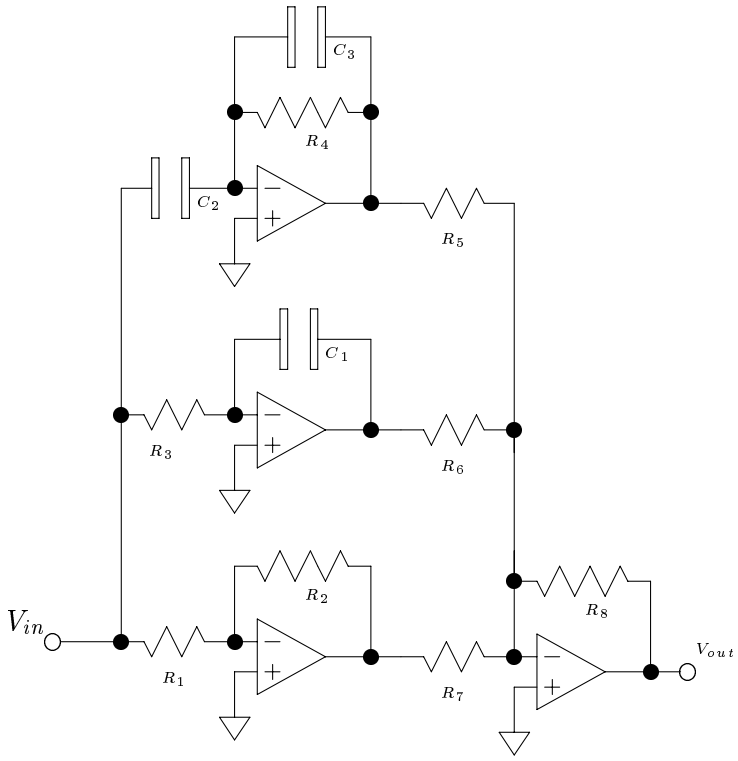

$$
\begin{aligned}
G(s) &= \frac{V_{out}(s)}{V_{in}(s)} \\
&= \frac{R_2 R_8}{R_1 R_7} && \text{P} \\
&\quad + \frac{R_8}{s C_1 R_3 R_6} && \text{I} \\
&\quad + \frac{s C_3 R_4 R_8}{R_5 (1 + s C_3 R_4)} && \text{D}
\end{aligned}
$$

7.5 Analog Controller: Principal Restrictions

Maximum voltage at each internal amplifier output: ± 12 volts

Maximum slew rate: ± 10 V$/\mu$ sec

Noise level: usually about 1–10 mV with good circuit design.

Selection of gains throughout the controller is critical in protecting the signal to noise ratio! Best you can do is *maybe* 80 dB. More likely to be on the order of 40 dB.

7.6 Simple Design Rules: Analog Controllers

1. Never: attenuate a signal and then amplify it:

$$V_2 = 0.15V_1 \quad V_3 = 7V_2$$

The noise is added at the attenuated level and the amplified along with the signal.

2. each component (single amplifier) filter should be strictly proper (more poles than zeros)

$$G(s) = a\frac{\prod_{j=1}^{n} s - z_j}{\prod_{k=1}^{m} s - p_k} \qquad m > n$$

3. no single filter should have a pole – zero ratio greater than about 20:

$$G(s) = a\frac{s+b}{(s+c)(s+d)} \qquad \min(c,d) < 20b$$

7.7 Simple Grounding Rules: Analog Controllers

1. all circuit board grounds in an enclosure should be joined at a single point: “star ground”

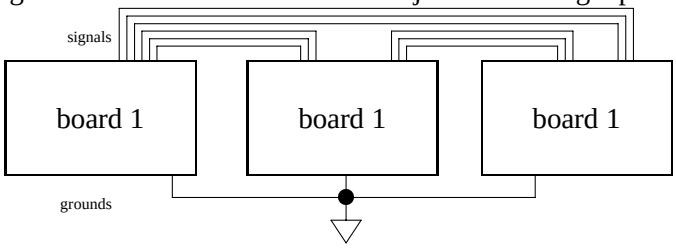

2. all shielded cables should have the shield connected to ground at a single point – even when interconnecting enclosures: use a single additional ground wire to interconnect the grounds

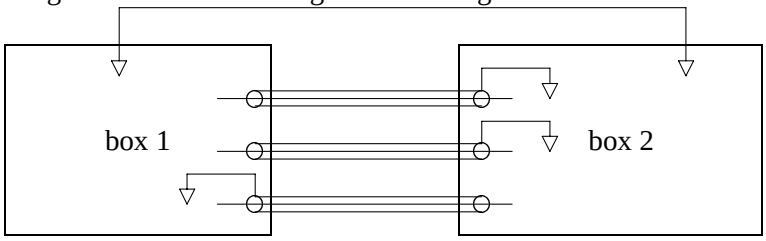

3. use differential transmitter–receiver pairs between widely separated boards to minimize noise, ground differential effects

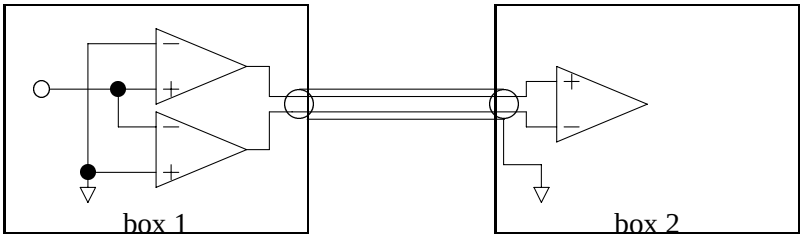

7.8 Some Other Useful Guidelines

- avoid resistances larger than about 470 kΩ: too noisy
- avoid resistances smaller than about 220 Ω: too much load on op–amps
- always bypass power supply lines to ground very close to op–amps with about $0.1\mu f$ capacitance: avoid the effects of power supply line inductance

7.9 Digital Controller - Simple

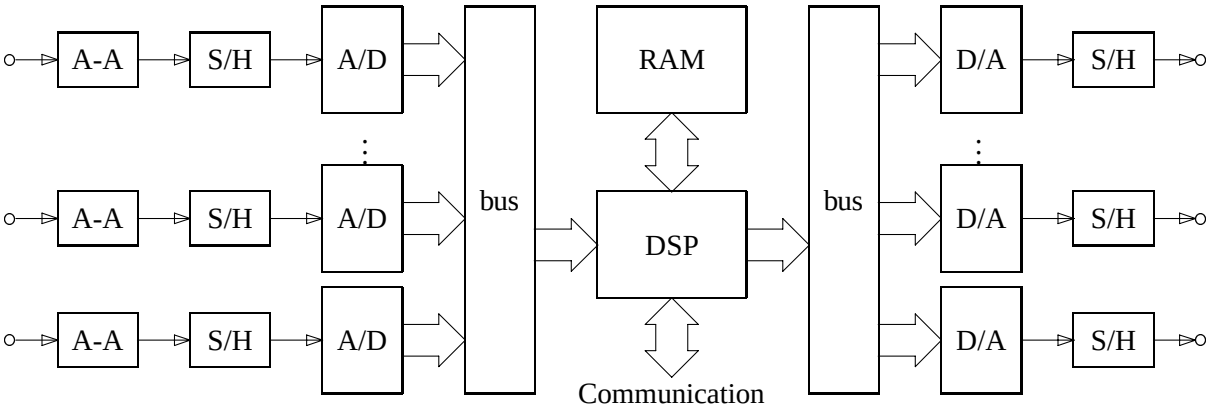

7.10 Digital Controller Components: Sample and Hold

Grabs an analog signal at its input and holds it constant at its output in response to the state of a control line.

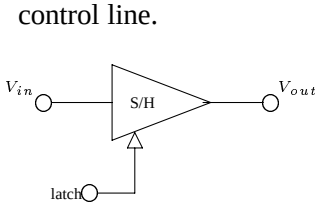

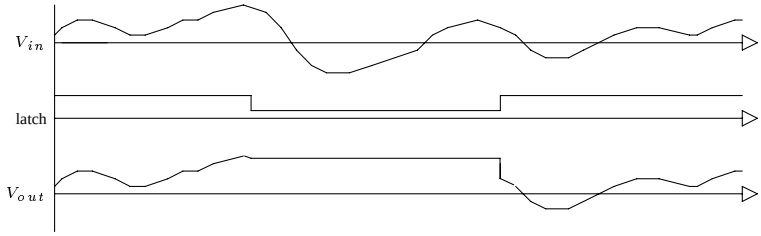

Used to enforce simultaneous sampling of inputs, simultaneous delivery of outputs, and to prevent bit transition glitches on the outputs.

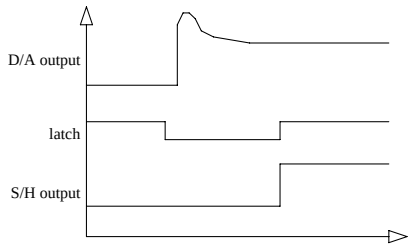

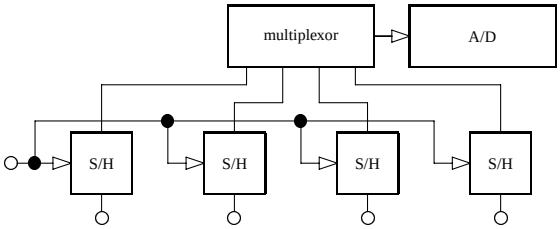

7.11 Digital Controller Components: D/A

Converts a digital number to an analog voltage. Usually linear conversion: $V_{out} = aD_{in} + b$. Typical resolution: 12–16 bits. Typical conversion time (settling time): 50 nanoseconds.

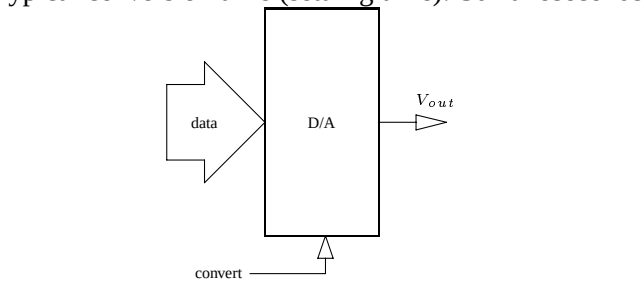

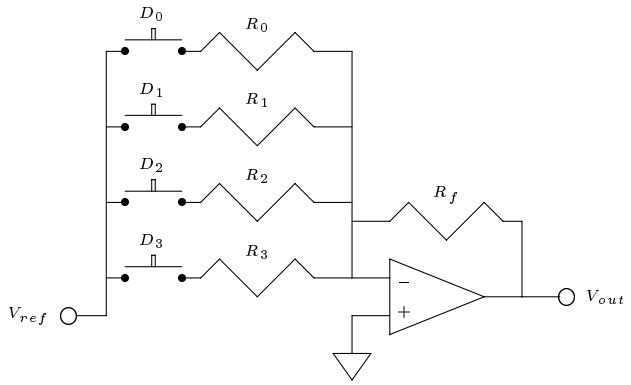

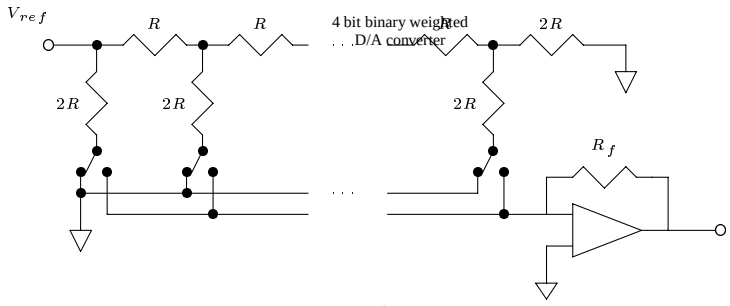

4 bit binary weighted D/A converter

ladder circuit for multibit D/A converter

7.12 Digital Controller Components: A/D

Converts an analog signal (voltage) to digital representation. Usually implemented as a D/A converter in a feedback loop, iterative conversion. Typical resolution: 10–14 bits. Typical conversion time: 1–3 microseconds.

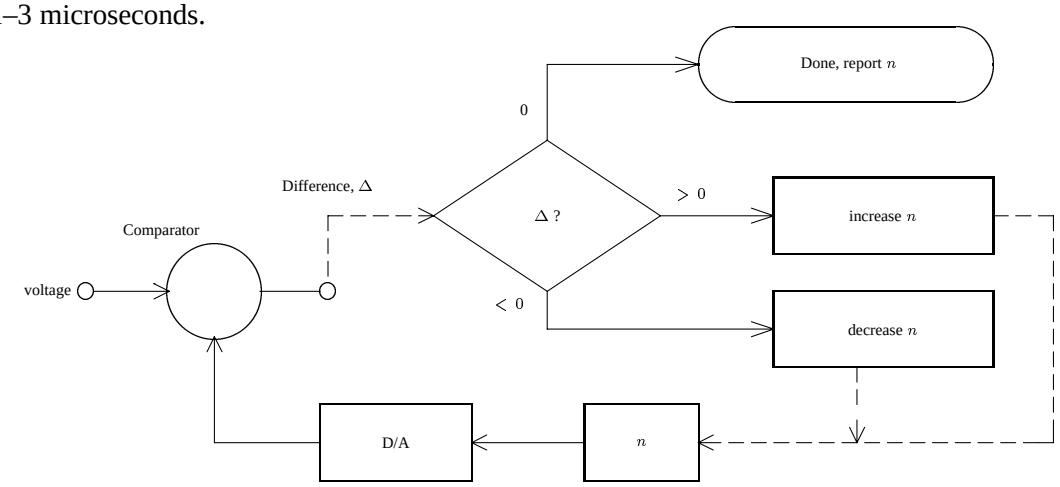

7.13 Digital Controller Components

Digital Signal Processor (DSP): Optimized for very rapid multiply and accumlate, very fast at the calculation

$$y_i = \sum_{j=i-k}^{i-1} a_i x_i + \sum_{j=i-m}^{i-1} b_i y_i$$

Floating point DSPs now common Single computation time: 50 nsec multiply, 50–100 nsec fetch, some parallelism possible.

Random Access Memory (RAM): Stores digital information for use by the DSP or other CPU. Various kinds: SRAM, DRAM, on–chip cache – have varying access times, affect speed of computation.

Bus: Permits multiple input/output devices to be addressed through single CPU I/O port. May permit parallelism: I/O deviced talk directly to RAM without passing through CPU; multiple CPUs can share same bus, RAM, I/O devices.

7.14 Operation Sequence

	CPU	A/D	D/A
1	requests A/D conversion		
2	computes next out–put from last data	locks S/H amps	
3	delivers next output to D/A	begins conversion(s)	
4	requests D/A conver-sion	completes conver–sion(s), notifies CPU	
5	retrieves data from A/D		converts output data

7.15 Aliasing

The most important limitation associated with a sampled data system is that of finite, discrete sampling which leads to aliasing.

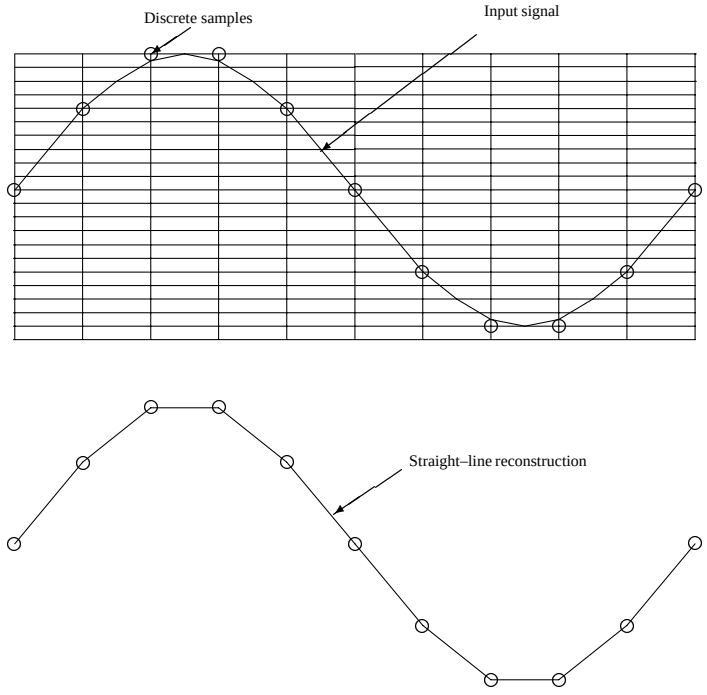

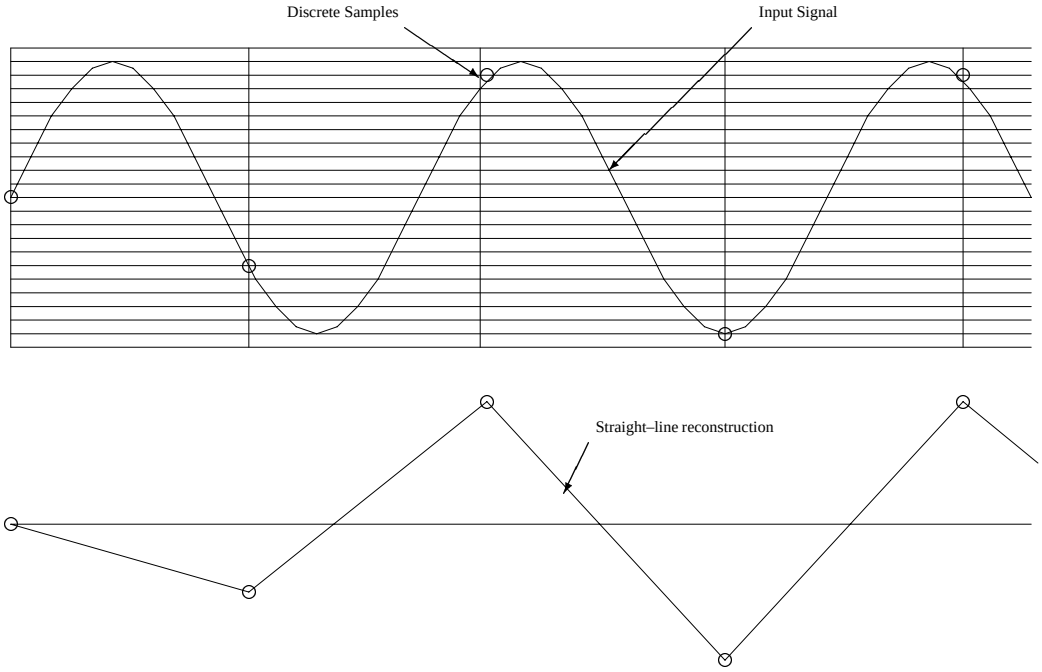

If a signal is sampled at a frequency f_s, the highest signal frequency which can be reconstructed from the data is $0.5f_s$. This is only with an infinite length sample. (Shannon's sampling theorem.)

Signals with higher frequency will appear in the data at a lower frequency – aliased.

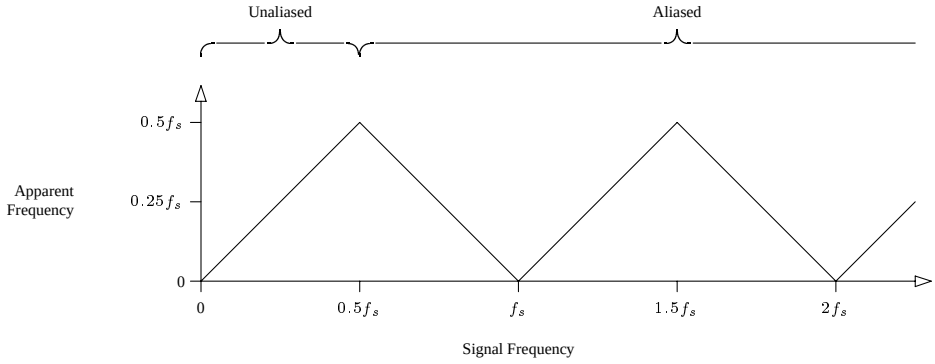

The practical limit to sampling is that the sampling frequency should be at least five times the highest significant frequency.

It is common to insert an *anti–aliasing* filter before the A/D converter to minimize the effect of aliased signals.

7.16 Anti–Aliasing Filters

The input signal to a sampled data system inevitably contains frequency components above half the sampling rate.

It is usual to insert a low pass filter ahead of the A/D converter (or S/H amplifier) to attenuate these components. This low pass filter is called an **anti–aliasing filter**.

In data acquisition systems where time delays are unimportant, high performance "brick–wall" filters are used. Such filters have 8 to 12 poles and provide extremely rapid roll–off beyond the filter bandwidth. However, they accomplish this rapid roll–off by introducing a group delay on the order of hundreds of milliseconds.

In digital control systems, this group delay would destabilize the system so such "brick–wall" filters cannot be used. Instead, simpler first or second order low pass filters are used with some transmission of aliased signals.

7.17 DSP Computations

Usually, DSP algorithms emulate linear controllers or filters. DSP propagates a real time simulation of the desired dynamic system.

Key idea: input is sampled (converted) regularly (τ); past input and output is used to generate new output

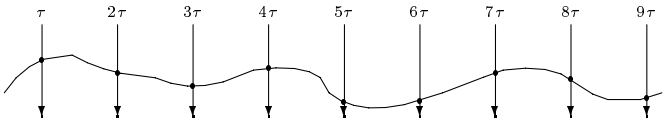

The approach: simulate the filter

$$G(s) = \frac{Y(s)}{X(s)} = \frac{a}{s+b}$$

In the time domain:

$$\dot{y} + by = ax$$

Approximate $\dot{y}$ as:

$$\dot{y} \approx \frac{y(t) - y(t-\tau)}{\tau}$$

to get

$$y(t) - y(t-\tau) + b\tau y(t) = a\tau x(t)$$

or,

$$y(t) = \frac{1}{1+b\tau} y(t-\tau) + \frac{a\tau}{1+b\tau} x(t)$$

Of course, in generating the next output, $y(t)$, we do not have the *next* input, $x(t)$, so

$$y(t) = \frac{1}{1+b\tau} y(t-\tau) + \frac{a\tau}{1+b\tau} x(t-\tau)$$

7.18 Difference Equations

The equation propagated on the DSP is called a **difference equation**.

Difference equations can be generated formally from differential equations (or transfer functions) by a transformation such as the Tustin transform:

1. separate the differential equation to put all terms in the output variable on one side, all terms in the input variable on the other:

$$\sum_{i=0}^{n} a_i \frac{d^i y}{dt^i} = \sum_{j=0}^{m} b_j \frac{d^j x}{dt^j}$$

2. replace each instance of $\frac{d^n}{dt^n}$ with $\left(\frac{2}{\tau}\,\frac{z-1}{z+1}\right)^n$:

$$\sum_{i=0}^{n} a_i \left(\frac{2}{\tau}\frac{z-1}{z+1}\right)^i y = \sum_{j=0}^{m} b_j \left(\frac{2}{\tau}\frac{z-1}{z+1}\right)^j x$$

3. multiply each side of the equation by the highest power of $z+1$ to obtain polynomials in z on each side

$$\sum_{i=0}^{n} a_i \frac{2^i}{\tau^i}(z-1)^i(z+1)^{n-i} y = \sum_{j=0}^{m} b_j \frac{2^j}{\tau^j}(z-1)^j(z+1)^{n-j} x$$

4. rearrange as simple polynomials in z:

$$y \sum_{i=0}^{n} \alpha_i z^i = x \sum_{j=0}^{n} \beta_j z^j$$

5. divide both sides by the highest power in z:

$$y \sum_{i=0}^{n} \alpha_i z^{n-i} = x \sum_{j=0}^{n} \beta_j z^{n-j}$$

6. rewrite as a difference equation, substituting $t - k\tau$ for z^{-k}:

$$\sum_{i=0}^{n} \alpha_i y(t-(n-i)\tau) = \sum_{j=0}^{n} \beta_j x(t-(n-j)\tau)$$

7. finally, solve for $y(t)$ and delay the input by one sample:

$$y(t) = -\sum_{i=0}^{n-1} \frac{\alpha_i}{\alpha_n} y(t-(n-i)\tau) + \sum_{j=0}^{n} \frac{\beta_j}{\alpha_n} x(t-(n-j+1)\tau)$$

7.19 Tustin Transform: A Simple Example

Assuming a sampling rate of $\tau = 0.0001$ seconds, generate the difference equation for

$$G(s) = \frac{Y(s)}{X(s)} = \frac{s + 200}{s^2 + 30s + 200}$$

1. arrange the equivalent differential equation:

$$\frac{d^2y}{dt^2} + 30\frac{dy}{dt} + 200y = \frac{dx}{dt} + 200x$$

2. substitute:

$$\left(4 \times 10^8 \frac{z^2 - 2z + 1}{z^2 + 2z + 1} + 6 \times 10^5 \frac{z - 1}{z + 1} + 200\right) y = \left(2 \times 10^4 \frac{z - 1}{z + 1} + 200\right) x$$

3. eliminate denominator:

$$\begin{aligned}\left(4 \times 10^8 (z^2 - 2z + 1) + 6 \times 10^5 (z^2 - 1) + 200(z^2 + 2z + 1)\right) y = \\ \left(2 \times 10^4 (z^2 - 1) + 200(z^2 + 2z + 1)\right) x\end{aligned}$$

4. convert to simple polynomials:

$$\left(4006002z^2 - 7999996z + 3994002\right) y = \left(202z^2 + 4z - 198\right) x$$

5. divide by the highest power of z:

$$\left(4006002 - 7999996z^{-1} + 3994002z^{-2}\right) y = \left(202 + 4z^{-1} - 198z^{-2}\right) x$$

6. substitute delay times for powers of z:

$$4006002y(t) - 7999996y(t - \tau) + 3994002y(t - 2\tau) = 202x(t) + 4x(t - \tau) - 198x(t - 2\tau)$$

7. finally, solve for $y(t)$ and delay x:

$$\begin{aligned}y(t) &= 1.9970025y(t - \tau) - 0.9970045y(t - 2\tau) \\ &\quad +5.042 \times 10^{-5} x(t - \tau) + 0.100 \times 10^{-5} x(t - 2\tau) - 4.942 \times 10^{-5} x(t - 3\tau)\end{aligned}$$

7.20 Example

Note that, if we truncate the coefficients,

$$\begin{aligned}y(t) &= 1.9970y(t - \tau) - 0.9970y(t - 2\tau) \\ &\quad +5.04 \times 10^{-5} x(t - \tau) + 0.10 \times 10^{-5} x(t - 2\tau) - 4.94 \times 10^{-5} x(t - 3\tau)\end{aligned}$$

the difference equation becomes unstable. To see this, assume a steady state solution: x is constant so y should also be constant:

$$y + 0.997y - 1.997y = 0y = 0.2 \times 10^{-5}x$$

that is, the final value of y is unbounded. This need to retain lots of digits in the coefficients is an indication of overly fast sampling: the difference equation evolves so slowly between samples that it is likely that the changes will be lost in underflow with finite sampling precision.

If the system is sampled more slowly: $\tau = 0.001$ seconds, the equation becomes:

$$\begin{aligned} y(t) &= 1.9702y(t-\tau) - 0.9704y(t-2\tau) \\ &\quad +5.42 \times 10^{-4}x(t-\tau) + 0.99 \times 10^{-4}x(t-2\tau) - 4.43 \times 10^{-5}x(t-3\tau) \end{aligned}$$

which is stable.

7.21 Difference Equations

An alternative way to look at the problem of numerical underflow as seen above is to say that the *form* of the difference equation is poor - in the same manner that it is numerically bad to represent a transfer function in coefficient form. Instead, write two difference equations (sampled every 100 μsec):

$$\begin{aligned} y(t) &= y(t-\tau) + \delta(t) \\ \delta(t) &= y(t) - y(t-\tau) \\ &= -2 \times 10^{-6}\delta(t-\tau) + 5.04 \times 10^{-5}x(t-\tau) \\ &\quad +0.10 \times 10^{-5}x(t-2\tau) - 4.94 \times 10^{-5}x(t-3\tau) \end{aligned}$$

Now, the equation coefficients are better balanced and do not need to retain as many digits.

This is a state space approach and generally leads to better numerical conditioning.

Rearrangement/balancing of the equations in a digital controller to improve numerical conditioning is equivalent to careful analog circuit design to protect signal–to–noise ratio.

7.22 State Space Form

Another form for the controller differential equations to take is:

$$\begin{aligned} \underline{\dot{x}} &= A\underline{x} + B\underline{u} \\ \underline{y} &= C\underline{x} \end{aligned}$$

To take the Tustin transform, first make the approximation:

$$\frac{1}{2}\left(\underline{\dot{x}}(t+\tau) + \underline{\dot{x}}(t)\right) \approx \frac{1}{\tau}\left(\underline{x}(t+\tau) - \underline{x}(t)\right)$$

Next, substitute the differential equation for $\underline{\dot{x}}$:

$$\frac{1}{2}\left(A\underline{x}(t+\tau) + B\underline{u}(t+\tau) + A\underline{x}(t) + B\underline{u}(t)\right) \approx \frac{1}{\tau}\left(\underline{x}(t+\tau) - \underline{x}(t)\right)$$

Now, assume that the input is delayed by one sample:

$$\frac{1}{2}\left(A\underline{x}(t+\tau)+B\underline{u}(t)+A\underline{x}(t)+B\underline{u}(t-\tau)\right)\approx\frac{1}{\tau}\left(\underline{x}(t+\tau)-\underline{x}(t)\right)$$

and solve for $\underline{x}(t+\tau)$:

$$\begin{aligned}\underline{x}(t+\tau) &= \left[I-0.5\tau A\right]^{-1}\left[I+0.5\tau A\right]\underline{x}(t)+0.5\tau\left[I-0.5\tau A\right]^{-1}B\left(\underline{u}(t)+\underline{u}(t-\tau)\right)\\ \underline{y}(t+\tau) &= C\underline{x}(t+\tau)\end{aligned}$$

So, define

$$\Phi\doteq\left[I-0.5\tau A\right]^{-1}\left[I+0.5\tau A\right]$$

and

$$V\doteq 0.5\tau\left[I-0.5\tau A\right]^{-1}B$$

so that the difference equation takes the simple form

$$\begin{aligned}\underline{x}(t+\tau) &= \Phi\underline{x}(t)+V\left(\underline{u}(t)+\underline{u}(t-\tau)\right)\\ \underline{y}(t+\tau) &= C\underline{x}(t+\tau)\end{aligned}$$

Note that it is reasonably simple to find a transformation, T, so that the numerical properties (conditioning) of the matrix

$$\hat{\Phi}=T\Phi T^{-1}$$

are better than for the original Φ. This transformation can be used by introducing the substitution

$$\underline{w}=T\underline{x}$$

so that

$$\begin{aligned}\underline{w}(t+\tau) &= T\Phi T^{-1}\underline{w}(t)+TV\left(\underline{u}(t)+\underline{u}(t-\tau)\right)\\ \underline{y}(t+\tau) &= CT^{-1}\underline{w}(t+\tau)\end{aligned}$$

The transformation T can be computed using standard numerical algorithms such as the method of Parlett and Reinsch[1] as implemented in the public software package EISPACK.

The delay which was introduced in order to make the controller causal can be somewhat mitigated by delaying only one of the input signal components rather than both of them. Thus,

$$\frac{1}{2}\left(A\underline{x}(t+\tau)+B\underline{u}(t+\tau)+A\underline{x}(t)+B\underline{u}(t)\right)\approx\frac{1}{\tau}\left(\underline{x}(t+\tau)-\underline{x}(t)\right)$$

becomes

$$\frac{1}{2}\left(A\underline{x}(t+\tau)+B\underline{u}(t)+A\underline{x}(t)+B\underline{u}(t)\right)\approx\frac{1}{\tau}\left(\underline{x}(t+\tau)-\underline{x}(t)\right)$$

[1] B. N. Parlett and C. Reinsch (1969). "Balancing a Matrix for Calculation of Eigenvalues and Eigenvectors," *Numerical Mathematics 13*, 292-304.

or

$$\frac{1}{2}\left(A\underline{x}(t+\tau)+A\underline{x}(t)+2B\underline{u}(t)\right)\approx\frac{1}{\tau}\left(\underline{x}(t+\tau)-\underline{x}(t)\right)$$

Again, solve for $\underline{x}(t+\tau)$ to obtain

$$\underline{x}(t+\tau)\approx\left[I-0.5\tau A\right]^{-1}\left[I+0.5\tau A\right]\underline{x}(t)+\tau\left[I-0.5\tau A\right]^{-1}B\underline{u}(t)$$

Finally, define

$$\Phi\doteq\left[I-0.5\tau A\right]^{-1}\left[I+0.5\tau A\right]\approx e^{A\tau}$$

and

$$V\doteq\tau\left[I-0.5\tau A\right]^{-1}B\approx\int_0^\tau e^{A(\tau-\sigma)}B\;d\sigma$$

to give the most commonly used difference equation

$$\underline{x}(t+\tau)=\Phi\underline{x}(t)+V\underline{u}(t)$$

7.22.1 State Space Example

To demonstrate this arithmetic, consider the preceding example where we wish to implement the control

$$G(s)=\frac{s+200}{s^2+30s+200}=\frac{Y(s)}{U(s)}$$

We can easily convert this transfer function to state space form through the following procedure. First, introduce the dummy variable, x:

$$\begin{aligned}\frac{X(s)}{U(s)} &= \frac{1}{s^2+30s+200}\\ \frac{Y(s)}{X(s)} &= s+200\end{aligned}$$

Next convert these transfer functions back to differential equations:

$$\begin{aligned}\ddot{x}+30\dot{x}+200x &= u\\ y &= \dot{x}+200x\end{aligned}$$

Now, introduce the state variables

$$x_0=x\quad,\quad x_1=\dot{x}$$

to obtain the simultaneous equations

$$\begin{aligned}\dot{x_0} &= x_1\\ \dot{x_1} &= -200x_0-30x_1+u\\ y &= 200x_0+x_1\end{aligned}$$

or, in matrix form

$$\begin{aligned} \frac{d}{dt}\left\{ \begin{array}{c} x_0 \\ x_1 \end{array} \right\} &= \left[\begin{array}{cc} 0 & 1 \\ -200 & -30 \end{array} \right] \left\{ \begin{array}{c} x_0 \\ x_1 \end{array} \right\} + \left[\begin{array}{c} 0 \\ 1 \end{array} \right] u \\ y &= \left[\begin{array}{cc} 200 & 1 \end{array} \right] \left\{ \begin{array}{c} x_0 \\ x_1 \end{array} \right\} \end{aligned}$$

so that

$$A = \left[\begin{array}{cc} 0 & 1 \\ -200 & -30 \end{array} \right] \quad , \quad B = \left[\begin{array}{c} 0 \\ 1 \end{array} \right] \quad \text{and} \quad C = \left[\begin{array}{cc} 200 & 1 \end{array} \right]$$

Assuming a sampling period of $\tau = 0.0001$, the matrices Φ and V are easily computed:

$$\Phi = \left[I - 0.5\tau A \right]^{-1} \left[I + 0.5\tau A \right] = \left[\begin{array}{cc} 1 & 0.00009985 \\ -0.01997 & 0.997 \end{array} \right]$$

$$V = \tau \left[I - 0.5\tau A \right]^{-1} B = 10^{-4} \left[\begin{array}{c} 0.00004995 \\ 0.9985 \end{array} \right]$$

so that

$$\begin{aligned} x_0(t+\tau) &= x_0(t) + 0.00009985 x_1(t) + 4.995 \times 10^{-9} u(t) \\ x_1(t+\tau) &= -0.01997 x_0(t) + 0.997 x_1(t) + 9.985 \times 10^{-5} u(t) \\ y(t+\tau) &= 200 x_0(t+\tau) + x_1(t+\tau) \end{aligned}$$

We can easily produce a numerical improvement for this problem by increasing the magnitude of the first state. Let

$$\hat{x}_0 = 14.142 x_0 \quad \text{and} \quad \hat{x}_1 = x_1$$

which produces

$$\begin{aligned} \hat{x}_0(t+\tau) &= \hat{x}_0(t) + 0.001412 \hat{x}_1(t) + 7.064 \times 10^{-8} u(t) \\ \hat{x}_1(t+\tau) &= -0.001412 \hat{x}_0(t) + 0.997 \hat{x}_1(t) + 9.985 \times 10^{-5} u(t) \\ y(t+\tau) &= 14.142 \hat{x}_0(t+\tau) + \hat{x}_1(t+\tau) \end{aligned}$$

7.23 Integrator Reset Windup: Saturation

Reset windup stems from fundamental instability of controllers with integrator: pole at $s = 0$.

Suppose that the controller contains a saturating nonlinearity at controller output or actuator: no matter how large the integrator output is, the input to the plant is fixed at some limit.

Once this limit is reached, the feedback loop is essentially broken and the instability of the integrator results in “unbounded” controller output.

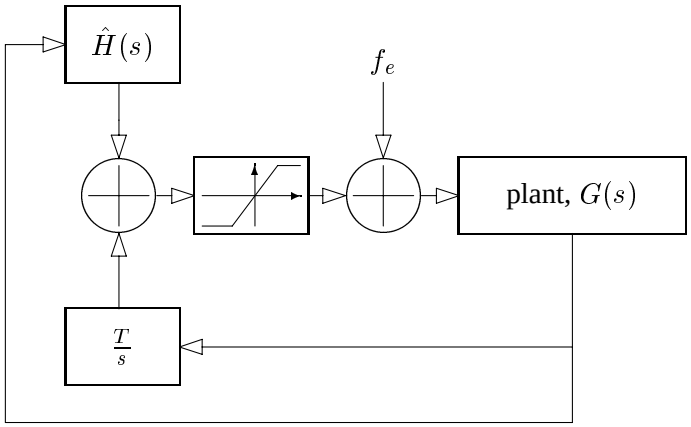

7.24 Cruise Control

The problem is really obvious with automobile speed (cruise) controls.

Suppose the car is climbing a hill and has not enough power to maintain a requested speed of 100 km/hr: with full power, it maintains 90 km/hr.

When the car reaches the top of the hill, the integrator has reached an enormous value: 10 t where t is the period during which the car was unable to maintain 100 km/hr.

Now, at the top of the hill, very little power is required to maintain 100 km/hr, but the integrator has a very large value! The speed of the car increases rapidly to produce a negative error (speed $>$ 100 km/hr) and integrator begins to **unwind**. Car may reach a very high peak velocity before finally settling down to the desired 100 km/hr.

7.24.1 Saturation

Steady state bearing force, displacement, and integrator output.

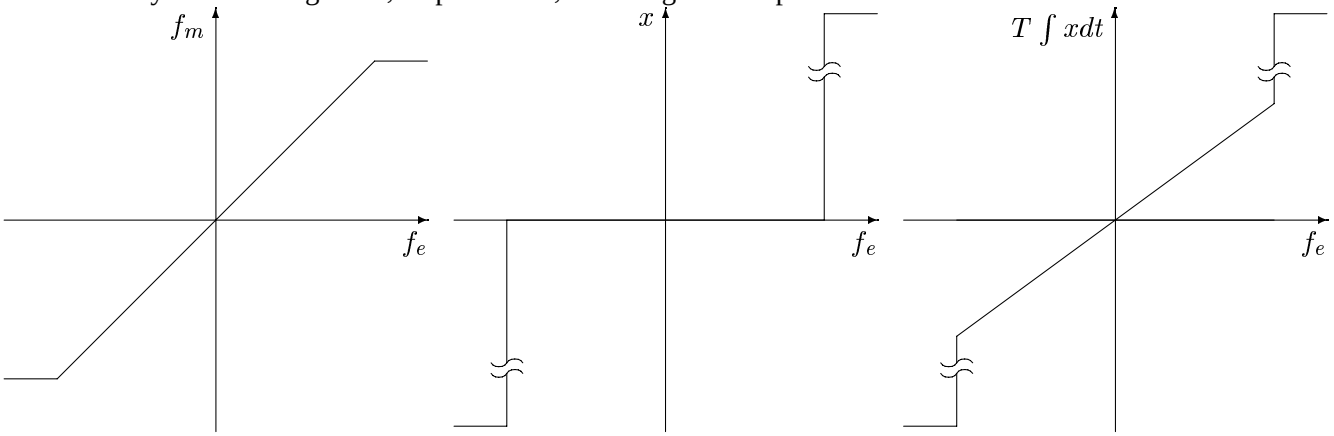

7.24.2 Normal Transient Response

If a constant load which does not exceed the saturation limit is applied, the error quickly converges to zero and the integrator output matches the load.

When the load is removed, the response is just the opposite of the applied response: the error quickly converges to zero and the integrator output returns to zero.

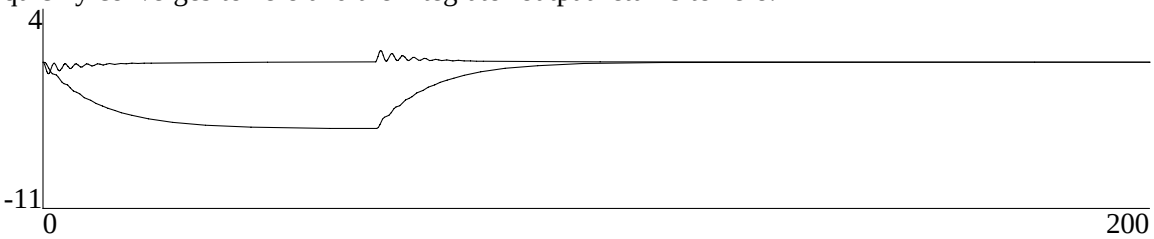

7.24.3 Reset Windup

If a constant load which exceeds the saturation limit is applied, the error does not go to zero and the integrator output climbs until it reaches its own (internal) saturation limit: it **winds up** like a clock spring.

When the load is removed, the integrator must **unwind** before it even gets back to the level which would match the original load. As a result, the plant error can take a long time to converge to zero.

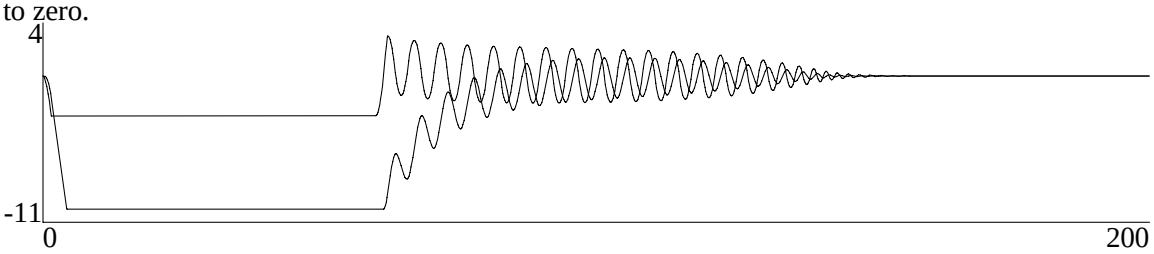

7.24.4 Preventing Reset Windup

Solution: use an additional input to the integrator to prevent the output from actually reaching saturation.

Normal integrator:

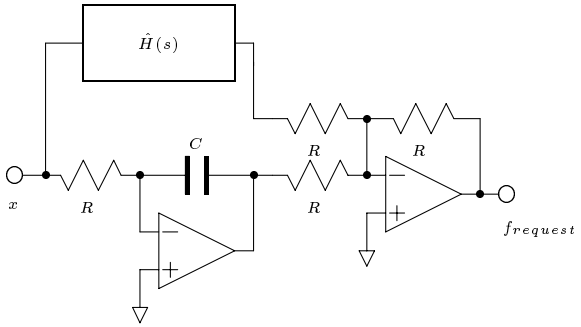

With limiting:

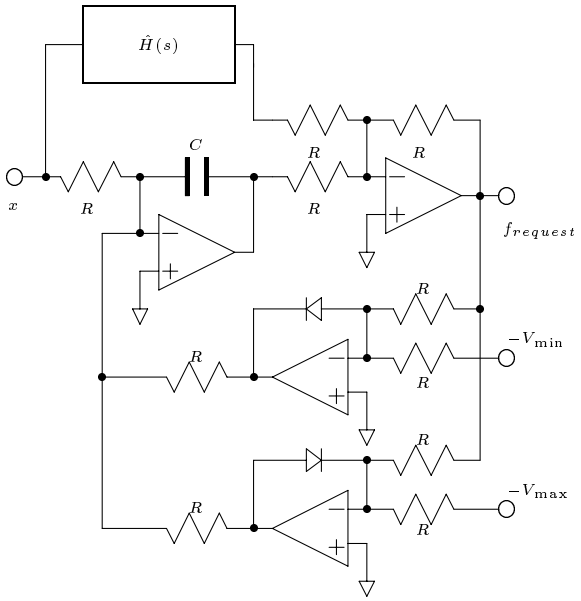

7.24.5 Real Effects in Single Mass Models

Some improvements in recovery from saturation can be obtained with reset windup limiting

Primary effect of force limit saturation in step response is loss of peak force associated with damping — loss of stability. Peak force occurs shortly after application of the load, is almost two times the load.

Results are very sensitive to parameter selection. As a result, it is hard to compare systems with and without reset windup limiting.

Chapter 8

Control of Flexible Structures and Rotors

When rotor flexibility is introduced, the system of equations quickly becomes too complicated to manage using simple transfer functions.

Instead, a systems approach is taken where the components of the system: the rotor, sensors, amplifiers/magnetics, and controller are modeled using a standard state space formulation.

The resulting (large) first order differential equation can be used to determine system stability and forced response.

8.1 Rotordynamic Model

The conventional model for the rotor has the form

$$\begin{bmatrix} M & 0 \\ 0 & M \end{bmatrix} \begin{Bmatrix} \ddot{\underline{w}}_x \\ \ddot{\underline{w}}_y \end{Bmatrix} + \begin{bmatrix} C & \Omega G \\ -\Omega G & C \end{bmatrix} \begin{Bmatrix} \dot{\underline{w}}_x \\ \dot{\underline{w}}_y \end{Bmatrix} + \begin{bmatrix} K & 0 \\ 0 & K \end{bmatrix} \begin{Bmatrix} \underline{w}_x \\ \underline{w}_y \end{Bmatrix} = \begin{Bmatrix} \underline{f}_x \\ \underline{f}_y \end{Bmatrix}$$

The magnetic actuators for operate at specific points along the shaft, so the magnetic forces, $\underline{f}_m$, can be inserted as:

$$\underline{f}_x = B_{m,x} f_{m,x} + B_{e,x} f_{e,x} \qquad \underline{f}_y = B_{m,y} f_{m,y} + B_{e,y} f_{e,y}$$

The sensors measure the displacement of the rotor at specific points along the shaft, so the sensor measurements can be represented by:

$$\underline{y}_x = C_x \underline{w}_x \qquad \underline{y}_y = C_y \underline{w}_y$$

8.1.1 Eliminating the Mass Matrix

The mass matrix is usually banded and is always symmetric so it is easy to invert. Use the Choleski decomposition to preserve symmetry:

$$M = M_R' M_R$$

and define

$$\underline{v}_x \doteq M_R \underline{w}_x \qquad \underline{v}_y \doteq M_R \underline{w}_y \qquad \mathcal{C} \doteq M_R^{-\top} C M_R^{-1} \qquad \mathcal{G} = M_R^{-\top} G M_R^{-1} \qquad \mathcal{K} \doteq M_R^{-\top} K M_R^{-1}$$

which gives

$$\left\{ \begin{array}{c} \underline{\ddot{v}}_x \\ \underline{\ddot{v}}_y \end{array} \right\} + \left[\begin{array}{cc} \mathcal{C} & \Omega\mathcal{G} \\ -\Omega\mathcal{G} & \mathcal{C} \end{array} \right] \left\{ \begin{array}{c} \underline{\dot{v}}_x \\ \underline{\dot{v}}_y \end{array} \right\} + \left[\begin{array}{cc} \mathcal{K} & 0 \\ 0 & \mathcal{K} \end{array} \right] \left\{ \begin{array}{c} \underline{v}_x \\ \underline{v}_y \end{array} \right\} = \left[\begin{array}{cc} M_R^{-\top} B_{m,x} & 0 \\ 0 & M_R^{-\top} B_{m,y} \end{array} \right] \left\{ \begin{array}{c} \underline{f}_x \\ \underline{f}_y \end{array} \right\}$$

$$\underline{y}_x = C_x M_R^{-1} \underline{v}_x \qquad \underline{y}_y = C_y M_R^{-1} \underline{v}_y$$

8.1.2 State Space Form

The second order form is only convenient for systems whose governing differential equations are even–ordered. Any linear differential equation can be represented in first order form:

$$\underline{\ddot{w}} + C(\Omega)\underline{\dot{w}} + K\underline{w} = B\underline{f} \qquad \underline{y} = C_x \underline{w}$$

becomes

$$\frac{d}{dt} \left\{ \begin{array}{c} \underline{w} \\ \underline{\dot{w}} \end{array} \right\} + \left[\begin{array}{cc} 0 & -I \\ K & C(\Omega) \end{array} \right] \left\{ \begin{array}{c} \underline{w} \\ \underline{\dot{w}} \end{array} \right\} = \left[\begin{array}{c} 0 \\ B \end{array} \right] \underline{f}$$

define

$$\underline{x}_R = \left\{ \begin{array}{c} \underline{w} \\ \underline{\dot{w}} \end{array} \right\} \qquad \mathbf{A}_R(\Omega) = \left[\begin{array}{cc} 0 & I \\ -K & -C(\Omega) \end{array} \right] \qquad \mathbf{B}_R = \left[\begin{array}{c} 0 \\ -B \end{array} \right] \qquad \mathbf{C}_R = \left[\begin{array}{cc} C_x & 0 \end{array} \right]$$

to produce

$$\begin{aligned} \underline{\dot{x}}_R &= \mathbf{A}_R(\Omega)\underline{x}_R + \mathbf{B}_R\underline{f} \\ \underline{y}_R &= \mathbf{C}_R\underline{x}_R \end{aligned}$$

8.2 State–Space Models from Transfer Functions

Many filters and simple dynamic systems are described in terms of their transfer functions:

$$\frac{r(s)}{u(s)} = G(s) = \frac{\sum_{i=0}^{m} \alpha_i s^i}{\sum_{i=0}^{n} \beta_i s^i} \quad m \leq n-1$$

First, introduce a variable, x:

$$\frac{x(s)}{u(s)} = \frac{1}{\sum_{i=0}^{n} \beta_i s^i}$$

Then, note that

$$r(s) = x(s) \sum \alpha_i s^i$$

Convert the former equation to a differential equation

$$\sum_{i=0}^{n} \beta_i x^{(i)}(t) = u(t)$$

Introduce the state variables $x_i = x^{(i)}$ and solve for x_i:

$$x_i = \dot{x}_{i-1} \qquad i = 1 \ldots n-1$$

$$x_n = \dot{x}_{n-1} = \frac{1}{\beta_n}\left(u - \sum_{i=0}^{n-1}\right)\beta_i x_i$$

Finally, the output variable is given in terms of the states:

$$r(t) = \sum_{i=1}^{m} \alpha_i x_i$$

8.2.1 Controllable Canonical Form

The result is that the transfer function can be converted, by inspection, to a state space time domain differential equation. The form is called the Controllable Canonical Form:

$$\frac{r(s)}{u(s)} = G(s) = \frac{\sum_{i=0}^{m} \alpha_i s^i}{\sum_{i=0}^{n} \beta_i s^i} \quad m \leq n-1$$

$$\frac{d}{dt}\begin{Bmatrix} x_1 \\ x_2 \\ \vdots \\ x_{n-2} \\ x_{n-1} \end{Bmatrix} = \begin{bmatrix} 0 & 1 & \cdots & 0 & 0 \\ 0 & 0 & \ddots & 0 & 0 \\ & \vdots & & \ddots & \vdots \\ 0 & 0 & \cdots & 0 & 1 \\ -\frac{\beta_0}{\beta_n} & -\frac{\beta_1}{\beta_n} & \cdots & & -\frac{\beta_{n-1}}{\beta_n} \end{bmatrix} \begin{Bmatrix} x_1 \\ x_2 \\ \vdots \\ x_{n-2} \\ x_{n-1} \end{Bmatrix} + \begin{Bmatrix} 0 \\ 0 \\ \vdots \\ 0 \\ 1 \end{Bmatrix} u$$

$$r = \begin{Bmatrix} \alpha_0 & \alpha_1 & \cdots & \alpha_{n-2} & \alpha_{n-1} \end{Bmatrix} \begin{Bmatrix} x_1 \\ x_2 \\ \vdots \\ x_{n-2} \\ x_{n-1} \end{Bmatrix}$$

8.3 Sensor Model

The sensors can typically be modeled as first or second order:

$$\dot{x}_s = \begin{bmatrix} -a \end{bmatrix} x_s + K_s x_{in}$$

$$v_{out} = [a]\, x_s$$

$$\frac{v_{out}(s)}{x_{in}(s)} = K_s \frac{a}{s+a}$$

$$\begin{aligned} \underline{\dot{x}}_s &= \begin{bmatrix} 0 & 1 \\ -\omega^2 & -2\xi\omega \end{bmatrix} x_s + \begin{bmatrix} 0 \\ K_s \end{bmatrix} x_{in} \\ v_{out} &= \begin{bmatrix} \omega^2 & 0 \end{bmatrix} x_s \end{aligned}$$

$$\frac{v_{out}(s)}{x_{in}(s)} = K_s \frac{\omega^2}{s^2 + 2\xi\omega s + \omega^2}$$

Generically,

$$\begin{aligned} \underline{x}_s &= \mathbf{A}_s \underline{x}_s + \mathbf{B}_s \underline{x}_{in} \\ \underline{v}_{out} &= \mathbf{C}_s \underline{x}_s \end{aligned}$$

This model may contain any number of sensors.

8.4 Rotor–Sensor Model

Simply combine the rotor and sensor models by setting the sensor input equal to the rotor output (assuming that $\mathcal{C}_R$ has been designed properly):

$$\underline{x}_{in} = \underline{y}_R$$

to obtain the combined system model

$$\begin{aligned} \frac{d}{dt}\left\{ \begin{array}{c} \underline{x}_R \\ \underline{x}_S \end{array} \right\} &= \left[\begin{array}{cc} A_R & 0 \\ B_S C_R & A_S \end{array} \right] \left\{ \begin{array}{c} \underline{x}_R \\ \underline{x}_S \end{array} \right\} \\ &\quad + \left[\begin{array}{ccc} B_m & B_e & 0 \\ 0 & 0 & I \end{array} \right] \left\{ \begin{array}{c} \underline{f}_m \\ \underline{f}_e \\ \underline{\eta}_S \end{array} \right\} \\ \underline{v}_S &= \left[\begin{array}{cc} 0 & C_S \end{array} \right] \left\{ \begin{array}{c} \underline{x}_R \\ \underline{x}_S \end{array} \right\} \end{aligned}$$

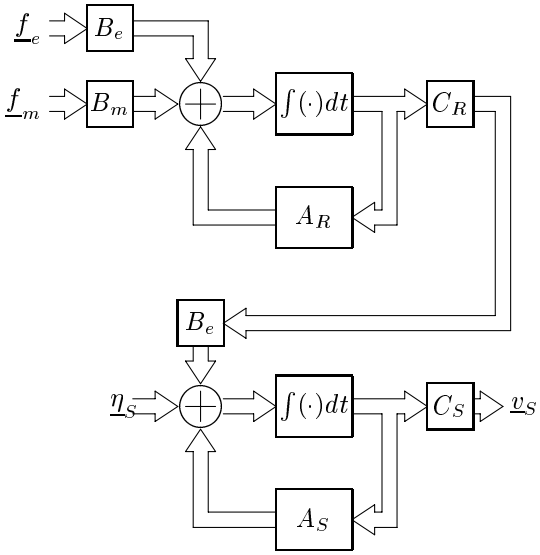

8.5 Amplifier / Magnetics Model

The linearized magnetics model for a single actuator has the form

$$\left\{ \begin{array}{c} f_x \\ f_y \end{array} \right\} = - \left[\begin{array}{cc} K_{xx} & K_{xy} \\ K_{yx} & K_{yy} \end{array} \right] \left\{ \begin{array}{c} w_x \\ w_y \end{array} \right\} + \left[\begin{array}{cc} K_{i,xx} & K_{i,xy} \\ K_{i,yx} & K_{i,yy} \end{array} \right] \left\{ \begin{array}{c} c_x \\ c_y \end{array} \right\}$$

where $K_{i,xy}$ and $K_{i,yx}$ are normally zero. The variables c_x and c_y have units of current. In the simplest case, they are the perturbation currents.

The desired coil currents are given by

$$\underline{I}_d = \mathcal{C}V \begin{bmatrix} 1/\beta & 0 & 0 \\ 0 & 1/\beta & 0 \\ 0 & 0 & \beta \end{bmatrix} \begin{Bmatrix} c_x \\ c_y \\ c_b \end{Bmatrix}_d$$

where V is the current selection matrix and $\mathcal{C}$ is the coil connection matrix.

- $\mathcal{C}$ is a physical property of the magnetic bearing stator.
- V, β, and c_b are constants provided by the controller (or intervening preamplifier)
- c_x and c_y are the control signals generated by the controller

As with the sensors, the amplifiers have a finite bandwidth and can be modeled individually as

$$\begin{aligned} \dot{x}_a &= \begin{bmatrix} -a \end{bmatrix} x_a + K_a v_{in} \\ i_{out} &= [a]\, x_a \end{aligned}$$

$$\frac{i_{out}(s)}{v_{in}(s)} = K_a \frac{a}{s+a}$$

$$\begin{aligned} \underline{\dot{x}}_a &= \begin{bmatrix} 0 & 1 \\ -\omega^2 & -2\xi\omega \end{bmatrix} x_s + \begin{bmatrix} 0 \\ K_a \end{bmatrix} v_{in} \\ i_{out} &= \begin{bmatrix} \omega^2 & 0 \end{bmatrix} x_s \end{aligned}$$

$$\frac{i_{out}(s)}{v_{in}(s)} = K_a \frac{\omega^2}{s^2 + 2\xi\omega s + \omega^2}$$

Thus, the actual currents delivered in the bearing stators are given by

$$\begin{aligned} \underline{\dot{x}}_a &= \mathbf{A}_a \underline{x}_a + \hat{\mathbf{B}}_a \underline{v}_{in} \\ \underline{I} &= \hat{\mathbf{C}}_a \underline{x}_a \end{aligned}$$

Continuing the formal development requires examining the nonlinear dynamics. The essential result is that the actual delivered variables c_x and c_y are related to the controller output variables $c_{x,d}$ and $c_{y,d}$ by simple transfer functions with the bandwidth of the power amplifiers and gains K_a. This bandwidth limitation can, as a result, include poles due to eddy current effects in the bearing stator. It can be shown that the dynamics which limit the actuator bandwidth (K_i term) also limit the bandwidth of the open–loop stiffness term.

The amplifier dynamics and the magnetic properties for any number of stators can be combined into a unit:

$$\begin{aligned} \underline{\dot{x}}_a &= A_a \underline{x}_a + B_a \left(K_a K_i \underline{c}_c - K_x \mathbf{C}_{m,x} \underline{x}_R \right) \\ \underline{f}_m &= C_a \underline{x}_a \end{aligned}$$

where the matrix $\mathbf{C}_{m,x}$ measures the motion of the journal degrees of freedom. K_a is a diagonal matrix of amplifier gains and the state space model has a diagonal transfer function with unit gain.

8.6 Amplifier/Magnetics – Rotor – Sensor Model

Again, combine the rotor, sensor, and amplifier/magnetics models by setting the rotor input equal to the bearing output to obtain the combined system model

$$\frac{d}{dt}\begin{Bmatrix} \underline{x}_R \\ \underline{x}_S \\ \underline{x}_A \end{Bmatrix} = \begin{bmatrix} A_R & 0 & B_m C_A \\ B_S C_R & A_S & 0 \\ B_a K_x C_{m,x} & 0 & A_A \end{bmatrix} \begin{Bmatrix} \underline{x}_R \\ \underline{x}_S \\ \underline{x}_A \end{Bmatrix} + \begin{bmatrix} B_e & 0 & 0 & 0 \\ 0 & I & 0 & 0 \\ 0 & 0 & B_A K_a K_i & I \end{bmatrix} \begin{Bmatrix} \underline{f}_e \\ \underline{\eta}_S \\ \underline{c} \\ \underline{\eta}_A \end{Bmatrix}$$

$$\underline{v}_S = \begin{bmatrix} 0 & C_S & 0 \end{bmatrix} \begin{Bmatrix} \underline{x}_R \\ \underline{x}_S \\ \underline{x}_A \end{Bmatrix}$$

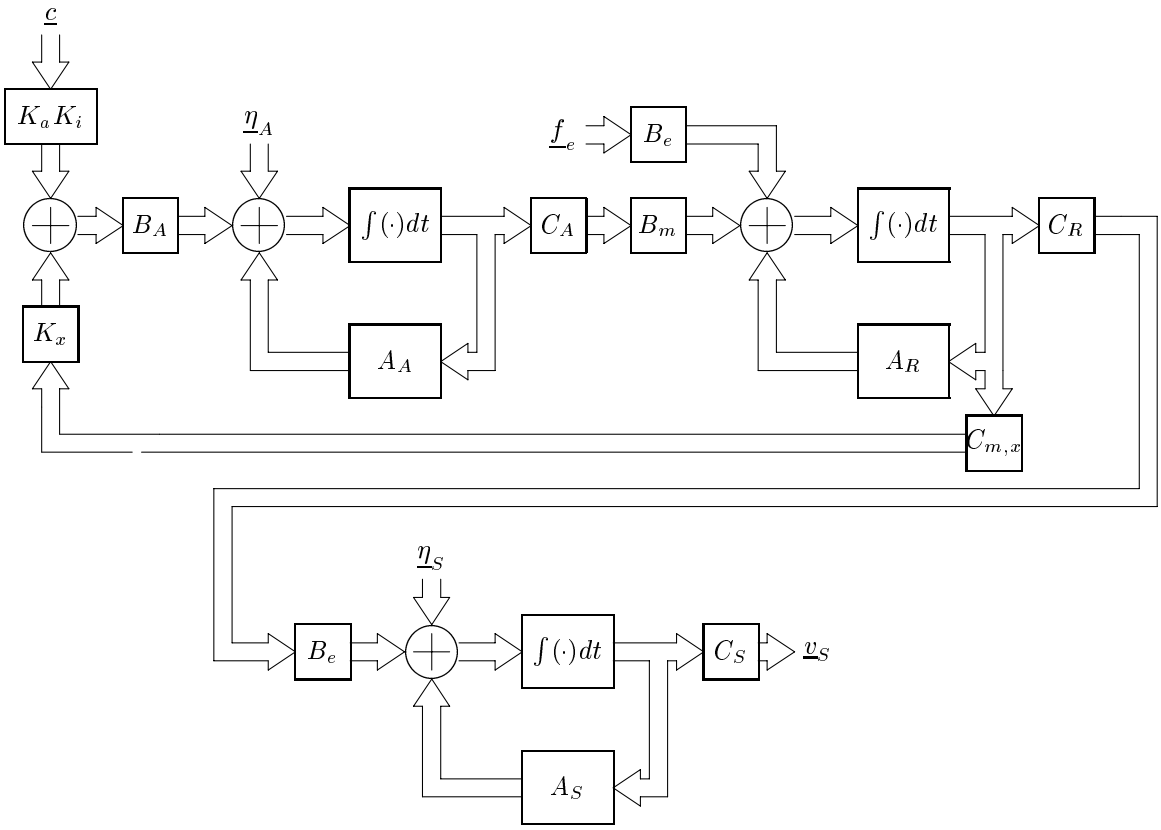

8.7 Controller Model

The controller may consist of several (typically four) local feedback controllers or it may be more complicated, using state space methods with state estimators and so forth. In any case, the controller takes as its input the sensor voltages, $\underline{v}_s$ and delivers as its output the amplifier input voltages, $\underline{c}$. The controller dynamics can always be represented by

$$\begin{aligned} \dot{\underline{x}}_C &= \mathbf{A}_C \underline{x}_C + \mathbf{B}_C \underline{v}_s + \underline{\eta}_C \\ \underline{c} &= \mathbf{C}_C \underline{x}_C \end{aligned}$$

8.8 System Model

The final system model can be assembled simply by connecting the output of the sensor model to the input of the controller model and the output of the controller model to the input of the amplifier/magnetics model:

$$\frac{d}{dt}\begin{Bmatrix} \underline{x}_R \\ \underline{x}_S \\ \underline{x}_A \\ \underline{x}_C \end{Bmatrix} = \begin{bmatrix} A_R & 0 & B_m C_A & 0 \\ B_S C_R & A_S & 0 & 0 \\ B_a K_x C_{m,x} & 0 & A_A & B_A K_a K_i C_C \\ 0 & B_C C_S & 0 & A_C \end{bmatrix} \begin{Bmatrix} \underline{x}_R \\ \underline{x}_S \\ \underline{x}_A \\ \underline{x}_C \end{Bmatrix} + \begin{bmatrix} B_e & 0 & 0 & 0 \\ 0 & I & 0 & 0 \\ 0 & 0 & I & 0 \\ 0 & 0 & 0 & I \end{bmatrix} \begin{Bmatrix} \underline{f}_e \\ \underline{\eta}_S \\ \underline{\eta}_A \\ \underline{\eta}_C \end{Bmatrix}$$

$$\underline{v}_S = \begin{bmatrix} 0 & C_S & 0 & 0 \end{bmatrix} \begin{Bmatrix} \underline{x}_R \\ \underline{x}_S \\ \underline{x}_A \\ \underline{x}_C \end{Bmatrix}$$

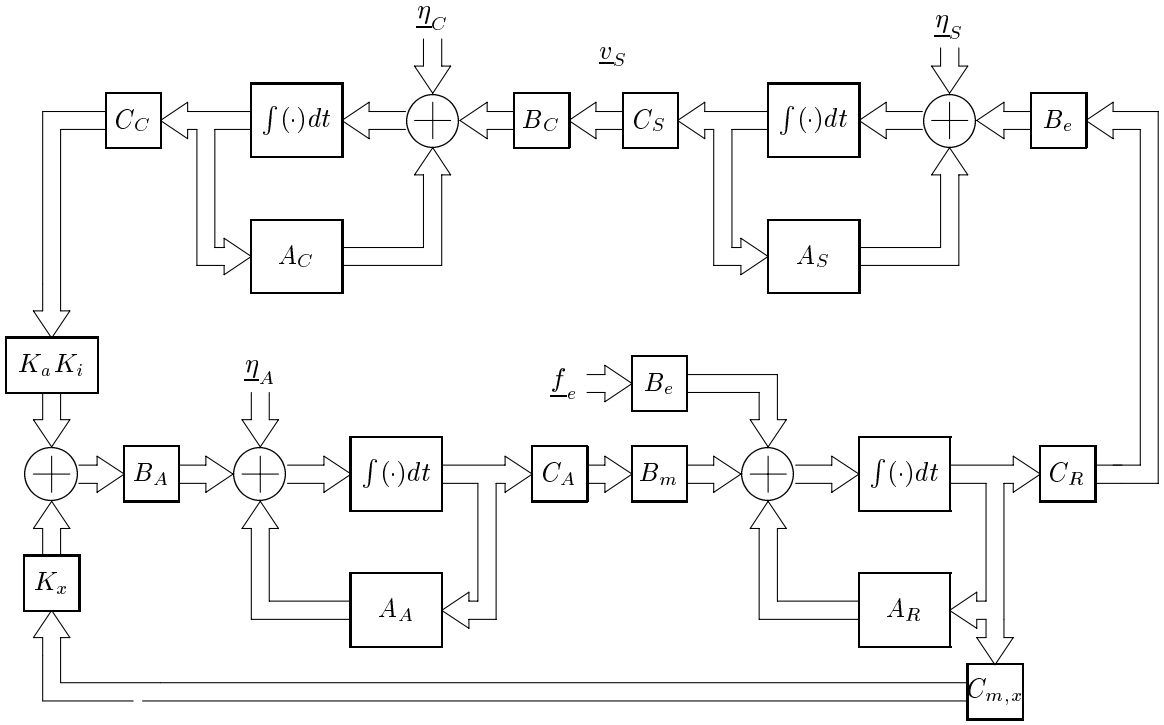

8.9 System Stability

Since the overall system can now be represented concisely by the system differential equation

$$\begin{aligned} \dot{\underline{x}} &= A\underline{x} + B\underline{f}_e \\ \underline{v} &= C\underline{x} \end{aligned}$$

we can determine stability by simply (!) computing the eigenvalues of the matrix A. If the eigenvalues all have negative real part, then the system is stable.

Computing the eigenvalues is non–trivial. The overall system model is non symmetric ($A \neq A'$) so we have to use a general eigenvalue solver. One of the better methods is the Francis $Q - R$ algorithm for computing the eigenvalues of a matrix in upper Hessenberg form. This method is referred to as HQR and software is publically available: EISPACK. Essentially, the process has three steps:

1. balance the matrix to improve numerical conditioning (`BALANC`)
2. transform to upper Hessenberg form (`ORTHES`)
3. compute the eigenvalues using the Francis $Q - R$ algorithm (`HQR`)

8.10 System Forced Response

Forced response of the system is computed in a straight forward manner. For step or impulse response, the differential equations are simply integrated:

$$\underline{v}(t) = C\underline{x}(t) \quad : \quad \underline{x}(t) = C\int_0^t \left(A\underline{x}(\tau) + B\underline{f}_e(\tau)\right) d\tau = e^{At}\underline{x}(0) + \int_0^t e^{A(t-\tau)}B\underline{f}_e(\tau)\tau$$

For frequency response (steady state, assuming stability), use a Bode plot approach:

$$\begin{aligned} \underline{\dot{x}} &= A\underline{x} + B\underline{f}_e \\ \underline{v} &= C\underline{x} \end{aligned}$$

$$\Rightarrow \qquad \underline{v}(s) = C\left(sI - A\right)^{-1} B\underline{f}_e(s)$$

For a sinusoidal input $f_e(t) = \underline{F}e^{j\omega t}$, the response is simply

$$\underline{V} = C\left(j\omega I - A\right)^{-1} B\underline{F} \qquad \underline{v}(t) = \underline{V}e^{j\omega t}$$

8.11 System Model: Modal Coordinates

Usually, it is easier and cheaper to compute forced response in modal (or nearly modal) coordinates. The normal system differential equation is converted to modal coordinates:

$$\begin{aligned} \underline{\dot{x}} &= A\underline{x} + B\underline{f}_e \\ \underline{v} &= C\underline{x} \end{aligned}$$

with the modal transformation:

$$A\Phi = \Phi\Lambda \quad \Rightarrow \underline{x} = \Phi\underline{z}$$

to obtain

$$\begin{aligned} \Phi\underline{\dot{z}} &= \Phi\Lambda\underline{z} + B\underline{f}_e \\ \underline{v} &= C\Phi\underline{z} \end{aligned}$$

or,

$$\begin{aligned} \underline{\dot{z}} &= \Lambda\underline{z} + \Phi^{-1}B\underline{f}_e \\ \underline{v} &= C\Phi\underline{z} \end{aligned}$$

8.11.1 Nearly Modal Coordinates

In general, both Λ and Φ are complex and the resulting arithmetic ends up being complex also. However, we can convert to nearly modal coordinates in the following manner. Assume that the complex eigenvalues and are produced in conjugate pairs:

$$\Lambda = \begin{bmatrix} \sigma_1 + j\omega_1 & 0 & \cdots & 0 & 0 \\ 0 & \sigma_1 - j\omega_1 & & & \vdots \\ \vdots & 0 & \ddots & & \\ 0 & 0 & \cdots & \sigma_{n/2} + j\omega_{n/2} & 0 \\ 0 & & & 0 & \sigma_{n/2} - j\omega_{n/2} \end{bmatrix}$$

$$\Phi = \begin{bmatrix} \underline{\phi}_1 & \overline{\underline{\phi}}_1 & \cdots & \underline{\phi}_{n/2} & \overline{\underline{\phi}}_{n/2} \end{bmatrix}$$

Introduce the simple transformation

$$T = \begin{bmatrix} T_1 & 0 & \cdots & 0 \\ 0 & \ddots & & \vdots \\ \vdots & & \ddots & \\ 0 & \cdots & 0 & T_{n/2} \end{bmatrix} \quad \text{where} \quad T_i = \frac{1}{\sqrt{2}} \begin{bmatrix} 1 & -j \\ 1 & j \end{bmatrix}$$

The products $T\Lambda T^*$ and ΦT^* are real and the product $T^*T = I$:

$$\hat{\Lambda} \doteq T\Lambda T^* = \begin{bmatrix} \sigma_1 & -\omega_1 & \cdots & 0 & 0 \\ \omega_1 & \sigma_1 & & & \vdots \\ \vdots & 0 & \ddots & & \\ 0 & 0 & \cdots & \sigma_{n/2} & -\omega_{n/2} \\ 0 & & & \omega_{n/2} & \sigma_{n/2} \end{bmatrix}$$

$$\Phi T^* = \sqrt{2} \begin{bmatrix} \Re(\underline{\phi}_1) & \Im(\underline{\phi}_1) & \cdots & \Re(\underline{\phi}_{n/2}) & \Im(\underline{\phi}_{n/2}) \end{bmatrix}$$

1) apply the transformation ΦT^*

$$\begin{aligned} \underline{x} &= \Phi T^* \underline{z} \\ \Phi T^* \dot{\underline{z}} &= A\Phi T^* \underline{z} + B\underline{f}_e \\ \underline{v} &= C\Phi T^* \underline{z} \end{aligned}$$

2) invert the real matrix ΦT^* to obtain

$$\begin{aligned} \dot{\underline{z}} &= (\Phi T^*)^{-1} \Phi \Lambda T^* \underline{z} + (\Phi T^*)^{-1} B\underline{f}_e \\ \underline{v} &= C\Phi T^* \underline{z} \end{aligned}$$

3) insert the identity T^*T:

$$\begin{aligned} \dot{\underline{z}} &= (\Phi T^*)^{-1} \Phi T^* T \Lambda T^* \underline{z} + (\Phi T^*)^{-1} B\underline{f}_e \\ \underline{v} &= C\Phi T^* \underline{z} \end{aligned}$$

4) and, finally,

$$\begin{aligned} \dot{\underline{z}} &= \hat{\Lambda}\underline{z} + (\Phi T^*)^{-1} B\underline{f}_e \\ \underline{v} &= C\Phi T^* \underline{z} \end{aligned}$$

which is conveniently block diagonal (with blocks of dimension 2) and all real.

The advantage of this form is that the computation

$$C\Phi T^* \left(j\omega I - \hat{\Lambda}\right)^{-1} (\Phi T^*)^{-1} B$$

can be performed without computing a full matrix inverse. This is because the inverse of a matrix which is block diagonal is the block diagonal matrix of inverse blocks:

$$M = \begin{bmatrix} M_{11} & 0 & \cdots & 0 \\ 0 & M_{22} & & \vdots \\ \vdots & & \ddots & \\ 0 & \cdots & 0 M_{nn} & \end{bmatrix} = \text{diag}\,(M_{ii})$$

$$M^{-1} = \begin{bmatrix} M_{11}^{-1} & 0 & \cdots & 0 \\ 0 & M_{22}^{-1} & & \vdots \\ \vdots & & \ddots & \\ 0 & \cdots & 0 M_{nn}^{-1} & \end{bmatrix} = \text{diag}\left(M_{ii}^{-1}\right)$$

Thus,

$$\left(j\omega I - \hat{\Lambda}\right)^{-1} = \text{diag}\left(\begin{bmatrix} j\omega - \sigma_i & \omega_i \\ -\omega_i & j\omega - \sigma_i \end{bmatrix}^{-1}\right) = \text{diag}\left(\frac{1}{(j\omega - \sigma_i)^2 + \omega_i^2} \begin{bmatrix} j\omega - \sigma_i & -\omega_i \\ \omega_i & j\omega - \sigma_i \end{bmatrix}\right)$$

which is enormously cheaper to compute than is the general complex inverse. Finally, because the inverse is block diagonal with 2×2 blocks, we can define the input and output matrices in terms of $n/2$ $2 \times m$ rows or $n/2$ $p \times 2$ rows:

$$(\Phi T^*)^{-1} B = \begin{bmatrix} \hat{B}_1 \\ \hat{B}_2 \\ \vdots \\ \hat{B}_{n/2} \end{bmatrix} \qquad C\Phi T^* = \begin{bmatrix} \hat{C}_1 & \hat{C}_2 & \cdots & \hat{C}_{n/2} \end{bmatrix}$$

Using this notation, the forced response becomes

$$\underline{V} = C\left(j\omega I - A\right)^{-1} B\underline{F} = \left(\sum_{i=1}^{n/2} \hat{C}_i \frac{1}{(j\omega - \sigma_i)^2 + \omega_i^2} \begin{bmatrix} j\omega - \sigma_i & -\omega_i \\ \omega_i & j\omega - \sigma_i \end{bmatrix} \hat{B}_i\right) \underline{F}$$

If the forced response is to be computed only at a single frequency, then this procedure, which relies on computation of the eigenvectors and eigenvalues is not very efficient. However, if the forced response is to be computed at many frequencies, then this approach is much more efficient than direct inversion of $j\omega I - A$.

8.12 Rotor Model: Modal Truncation

To obtain an accurate representation of the rotor even at low frequencies, it is usually necessary to use a lot of degrees of freedom (mass stations). As a result, the rotor model has many eigenvalues

The higher eigenvalues are probably not important:

- they are inaccurate
- large response in the higher modes cannot be attained
  - small angle assumptions violated
  - actuator capacity at these frequencies is very limited

Modal truncation is employed to eliminate the poorly modeled modes. Use the free–free planar modes without damping and without gyroscopics. These are the easiest to compute and provide enough information to permit accurate model reduction.

The initial model:

$$\begin{bmatrix} M & 0 \\ 0 & M \end{bmatrix} \begin{Bmatrix} \underline{\ddot{w}}_x \\ \underline{\ddot{w}}_y \end{Bmatrix} + \begin{bmatrix} C & \Omega G \\ -\Omega G & C \end{bmatrix} \begin{Bmatrix} \underline{\dot{w}}_x \\ \underline{\dot{w}}_y \end{Bmatrix} + \begin{bmatrix} K & 0 \\ 0 & K \end{bmatrix} \begin{Bmatrix} \underline{w}_x \\ \underline{w}_y \end{Bmatrix} = \begin{Bmatrix} \underline{f}_x \\ \underline{f}_y \end{Bmatrix}$$

Compute the eigenvalues and eigenvectors for the pair M and K:

$$\Phi' M \Phi = I \qquad \Phi' K \Phi = \Lambda^2$$

Without truncation, the responses $\underline{w}_x$ and $\underline{w}_y$ can be represented as

$$\underline{w}_x = \Phi \underline{m}_x \qquad \underline{w}_y = \Phi \underline{m}_y$$

So that the model becomes

$$\begin{bmatrix} M\Phi & 0 \\ 0 & M\Phi \end{bmatrix} \begin{Bmatrix} \underline{\ddot{m}}_x \\ \underline{\ddot{m}}_y \end{Bmatrix} + \begin{bmatrix} C\Phi & \Omega G\Phi \\ -\Omega G\Phi & C\Phi \end{bmatrix} \begin{Bmatrix} \underline{\dot{m}}_x \\ \underline{\dot{m}}_y \end{Bmatrix} + \begin{bmatrix} K\Phi & 0 \\ 0 & K\Phi \end{bmatrix} \begin{Bmatrix} \underline{m}_x \\ \underline{m}_y \end{Bmatrix} = \begin{Bmatrix} \underline{f}_x \\ \underline{f}_y \end{Bmatrix}$$

Premultiply by Φ' to obtain the differential equation in modal coordinates:

$$\begin{Bmatrix} \underline{\ddot{m}}_x \\ \underline{\ddot{m}}_y \end{Bmatrix} + \begin{bmatrix} \Phi' C \Phi & \Omega \Phi' G \Phi \\ -\Omega \Phi' G \Phi & \Phi' C \Phi \end{bmatrix} \begin{Bmatrix} \underline{\dot{m}}_x \\ \underline{\dot{m}}_y \end{Bmatrix} + \begin{bmatrix} \Lambda^2 & 0 \\ 0 & \Lambda^2 \end{bmatrix} \begin{Bmatrix} \underline{m}_x \\ \underline{m}_y \end{Bmatrix} = \begin{Bmatrix} \Phi' \underline{f}_x \\ \Phi' \underline{f}_y \end{Bmatrix}$$

If C and G were zero, this transformation would completely decouple the equations, as usual. However, that is not the objective. Rearrange according to the modes which are to be retained and those which are to be truncated (removed):

$$\begin{Bmatrix} \underline{m}_{m,x} \\ \underline{m}_{s,x} \end{Bmatrix} = \begin{bmatrix} T_m \\ T_s \end{bmatrix} \underline{m}_x \qquad \begin{Bmatrix} \underline{m}_{m,y} \\ \underline{m}_{s,y} \end{Bmatrix} = \begin{bmatrix} T_m \\ T_s \end{bmatrix} \underline{m}_y$$

Note that, since this is a permutation matrix, $T'T = I$. Define

$$\begin{bmatrix} \Lambda_{mm} & 0 \\ 0 & \Lambda_{ss} \end{bmatrix} \doteq \begin{bmatrix} T'_m T'_s \end{bmatrix} \Phi' K \Phi \begin{bmatrix} T_m \\ T_s \end{bmatrix} = \begin{bmatrix} \Phi'_m \\ \Phi'_s \end{bmatrix} \qquad \begin{bmatrix} B_m \\ B_s \end{bmatrix} \doteq \begin{bmatrix} T'_m T'_s \end{bmatrix} \Phi'$$

and

$$\begin{bmatrix} C_{mm} & C_{ms} \\ C_{sm} & C_{ss} \end{bmatrix} \doteq \begin{bmatrix} T'_m T'_s \end{bmatrix} \Phi' C \Phi \begin{bmatrix} T_m \\ T_s \end{bmatrix} \qquad \begin{bmatrix} G_{mm} & G_{ms} \\ G_{sm} & G_{ss} \end{bmatrix} \doteq \begin{bmatrix} T'_m T'_s \end{bmatrix} \Phi' G \Phi \begin{bmatrix} T_m \\ T_s \end{bmatrix}$$

Normally, the choice of T dictates that $\Lambda^2_{mm} < \Lambda^2_{ss}$.

Thus the model becomes,

$$\begin{Bmatrix} \ddot{\underline{m}}_{m,x} \\ \ddot{\underline{m}}_{s,x} \\ \ddot{\underline{m}}_{m,y} \\ \ddot{\underline{m}}_{s,y} \end{Bmatrix} + \begin{bmatrix} C_{mm} & C_{ms} & \Omega G_{mm} & \Omega G_{ms} \\ C_{sm} & C_{ss} & \Omega G_{sm} & \Omega G_{ss} \\ -\Omega G_{mm} & -\Omega G_{ms} & C_{mm} & C_{ms} \\ -\Omega G_{sm} & -\Omega G_{ss} & C_{sm} & C_{ss} \end{bmatrix} \begin{Bmatrix} \dot{\underline{m}}_{m,x} \\ \dot{\underline{m}}_{s,x} \\ \dot{\underline{m}}_{m,y} \\ \dot{\underline{m}}_{s,y} \end{Bmatrix}$$
$$+ \begin{bmatrix} \Lambda_{mm}^2 & 0 & 0 & 0 \\ 0 & \Lambda_{ss}^2 & 0 & 0 \\ 0 & 0 & \Lambda_{mm}^2 & 0 \\ 0 & 0 & 0 & \Lambda_{ss}^2 \end{bmatrix} \begin{Bmatrix} \underline{m}_{m,x} \\ \underline{m}_{s,x} \\ \underline{m}_{m,y} \\ \underline{m}_{s,y} \end{Bmatrix} = \begin{bmatrix} B_{m,x} & 0 \\ B_{m,s} & 0 \\ 0 & B_{m,y} \\ 0 & B_{s,y} \end{bmatrix} \begin{Bmatrix} \underline{f}_x \\ \underline{f}_y \end{Bmatrix}$$

where

$$\underline{w}_x = \Phi^{-1} T_m \underline{m}_{m,x} + \Phi^{-1} T_s \underline{m}_{s,x} \qquad \underline{w}_y = \Phi^{-1} T_m \underline{m}_{m,y} + \Phi^{-1} T_s \underline{m}_{s,y}$$

The equation can be rearranged to separate the master and slave modal degrees of freedom:

$$\begin{Bmatrix} \ddot{\underline{m}}_{m,x} \\ \ddot{\underline{m}}_{s,x} \\ \ddot{\underline{m}}_{m,y} \\ \ddot{\underline{m}}_{s,y} \end{Bmatrix} + \begin{bmatrix} C_{mm} & \Omega G_{mm} & C_{ms} & \Omega G_{ms} \\ -\Omega G_{mm} & C_{mm} & -\Omega G_{ms} & C_{ms} \\ C_{sm} & \Omega G_{sm} & C_{ss} & \Omega G_{ss} \\ -\Omega G_{sm} & C_{sm} & -\Omega G_{ss} & C_{ss} \end{bmatrix} \begin{Bmatrix} \dot{\underline{m}}_{m,x} \\ \dot{\underline{m}}_{m,y} \\ \dot{\underline{m}}_{s,x} \\ \dot{\underline{m}}_{s,y} \end{Bmatrix}$$
$$+ \begin{bmatrix} \Lambda_{mm}^2 & 0 & 0 & 0 \\ 0 & \Lambda_{mm}^2 & 0 & 0 \\ 0 & 0 & \Lambda_{ss}^2 & 0 \\ 0 & 0 & 0 & \Lambda_{ss}^2 \end{bmatrix} \begin{Bmatrix} \underline{m}_{m,x} \\ \underline{m}_{m,y} \\ \underline{m}_{s,x} \\ \underline{m}_{s,y} \end{Bmatrix} = \begin{bmatrix} B_{m,x} & 0 \\ 0 & B_{m,y} \\ B_{m,s} & 0 \\ 0 & B_{s,y} \end{bmatrix} \begin{Bmatrix} \underline{f}_x \\ \underline{f}_y \end{Bmatrix}$$

where, again,

$$\underline{w}_x = \Phi^{-1} T_m \underline{m}_{m,x} + \Phi^{-1} T_s \underline{m}_{s,x} \qquad \underline{w}_y = \Phi^{-1} T_m \underline{m}_{m,y} + \Phi^{-1} T_s \underline{m}_{s,y}$$

8.12.1 Modal Truncation, Assumptions

Finally, assume that $B_{s,x} \approx 0$, $B_{s,y} \approx 0$, $C_{sm} \approx 0$, and $G_{sm} \approx 0$:

$$\begin{Bmatrix} \ddot{\underline{m}}_{m,x} \\ \ddot{\underline{m}}_{s,x} \\ \ddot{\underline{m}}_{m,y} \\ \ddot{\underline{m}}_{s,y} \end{Bmatrix} + \begin{bmatrix} C_{mm} & \Omega G_{mm} & C_{ms} & \Omega G_{ms} \\ -\Omega G_{mm} & C_{mm} & -\Omega G_{ms} & C_{ms} \\ 0 & 0 & C_{ss} & \Omega G_{ss} \\ 0 & 0 & -\Omega G_{ss} & C_{ss} \end{bmatrix} \begin{Bmatrix} \dot{\underline{m}}_{m,x} \\ \dot{\underline{m}}_{m,y} \\ \dot{\underline{m}}_{s,x} \\ \dot{\underline{m}}_{s,y} \end{Bmatrix}$$
$$+ \begin{bmatrix} \Lambda_{mm}^2 & 0 & 0 & 0 \\ 0 & \Lambda_{mm}^2 & 0 & 0 \\ 0 & 0 & \Lambda_{ss}^2 & 0 \\ 0 & 0 & 0 & \Lambda_{ss}^2 \end{bmatrix} \begin{Bmatrix} \underline{m}_{m,x} \\ \underline{m}_{m,y} \\ \underline{m}_{s,x} \\ \underline{m}_{s,y} \end{Bmatrix} = \begin{bmatrix} B_{m,x} & 0 \\ 0 & B_{m,y} \\ 0 & 0 \\ 0 & 0 \end{bmatrix} \begin{Bmatrix} \underline{f}_x \\ \underline{f}_y \end{Bmatrix}$$

If these assumptions are good and the slave modes are stable, then $\underline{m}_{s,x} = \underline{m}_{s,y} = 0$

8.12.2 Modally Reduced Model

Since the slave modal degrees of freedom aren't doing anything, ignore them to obtain the reduced order model

$$\left\{ \begin{array}{c} \underline{\ddot{m}}_{m,x} \\ \underline{\ddot{m}}_{m,y} \end{array} \right\} + \left[\begin{array}{cc} C_{mm} & \Omega G_{mm} \\ -\Omega G_{mm} & C_{mm} \end{array} \right] \left\{ \begin{array}{c} \underline{\dot{m}}_{m,x} \\ \underline{\dot{m}}_{m,y} \end{array} \right\}$$
$$+ \left[\begin{array}{cc} \Lambda^2_{mm} & 0 \\ 0 & \Lambda^2_{mm} \end{array} \right] \left\{ \begin{array}{c} \underline{m}_{m,x} \\ \underline{m}_{m,y} \end{array} \right\} = \left[\begin{array}{cc} B_{m,x} & 0 \\ 0 & B_{m,y} \end{array} \right] \left\{ \begin{array}{c} \underline{f}_x \\ \underline{f}_y \end{array} \right\}$$

From which the physical degrees of freedom can be obtained using

$$\underline{w}_x = \Phi^{-1} T_m \underline{m}_{m,x} \qquad \underline{w}_y = \Phi^{-1} T_m \underline{m}_{m,y}$$

Note that the dimension of $\underline{m}_{m,x}$ is much less than that of $\underline{w}_x$: the matrix $\Phi^{-1}T_m$ is a modal interpolation matrix.

The real advantage to this approach lies in that the component matrices, C_{mm}, G_{mm}, Λ^2_{mm}, $\Phi^{-1}T_m$, and B_m can be obtained without computing the eigenvalues or mode shapes for the truncated modes: only the lowest modes which are to be retained need to be computed. This is a normal approach in finite element analysis or in modal testing.

8.13 Primary Issues in Flexible Structures

- sensor–actuator collocation

  when sensor–actuator pairs act at the same point in the structure, local phase lead feedback can be shown to be robust to most uncertainties

- robustness to uncertainty in structural damping

  design of strictly proper controllers is sensitive to assumptions about structural damping

- spill–over of unmodeled dynamics

  The structural model is always truncated and ignores some high frequency dynamics. These unmodeled dynamics may affect system stability.

8.13.1 Simple Flexible Beam, One End Simply Supported

To make it easy to understand these issues, we will examine the dynamics of a uniform beam 1 cm in diameter and 60 cm long which is simply supported at a point 10 cm from the left end as indicated in Figure 8.1. The actuator will be placed 45 cm from the left end. The sensor can either be placed 45 cm from the left end (collocated) or somewhere else (noncollocated). The modeshapes for this pivoted beam are shown in Figure 8.2.

Figures 8.3 and 8.4 illustrate the effect of sensor position on the transfer function from actuator input to sensor output. The former assumes 0.5 percent damping in each of the flexible modes while the latter assumes 2 percent. In each case, the sensor is moved from 5 cm to the left of the actuator (which is 45 cm from the left end of the beam) to 5 cm to the right of the actuator. Notice that the maxima of the transfer functions (poles) are independent of the sensor location while the minima (zeros) are very sensitive to sensor location.

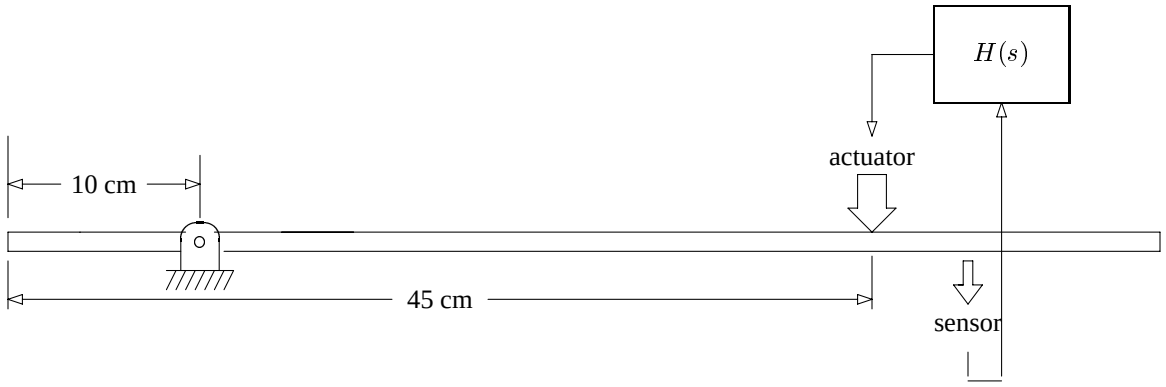

Figure 8.1: Flexible Beam with one Pinned Support

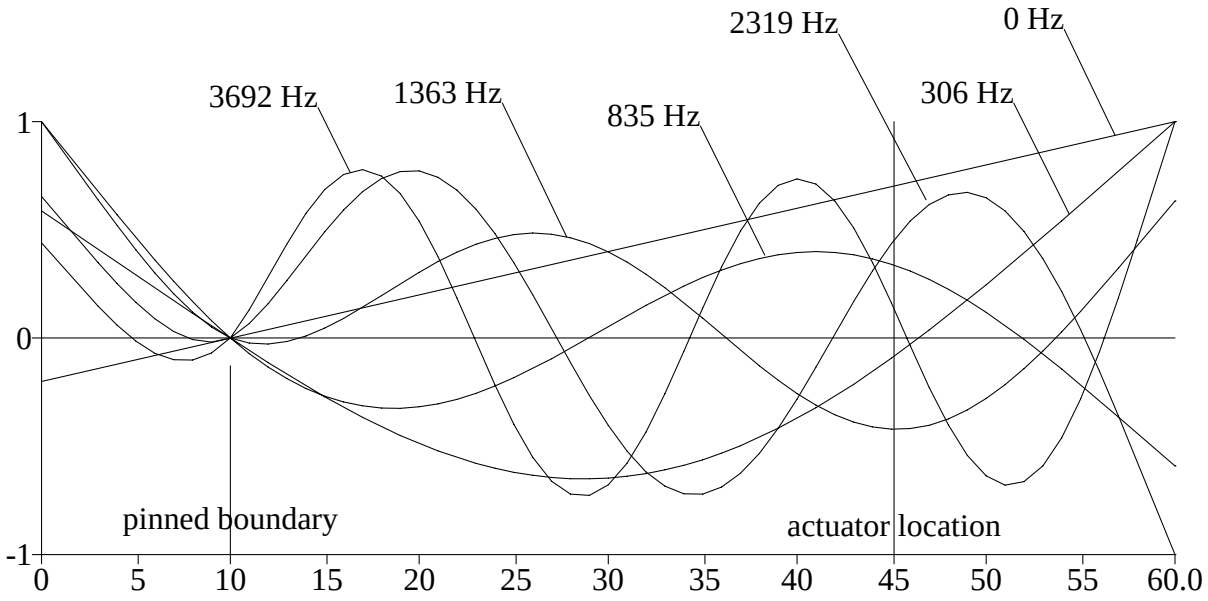

Figure 8.2: Flexible Beam with one Pinned Support: Mode Shapes

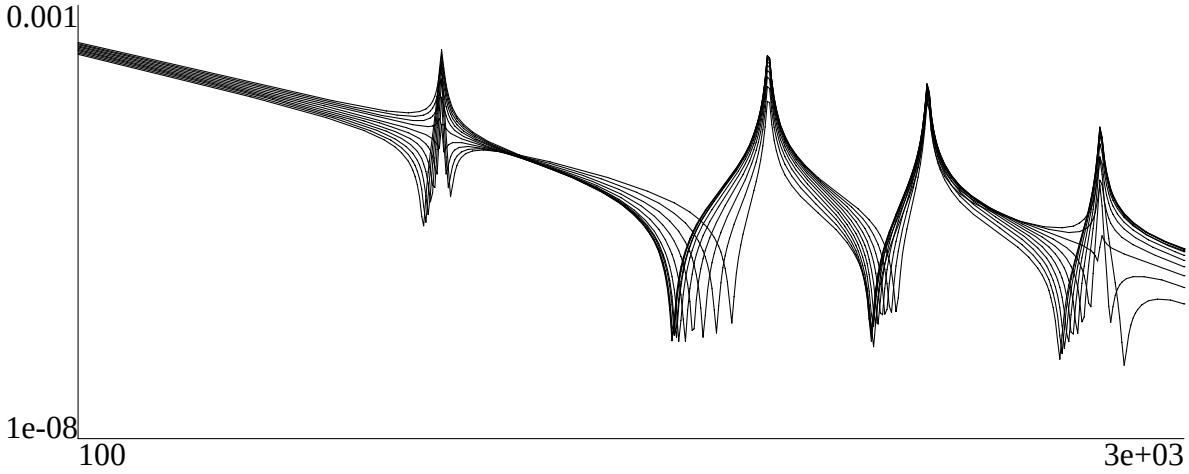

Figure 8.3: Flexible beam transfer functions, 0.5% damping; sensor location is moved from 40 cm to 50 cm in 1 cm increments.

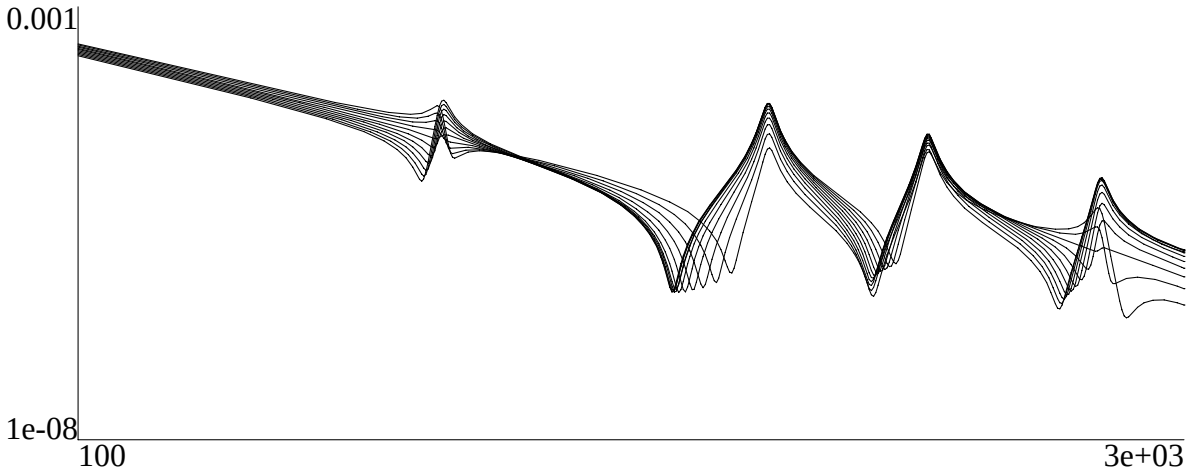

Figure 8.4: Flexible beam transfer functions, 2.0% damping; sensor location is moved from 40 cm to 50 cm in 1 cm increments.

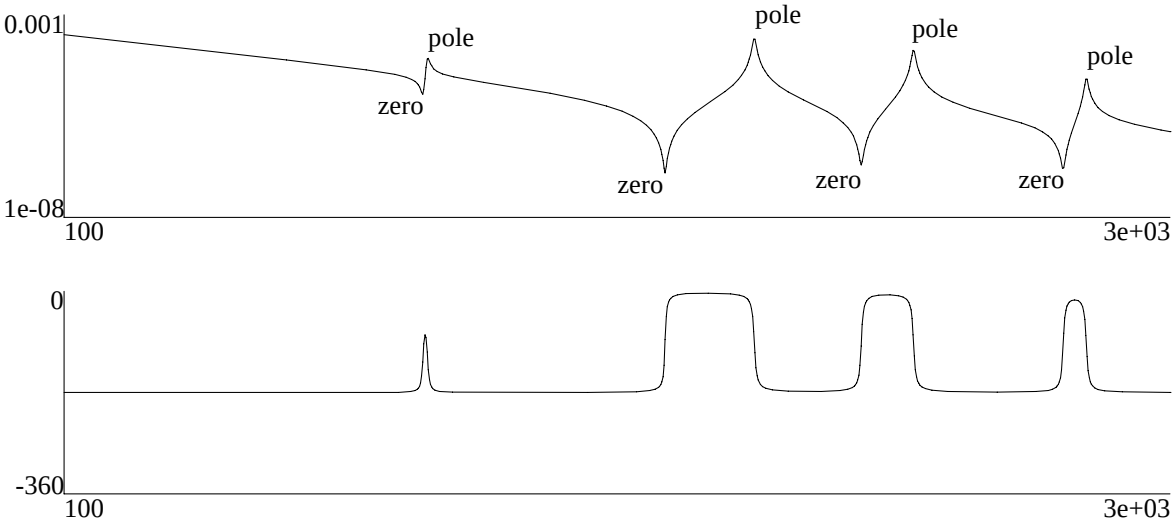

Figure 8.5: Collocated transfer function, 0.5% damping

Figure 8.5 illustrates the magnitude and phase of the transfer function from actuator input to sensor output when the two devices act at the same point along the shaft. Notice that poles and zeros are *interlaced*, so that the phase is between 0 and -180°. Starting at the low frequency end of the transfer function, the first feature encountered is a minimum or zero where the phase recovers nearly to 0. This is followed by a maximum or pole where the phase returns nearly to -180. This sequence of zero followed by pole continues throughout the plotted range.

Figure 8.6 superimposes the sensor and actuator locations on the modeshapes for the collocated case. Notice that the product of the modal displacement at the sensor location times the modal displacement at the actuator location is always positive. (It *must* be because the displacements are the same and $x^2 >= 0$.) This is characteristic of a flexible beam with collocated sensor and actuator.

8.14 Stability and $H(S)$

From the Nyquist criterion, the closed loop system is stable as long as the point $(-1, 0)$ in the complex plane is not clockwise encircled. That is, when the product of the $H(s)$ and the plant transfer function is 1.0, the phase must be greater than -180°. This is the concept of cross-over phase used in Bode analysis.

Since the plant transfer function is always less than 0 but greater than -180° we need only ensure that the controller phase lies between 0 and $+180^\circ$ to guarantee stability for *any* loop gain! Such a controller is called *strictly positive* and it is a widely used theorem of structural mechanics that such a controller is always stabilizing when the sensor and actuator are collocated. A system which is stable for any gain is referred to as *phase stabilized.*

8.14.1 Stabilizing Controllers: Collocated Case

If the sensor and actuator are collocated then the system is stabilized by any *proper* PD controller. Further, a proper PID controller will also stabilize the system as long as the initial -90° phase of the controller recovers to a positive value before cross–over. This means that a proper PID controller

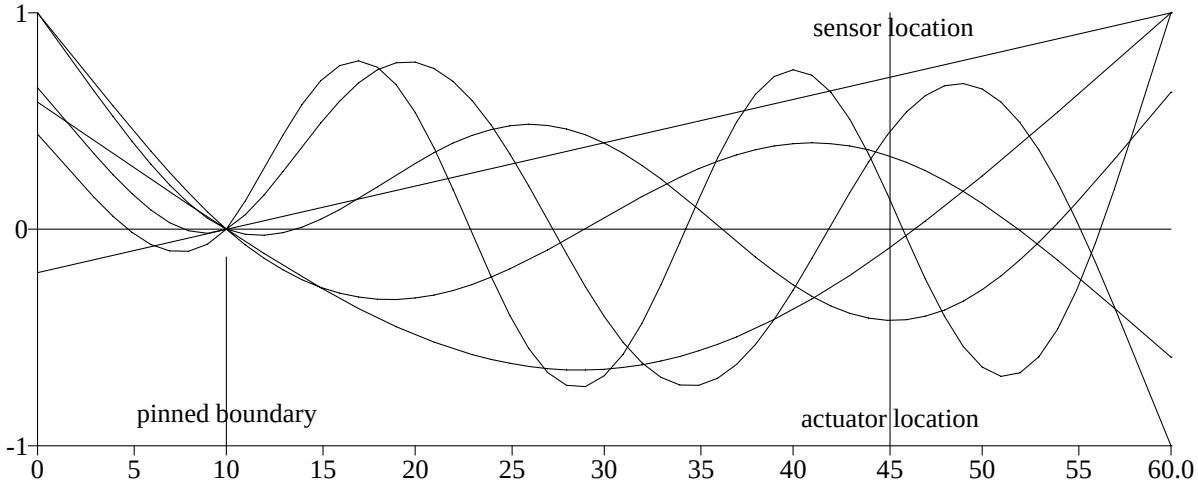

Figure 8.6: Modeshapes with sensor collocated.

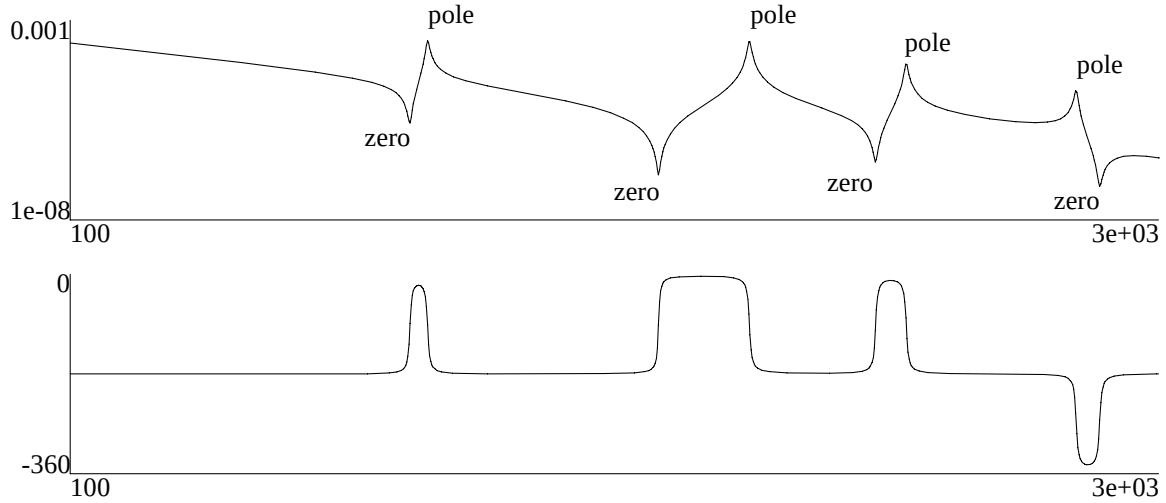

Figure 8.7: Bode diagram with sensor located at 50 cm (5 cm to the right of the actuator).

has a lower gain limit below which the system is unstable. It has no upper gain limit. This is the main reason for which PID control is so popular in stabilizing flexible structures!

8.14.2 Sensor at 40 cm: Noncollocated, 0.5% Damping

When the sensor and actuator are not collocated, this property is lost. Figure 8.7 shows the Bode diagram when the sensor is placed at 40 cm, 5 cm to the left of the actuator. Notice that the poles and zeros are no longer interlaced and the phase is less than -180° at some frequencies.

Figure 8.8 shows the modeshapes, sensor location, and actuator location for this case. Notice that the product of the modal displacement at the sensor location times the modal displacement at the actuator location is no longer always positive: mode 5 at 2319 Hz has a node between the sensor and the actuator leading to a sign reversal.

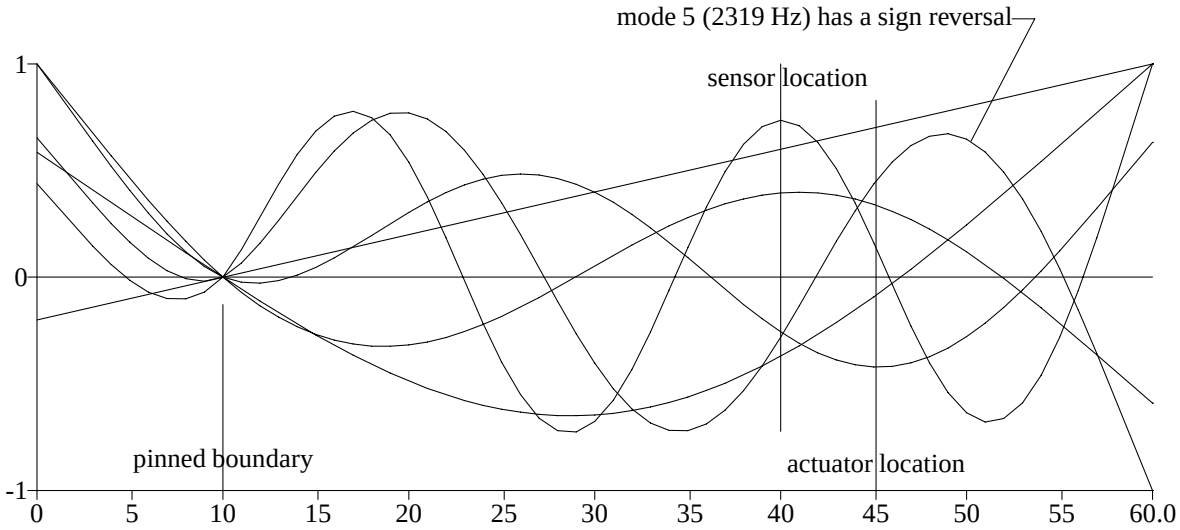

Figure 8.8: Modeshapes, sensor, and actuator locations: 40 cm sensor location.

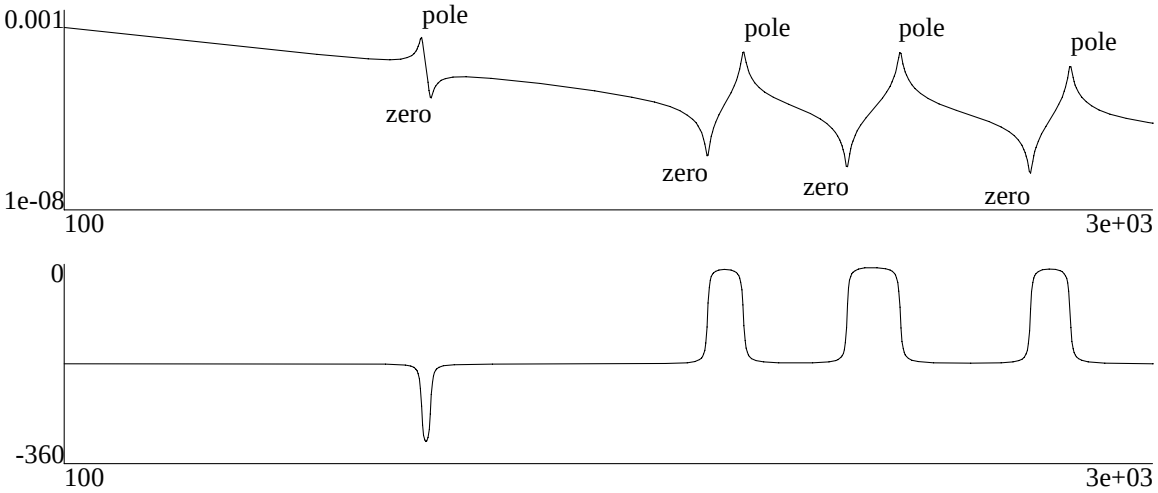

Figure 8.9: Bode diagram with sensor located at 50 cm (5 cm to the right of the actuator).

8.14.3 Sensor at 50 cm: Noncollocated, 0.5% Damping

When the sensor is moved to 50 cm, 5 cm to the right of the actuator, the interlacing violation occurs in the second mode and the phase falls below -180° at a very low frequency: about 320 Hz as illustrated in Figure 8.9. This is a real problem!

Figure 8.10 shows the modeshapes of the beam, superimposing the actuator and sensor locations with the sensor at 50 cm, 5 cm to the right of the actuator. Notice that the product of the modal displacement at the sensor location times the modal displacement at the actuator location is negative for modes 2 at 306 Hz and 6 at 3692 because these modes have nodes located between the sensor and the actuator. Comparing to Figure 8.9, this sign change is directly associated with the excess phase lag in the actuator–sensor transfer function.

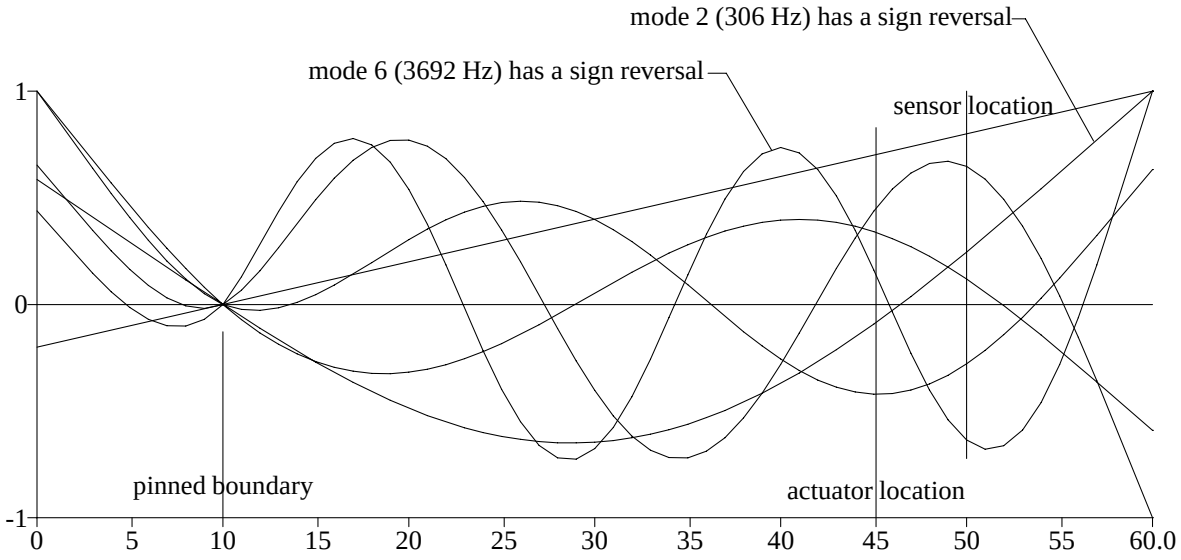

Figure 8.10: Modeshapes, sensor, and actuator locations: 50 cm sensor location.

8.14.4 Stability with Noncollocation

This excess phase associated with noncollocation produces a stability problem, substantially complicating the design of the controller. The problem is easy to understand using a root locus. The zeros attract the poles and the loci do not cross. When the poles and zeros are interlaced, the loci can stay in the left half plane without any difficulty: the left to right motion of the pole associated with a simple phase lead controller is sufficient to attract the loci into the left half plane.

When the poles and zeros are not interlaced, some of the loci must "skip" over a pole and they do this by traveling into the right half plane, producing instability, as illustrated in the root locus of Figure 8.11.

The problem can be "fixed" if the controller adds some poles and zeros which "repair" the interlacing violation, as illustrated in Figure 8.12. Obviously, this repair can be made and the gain margin appears to become again infinite, but the result is very sensitive to the exact dynamics of the beam: it wasn't in the case of collocated control because the interlacing is a fundamental property of such structures. Here, if the controller misplaces its added poles and zeros relative to the *actual* plant poles and zeros, the system may be unstable rather than stable.

8.14.5 The Spill–over Problem

Since the strategy for stabilizing the noncollocated system is to fix any interlacing violations by adding controller pole–zero pairs, it is clear that any unmodeled poles (higher frequency dynamics) will not be considered in this "repair job". Further, the mode shapes associated with the higher modes have more nodes and so, are more likely to produce interlacing violations. The result is that, no matter how much effort is put into stabilizing the modeled plant, some part of the unmodeled plant will *always* produce instability in the final system.

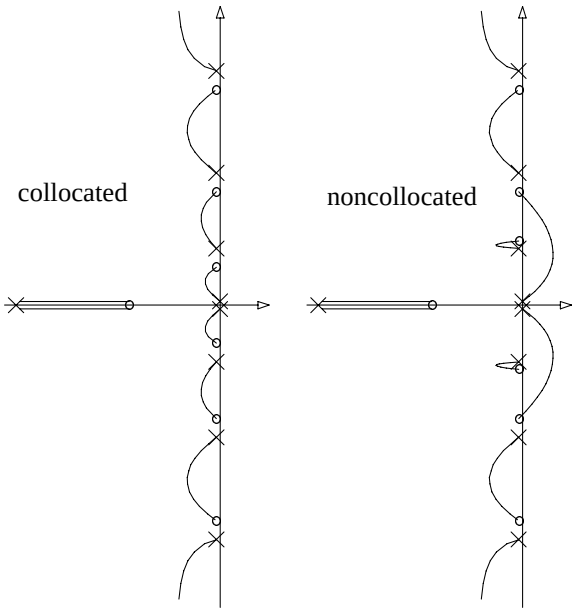

Figure 8.11: Root locus of actuator–controller transfer function: collocated case compared to noncollocated case.

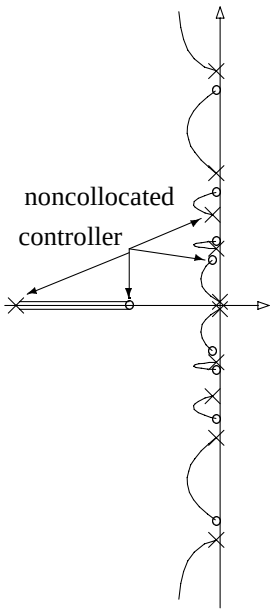

Figure 8.12: Root locus of actuator–controller transfer function with interlacing repair.

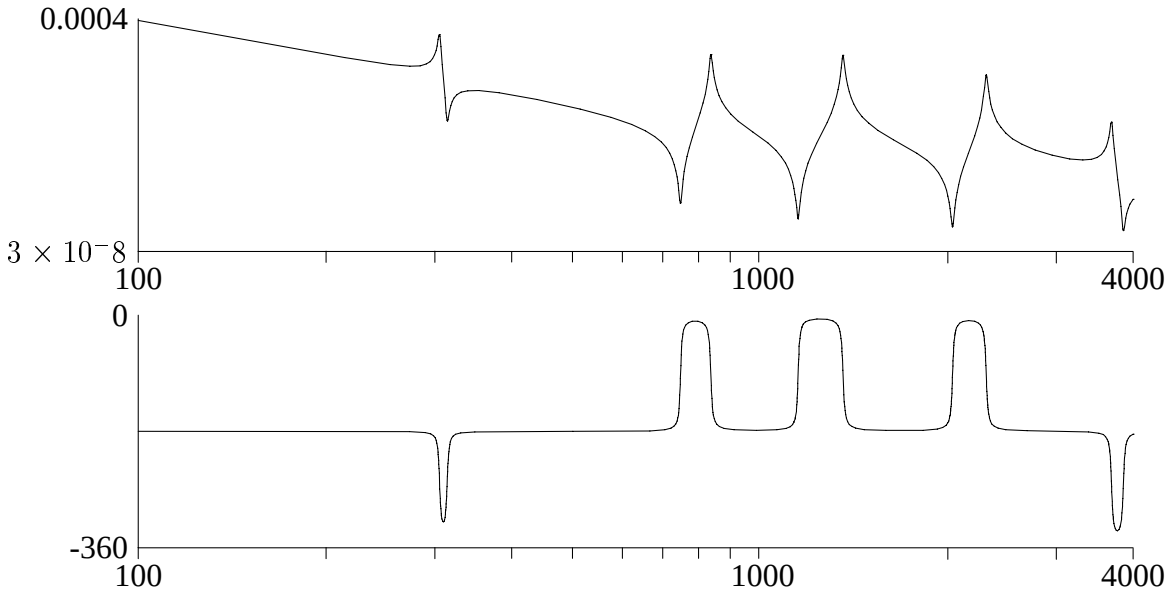

Figure 8.13: Bode plot of flexible beam, actuator at 45 cm, sensor at 50 cm, 0.5% modal damping.

8.15 Controller Design: Single Input–Single Output

The controller is essentially a strictly proper PID controller. If the sensor and actuator are not collocated, then some pole–zero pairs are added near to the $j\omega$ axis to repair the interlacing violations.

Selection of the actual controller gains: proportional, derivative, integral and high frequency roll–off follows the following sequence:

1. a critical speed map is generated for the beam (rotor) to determine what the nominal bearing stiffness should be.

2. the first roll–off frequency will be at 10–20 times the zero at K/C. This means that the peak phase will be attained at a frequency of $\sqrt{\alpha}K/C$ where α is the pole–zero ratio (10–20). The peak phase should probably occur at the first bending mode as this is the most difficult mode to control.

3. the second roll–off frequency is selected to prevent destabilizing the higher modes - a Bode plot gives the necessary information.

4. the integrator gain is selected to provide adequate damping in the first closed loop mode. Again, a Bode plot gives the necessary information.

8.15.1 Simple Pinned Beam

Again, we will examine the dynamics of a uniform beam 1 cm in diameter and 60 cm long which is simply supported at a point 10 cm from the left end. The actuator will be placed 45 cm from the left end. The sensor will be placed 50 cm from the left end to provide some non–collocation. Assume 0.5% modal damping in the beam. Figure 8.13 illustrates the plant Bode diagram from actuator input to sensor output while Table 8.1 lists the poles and zeros of this transfer function..

Table 8.1: Poles and zeros for flexible beam, actuator at 45 cm, sensor at 50 cm, 0.5% modal damping.

frequency (Hz)	damping (%)	pole	zero
0	0	√	
306	0.5	√	
314	0.52		√
747	0.43		√
835	0.5	√	
1155	0.44		√
1363	0.5	√	
2047	0.47		√
2319	0.5	√	
3692	0.5	√	
3856	0.51		√

Interlacing Repair

First, the controller must repair the interlacing. A complex pair of zeros is added at 280 Hz with a damping ratio of 0.5% and a complex pair of poles is added at 320 Hz with a damping ratio of 0.5%. This repairs the first interlacing violation. In addition, a complex pair of zeros is added at 3500 Hz with a damping ratio of 0.5% and a complex pair of poles is added at 3900 Hz with a damping ratio of 0.5%. Table 8.2 illustrates the insertion of these compensating poles and zeros.

The resulting initial controller transfer function is

$$H_{ir}(s) = \frac{1.3061s^2 + 11.489s + 4.0426 \times 10^6}{s^2 + 10.053s + 4.0426 \times 10^6} \frac{1.2416s^2 + 136.53s + 6.0047 \times 10^8}{s^2 + 122.52s + 6.0047 \times 10^8}$$

and the Bode plot of this controller acting in series with the noninterlaced plant is illustrated in Figure 8.14. Notice that the phase of the compensated transfer function stays between 0 and -180° throughout the frequency range.

Choose Nominal PD Gains

Figure 8.15 is a critical speed map for this flexible beam. It is a plot of the imaginary part of the system eigenvalues as a function of the stiffness of a spring acting at the actuator location. To design the PID portion of the controller, select the bearing stiffness to correspond to sections of the critical speed map where the curves have significant slope: this is where the bearing/rotor interaction is strongest. Figure 8.16 expands the region of interest.

From the critical speed map, it will only be possible to do this for the first two modes – at a stiffness of about 9×10^6 N/m. Use a pole–zero ratio of 15 and put the peak phase at the average of the two critical speeds, from the critical speed map: 331 Hz. Thus, the PD portion of the controller is

$$H_{PD}(s) = 9 \times 10^6 \frac{0.00186s + 1}{0.000124s + 1}$$

Figure 8.17 illustrates the open loop transfer function of the beam acting in series with the PD controller and interlacing repair filter.

Table 8.2: Compensated poles and zeros for flexible beam, actuator at 45 cm, sensor at 50 cm, 0.5% modal damping.

freq. (Hz)	damp. (%)	pole	zero
0	0	√	
⇒ 280	0.5		√
306	0.5	√	
314	0.52		√
⇒ 320	0.5	√	
747	0.43		√
835	0.5	√	
1155	0.44		√
1363	0.5	√	
2047	0.47		√
2319	0.5	√	
⇒ 3500	0.5		√
3692	0.5	√	
3856	0.51		√
⇒ 3900	0.5	√	

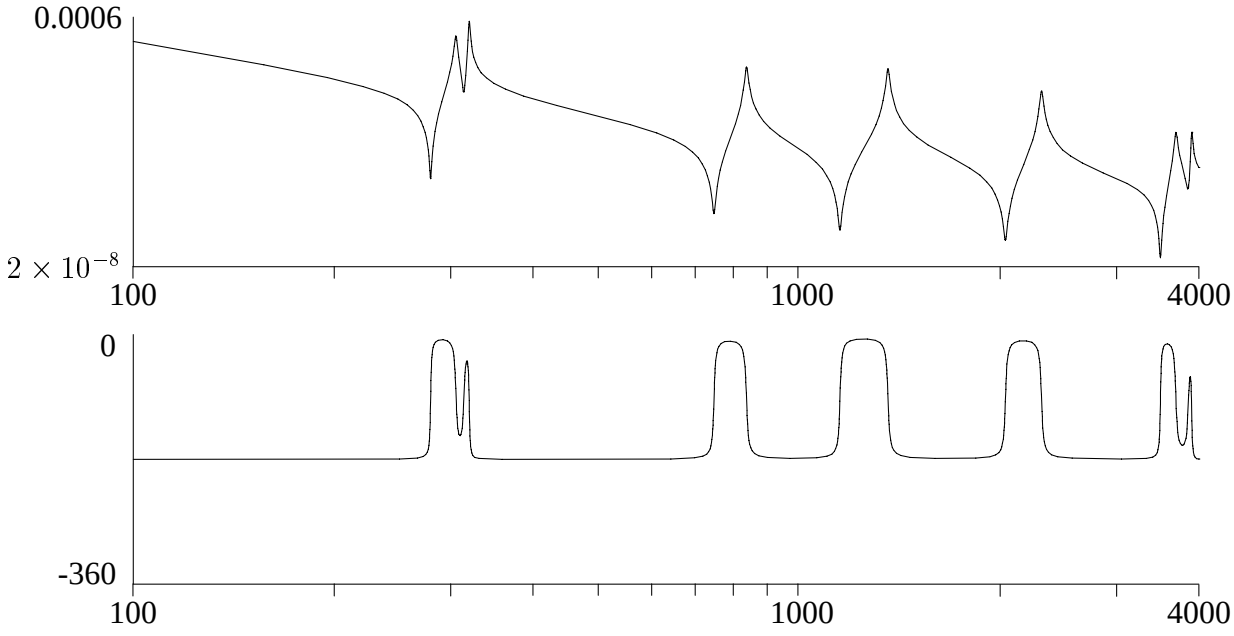

Figure 8.14: Bode Plot of Plant with Interlacing Repairs

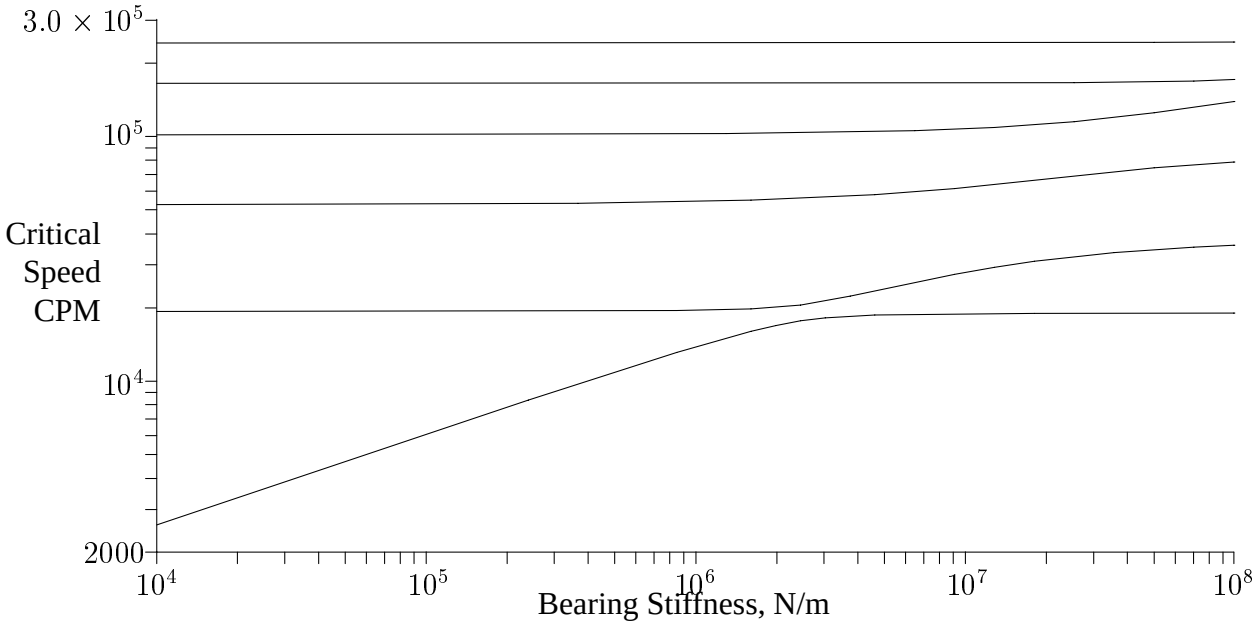

Figure 8.15: Critical Speed Map of Flexible Beam

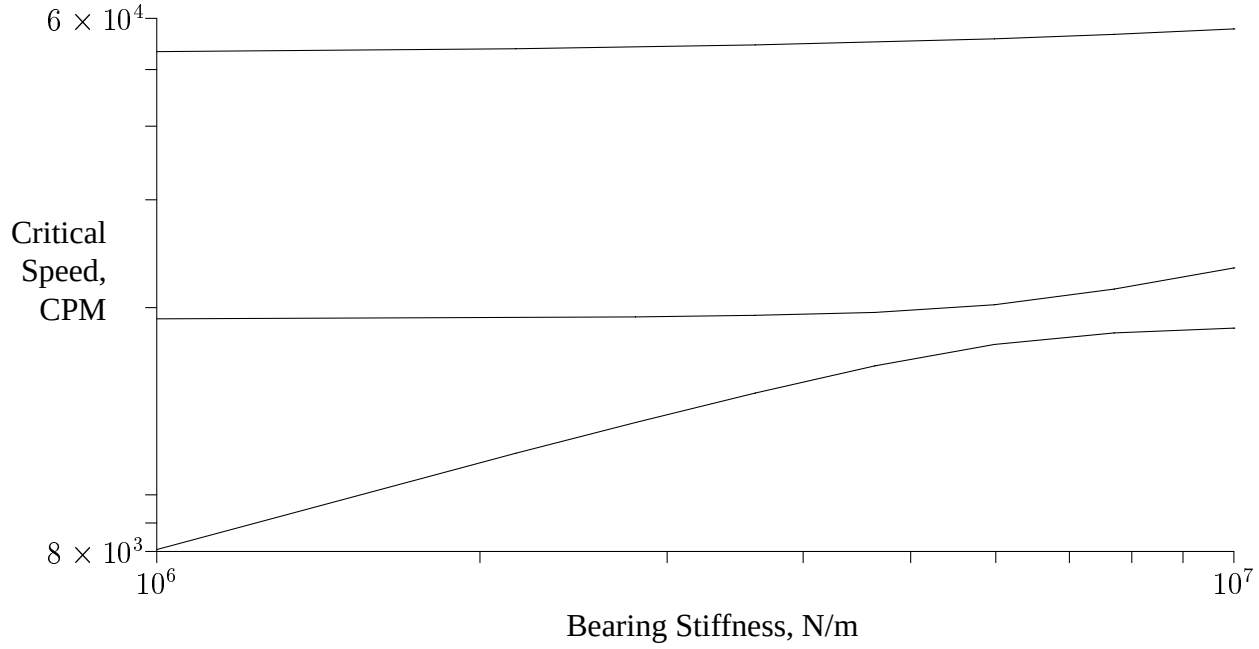

Figure 8.16: Critical Speed Map Detail

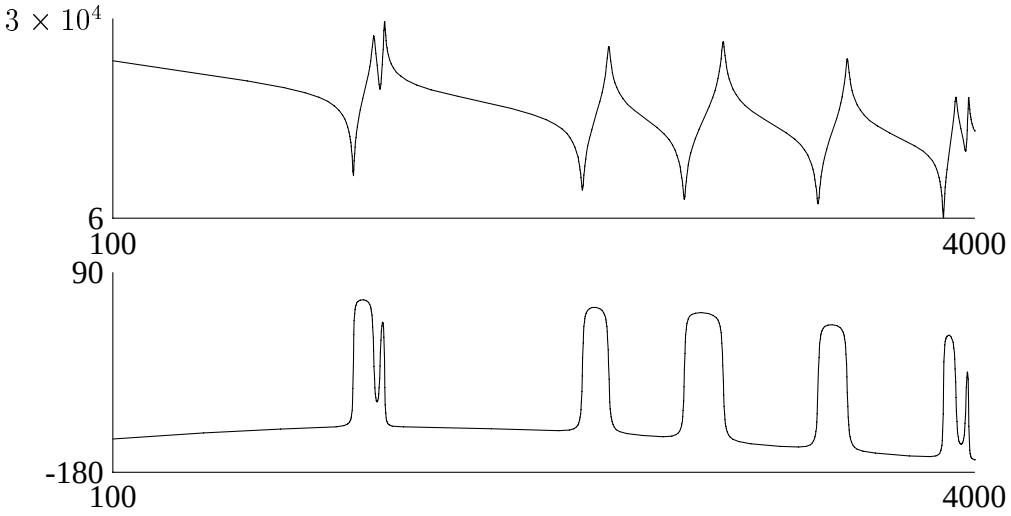

Figure 8.17: Bode plot of beam with PD controller.

Integrator Design

Adding an integrator to the PD controller introduces a pole at the origin and a zero at some other frequency, which depends on the integrator gain:

$$\begin{aligned} H_{PID}(s) &= \frac{T}{s} + K\frac{C/Ks+1}{0.067C/Ks+1} \\ &= \frac{T(0.067C/Ks+1)+K(C/Ks^2+s)}{s(0.067C/Ks+1)} \end{aligned}$$

From the Bode plot of the combined controller and flexible beam, the zero should be at a frequency well below the PD controller zero at about 85 Hz. Put it at 5 Hz:

$$\begin{aligned} H_{PID}(s) &= \frac{3\times 10^8}{s} + 9\times 10^6 \frac{0.00186s+1}{0.000124s+1} \\ &= 9\times 10^6 \frac{0.00186s^2+1.0041s+33.3}{0.000124s^2+s} \end{aligned}$$

The resulting plant and controller Bode diagram is illustrated in Figure 8.18.

Stability of the closed loop system is assessed by computing the eigenvalues of the closed loop dynamic matrix. Table 8.3 is the output of a stability code when the closed loop model is submitted.

Strictly Proper Controller

The controller designed so far is a proper controller but not strictly proper. The gain at infinite frequency is 2.2×10^8 N/m. To make the controller strictly proper, we need to add one or two poles at high frequency. One option is to add a pole at a frequency well beyond the last plant mode – at 5 kHz, for example. The problem with this is that the plant certainly has unmodeled (truncated) dynamics at these frequencies – it is better if the controller bandwidth is less than the nominal plant bandwidth.

Instead, we would like to limit the controller bandwidth to less than 3500 Hz. Figure 8.19 plots the real part of the first four eigenvalues as a function of the controller bandwidth (the frequency

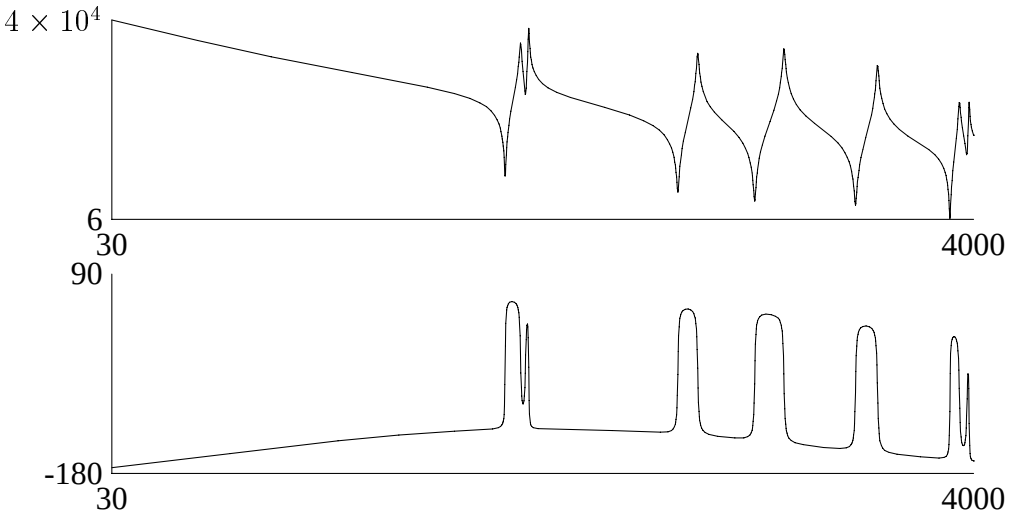

Figure 8.18: Bode Plot of Beam with Proper PID controller

Table 8.3: Closed Loop System With Proper PID Controller

```
Program EIGS Compiled Jun 07 1995 at 20:18:51
Version 1.1
Copyright (c) 1995, ROMAC Laboratories, University of Virginia
Run time is Mon Jun 26 18:17:59 1995

"A" matrix file:        sysa.mat

Real eigenvalues:
    exponent  time constant (sec)
     -32.995     0.0303077
    -559.155    0.00178841

Complex eigenvalues:
        real     imaginary      log. dec.        Hertz          CPM
    -24.0664       1749.77      0.086419       278.484       16709.1
    -11.3008       1973.89     0.0359721       314.155       18849.3
    -200.228       4601.43      0.273408       732.341       43940.5
    -376.909       6949.36      0.340778       1106.02       66361.5
    -769.427       11876.8      0.407049       1890.26        113416
    -1557.69       18526.8      0.528277       2948.63        176918
    -310.729       23922.5     0.0816122       3807.38        228443
    -819.642       25596.1      0.201201       4073.75        244425
```

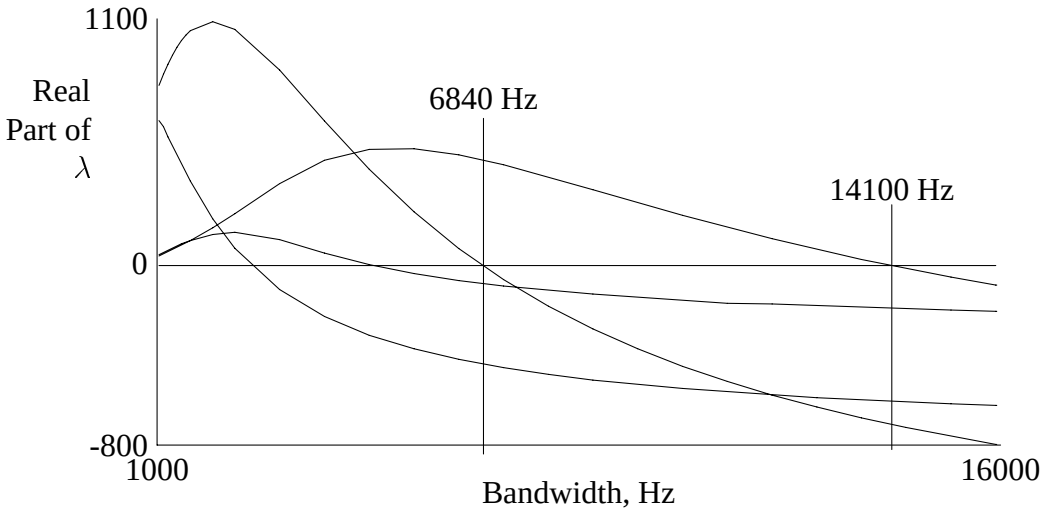

Figure 8.19: Effect of Controller Bandwidth on Stability

of the added pole which makes the controller strictly proper. If the controller bandwidth is greater than 14,100 Hz, then all of these modes are stable. When the controller bandwidth is dropped below this frequency, the highest mode is destabilized. The remaining modes remain stable until the controller bandwidth drops to 6840 Hz, at which point the next highest mode is also destabilized. Unfortunately, at this point the controller bandwidth still exceeds the plant model bandwidth, so this approach to obtaining gain stabilization for the remaining modes will not work.

8.15.2 Repeat with 2.0% Damping

Plant Bode Diagram:

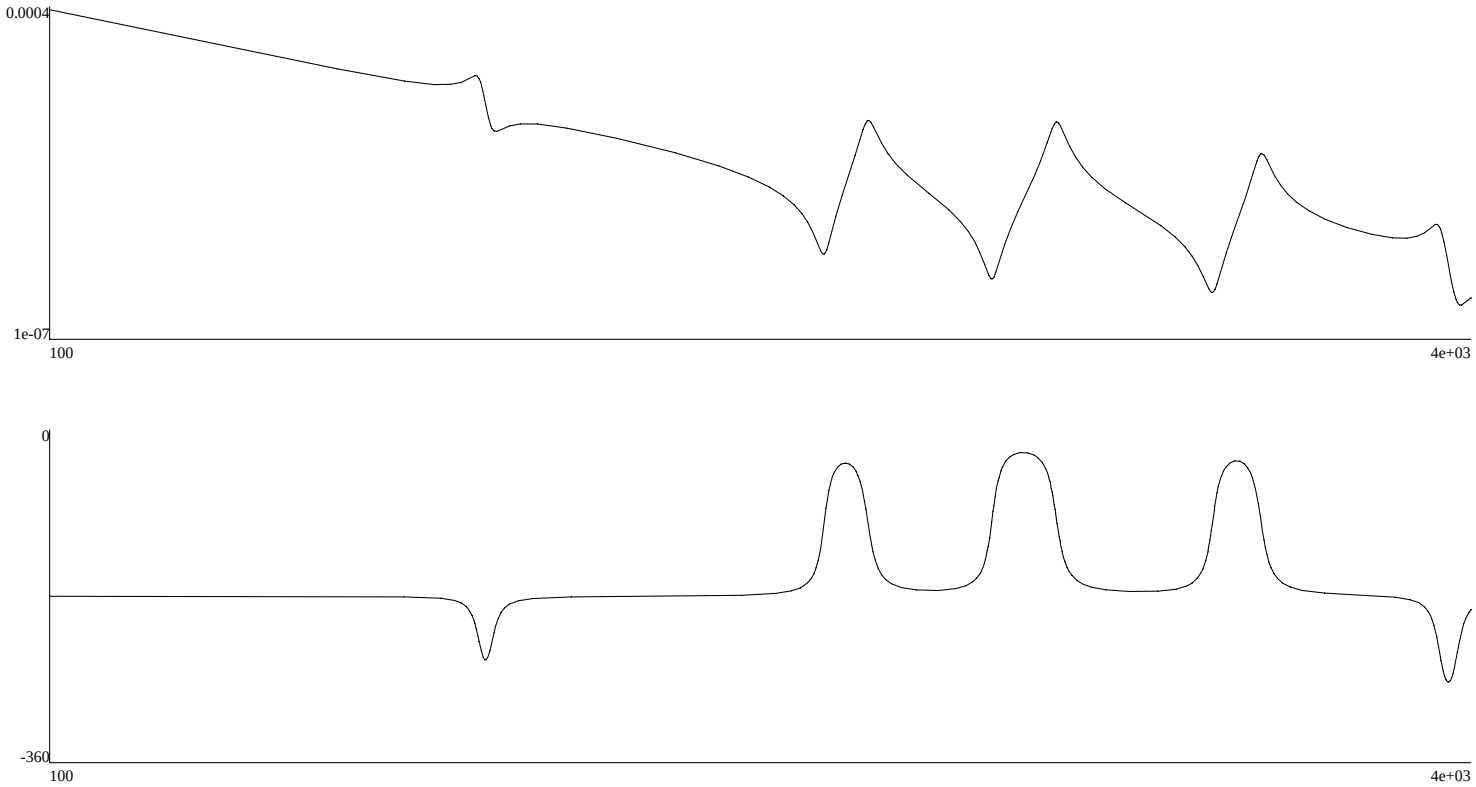

Interlacing Repair

Put a complex pair of zeros at 280 Hz with a damping ratio of 2.0% and a complex pair of poles at 320 Hz with a damping ratio of 2.0%. In addition, put a complex pair of zeros at 3500 Hz with a damping ratio of 2.0% and a complex pair of poles at 3900 Hz with a damping ratio of 2.0%.

$$H_{ir}(s) = \frac{1.3s^2 + 46.0s + 4.04 \times 10^6}{s^2 + 40.2s + 4.04 \times 10^6} \; \frac{1.24s^2 + 546s + 6.0 \times 10^8}{s^2 + 490s + 6.0 \times 10^8}$$

Figure 8.20 shows the Bode diagram of the plant in series with this interlacing repair filter.

PID Controller

Since the plant is substantially the same, use the same PID controller section to obtain the desired stiffness and damping:

$$\begin{aligned} H_{PID}(s) &= \frac{3 \times 10^8}{s} + 9 \times 10^6 \frac{0.00186s + 1}{0.000124s + 1} \\ &= 9 \times 10^6 \frac{0.00186s^2 + 1.0041s + 33.3}{0.000124s^2 + s} \end{aligned}$$

Table 8.4 shows the result of the stability analysis for the closed loop system.

8.16 Harmonic Control: Basic Concept

Most rotor excitation is sinusoidal and synchronized with the shaft rotation:

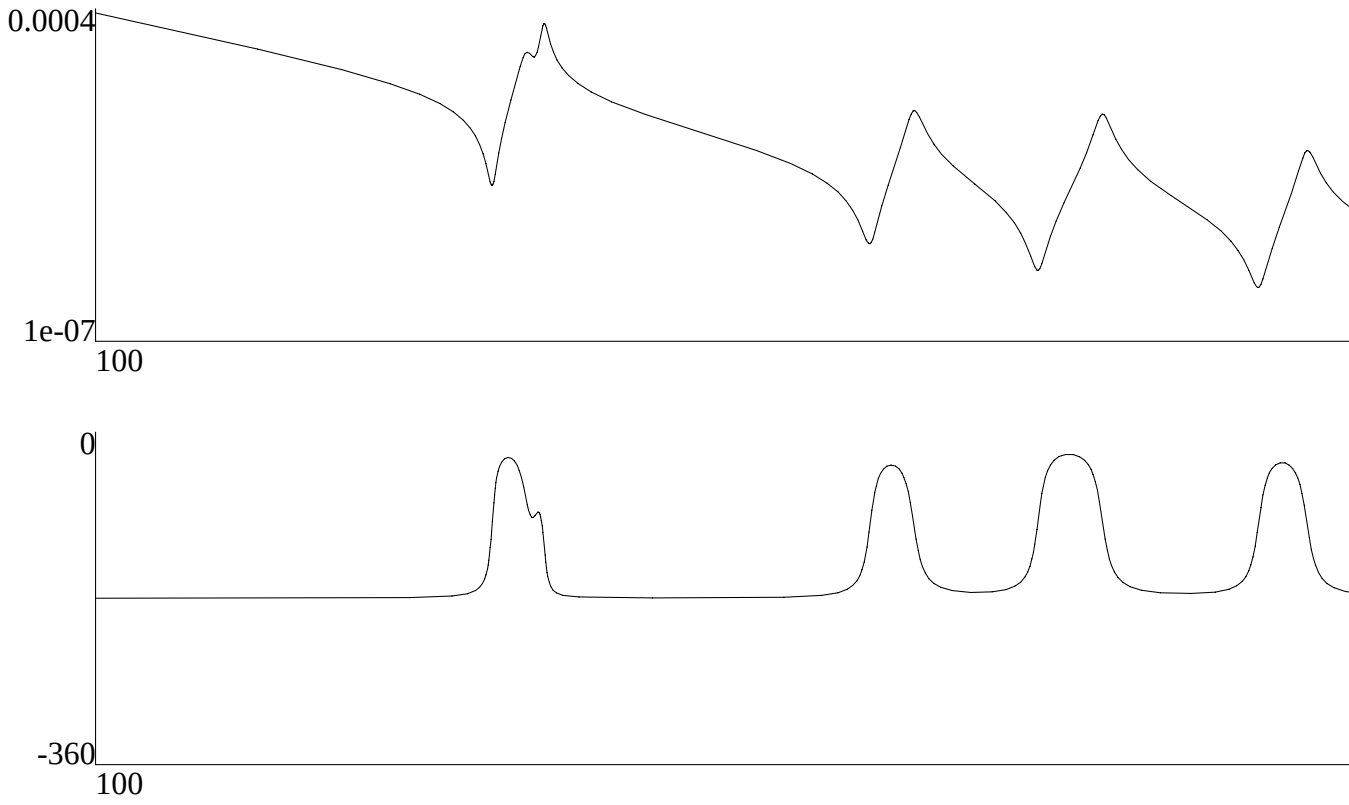

Figure 8.20: Bode plot of plant with interlacing repairs, 2% modal damping.

Table 8.4: Stability with proper PID controller: 2% modal damping.

```
Program EIGS Compiled Jun 07 1995 at 20:18:51
Version 1.1
Copyright (c) 1995, ROMAC Laboratories, University of Virginia
Run time is Tue Jun 27 10:03:41 1995

"A" matrix file:        sysa.mat

Real eigenvalues:
    exponent  time constant (sec)
     -32.995     0.0303077
    -559.167    0.00178837

Complex eigenvalues:
        real     imaginary      log. dec.        Hertz           CPM
     -36.969       1749.06      0.132805       278.371       16702.3
     -42.102       1973.97      0.134012       314.167         18850
    -254.825       4591.89      0.348683       730.822       43849.3
    -458.245       6939.36      0.414913       1104.43         66266
    -904.586       11859.6      0.479248       1887.51        113251
    -1698.05       18564.5      0.574709       2954.63        177278
    -862.878       23871.5      0.227117       3799.27        227956
     -813.77       25641.8      0.199404       4081.02        244861
```

mass imbalance

shaft bow

aerodynamic excitation

sensor surface runout

Because the excitation is steady, it can be *predicted* on the basis of past observations. If it can be predicted, then a counteracting force can be applied which minimizes the system response.

8.16.1 Parallel Control

This harmonic control is some sinusoidal force applied to the system in order to counter-act (cancel) the effect of the steady disturbance. The magnitude and phase of the harmonic control will be changed very slowly (every 0.05 seconds?) so there is no effect on linear system stability. Because this is not a stabilizing control, some feedback control must also be used. The two controls then function in parallel as illustrated in Figure 8.21.

8.16.2 Single Mass Model

The underlying idea is best illustrated through the example of controlling a simple mass. The model of the simple mass is

$$M\ddot{x} = f_b + f_e$$

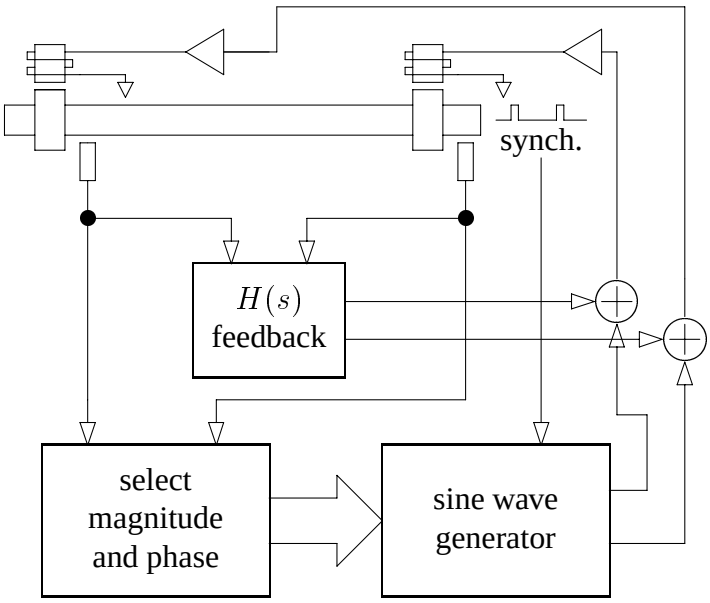

Figure 8.21: Parallel control architecture.

Examine simple feedback control. Assume $f_b = -Kx - C\dot{x}$:

$$M\ddot{x} + C\dot{x} + Kx = f_e$$

Choose C for damping ξ: $C = 2\xi\sqrt{KM}$. The steady state load response is

$$\frac{x(s)}{f_e(s)} = \frac{1}{Ms^2 + Cs + K}$$

Normalize by the last coefficient and substitute the defining relationship for C. Now, define the nondimensional frequency

$$\sigma \doteq s\sqrt{\frac{M}{K}}$$

to obtain

$$\frac{x(\sigma)}{f_e(\sigma)} = \frac{1}{K}\frac{1}{\sigma^2 + 2\xi\sigma + 1}$$

The required bearing force is

$$\frac{f_b(\sigma)}{f_e(\sigma)} = (K + Cs)\frac{x(\sigma)}{f_e(\sigma)} = \frac{1 + 2\xi\sigma}{\sigma^2 + 2\xi\sigma + 1}$$

Figure 8.22 shows the worst case amplification from the unbalance load, f_e, to the bearing force, f_b, as a function of the damping ratio, ξ.

8.16.3 Single Mass Model: Quadratic Optimization

Clearly, with a feedback solution, we want very high stiffness and very high damping to minimize the forced response while using the least force. As an alternative, assume that $f_e = F_e \sin \omega t$. If

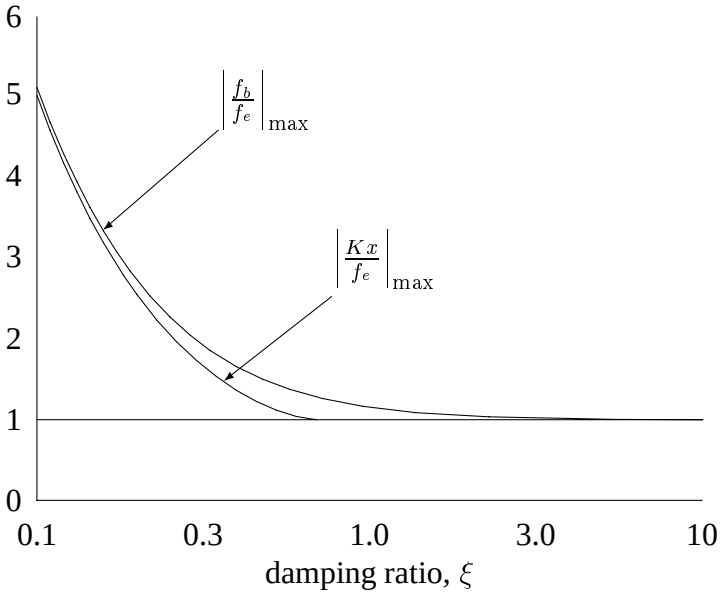

Figure 8.22: Single mass bearing, worst amplification *vs* damping ratio.

$f_b = F_b \sin\omega t = -f_e$ then the response, $x = X \sin\omega t$, is identically zero and the force is always smaller than with feedback.

In general, we wish to reach some sort of trade–off between bearing force and response:

$$F_b^* = \arg\min_{F_b} \left(|F_b/\alpha|^2 + |X/\beta|^2 \right) \quad : \quad X = \frac{1}{m\omega^2} \left(F_b + F_e \right)$$

This allows the force to go to zero at high frequencies if α is finite and β is non–zero:

$$F_b^* = -\frac{\alpha^2}{\alpha^2 + \beta^2 m^2 \omega^4} F_e$$

Notice that the force is always 180° out of phase with the excitation. This cannot be achieved stably using only feedback.

Solution of the Quadratic Minimization

The problem posed is to minimize J by choice of F_b:

$$J = \left(|F_b/\alpha|^2 + |X/\beta|^2 \right)$$

subject to the constraint:

$$X = \frac{1}{m\omega^2} \left(F_b + F_e \right)$$

Thus, J can be expanded as

$$J = \frac{F_b^2}{\alpha^2} + \frac{1}{m^2\omega^4} \left(F_b^2 + 2F_bF_e + F_e^2 \right)$$

Differentiate with respect to F_b:

$$\frac{dJ}{dF_b} = 2\frac{F_b}{\alpha^2} + \frac{1}{\beta^2 m^2 \omega^4} \left(2F_b + 2F_e \right)$$

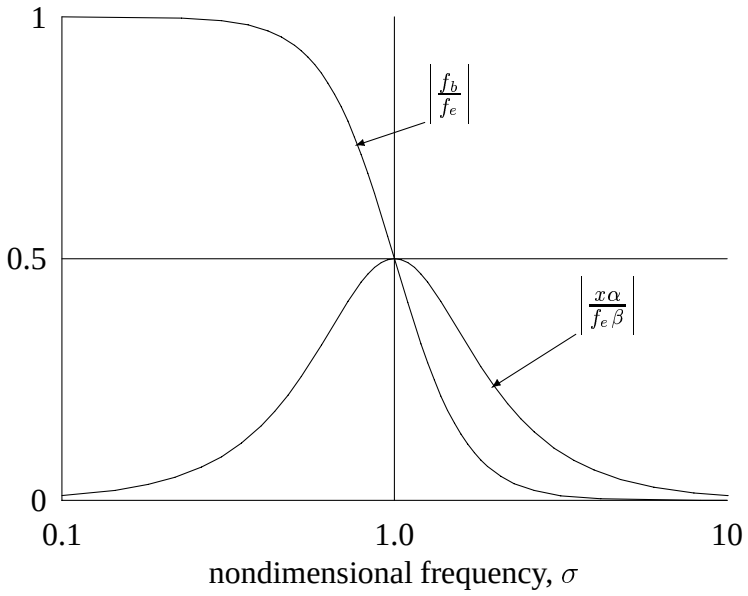

Figure 8.23: Single mass: quadratically optimized bearing force amplification *vs* nondimensional frequency.

The minimizer occurs where the derivative is zero, so

$$F_b^*\left(\frac{1}{\alpha^2}+\frac{1}{\beta^2 m^2\omega^4}\right) = -\frac{1}{\beta^2 m^2\omega^4}F_e \quad \Rightarrow \quad F_b^* = -\frac{\alpha^2}{\alpha^2+\beta^2 m^2\omega^4}F_e$$

Quadratic Optimized Solution: Single Mass

With this quadratic optimization, the bearing force and mass response magnitudes are:

$$\left|\frac{F_b}{F_e}\right| = \frac{\alpha^2}{\alpha^2+\beta^2 m^2\omega^4}$$

$$\left|\frac{X}{F_e}\right| = \frac{1}{m\omega^2}\frac{\beta^2 m^2\omega^4}{\alpha^2+\beta^2 m^2\omega^4}$$

Or, define $\sigma \doteq \omega\sqrt{\beta m/\alpha}$ to obtain the nondimensional forms

$$\left|\frac{F_b}{F_e}\right| = \frac{1}{1+\sigma^4} \qquad \left|\frac{X\alpha}{F_e\beta}\right| = \frac{\sigma^2}{1+\sigma^4}$$

Figure 8.23 illustrates this solution. Notice that this response looks like a mass with PID control. It has a "resonance" and is zero as $\sigma \to 0$ and as $\sigma \to \infty$.

8.16.4 Similar PID Control

For comparison, a PID controller was designed for a mass of 0.387 units. The PID parameters were:

$$K = 2.309 \quad C = 1.638 \quad T = 1.085$$

The Bode plots of force and displacement are shown in Figure 8.16.4. The displacement response is somewhat similar to that obtained with quadratic optimization but the control forces are substantially larger.

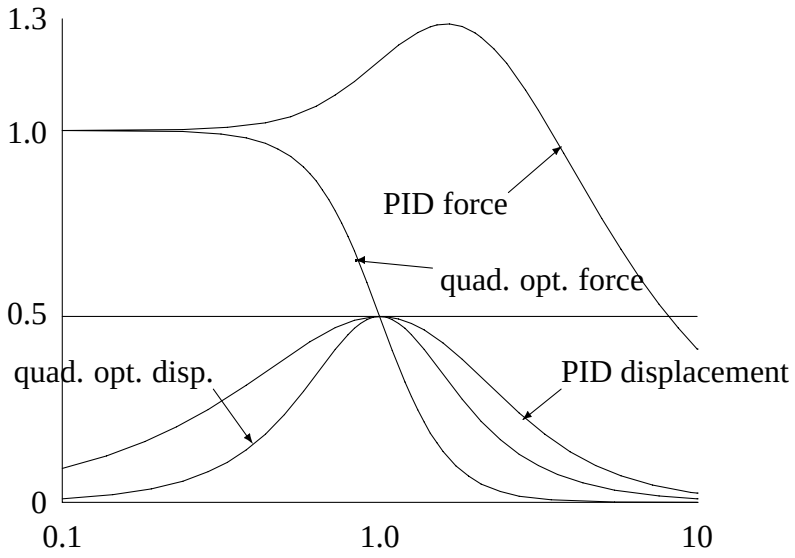

Quadratic Optimization: Choice of Parameters

How are the parameters α and β selected? Notice that these parameters nondimensionalize the displacement and bearing force in the cost function:

$$F_b^* = \arg\min_{F_b} \left(|F_b/\alpha|^2 + |X/\beta|^2 \right) \quad : \quad X = \frac{1}{m\omega^2} \left(F_b + F_e \right)$$

As a result, an obvious choice is to let α equal the largest expected force *or* the bearing load capacity and β equal the largest allowed motion.

It is perfectly reasonable for α or β to depend on frequency. This is especially useful with α where the bearing load capacity is frequency dependent: at low frequency, the capacity is set by saturation and at high frequency, it is set by slew rate:

$$\alpha = f_{\max,DC} \sqrt{\frac{\omega_o^2}{\omega^2 + \omega_o^2}} \quad : \quad \omega_o = \frac{\dot{f}_{\max}}{f_{\max}}$$

8.16.5 Computing F_b

In the presentation so far, it is assumed that F_e is known so that F_b can be computed directly. However, it is usual to know only x: how do we compute F_b?

The answer is that the cost function itself can be evaluated for a given choice of F_b and then F_b is iterated until the cost function is minimized:

$$F_b^*(\omega) = \arg\min_{F_b} \left(|F_b/\alpha(\omega)|^2 + |X/\beta|^2 \right) \quad : \quad X = k_b(F_b;\omega) + k_e(F_e;\omega)$$

The functions k_b and k_e define the plant. For the single mass example, both are simply $F/m\omega^2$. In general, they do not have to be linear in the force: any monotonic relationship will work!

In iterating F_b, it is assumed that ω, k_b, k_e, and F_e are constant. Thus, the solution F_b^* is found in the same way as a numerical optimization is performed. Since the cost function is quadratic and the plant functions (k_e and k_b) are monotonic, the problem has a single global minimum. Figure 8.24 illustrates the algorithm.

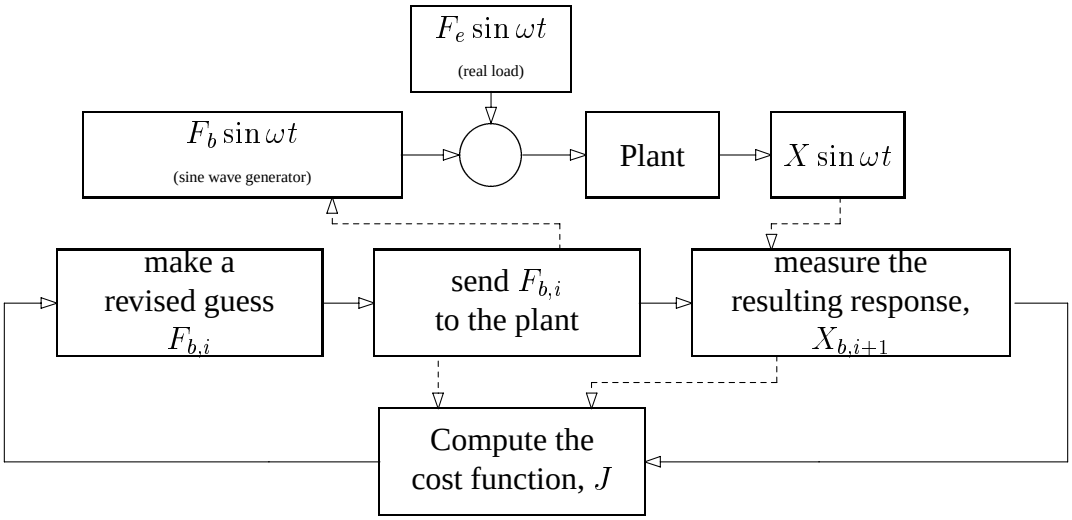

Figure 8.24: Harmonic control: the essential algorithm.

Requirements

Since the problem is stated in the frequency domain, we require a few things.

1. The plant must be stable. Otherwise, we can't talk about (or measure) steady state response. Typically, this means that the plant must be stabilized with feedback control.
2. There must be a way of selecting the frequency and staying synchronized with it. For rotors, the frequency is usually a multiple of the shaft speed and is monitored with a *key phasor* signal: a pulse which is issued once per revolution.
3. We need to be able to evaluate the cost function: this means that we need to measure F_b and X. F_b is assumed known. X is measured by integrating the product of the measured response with synchronized sine and cosine waves (to generate Fourier coefficients):

$$X = \frac{\omega}{n\pi} \int_0^{\frac{2\pi n}{\omega}} x(t) \cos \omega t dt + j \frac{\omega}{n\pi} \int_0^{\frac{2\pi n}{\omega}} x(t) \sin \omega t dt$$

8.16.6 Generalizing to Flexible Rotors

The harmonic response model for a rotor is fairly simple. For instance, if the rotor differential equation is

$$\begin{aligned} M\underline{\ddot{x}} + C(\Omega)\underline{\dot{x}} + K\underline{x} &= B_c \underline{f}_b + B_e \underline{f} \\ \underline{y} &= W\underline{x} \end{aligned}$$

then the harmonic response model is

$$\underline{Y} = W \left(K - \omega^2 M + j\omega C(\Omega) \right)^{-1} (B_c \underline{F}_b + B_e \underline{F})$$

In simpler form, the response is

$$\underline{Y} = T(\Omega)\underline{F}_b + \underline{Y}_0(\Omega)$$

This is the general form for a linear differential equation, but even a nonlinear differential equation can be linearized about a present operating point to produce this same form.

Cost Functions for Large Plants

The quadratically optimized harmonic control is based on a quadratic cost function. For the single mass, this was

$$J = |F_b/\alpha(\omega)|^2 + |X/\beta|^2$$

In general, we use

$$J = \sum_{i=1}^{N_f} |F_{b,i}/\alpha_i(\omega)|^2 + \sum_{i=1}^{N_y} |Y_i/\beta_i|^2$$

In matrix notation, this is

$$J = \underline{F_b}^* R \underline{F_b} + \underline{Y}^* Q \underline{Y}$$

(where $(\cdot)^*$ means the conjugate transpose)

The matrices R and Q are

$$R = \begin{bmatrix} 1/\alpha_1^2 & & \\ & \ddots & \\ & & 1/\alpha_n^2 \end{bmatrix} \quad Q = \begin{bmatrix} 1/\beta_1^2 & & \\ & \ddots & \\ & & 1/\beta_n^2 \end{bmatrix}$$

As before, the α_i compare the bearing forces to maximum capacity and the β_i compare the response to the maximum allowed response.

We can substitute the harmonic model for $\underline{Y}$ to obtain

$$J = \underline{F_b}^* R \underline{F_b} + \left(\underline{F_b}^* T^*(\Omega) + \underline{Y_0}^*(\Omega)\right) Q \left(T \underline{F_b} + \underline{Y_0}\right)$$

This expression is differentiated with respect to $\underline{F_b}$ and the result set to zero:

$$\frac{dJ}{d\underline{F_b}} = 2R\underline{F_b} + 2T^*(\Omega)QT\underline{F_b} + 2T^*(\Omega)Q\underline{Y_0} = 0$$

The best control bearing control is the solution to this minimization:

$$\underline{F_b}_{i+1} = -\left(R + T^*(\Omega)QT\right)^{-1} T^*(\Omega)Q\underline{Y_0}$$

As with the single mass problem, we do not know what $\underline{Y_0}$ is, but we can estimate it from previous solutions:

$$\underline{Y_0}(\Omega) = \underline{Y_i} - T(\Omega)\ \underline{F_b}_i$$

which defines a recursive relationship for $\underline{F_b}$:

$$\underline{F_b}_{i+1} = -\left(R + T^*(\Omega)QT\right)^{-1} T^*(\Omega)Q\left(T(\Omega)\underline{F_b}_i - \underline{Y_i}\right)$$

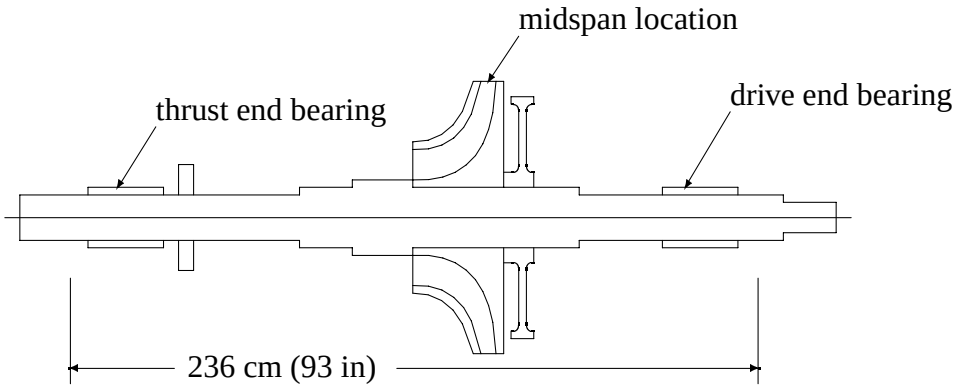

Figure 8.25: Gas pipeline compressor rotor.

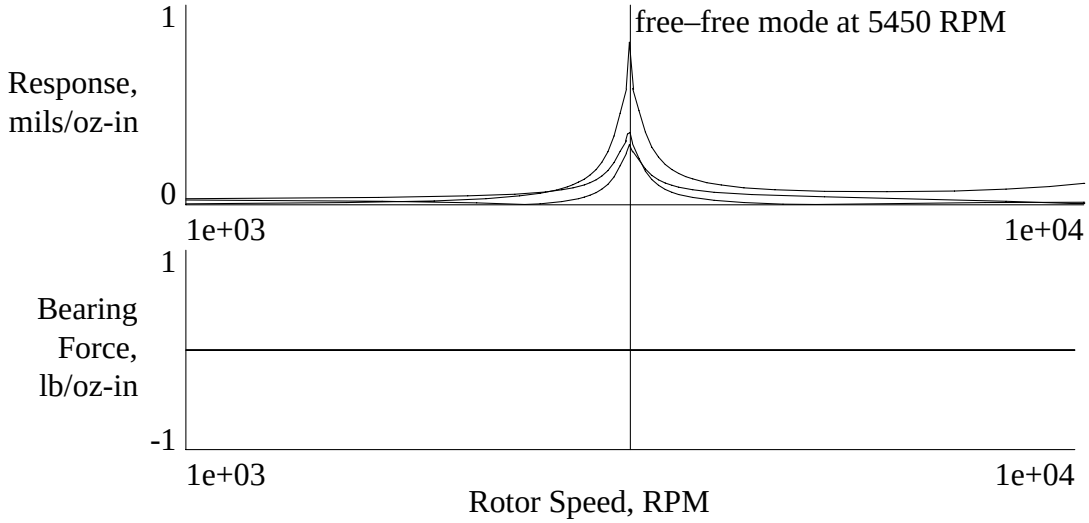

Figure 8.26: Free–free response of a pipeline compressor rotor to midspan unbalance.

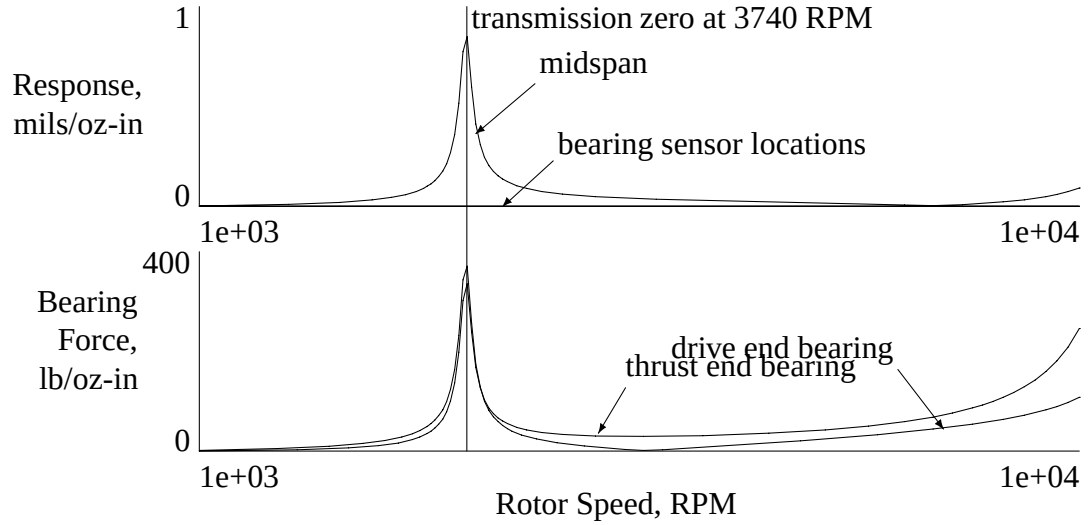

Figure 8.27: Clamped response of a pipeline compressor rotor to mass unbalance at midspan.

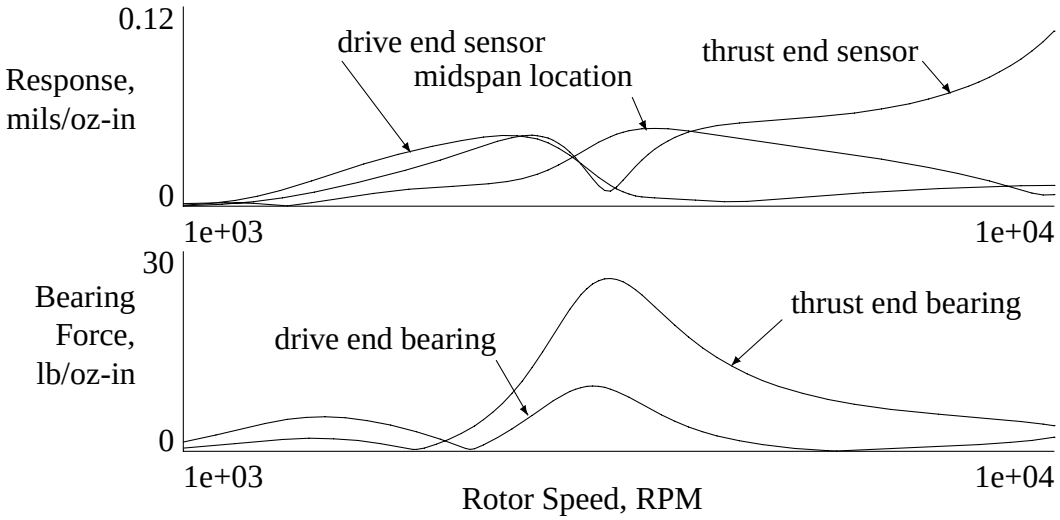

Figure 8.28: Mixed optimization response of a pipeline compressor rotor to mass unbalance at midspan.

Example Compressor

Gas pipeline compressor. Rotor mass = 1050 kg. First free–free resonance = 5433 CPM. Depicted in Figure 8.25.

The simplest result is when the cost of response (Q) is zero and the cost of control (R) is not. This produces the rotor free–free response illustrated in Figure 8.26 Clearly, this approach of eliminating the bearing effect at the synchronous speed causes problems at any free–free natural frequencies!

The opposite extreme uses no cost of control: $R = 0$ to absolutely minimize the rotor response. Figure 8.27 illustrates the resulting rotor response and bearing forces. In contrast to the minimum bearing force solution, the minimum response solution causes problems at frequencies other than the free–free resonances. The problem frequencies correspond to transmission zeros for the transfer matrix from actuator input to cost function (β weighted) output.

The problems associated with either of these extreme solutions can be avoided simply by using a mixed optimization in which neither the cost of control nor the cost of response is zero. As an example, the bearing control forces for the present rotor are normalized by their capacity of 2230 pounds force and the journal motions are normalized by a clearance of 0.007 inches. The resulting unbalance response and bearing forces are illustrated in Figure 8.28.

Chapter 9

Auxilliary Bearings

9.1 Introduction

In application to commercial rotating machinery, magnetic bearings usually require some form of auxiliary bearing. Fundamental limits to the static and dynamic capacity of magnetic bearings dictate that excessive shaft loads will, at some point in the life of the bearing, force the shaft out of support.[6] To protect the shaft and surrounding components such as seals and impellers which are likely to be damaged in the event of excessive shaft vibration, auxiliary bearings are introduced to limit the shaft motion to some acceptable level. These auxiliary bearings generally take the form of either a rolling element bearing or a bushing. In either case, the inner bore is oversized to provide a clearance between the auxiliary bearing and the shaft. In this manner, the shaft does not contact the auxiliary bearing until it moves beyond a limit point equal to the radial clearance in the auxiliary bearing. Smaller motions of the shaft are controlled by the magnetic bearing.

The transient behavior governing the transfer of support of the rotor from magnetic bearings onto auxiliary bearings has been examined in detail in the context of general rotor rubs by Muszynska [7] and Choy [2] and in the specific context of auxiliary bearings by Ishii [4] and Kirk [5]. This behavior is very complex and dependent upon the precise conditions at the moment of loss of support as well as the details of the friction at the interface between rotor and auxiliary bearing inner race and auxiliary bearing dynamic compliance. As a result, it is very difficult to draw general conclusions from either transient simulations or actual drop tests.

However, one important property of the steady behavior following such a transition is whether or not the rotor enters full rolling whirl in the auxiliary bearing clearances. This is important because fully developed circular whirl typically results in much larger shaft deflections than does the more random bouncing which may characterize the transient response or, ideally, the small oscillations about a steady operating point at the bottom of the clearance space.

The conditions for a sustained circular whirl can be computed without relying on a transient simulation. Black [1] carried out an elegant study of steady whirl at a single point of rub in a simple single mass rotor. Feeny [3] explored the stability of various classes of whirls in rigid rotors on rigid auxiliary bearings using perturbation analysis. While prediction of the *possibility* of full whirl does not imply that it will occur – this depends on the precise initial conditions of the drop – prediction that whirl is impossible precludes such behavior. The present work develops a general condition for steady circular whirl when the rotor and auxiliary bearing support are circularly isotropic.

Nomenclature

a	amplitude	R	receptance matrix (function of ω and Ω)
$\underline{c}$	vector of complex clearance components	t	time
C	damping matrix	V	journal force selection matrix
D	whirl direction matrix, diag$[\pm 1]$	w_x	generalized displacements in the $x-z$ plane
f	generalized force	w_y	generalized displacements in the $y-z$ plane
G	gyroscopic matrix	$\underline{X}$	vector of complex planar rotor motions
H	output selection matrix	$\underline{Y}$	vector of complex planar rotor journal motions
j	$\sqrt{-1}$	$\underline{\epsilon}$	vector of complex bearing motions
J	cost, worst case phase error	ϕ	phase angle
K	stiffness matrix	γ	spin/whirl ratio: Ω/ω
$\mathcal{K}$	frequency dependent stiffness matrix	μ_k	kinematic coefficient of friction
M	mass matrix	ω	shaft whirl speed
n	number of mass stations in the rotor model	Ω	shaft spin speed
n_c	number of contact points along the rotor	σ	dimensionless whirl frequency
P	permutation matrix	ξ	damping ratio

9.2 Model

The interaction between the rotor journals and oversized bearing bores is potentially quite complicated. However, if the system components are circularly isotropic, this interaction becomes considerably simpler, permitting a relatively compact formulation. In the following subsections, the complex analysis which permits this compact formulation is discussed to highlight the model assumptions necessary for its use. The rotor and bearing models are then examined to demonstrate their suitability to such a formulation.

9.2.1 Complex Notation

Assume that the harmonic motions of the journals in a rotor spinning at a rate Ω in response to harmonic forces applied to the journals at a frequency ω can be componentiated in the x and y planes and computed as

$$\left\{ \begin{array}{c} \underline{w}_x \\ \underline{w}_y \end{array} \right\} = \left[\begin{array}{cc} R_{xx} & R_{xy} \\ R_{yx} & R_{yy} \end{array} \right] (\omega;\Omega) \left\{ \begin{array}{c} \underline{f}_x \\ \underline{f}_y \end{array} \right\} \tag{9.1}$$

(a model of this form for the rotor will be developed in the next section.) If the motion is uniformly circular so that

$$w_{x,i}(t) = a_i \cos(\omega t + \phi_i)$$

and

$$w_{y,i}(t) = a_i \sin(\omega t + \phi_i)$$

then the motion can be represented in terms of the complex notation

$$W_i(t) = w_{x,i}(t) + j w_{y,i}(t) = a_i e^{j(\omega t + \phi_i)}$$

or

$$W_i(t) = a_i e^{j\phi_i} e^{j\omega t}$$

The term *uniformly circular* implies that the magnitude and sign of ω are the same at every station, i. In this manner, each element of the vector is distinguished from each other only in terms of its magnitude, a_i, and phase, ϕ_i. This permits the simple vector notation

$$\underline{W}(t) = \underline{A}_w e^{j\omega t}$$

where $\underline{A}_w$ is a complex vector indicating both magnitude and phase at each station, i.

This notation is useful only if the dynamics of the system are suitable. That is, assume that the bearing forces are to be represented as

$$\underline{F}(t) = \underline{f}_x(t) + j\underline{f}_y(t) = \underline{A}_f e^{j\omega t}$$

Then the relationship (9.1) must be able to be compactly represented as

$$\underline{W}(t) = R(\omega;\Omega)\underline{F}(t) \tag{9.2}$$

or, equivalently,

$$\underline{w}_x + j\underline{w}_y = (R_r + jR_i)\left(\underline{f}_x + j\underline{f}_y\right) \tag{9.3}$$

Expanding (9.3) produces

$$\underline{w}_x + j\underline{w}_y = R_r\underline{f}_x - R_i\underline{f}_y + j(R_i\underline{f}_x + R_r\underline{f}_y) \tag{9.4}$$

Comparing (9.4) to (9.1) implies that

$$R_r(\omega;\Omega) = R_{xx}(\omega;\Omega) = R_{yy}(\omega;\Omega)$$

and

$$R_i(\omega;\Omega) = -R_{xy}(\omega;\Omega) = R_{yx}(\omega;\Omega)$$

Thus, the complex notation is useful only for systems with the form

$$\left\{ \begin{array}{c} \underline{w}_x \\ \underline{w}_y \end{array} \right\} = \left[\begin{array}{cc} R_{xx} & R_{xy} \\ -R_{xy} & R_{xx} \end{array} \right](\omega;\Omega) \left\{ \begin{array}{c} \underline{f}_x \\ \underline{f}_y \end{array} \right\} \tag{9.5}$$

Such systems will be referred to as circularly isotropic. The arguments Ω and ω imply that the isotropy may only hold at specific values of Ω and ω. Linear systems will usually be isotropic for all values of these parameters if for any.

9.2.2 The Rotor

The rotor is assumed to have the rather conventional circularly symmetric model of the form

$$\begin{aligned} \left[\begin{array}{cc} M & 0 \\ 0 & M \end{array} \right] \left\{ \begin{array}{c} \ddot{\underline{w}}_x \\ \ddot{\underline{w}}_y \end{array} \right\} + \left(\Omega \left[\begin{array}{cc} 0 & G \\ -G & 0 \end{array} \right] + \left[\begin{array}{cc} C & 0 \\ 0 & C \end{array} \right] \right) \left\{ \begin{array}{c} \dot{\underline{w}}_x \\ \dot{\underline{w}}_y \end{array} \right\} & \\ + \left[\begin{array}{cc} K & 0 \\ 0 & K \end{array} \right] \left\{ \begin{array}{c} \underline{w}_x \\ \underline{x}_y \end{array} \right\} &= \left\{ \begin{array}{c} \underline{f}_x \\ \underline{f}_y \end{array} \right\} \end{aligned} \tag{9.6}$$

where $\underline{w}_x$ and $\underline{w}_y$ are generalized displacements (translations and rotations) in the $x-z$ and $y-z$ planes, Ω is the shaft spin rate, and any gyroscopic effects are described by the matrix G. Physical considerations imply that M, C, G, and K are all symmetric. Typically, the matrices M and G are diagonal, but need not be. For the problem of whirl in the auxiliary bearing clearance, it is assumed that $\underline{f}_x$ and $\underline{f}_y$ are solely bearing contact forces: gravity, mass unbalance, and aero- or hydro-dynamic effects are neglected. These effects can be added back in as a linear perturbation to the solution subject to some easily established constraints on the magnitude of the additional forces relative to those exerted by the bearings.

Given the isotropic nature of the rotor and the auxiliary bearings, it is assumed that the steady state motion of the rotor consists of circular orbits at each mass station:

$$w_{x,i} = X_i e^{j\omega t} \qquad w_{y,i} = \pm j X_i e^{j\omega t} \tag{9.7}$$

or, more compactly

$$\underline{w}_x = \underline{X} e^{j\omega t} \qquad \underline{w}_y = -jD\underline{X} e^{j\omega t} \quad : \qquad \underline{X} \in \mathbf{C}^n \tag{9.8}$$

where $D = \text{diag}(\pm 1)$ which has the property $DD = I$. For an isotropic bearing model, this type of orbit should give rise to bearing forces of the form

$$\underline{f}_x = \underline{F} e^{j\omega t} \qquad \underline{f}_y = -jD\underline{F} e^{j\omega t} \quad : \qquad \underline{F} \in \mathbf{C}^n \tag{9.9}$$

Such a model for the bearing forces presupposes *only* that the bearing forces precess in the same direction and at the same rate as the motion of the associated journals.

This model produces a simultaneous pair of algebraic equations for the steady state response

$$\left[-\omega^2 M + \omega\Omega GD + j\omega C + K\right] \underline{X} = \underline{F} \tag{9.10}$$

and

$$-j\left[-\omega^2 MD + \omega\Omega G j\omega CD + KD\right] \underline{X} = -jD\underline{F} \tag{9.11}$$

Multiply (9.11) by jD to obtain

$$\left[-\omega^2 DMD + \omega\Omega DG + jDCD + DKD\right] \underline{X} = \underline{F} \tag{9.12}$$

Now, introduce the permutation matrix P where

$$PDP' \doteq \begin{bmatrix} I & 0 \\ 0 & -I \end{bmatrix} \quad , \quad P'P = I \tag{9.13}$$

Apply the transformation

$$P' \begin{Bmatrix} \underline{X}_+ \\ \underline{X}_- \end{Bmatrix} \doteq \underline{X} \qquad P' \begin{Bmatrix} \underline{F}_+ \\ \underline{F}_- \end{Bmatrix} \doteq \underline{F} \tag{9.14}$$

and define

$$P'MP \doteq \begin{bmatrix} M_{++} & M_{+-} \\ M_{-+} & M_{--} \end{bmatrix}$$
$$P'GP \doteq \begin{bmatrix} G_{++} & G_{+-} \\ G_{-+} & G_{--} \end{bmatrix}$$
$$P'CP \doteq \begin{bmatrix} C_{++} & C_{+-} \\ C_{-+} & C_{--} \end{bmatrix}$$
$$P'KP \doteq \begin{bmatrix} K_{++} & K_{+-} \\ K_{-+} & K_{--} \end{bmatrix}$$
$$\mathcal{K}_{++}(\omega;\Omega) \doteq -\omega^2 M_{++} + \omega\Omega G_{++} + j\omega C_{++} + K_{++}$$
$$\mathcal{K}_{+-}(\omega;\Omega) \doteq -\omega^2 M_{+-} - \omega\Omega G_{+-} + j\omega C_{+-} + K_{+-}$$
$$\mathcal{K}_{-+}(\omega;\Omega) \doteq -\omega^2 M_{-+} + \omega\Omega G_{-+} + j\omega C_{-+} + K_{-+}$$
$$\mathcal{K}_{--}(\omega;\Omega) \doteq -\omega^2 M_{--} - \omega\Omega G_{--} + j\omega C_{--} + K_{--}$$

to convert the algebraic equations (9.10) and (9.12) to

$$\begin{bmatrix} \mathcal{K}_{++}(\omega;\Omega) & \mathcal{K}_{+-}(\omega;\Omega) \\ \mathcal{K}_{-+}(\omega;\Omega) & \mathcal{K}_{--}(\omega;\Omega) \end{bmatrix} \begin{Bmatrix} \underline{X}_+ \\ \underline{X}_- \end{Bmatrix} = \begin{Bmatrix} \underline{F}_+ \\ \underline{F}_- \end{Bmatrix} \tag{9.15}$$

and

$$\begin{bmatrix} \mathcal{K}_{++}(\omega;\Omega) & -\mathcal{K}_{+-}(\omega;\Omega) \\ -\mathcal{K}_{-+}(\omega;\Omega) & \mathcal{K}_{--}(\omega;\Omega) \end{bmatrix} \begin{Bmatrix} \underline{X}_+ \\ \underline{X}_- \end{Bmatrix} = \begin{Bmatrix} \underline{F}_+ \\ \underline{F}_- \end{Bmatrix} \tag{9.16}$$

where the off diagonal terms M_{+-}, M_{-+}, G_{+-}, and G_{-+} would typically be zero. The block components $\underline{X}_+$ and $\underline{X}_-$ are associated with forward and backward whirl, respectively. Recombine these simultaneous equations by forming half the sum of the two equations and half the difference:

$$\begin{bmatrix} \mathcal{K}_{++}(\omega;\Omega) & 0 \\ 0 & \mathcal{K}_{--}(\omega;\Omega) \end{bmatrix} \begin{Bmatrix} \underline{X}_+ \\ \underline{X}_- \end{Bmatrix} = \begin{Bmatrix} \underline{F}_+ \\ \underline{F}_- \end{Bmatrix} \tag{9.17}$$

and

$$\begin{bmatrix} 0 & \mathcal{K}_{+-}(\omega;\Omega) \\ \mathcal{K}_{-+}(\omega;\Omega) & 0 \end{bmatrix} \begin{Bmatrix} \underline{X}_+ \\ \underline{X}_- \end{Bmatrix} = \begin{Bmatrix} \underline{0} \\ \underline{0} \end{Bmatrix} \tag{9.18}$$

These equations imply that the forward component of the response, $\underline{X}_+$, is independent of the backward component of the response, $\underline{X}_-$. However, each response must simultaneously satisfy a pair of equations of the form

$$\left[-\omega^2 M_{\pm\pm} \pm \omega\Omega G_{\pm\pm} + j\omega C_{\pm\pm} + K_{\pm\pm}\right] \underline{X}_\pm = \underline{F}_\pm \tag{9.19}$$

and

$$\left[-\omega^2 M_{\mp\pm} \pm \omega\Omega G_{\mp\pm} + j\omega C_{\mp\pm} + K_{\mp\pm}\right] \underline{X}_\pm = 0 \tag{9.20}$$

In general, the coefficient matrix in (9.19) is full rank, so unless the coefficient matrix in (9.20) has zero rank, these equations cannot be simultaneously satisfied except for very specific cases of $\underline{F}_\pm$. The more general condition is satisfied when the coefficient matrix in (9.20) has zero rank; that

is, when the dimension of $\underline{X}_+$ or of $\underline{X}_-$ is zero. This implies that mixed whirl can only occur for this type of circularly isotropic system under very specific conditions whereas uniform whirl, either forward or backward, can occur under much more general conditions. As a result, the remaining analysis will assume that $D = \pm I$, which satisfies the assumption of uniform circular response discussed in the preceding section.

Defining

$$\gamma = \frac{\Omega}{\omega} \tag{9.21}$$

where γ can be either positive or negative: $\gamma > 0$ corresponds to forward whirl while $\gamma < 0$ corresponds to backward whirl, leads to the simpler formulation

$$\left(\omega^2[\gamma G - M] + j\omega C + K\right)\underline{X} = \underline{F} \tag{9.22}$$

In the present analysis, the interaction between the rotor and the auxiliary bearings occurs only at a few discrete points. Thus, it is convenient to extract from (9.22) that information which is relevant to this interaction. Define the displacement at the journals as

$$\underline{Y} = H\underline{X}$$

Further, assume that forces are only applied to the rotor at the discrete auxiliary bearing journals so that

$$\underline{F} = V\underline{F}_j$$

After solving (9.22) for $\underline{X}$, the input–output relationship can be reduced to

$$\underline{Y} = H\left(\omega^2[\gamma G - M] + j\omega C + K\right)^{-1} V\underline{F}_j \tag{9.23}$$

Comparing (9.23) to (9.2) reveals that the transfer function from journal forces to journal displacements is

$$R(\omega;\Omega) = H\left(\omega^2[\gamma G - M] + j\omega C + K\right)^{-1} V \tag{9.24}$$

9.2.3 Bearing Model

In the previous section, it was demonstrated that forced circular motion of the free–free shaft can be described by the relationship

$$\underline{Y}e^{j\omega t} = R(\omega;\Omega)\underline{F}_j e^{j\omega t} \tag{9.25}$$

in which the complex elements of the vector $\underline{Y}$ represent the planar displacements of the shaft at the points where it interacts with its auxiliary bearings and the complex elements of the vector $\underline{F}_j$ represent the planar forces applied to the system by the auxiliary bearings.

Further, if the displacements of the centers of the auxiliary bearings are given by the complex vector $\underline{\epsilon}$ then tangency of the journal surfaces to the auxiliary bearing bores requires that

$$\underline{Y} = \underline{\epsilon} + \underline{c} \quad : \qquad \underline{c} = \left\{ \begin{array}{c} c_1 e^{j\phi_1} \\ \vdots \\ c_{n_c} e^{j\phi_{n_c}} \end{array} \right\} \tag{9.26}$$

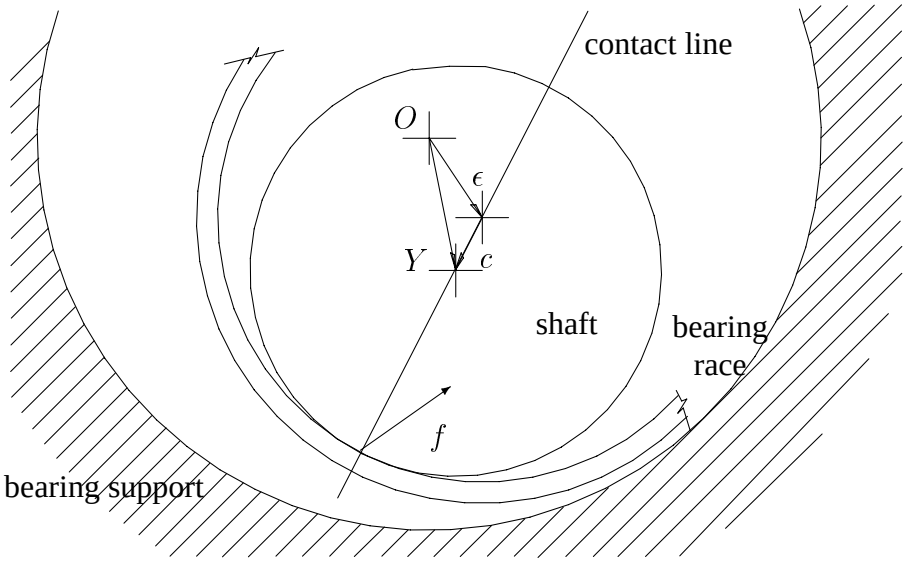

Figure 9.1: Rotor–bearing contact geometry

in which the elements of vector $\underline{c}$ are equal in magnitude to the clearance at each auxiliary bearing but whose phase (orientation) is, as yet, unknown. The geometry is indicated in Figure 9.1.

Finally, if the bearing compliance is circularly isotropic then the complex bearing force, $\underline{F}_j$ can be computed in terms of the complex bearing displacement as

$$\underline{F}_j = -\mathcal{K}_b(\omega;\Omega)\underline{\epsilon} \tag{9.27}$$

The interface between the rotor journal and the bearing bore can only sustain a positive normal force; a negative normal force would imply tension across this contact. In addition, assuming skidding at the interface, the tangential component of the contact force must equal the limit imposed by the contact kinematic coefficient of friction, μ_k. This means that the tangent of the angle between the bearing force and the surface inward normal must be equal to the kinematic coefficient of friction with sign determined by the sign of the ratio of the shaft spin to the shaft whirl:

$$\angle\left(\underline{F}_{j,i}\right) - \angle\left(-\underline{c}_i\right) = \text{sign}\left(\frac{\Omega}{\omega}\right)\tan^{-1}\mu_{k,i} \qquad i = 1\ldots n_c \tag{9.28}$$

at n_c points of contact along the rotor.

If μ_k is non–zero, the tangential component of the bearing force will produce a moment, or torque, on the shaft which will tend to slow the shaft spin unless there is an external torque acting on the shaft. In the present work, we assume either that the translational motion of the shaft is not coupled to its spin (usually gyroscopically) or that there is enough external torque or shaft inertia to make the effect of the friction on the shaft spin rate negligible (the time scale of loss in shaft spin rate is much larger than the period of the whirl.)

9.3 Whirl Condition

With these assumptions, the bearing motion $\underline{\epsilon}$ can easily be computed as

$$\underline{\epsilon} = -\left(I + R(\omega;\Omega)\mathcal{K}_b(\omega;\Omega)\right)^{-1}\underline{c} \tag{9.29}$$

This solution can be rearranged to a form which is more convenient to use:

$$\underline{c} + \underline{\epsilon} = (I + R\mathcal{K}_b)^{-1} R\mathcal{K}_b \underline{c} \tag{9.30}$$

Introducing the rotor transfer function *without auxiliary bearing clearance*,

$$R_{cl}(\omega;\Omega) = (I + R(\omega;\Omega)\mathcal{K}_b(\omega;\Omega))^{-1} R(\omega;\Omega) \tag{9.31}$$

permits the simple representation of the overall rotor journal motion for a given clearance vector,

$$\underline{c} + \underline{\epsilon} = R_{cl}\mathcal{K}_b \underline{c} \tag{9.32}$$

or,

$$\underline{\epsilon} = (R_{cl}\mathcal{K}_b - I)\,\underline{c} \tag{9.33}$$

In this manner, a general condition for sustainable whirl can be obtained by combining (9.27), (9.28), and (9.33):

$$\angle\left\{\mathcal{K}_b\left(R_{cl}\mathcal{K}_b - I\right)\underline{c}\right\}_i - \angle\underline{c}_i = \text{sign}\left(\frac{\Omega}{\omega}\right)\tan^{-1}\mu_{k,i} \qquad i = 1\ldots n_c \tag{9.34}$$

for some choice of phasings in the vector $\underline{c}$. When this condition is satisfied for a given $\underline{c}$, the total rotor journal response can be computed from (9.32).

9.3.1 Computation

When only one point of contact is possible, (9.34) is independent of the choice of clearance phase:

$$\angle ac - \angle c = \angle a$$

so no effort need be invested in determining the appropriate phase. Further, (9.34) describes the points of intersections of the phase of a rotor transfer function and the constant phase line corresponding to the coefficient of friction. These points of intersection can be found using any convenient root finding algorithm.

However, when two or more points of contact are possible, the problem immediately becomes more complicated. At each potential whirl frequency, the phases of the elements of $\underline{c}$ must be searched for an arrangement which satisfies (9.34). If the off–diagonal terms in $\mathcal{K}_b\left(R_{cl}\mathcal{K}_b - I\right)$ are negligible then, again, the choice of phase has no effect on satisfying the constraint. In this case the constraint is satisfied only at points of mutual intersection of $n_c + 1$ phase curves. Such an intersection may not exist for a real rotor model at any frequency. When the off–diagonal terms are not negligible, then the individual phases in $\underline{c}$ can be manipulated to change the shapes of the phase curves, leading to a better chance of finding such points of mutual intersection.

Consequently, in searching for whirl frequencies which satisfy (9.34), an optimization problem is posed at each potential frequency. Define a cost which is the maximum error in the agreement of phase:

$$J(\omega,\underline{c}) = \max_i \left| \angle\left\{\mathcal{K}_b\left(R_{cl}\mathcal{K}_b - I\right)\underline{c}\right\}_i - \angle\underline{c}_i - \text{sign}\left(\frac{\Omega}{\omega}\right)\tan^{-1}\mu_{k,i} \right| \tag{9.35}$$

then search on the elements of $\underline{c}$ to minimize J:

$$\underline{c}(\omega) = \arg\min_{\underline{c}} J(\omega,\underline{c}) \tag{9.36}$$

It is important to note that one of the phases in $\underline{c}$ is arbitrary. Factor $\underline{c}$ by the phase of c_1:

$$\underline{c} = \left\{ \begin{array}{c} c_1 \\ c_2 e^{j(\phi_2 - \phi_1)} \\ \vdots \\ c_{n_c} e^{j(\phi_{n_c} - \phi_1)} \end{array} \right\} e^{j\phi_1}$$

Clearly, the choice of ϕ_1 has no effect on the equality of (9.34) so it can be arbitrarily chosen equal to zero. In the case of rotors with two points of contact, (9.36) represents a scalar minimization at each potential frequency.

If (9.34) can be identically satisfied at a given frequency then the minimum cost achieved in (9.36) will be zero. Typically, this zero cost will not be achieved at any frequency for real rotors. However, the actual minimum cost achieved has a useful interpretation. Defining $J_{\min}(\omega)$ as the lowest cost achieved through (9.36), if the coefficients of friction at the rotor–bearing interfaces can be modified by an amount bounded by

$$\Delta\mu_{k,i} \leq \tan J_{\min}(\omega)$$

then whirl can be achieved at ω. Given the approximate nature of the model represented by the kinematic coefficient of friction, it seems reasonable to consider any frequency with a low enough bound, $\tan J_{\min}(\omega)$, to be a possible whirl frequency.

9.3.2 Multiple Auxiliary Bearings or Rubs

If a rotor system has more than two potential points of contact ($n_c > 2$), it may be that whirl involves some, but not all, of the contact points. In this case, it will be necesary to examine the possibility of whirl with all possible combinations of contact points. For each combination examined, if whirl appears feasible, the response at the other potential points of contact not included in the analysis set must be examined to ensure that the computed whirl does not produce contact at the excluded points.

9.4 Examples

9.4.1 Simple Disk

A simple example of this analysis is that of a disk rolling in a clearance. The geometry is illustrated in Figure 9.2. The disk has a mass M. The annular support (auxiliary bearing) has a stiffness of K and a damping C. The radial clearance between the disk and the bearing is c, the contact coefficient of friction is μ_k, and the clearance phase angle is assumed to be ϕ. Given this model, (9.34) becomes

$$\angle\left(\frac{M\omega^2(K + j\omega C)ce^{j\phi}}{K - M\omega^2 + j\omega C}\right) - \angle\left(ce^{j\phi}\right) = \text{sign}\left(\frac{\Omega}{\omega}\right)\tan^{-1}\mu_k$$

Introducing the damping ratio $\xi = C/2\sqrt{KM}$ and the whirl ratio $\sigma = \omega/\sqrt{K/M}$ produces

$$\angle\left(\frac{1 + 2\xi\sigma}{1 - \sigma^2 + 2\xi\sigma}\right) = \text{sign}\frac{\Omega}{\omega}\tan^{-1}\mu_k \tag{9.37}$$

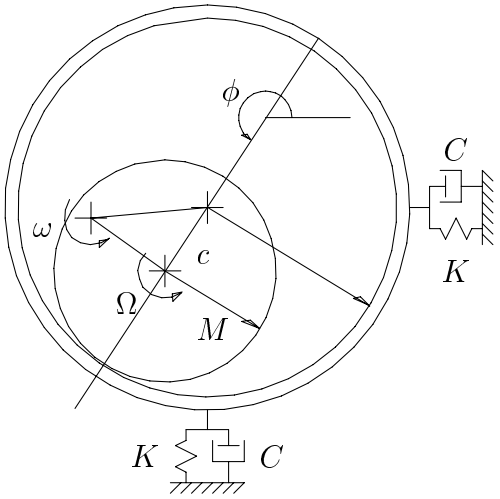

Figure 9.2: Geometry of simple disk example.

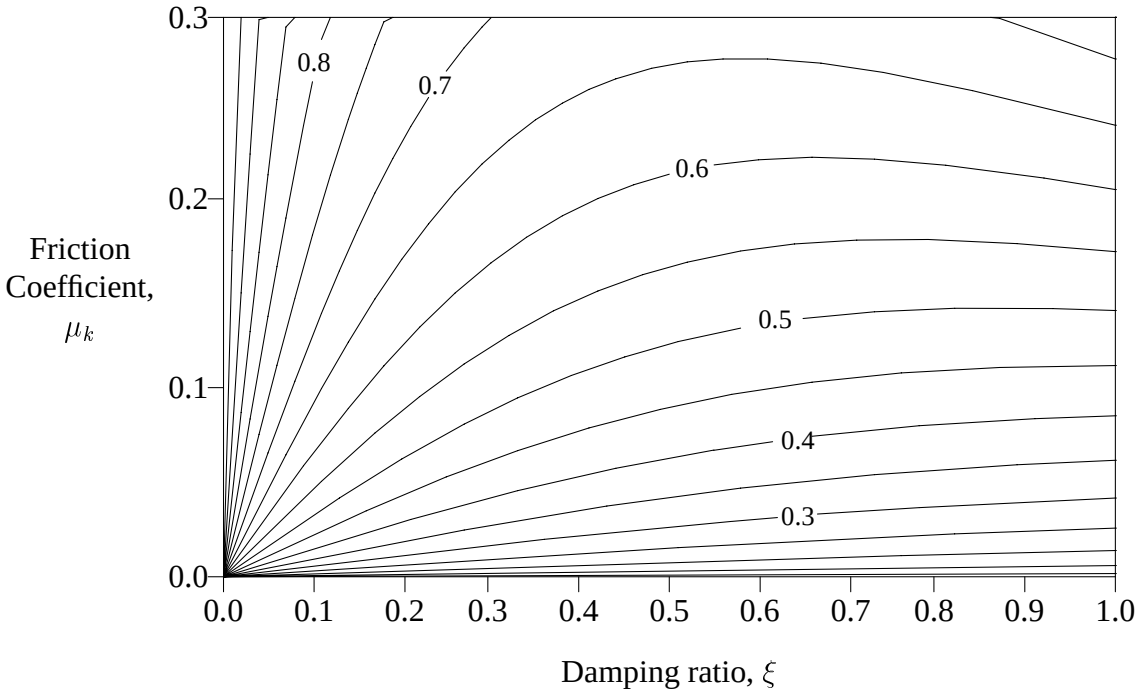

Figure 9.3: Contour map of whirl ratio σ *vs* damping ratio ξ and friction coefficient μ_k for a simple disk.

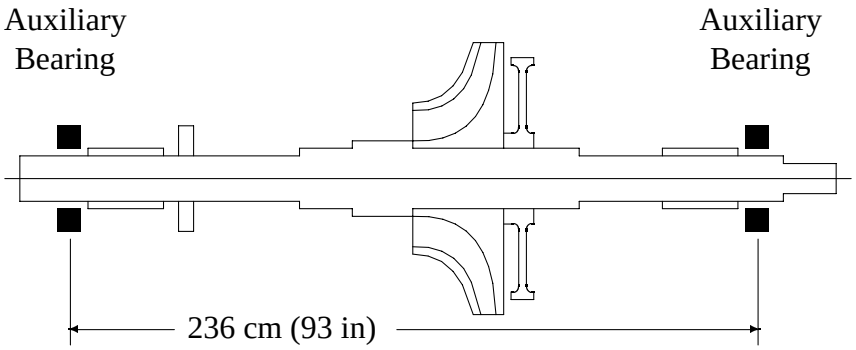

Figure 9.4: Compressor layout, showing impeller, balance piston, thrust bearing, and auxiliary bearing locations.

For $0 \leq \mu_k \leq 1$ and $\xi \geq 0$, (9.37) can only be satisfied if $\text{sign}(\Omega/\omega) = -1$: the wheel can only whirl *backwards*.

Figure 9.3 is a contour map of the whirl ratio, σ, *vs* damping ratio, ξ, and friction coefficient, μ_k. Of particular interest is that the contour lines converge at the origin. This means that the problem of clearance whirl is ill–posed in the absence of both friction and bearing dissipation. Further, in the limit as the damping ratio goes to zero, the whirl ratio converges to 1.0 for any non–zero friction coefficient. Finally, if $\mu_k = 0$ and $\xi > 0$, the disk cannot exhibit steady whirl. This last observation is no surprise: the whirl is driven by friction so, if the system is dissipative and there is no friction to drive the whirl, then any whirl produced by initial conditions would quickly collapse.

9.4.2 Commercial Compressor Rotor

The rotor of a large commercial compressor with a centrally mounted compressor wheel is depicted in Figure 9.4. The rotor has an auxiliary bearing span of 236 cm (93 inches) and a total rotor weight of 1050 kg (2320 pounds). The first free-free bending critical speed occurs at about 6500 CPM. The rotor model assumes about 0.2% modal damping in each of the rotor free–free modes. Figure 9.5 is a critical speed map for this rotor with gyroscopic effects neglected. This diagram shows the rotor/bearing resonances as a function of the bearing stiffness, assuming that the rotor is in contact with both auxiliary bearings and that they have identical stiffness and damping. For this rotor, which is fairly symmetric end–to–end, whirl is most likely to occur at a frequency slightly below the first resonance in the auxiliary bearings. As an example, Figure 9.6 shows the required variation in coefficient of friction for whirl to occur ($J_{\min}(\omega)$ in equation 9.36) at frequencies ranging from 500 CPM to 17000 CPM. In this example, the bearings are assumed to have a stiffness of 17,500,000 N/m and the effect of auxiliary bearing damping is illustrated by plotting the required variation for damping values ranging from 700 N-sec/m up to 70000 N-sec/m.

Figure 9.6 indicates that when the auxiliary bearing damping is slight there is a strong tendency to whirl at about 1650 CPM. It also suggests the possibility of whirl at about 2290 CPM or at about 11000 CPM when the damping is very light. Very heavy damping introduces the possibility of high frequency whirl at about 13500 CPM, associated with the fourth critical speed. Since the rotor is never operated beyond 7000 CPM, it is most likely that any whirl induced by a rotor drop onto auxiliary bearings would have a frequency lower than the first critical speed. A very similar result is reported by Ishii [4] on the basis of simulated rotor drops for a rotor with similar geometry.

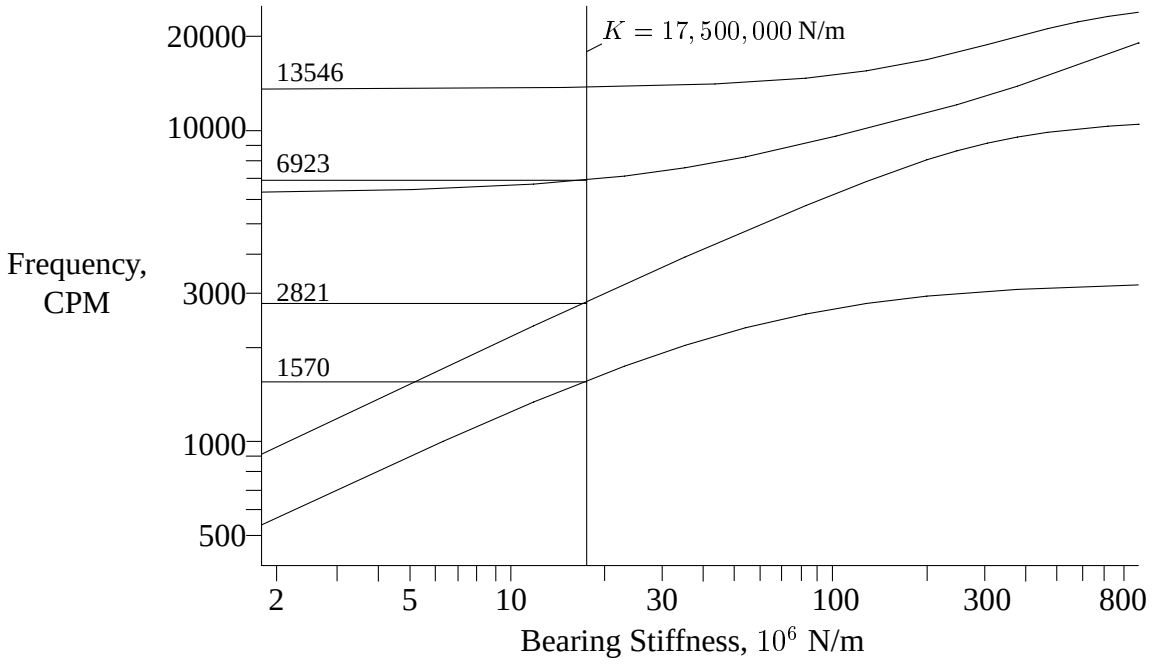

Figure 9.5: Critical speed map, gyroscopic effects suppressed

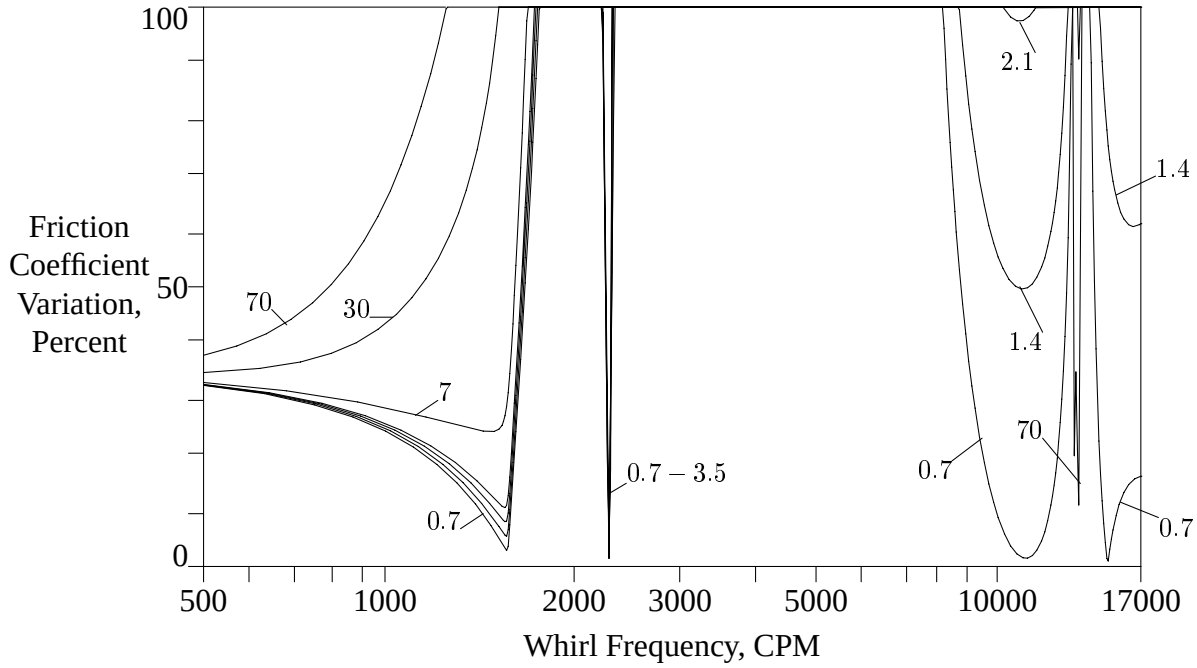

Figure 9.6: Commercial compressor rotor: required variation in coefficient of friction, μ_k, for whirl to occur. Auxiliary bearing stiffness = 17,500,000 N/m, damping is indicated in 10^3 N-sec/m.

9.5 Conclusions

An economical method of evaluating the whirl response of rotors supported in auxiliary bearings with an annular clearance has been developed. The method does not require simulation and the calculations involved are essentially similar to standard forced response analysis as widely employed in the rotordynamics community. As developed in this presentation, the generality of the method is limited only by the requirement of circular isotropy in the rotor and auxiliary bearings.

The primary value of the analysis lies not in predicting the possibility of whirl: almost any rotor/bearing system can probably whirl. Instead, the analysis permits regions of feasible whirl to be examined to determine the rotor response in an effort to ascertain the extent of attendant damage. Further, it permits direct comparison of various auxiliary bearing designs on the bases of likelihood and severity of whirl.

Bibliography

[1] Black, H. F., "Interaction of a Whirling Rotor with a Vibrating Stator Across a Clearance Annulus," *Journal of Mechanical Engineering Science*, VOL. 10, NO. 1, 1968, pp. 1–12.

[2] Choy, F. K., Padovan, J., and Qian, W., "Effects of Foundation Excitation on Multiple Rub Interations in Turbomachinery," *Journal of Sound and Vibration*,", VOL. 164, NO. 2, 1993, pp. 349–363.

[3] Feeny, B. F., "Stability of Cylindrical and Conical Motions of a Rigid Rotor in Retainer Bearings," *Proceedings of the Fourth International Symposium on Magnetic Bearings*, Zurich, August 1994, pp. 219–224.

[4] Ishii, T., and Kirk, R. G., "Transient Response Technique Applied to Active Magnetic Bearing Machinery During Rotor Drop," Rotating Machinery and Vehicle Dynamics Proceedings of the ASME 13^{th} Biennial Conference on Mechanical Vibration and Noise, Miami, September 22–25, 1991, pp. 191–199.

[5] Kirk, R. G, Swanson, E. E., Kavarna, F. H., and Wang, X., "Rotor Drop Test Stand for AMB Rotating Machinery, Part I: Description of Test Stand and Initial Results," *Proceedings of the Fourth International Symposium on Magnetic Bearings*, Zurich, August 1994, pp. 207–212.

[6] Maslen, E. H., Hermann, P., Scott, M. A., and Humphris, R. R., "Practical Limits to the Performance of Magnetic Bearings: Peak Force, Slew Rate, and Displacement Sensitivity," *ASME Journal of Tribology*, VOL. 111, NO. 2, April 1989, pp. 331-336.

[7] Muszynska, A., Franklin, W. D., and Hayashida, R. D., "Rotor–to–Stator Partial Rubbing and its Effects on Rotor Dynamic Response," NASA Conference Publication 2133: Rotordynamic Instability Problems in High–Performance Turbomachinery 1990, Texas A&M University, College Station, Texas, May 21–23, 1990, pp. 345–362.